Competing Pathways of Sugar-Nucleotide synthesis during the Biosynthesis of Plant Cell Walls

Sandra Christina Sharples

A thesis prepared in fulfilment of the requirements for the degree of Doctor of Philosophy (Ph.D.), University of Edinburgh 2005

Declaration

This thesis has been composed by myself and the work, of which it is a record, has been carried out by myself. All sources of information have been specifically acknowledged by means of a reference.

Sandra Christina Sharples

Acknowledgements

There a number of people I would like to thank who have made my time in the Edinburgh Cell Wall Group both memorable and enjoyable. I would first like to thank Prof. Fry for his time, patience, help and support throughout the years. It was both his enthusiasm for his subject and excellent lecturing skills that inspired me to research cell walls at Postgraduate level. I would also like to thank the members of the Edinburgh Cell Wall Group that I have known throughout the last four years: Janice Miller, Shona Lindsay, Harriet Parsons, Robert Vreeburg, Anna Kärkönen, Martha Green and Antonio Encina. It has been a pleasure working with all of you.

I would like to give a very special thank you to my family. To my fantastic Mum who "taught me everything I know" and who continues to teach me so much more. I can only aspire to her infinite positive qualities! To my wonderful Dad who remains my 4th emergency service with 100% reliability! To my sister who keeps my feet on *terra firma* and makes sure the shoes on them match my outfit. Finally I would like to thank Oma and Tante Else who always showed me great kindness and gave me so many happy memories.

The research conducted throughout this project was funded by the European COPOL project.

To Mum, Dad and Mel.

With all my love, always.

Abstract

In 1970 Leloir received the Nobel Prize for chemistry for his discovery of sugar nucleotides and their effect on the biosynthesis of carbohydrates. Sugar nucleotides are the only known donor substrates for plant cell wall polysaccharide formation. As the dry weight of a cell wall is composed of ~90% polysaccharides, the formation of the cell wall is heavily reliant on sugar nucleotides. More than one biochemical pathway may exist to form UDP-GlcA, UDP-GalA and GDP-Man. The project aim was to determine which of the competing pathways predominate(s) *in vivo* in the formation of the UDP-GlcA, GDP-GalA and UDP- Man utilised for plant cell wall synthesis.

The study utilised a novel 'trace' dual radiolabelling approach. Each NDP-sugar stems from one of four (or five) interconvertible 'core' metabolites (UDP-Gal ↔ UDP-Glc ↔ Glc 1-P ↔ Glc 6-P ↔ †Fru 6-P). The introduction of ^{14}C and ^{3}H at opposite ends of the 'core' metabolite pathway was predicted to form a gradient of ^{3}H:^{14}C ratios amongst the 'core' metabolites. The ^{3}H:^{14}C ratio that each NDP-sugar acquired was proposed to indicate the 'core' metabolite, and ultimately predominant pathway, that the NDP-sugar stemmed from.

The studies conducted on the ^{3}H:^{14}C ratios of plant cell wall residues at 8 h indicate that UDP-Gal is not a significant direct precursor of UDP-GalA. The ^{3}H:^{14}C ratios of the intermediary metabolites were studied over time. The results show that the ^{3}H:^{14}C ratio kinetics of UDP-GalA and UDP-Gal are vastly different from one another. These results also indicate that UDP-Gal is not a significant direct precursor of UDP-GalA. The ^{3}H:^{14}C ratios of the AIR (alcohol insoluble residue) -derived monosaccharides indicate that UDP-GlcA, UDP-GalA, UDP-Xyl, UDP-Ara and UDP-Api, like UDP-Rha, arose mainly from the UDP-Glc 'core' metabolite. The ^{3}H:^{14}C ratio kinetics of UDP-GalA, UDP-GlcA, UDP-Xyl and UDP-Ara are very distinct from the ^{3}H:^{14}C ratio kinetics of Glc 6-P but they are similar to the isotope ratio kinetics of UDP-Glc. The ^{3}H:^{14}C ratios of the AIR-derived monosaccharides and ^{3}H:^{14}C ratios of the intermediary metabolites give strong evidence that UDP-GalA and UDP-GlcA are predominantly formed by the UDP-Glc dehydrogenase pathway and not the *myo*-inositol pathway.

The ^{3}H:^{14}C ratio kinetics of UDP-Glc are approximately equal to those of Glc 1-P. It is observed that the ^{3}H:^{14}C ratio of the AIR-derived GalA residues is greater than for Man and Fuc. As UDP-GalA was determined to arise predominantly from UDP-Glc, GDP-Man and GDP-Fuc cannot also stem from Glc 1-P. The predominant pathway of GDP-Man synthesis must be via Glc 6-P or †Fru 6-P.

Although Rib is not considered a component of plant cell wall polysaccharides the AIR-derived Rib, thought to arise from RNA, gave an interesting and reproducible ^{3}H:^{14}C ratio. The ^{3}H:^{14}C ratio of Rib was similar to those of GalA, Ara, Xyl and Api. A pathway is known to exist that may convert UDP-Xyl to the RNA precursor Rib 5-P. The results suggest that this is the predominant pathway of Rib synthesis for RNA.

Triose phosphates that may be transported into the plastids from the cytosol are proposed to be the precursors of plastid Glc 1-P synthesis which, in turn, may form ADP-Glc. The formation of triose phosphates occurs by glycolysis. As glycolysis is 'distanced' from the 'core' metabolite Glc 6-P or †Fru 6-P, the ^{3}H:^{14}C ratio values of ADP-Glc were expected to be lower than the results obtained for any of the 'core' metabolites. However, the isotope ratio kinetics of ADP-Glc closely match the isotope ratio kinetics of total cellular Glc 1-P. As Glc 1-P is the direct precursor of ADP-Glc and both metabolites share similar ratio kinetics and values, ADP-Glc may be predominantly synthesised from Glc 1-P in the cytosol or taken up into plastids as Glc 1-P.

† This is classed as a 'core' metabolite when cells are fed [U-^{14}C]Fru. If cells are fed [U-^{14}C]Glc, this is not a 'core' metabolite

Table of contents

List of Figures

List of Tables

List of Appendices

Abbreviations

AIR	Alcohol-insoluble residue
Api	Apiose
Ara	Arabinose
ASF	Alcohol soluble fraction
BAB	Butan-1-one:acetic acid:saturated boric acid (9:1:1 by vol.)
BAW	Butanol:acetic acid:water
CB	Chlorobutanol
CMC	Chloroform:methanol:water (10:10:3 by vol., final concentration)
cpm	Counts per minute
dGlc	2-deoxyglucose
dpm	Disintegrations per minute
EPGase	Endopolygalacturonase
EPW	Ethylacetate:pyridine:water
FAW	Formic acid: acetic acid: water
Fuc	Fucose
Gal	Galactose
GalA	Galacturonic acid
Glc	Glucose
GlcA	Glucuronic acid
IsoP	Isoprimeverose
KDO	2-keto-3-deoxyoctonate
Man	Mannose

MES	2-[N-morpholino]ethane-sulphonic acid
NDP-sugar	nucleoside diphosphate sugar
PC	Paper chromatography
PE	Paper electrophoresis
PyAW	Pyridine:acetic acid: water (1:1:98 by vol., pH 4.7)
Rha	Rhamnose
Rib	Ribose
SA	Specific activity
SCV	Settled cell volume
Suc	Sucrose
TLC	Thin layer chromatography
Xyl	Xylose

1. Introduction

The plant cell wall is a unique, metabolically active sub-cellular compartment. The plant cell wall governs many aspects of a cell such as shape, size, growth rate and resistance to microbial digestion. The cell wall also plays a vital role in the strength and texture of plant tissue.

1.1 Plant cell wall structure

The two main types of plant cell walls that exist are classed as primary and secondary cell walls. Initially a thin, plastic primary cell wall is laid down whilst the cell undergoes expansion. There are two phases associated with primary cell walls: the microfibrillar phase and matrix phase. As this study is concerned with the formation of the primary plant cell wall details on each phase are provided (section 1.1.1 – section 1.1.2). The primary cell walls of non-gramineous plants have type I cell walls. Type I cell walls have a xyloglucan-cellulose network embedded in a pectin-rich matrix. Type I cell walls differ in composition from gramineous plants (type II cell walls) as they have a glucuronoarabinoxylan-cellulose network in a relatively pectin-poor matrix that is cross-linked by ferulate esters and aromatic compounds (Carpita, 1996).

Once cell expansion has ceased, certain cells begin to form a thick secondary cell wall. The deposition of the secondary cell wall renders the cell no longer capable of growth.

1.1.1 Microfibrillar phase

Cellulose is a highly insoluble unbranched chain of (1→4) β-linked Glc residues. Cellulose chains associate together along their long axis to form bundles called microfibrils. Microfibril size varies between organisms and can range from ~36 chains in elementary fibrils to greater than 200 chains in cellulosic algae (Delmer & Amor, 1995). Microfibrils form a rigid structure and have a skeletal role in the plant cell wall.

1.1.2 Matrix phase

The matrix phase of primary plant cell walls consists mainly of pectic and hemicellulosic polysaccharides. Other components, not described here, include proteins, glycoproteins, lignin and phenolic compounds. These are tissue-specific and occur in variable quantities.

Pectin mainly comprises GalA, Rha, Ara and Gal residues (Brett & Waldron, 1996). Pectin accounts for ~30% of the dry weight of type I primary cell walls and is present in only small amounts in type II cell walls (McNeil *et al.*, 1984). The main types of pectin include homogalacturonan, rhamnogalacturonan I, rhamnogalacturonan II, arabinan, galactan and arabinogalactan I. Pectin is highly hydrated and has a 'gel-like' property that is thought to have a lubrication and loosening role in cell expansion.

The main sugar residues that make up hemicellulose are Glc, Gal, Man, Fuc, Ara, Xyl and GlcA. The four main hemicelluloses are xylans, xyloglucans, mixed-linkage glucans and mannans. Hemicelluloses have a role in the control of cell expansion. They may tether the microfibrils via hydrogen bonds.

1.1.2 Plant cell wall polysaccharide precursors — NDP-sugars

The existence of an NDP-sugar was proposed by Cardini *et al.* (1950) who suggested that UDP-Glc (Fig. 1.1) could be a cofactor for the interconversion of Glc 1-P from Gal 1-P. It was Caputto *et al.* (1950) that first isolated and characterised UDP-Glc. The importance of UDP-Glc as a donor substrate for plant cell wall polysaccharide synthesis was realised by Feingold *et al.* (1958) who demonstrated the involvement of UDP-Glc in callose synthesis.

Approximately 90% of the dry weight of the primary plant cell wall is composed of polysaccharides. At present, NDP-sugars are the only known donor substrates of cell wall polysaccharide synthesis (Table 1.1). The glycosylpyrophosphate bond in an NDP-sugar has a large negative free energy ($\Delta G°'$) of hydrolysis and renders the non-ribose sugar residue in an 'activated' or 'high-energy' form. This enables the almost irreversible transfer of the non-ribose sugar residue of the NDP-sugar to a nascent wall polymer with the aid of a transferase.

1.2 Scope for research in NDP-sugar metabolism involved in plant cell wall synthesis

Research into the formation of NDP-sugars has revealed that UDP-GlcA (Reiter *et al.*, 2001), UDP-GalA (Feingold *et al.*, 1960; Carpita *et al.*, 2001) and GDP-Man (Dalessandro *et al.*, 1986; DeAsua *et al.*, 1966) may be formed by more than one biochemical pathway (Fig. 1.2, Fig. 1.3, Fig. 1.4, respectively). In each case the predominant pathway that is utilised for plant cell wall synthesis is debated. In addition to this, the NDP-sugar utilised for cellulose formation has, as yet, not been conclusively shown to be UDP-Glc or GDP-Glc.

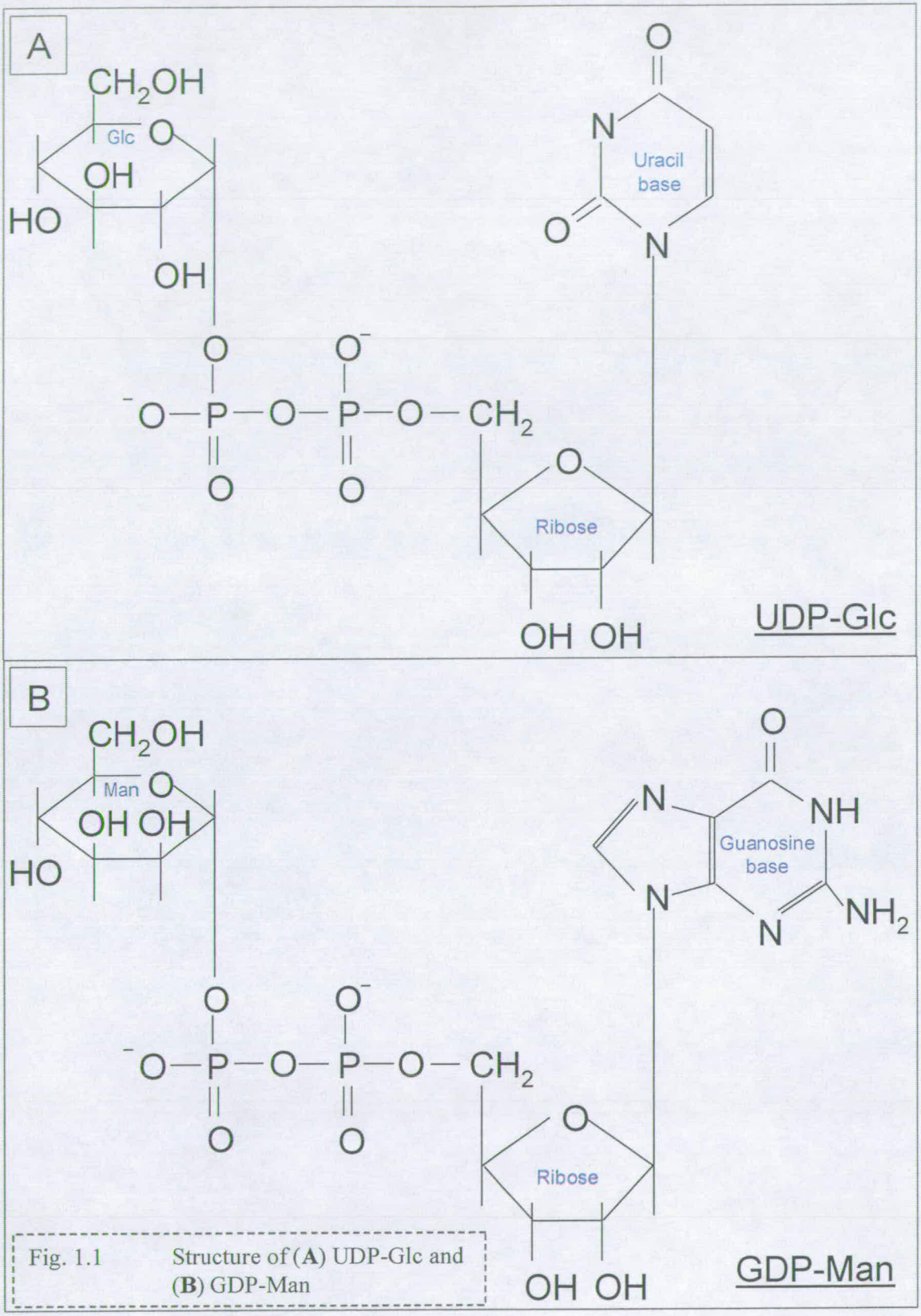

Fig. 1.1 Structure of (**A**) UDP-Glc and (**B**) GDP-Man

Nucelotide	NDP-sugar	Plant
ADP	ADP-Ara	Brown algae (Lin *et al.*, 1966)
	ADP-Fru	Larch (Cumming, 1970)
	ADP-Gal	Corn grain (Passeron *et al.*, 1964)
	ADP-Glc	*Chlorella* (Kauss *et al.*, 1962)
	ADP-Man	Corn grain (Dankert *et al.*, 1964)
GDP	GDP-Fuc	Brown algae (Lin *et al.*, 1966)
	GDP-D-Gal	Strawberry leaves (Selvendran *et al.*, 1967)
	GDP-L-Gal	Red algae (Su *et al.*, 1962 a,b)
	GDP-Glc	Sugar beet root (Katan *et al.*, 1965)
	GDP-Man	Brown algae (Lin *et al.*, 1966)
TDP	TDP-GalA	Sugar beet root (Katan *et al.*, 1965)
	TDP-Glc	Sugar beet root (Katan *et al.*, 1965)
UDP	UDP-Api	Parsley (Sanderman *et al.*, 1968 a,b)
	UDP-Ara	Mung bean seedlings (Ginsburg *et al.*, 1956)
	UDP-Fru	Dahlia tubers (Gonzalez *et al.*, 1963)
	UDP-Gal	Mung bean seedlings (Ginsburg *et al.*, 1956)
	UDP-GalA	Mung bean seedlings (Neufeld *et al.*, 1961)
	UDP-Glc	*Chlorella* (Kauss *et al.*, 1962)
	UDP-GlcA	Mung bean seedlings (Solms et al., 1957)
	UDP-Rha	Brown algae (Kauss, 1965)
	UDP-Xyl	Mung bean seedlings (Ginsburg *et al.*, 1956)

Table 1.1 Sugar nucleotides in plants

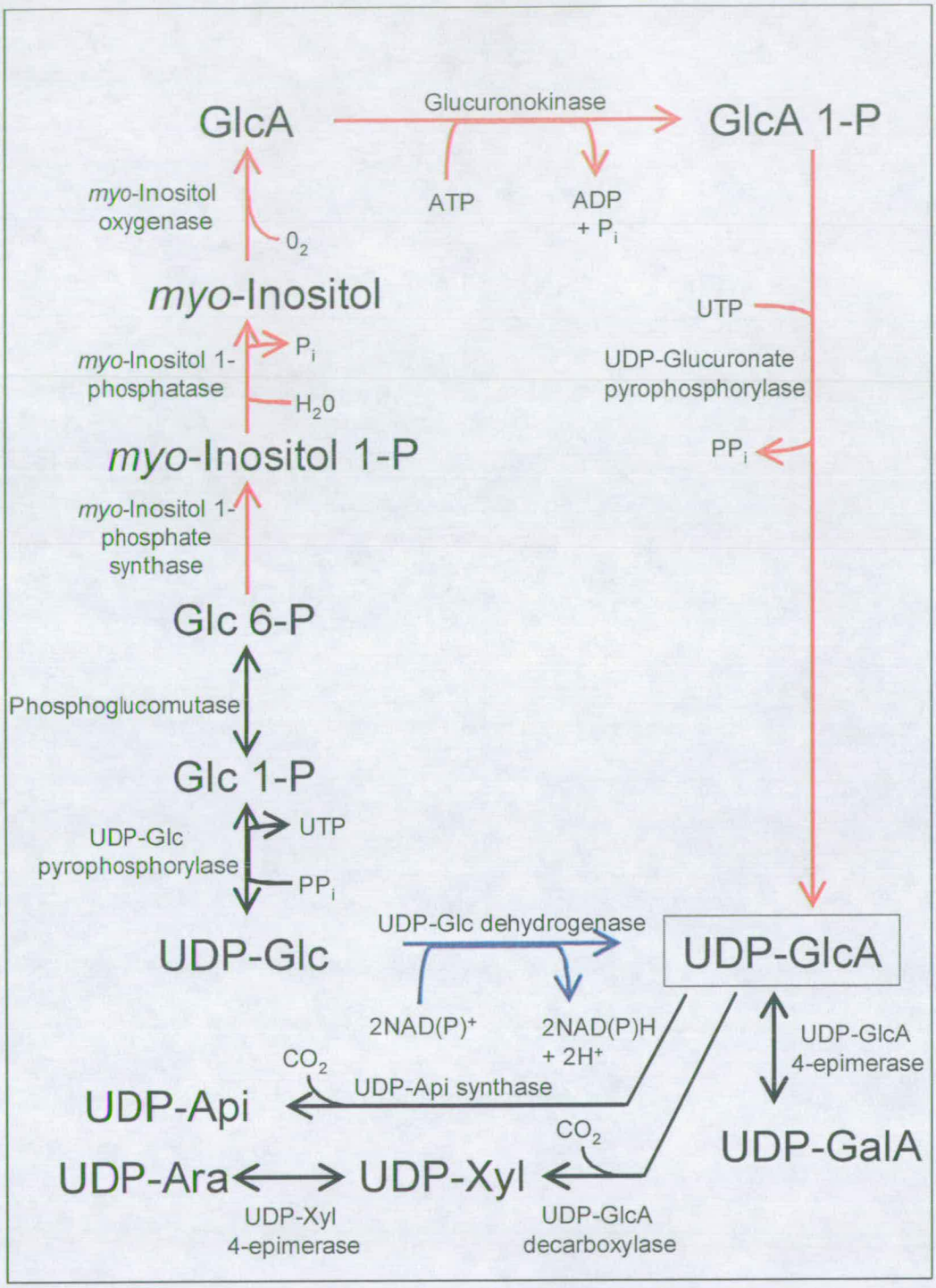

Figure 1.2 Production of UDP-GlcA by direct oxidation of UDP-Glc (blue arrows) or via the *myo*-inositol pathway (red arrows) and products of UDP-GlcA metabolism

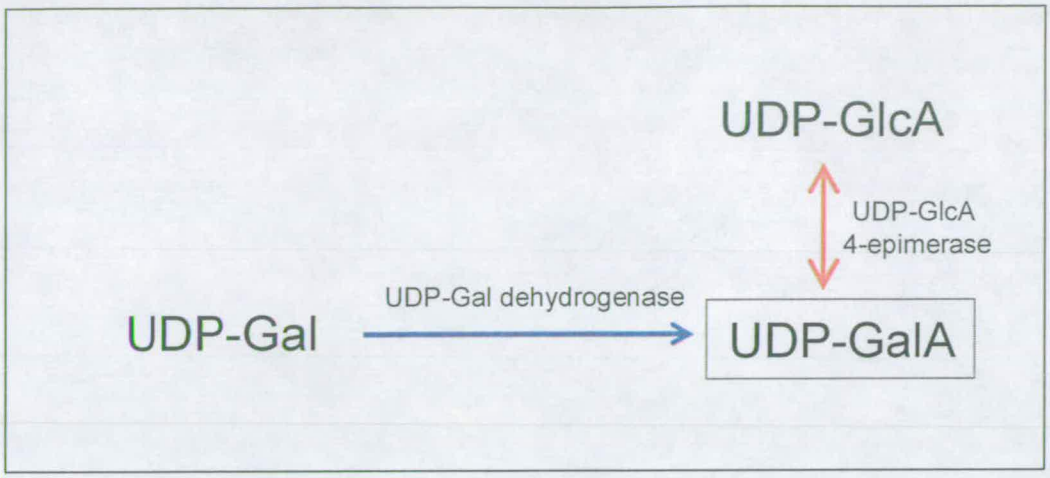

Figure 1.3 Production of UDP-GalA may be achieved by epimerisation of UDP-GlcA (red arrow) or by the dehydrogenation of UDP-Gal (blue arrow)

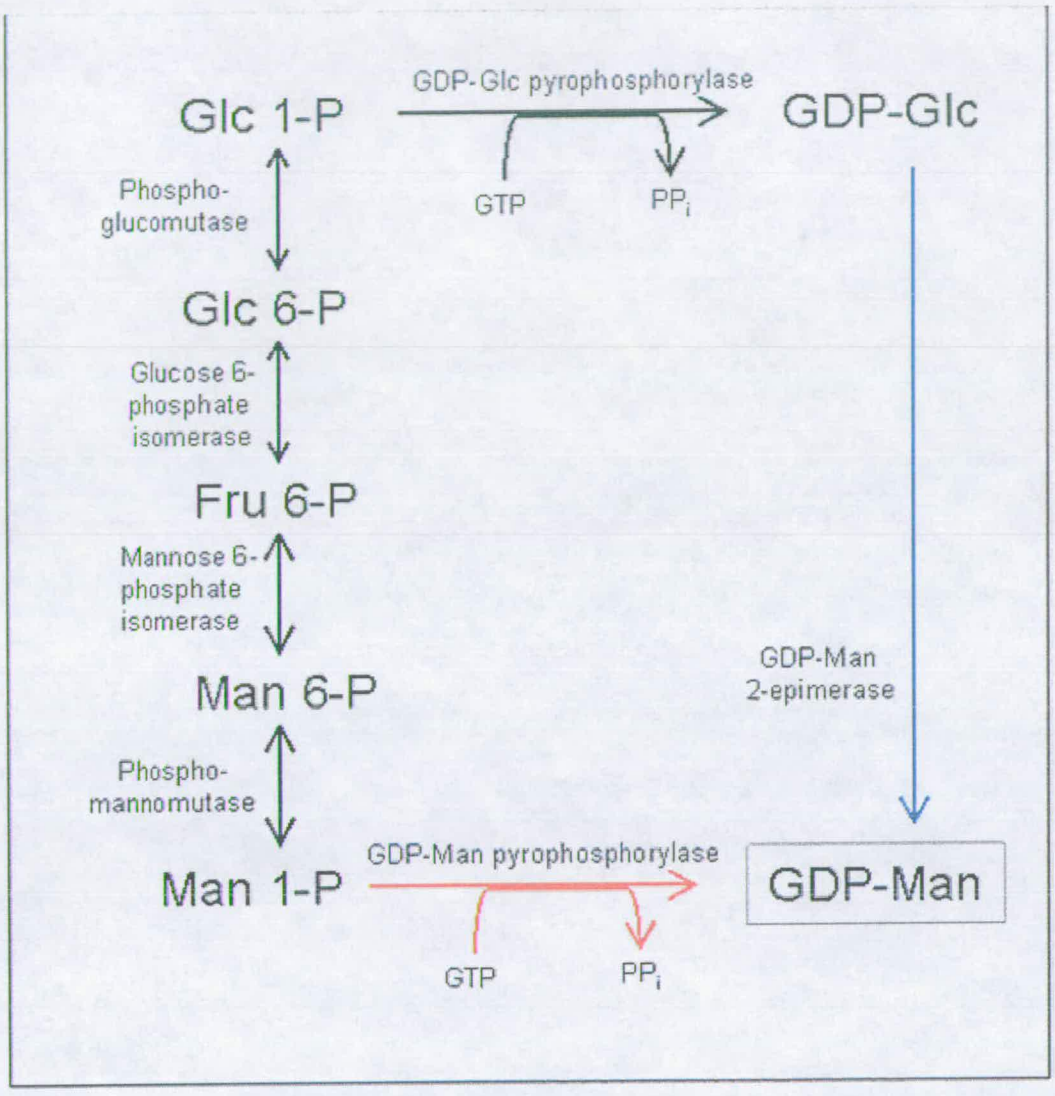

Figure 1.4 Production of GDP-Man from Man 1-P (red arrow) or via the 2-epimerisation of GDP-Glc (blue arrow)

Increased knowledge about the predominant pathways involved in NDP-sugar formation used for cell wall synthesis is necessary to allow researchers to alter or control plant cell wall precursor levels, and ultimately plant cell wall polymer synthesis, in a beneficial manner. One example of why it is important to understand the biochemical pathways involved in sugar nucleotide metabolism is illustrated by the results of an experiment conducted on alfalfa (lucerne; *Medicago sativa*) by Samac *et al.* (2004). Alfalfa is used as a forage crop for ruminants in temperate

regions. The stems of alfalfa have a large proportion of cellulose and hemicellulose that ruminants cannot digest or derive nutrition from. An increase in polysaccharide digestibility would yield carbohydrates that the microbes in the rumen could obtain energy from. It is thought that this would enhance amino acid uptake by the microbes and ultimately benefit the ruminant that digests the microbes. The current solution to improve this situation involves the addition of starch to the animal diet. This, however, often leads to acidosis and other health problems in the cattle. One solution to this problem is to increase the content of digestible plant cell wall polymers in the forage crop. Samac *et al.* (2004), without complete knowledge of the competing pathways involved, attempted to increase the availability of pectin precursors in alfalfa vascular tissues in the hope that this would be associated with an increase in pectin synthesis. To do this, Samac *et al.* (2004) expressed soybean UDP-Glc dehydrogenase cDNA in alfalfa under the control of promoters active in either xylem or phloem tissue. The transgenic plants did not show a significant increase in pectin or uronic acids in the polysaccharide fraction. An increase in Xyl content was detected that may have been counter productive as UDP-Xyl has been shown to have an inhibitory effect on UDP-Glc dehydrogenase (Davies *et al.*, 1972; Turner *et al.*, 2002; Hinterberg *et al.*, 2002; Robertson *et al.*, 1996). However, the inhibitory effect would depend on whether UDP-Glc dehydrogenase and UDP-Xyl were located in the same cellular compartment in alfalfa. Evidence has suggested that UDP-Xyl is formed in the Golgi lumen from UDP-GlcA that has been formed outwith this compartment in soybean (*Glycine max*) (Hayashi *et al.*, 1988).

The transgenic alfalfa plants showed a decrease in overall cell-wall polysaccharide (g/kg cell wall) content. This indicates that modification of plant cell

wall properties is not a simple process and experiments such as these would benefit from a more solid knowledge base of the pathways involved in cell wall precursor formation.

Section 1.2.1 – section 1.2.4 outlines the information known about each of the competing NDP-sugar pathways and the potential cellulosic precursors.

1.2.1 Formation of UDP-GlcA

UDP-GlcA has an important role in the generation of several other NDP-sugar precursors for pectin and hemicellulose synthesis. UDP-GlcA may act as the direct precursor of UDP-GalA, UDP-Api and UDP-Xyl, which itself can be epimerised to UDP-Ara (Fig. 1.2). Impressively, these sugars when incorporated account for ~50% of the biomass of an *Arabidopsis thaliana* plant cell wall (Seitz *et al.*, 2000). At present there are two proposed biochemical pathways that result in UDP-GlcA formation (Fig. 1.2). UDP-GlcA may be formed via UDP-Glc through the action of UDP-Glc dehydrogenase (EC 1.1.1.22). An alternative pathway that could result in the formation of UDP-GlcA is via the *myo*-inositol pathway. The importance of each pathway in relation to plant cell wall precursor synthesis is debated (Kärkönen, 2005). It is not easy to distinguish which pathway the component monosaccharide residues in the plant cell wall specifically arose from. Unfortunately the use of specifically labelled [^{14}C]Glc is unable to provide results that would answer this question as the carbons retain their locant throughout each of the pathways.

The knowledge that has been gained about each pathway is discussed (section 1.2.1.1 – section 1.2.1.2).

1.2.1.1 Direct oxidation of UDP-Glc

1.2.1.1.1 Characterisation of UDP-Glc dehydrogenase

The knowledge that UDP-GlcA could be formed from UDP-Glc by the action of a NAD-linked dehydrogenase in animal liver (Strominger *et al.*, 1954) sparked interest in the potential existence of this enzyme in plants. The presence of UDP-Glc dehydrogenase in plants was demonstrated in 'English Wonder' pea seedlings (Strominger *et al.*, 1957). The enzyme, purified 1000-fold, had a pH optimum of 9.0, catalysed an irreversible reaction where 1.8–1.9 moles of an electron acceptor (NAD) were reduced per mole of UDP-Glc that was added and yielded UDP-GlcA. The K_m value for UDP-Glc was 0.07 mM.

It has now been shown that UDP-Glc dehydrogenase exists in a number of diverse plant species such as soybean, sugarcane, poplar, maize, tobacco and liverwort, and it has been well characterised.

The advent of molecular cloning has enabled many researchers to characterise and compare UDP-Glc dehydrogenases from different species. A gene for UDP-Glc dehydrogenase was isolated from soybean and was found to be highly similar to the gene sequence of bovine UDP-Glc dehydrogenase (Tenhaken *et al.*, 1996). The sequence predicted a protein of M_r 52900, with a characteristic catalytic centre and NAD-binding site shown to be conserved between prokaryotes and eukaryotes. When antibodies were raised against soybean UDP-Glc dehydrogenase, immunoprecipitation in a crude protein extract occurred and soybean UDP-Glc dehydrogenase activity was inhibited. The highest expression level and activity of soybean UDP-Glc dehydrogenase was found in the roots and expanding leaves. This

correlated well with the areas of the plant that required precursors for hemicellulose synthesis.

UDP-Glc dehydrogenase was purified from the nodules of soybean (Stewart *et al.*, 1998). In this case the enzyme was thought to be hexameric and have a subunit mass of Mr 47000. The enzyme was specific for NAD^+ and showed activity with UDP-Glc as opposed to: UDP-Gal, UDP-acetylgalactosamine, UDP-acetylglucosamine, GDP-Man, Glc, Glc 1-P and ethanol. The enzyme had a K_m value for UDP-Glc of 0.05 mM. Some activity was noted when UDP-Gal or TDP-Glc were utilised as a substrate. However, it is uncertain whether the UDP-Glc dehydrogenase that was purified was a soybean or *Rhizobium* enzyme.

More recent studies conducted on soybean have enabled the production of large amounts of recombinant UDP-Glc dehydrogenase in *Escherichia coli* (Hinterberg *et al.*, 2002). Gel-permeation chromatography results revealed that UDP-Glc dehydrogenase had a M_r of 55000. The results from gel-permeation assays suggested that the enzyme is active as a monomer. The enzyme was specific for UDP-Glc and the K_m value for UDP-Glc was lower than previous reports at 22 ± 2 μM.

Other authors also claim to have isolated UDP-Glc dehydrogenase from French bean (*Phaseolus vulgaris* L.) cell-suspension cultures (Robertson *et al.*, 1996). In contrast to the work already described, the purified homogeneous French bean UDP-Glc dehydrogenase had a smaller subunit of M_r 40000 and a much greater K_m value for UDP-Glc of 5.5 ± 1.4 mM. Antibodies raised against the enzyme protein showed immunolocalisation in xylem and phloem of French bean hypocotyls. This suggested a role in secondary wall cell formation. In addition to this, the

enzyme isolated from French bean co-purified with ethanol dehydrogenase activity. Although it is possible that the UDP-Glc dehydrogenase exists in a different form in different species, it seems unlikely as the bovine and soybean sequences are very similar and soybean and French bean are closely related. It has been disputed (Tenhaken *et al.*, 1996) whether Robertson *et al.* (1996) isolated UDP-Glc dehydrogenase activity and ethanol dehydrogenase activity or ethanol dehydrogenase activity alone. Other authors have suggested that proteolysis of the native French bean enzyme may have resulted in altered enzyme properties where ethanol dehydrogenase activity may have been gained (Turner *et al.*, 2002). However, the additional ethanol dehydrogenase activity pertaining to purified UDP-Glc dehydrogenase may not be unique to French bean. Indeed, evidence in a xylogenic cell-suspension of tobacco (*Nicotiana tabacum*) suggests that UDP-Glc dehydrogenase may have an isoform that can also function as an ethanol dehydrogenase (Bindschedler *et al.*, 2005). UDP-Glc dehydrogenase was purified 195-fold to apparent homogeneity and was found to have a M_r of 43000 comparable to the previously described French bean enzyme. When the purified UDP-Glc dehydrogenase was enzymically digested the peptide sequence was similar to the French bean enzyme (Robertson *et al.*, 1996). In addition to this the substrate UDP-Glc could be replaced with ethanol. When the bifunctional UDP-Glc dehydrogenase cDNA was transferred into *E. coli* a protein with dual activity was only detected in bacteria with the UDP-Glc dehydrogenase construct (Bindschedler *et al.*, 2005). The expression pattern of the dual-specific enzyme with ethanol dehydrogenase activity was found in plant sections that were establishing secondary growth. This was also the conclusion of the previously described work carried out with French bean.

The monospecific enzyme isoform isolated from tobacco plants was more highly expressed in young developing tissues in agreement with the inability to purifiy this isoform from tobacco xylogenic cell-suspension culture. This suggested that it is not greatly involved in secondary plant cell wall synthesis.

Examination of a poplar (*Populus tremula* × *tremuloides*) cDNA clone of UDP-Glc dehydrogenase revealed a protein with a calculated M_r of 53100 that has 90% and 63% amino acid identity to soybean and bovine liver UDP-Glc dehydrogenase, respectively. Immunoblot techniques revealed that the UDP-Glc dehydrogenase protein was predominant in differentiating xylem and young leaves.

The first monocot UDP-Glc dehydrogenase was purified from sugarcane (*Saccharum* spp.) hybrids (Turner *et al.*, 2002). The monocot UDP-Glc dehydrogenase was similar to the monospecific enzyme determined in dicot species as it had a M_r 52000 with a K_m value for UDP-Glc of 18.7 $\pm$ 0.75 μM. Kärkönen & Fry (2005a, in press) studied UDP-Glc dehydrogenase in maize cell-suspension culture and obtained an estimated K_m value for UDP-Glc ($\approx$ 28 μM) that was in the same order as the K_m value for UDP-Glc in sugarcane. However, when Kärkönen *et al.* (2005b, in press) estimated the K_m values for UDP-Glc of two different isoforms of UDP-Glc dehydrogenase coded by *UDPGDH-A* and *UDPGDH-B* in crude cell extracts of maize plants, the K_m values were ca. 380 μM and 950 μM, respectively. These values are much higher than the K_m value for UDP-Glc in sugarcane and maize cell-suspension culture. There is a possibility that there is an additional isoform of UDP-Glc dehydrogenase in maize plants that has a much lower K_m value for UDP-Glc.

1.2.1.1.2 Importance of UDP-Glc dehydrogenase in plant cell wall precursor formation

The concentration of UDP-Glc correlated positively with extractable UDP-Glc dehydrogenase activity in liverwort (*Riella helicophylla*) (Witt, 1992). This result led the author to suggest that UDP-Glc dehydrogenase synthesis is regulated by its substrate UDP-Glc. An increase of UDP-Glc occurred from the zone of meristematic cells to expanding cells, but mature cells were found to have the lowest concentration of UDP-Glc. The high activity of UDP-Glc dehydrogenase, and correlating level of UDP-Glc in expanding cells, hinted that this reaction was the main method of UDP-GlcA synthesis needed for the production of plant cell wall polysaccharide precursors. However, one might equally argue that the concentration of UDP-Glc should be low if the activity of UDP-Glc dehydrogenase, the enzyme that oxidises it, is high.

A positive correlation between the concentration of UDP-GlcA and activity of UDP-Glc dehydrogenase was determined in studies conducted on periwinkle (*Catharanthus roseus*) synchronous cultures (Amino *et al.*, 1985). Amino *et al.* (1985) reported a high production of UDP-GlcA and a high concentration of UDP-Glc dehydrogenase in the G_1 growth phase. Plant cell wall synthesis was found to be most active in the G_1 phase. This indicated that UDP-Glc dehydrogenase could potentially regulate plant cell wall polysaccharide synthesis through substrate concentration. High UDP-Glc dehydrogenase activity was also found to be associated with an increase in the relative growth rates of *Arabidopsis thaliana* plants grown in an atmosphere of elevated carbon dioxide (Gibeaut *et al.*, 2001). An increase in UDP-Glc dehydrogenase activity was also witnessed in suspension-

cultured cells and the hypocotyls of French bean during cell growth and differentiation (Robertson *et al.*, 1995). In comparison to this, UDP-Xyl epimerase and UDP-Glc epimerase activities in French bean were not found to be associated with cell growth and differentiation. This agrees with the involvement of differentiation in secondary cell wall (mainly hemicellulose and some pectin) synthesis, which requires UDP-Glc, UDP-GlcA and UDP-Xyl, but little UDP-Gal and UDP-Ara. As cell growth is accompanied by cell wall formation it is thought that the increase in UDP-Glc dehydrogenase activity enables the provision of sufficient pectin and hemicellulose precursors.

Qualitative assays conducted on *Arabidopsis thaliana* seedlings showed UDP-Glc dehydrogenase gene expression patterns were localised in the root tissue compared to other parts of the seedlings (Reiter *et al.*, 2001). Plant roots may be subjected to anoxic conditions. The conversion of *myo*-inositol to GlcA requires O_2. Anoxic conditions would inhibit this. Seitz *et al.*, (2000) suggest that the use of UDP-Glc dehydrogenase in place of the *myo*-inositol pathway would overcome this and prevent any detrimental effects that a decrease in NDP-sugars would incur. However, Seitz *et al.* (2000) do not explain what would happen to the increased NADH concentration under anoxia that would be produced by the UDP-Glc dehydrogenase pathway. Indeed, NADH would not be converted back to NAD^+ in the absence of O_2 as the conversion of pyruvate to ethanol would only function if NAD^+ is used to form the pyruvate.

Despite previous claims that UDP-Glc dehydrogenase activity could not be detected in maize (Roberts *et al.*, 1973), work has now shown that UDP-Glc dehydrogenase is involved in pentose biosynthesis in maize (Kärkönen *et al.*, 2005b;

in press). In this case a maize plant homozygous for a mutation in one of the UDP-Glc dehydrogenase genes (*UDPGDH-A1*) was studied. The *udpgdh-A1* homozygote had a 35 – 45% reduction of Ara:Gal and Xyl:Gal ratios in non-cellulosic polysaccharides in comparison to the wild-type controls. This indicates that UDP-Glc dehydrogenase contributes to a large proportion of cell wall pentose residues in maize. Unlike the suggestion made by the authors, these results do not necessarily suggest that UDP-Glc dehydrogenase has greater importance in pentose residue formation than the *myo*-inositol pathway. Indeed, the Ara:Gal and Xyl:Gal ratios in the *udpgdh-A1* homozygote were not reduced by more than 45% so the majority of pentoses, at least in the mutant, must be formed by an alternative method. This could be via a different UDP-Glc dehydrogenase isoform or by the *myo*-inositol pathway (section 1.2.1.2).

1.2.1.2 The myo-inositol pathway

Inositols are isomers of hexahydroxycylohexane. There are, in total, nine stereoisomers of inositol. *epi*- and *allo*-inositol are the only stereoisomers that do not occur naturally.

The presence of *myo*-inositol in biological tissue has been noted since as early as 1850 in muscle extract. *myo*-Inositol is now classed as a compound that is ubiquitous in plants and is thought to have many diverse functions (Fig. 1.5). The formation of *myo*-inositol is only known to occur via the *myo*-inositol pathway in cyanobacteria, alagae, fungi, animals and plants (Loewus *et al.*, 2000). The *myo*-inositol pathway is outlined in Fig. 1.2. The first committed step in the *myo*-inositol pathway occurs when Glc 6-P is irreversibly isomerised to *myo*-inositol 1-phosphate

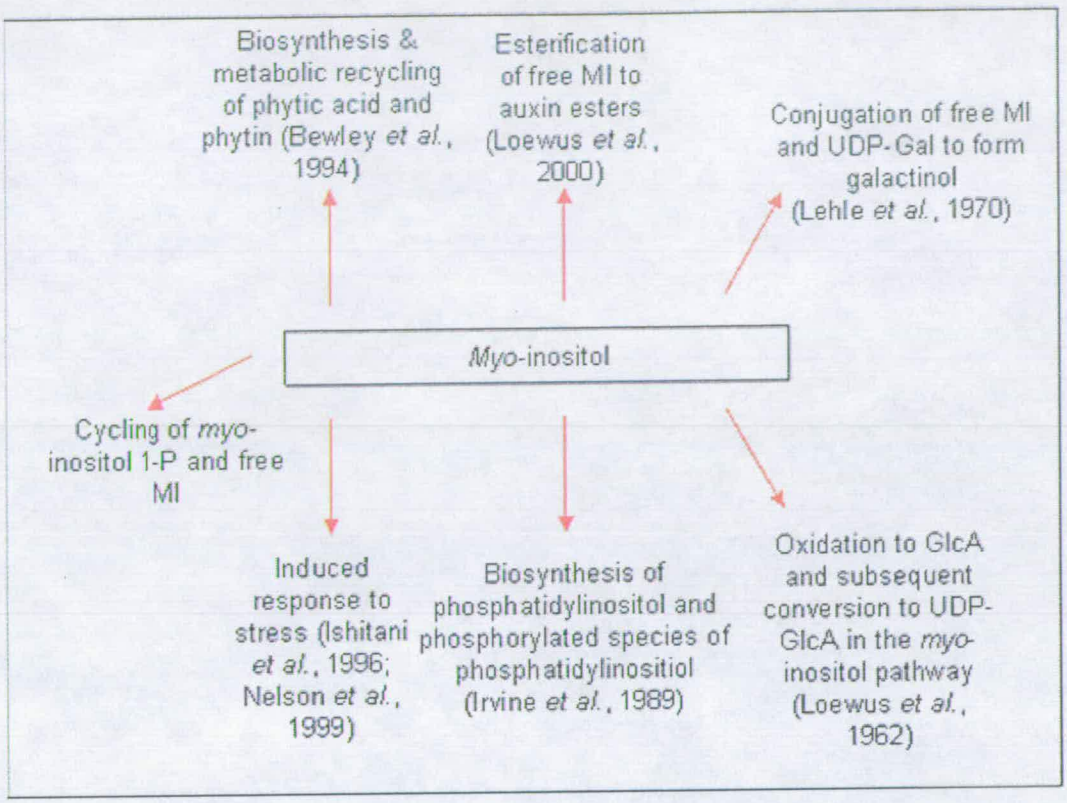

Figure 1.5 Functional roles of *myo*-inositol in plants

through the action of *myo*-inositol 1-phosphate synthase. Subsequent reactions yield UDP-GlcA.

The *myo*-inositol pathway was first proposed by Loewus *et al.* (1962). At that time it had been established that yeast and rat kidney metabolised *myo*-inositol to GlcA through the action of an oxidase. The products of GlcA metabolism in plants were also known. It was speculated that if *myo*-inositol was the precursor to GlcA in plants, labelled *myo*-inositol exogenously applied to plant tissue would yield labelled products characteristic of plant GlcA metabolism. Indeed, the application of *myo*-[2-^{3}H]inositol and *myo*-[2-^{14}C]inositol to the cut petioles of parsley leaves and to strawberry 'fruits' gave rise to labelled GalA, Xyl and Ara residues of pectin and hemicellulose.

Since the first proposition of the *myo*-inositol pathway (Loewus *et al.*, 1962) there has been similar experimental evidence that demonstrates the existence of a *myo*-inositol pathway that may contribute to plant cell wall polysaccharide precursors in a variety of plant species such as: oat seedlings (Albersheim, 1962), lily pollen (Chen *et al.*, 1977), maize roots (Roberts *et al.*, 1968) and cultured sycamore cells (Roberts *et al.*, 1966).

When excised maize roots were incubated with 0.1 M *myo*-inositol for 6 h, the intracellular *myo*-inositol concentration increased 100-fold (Roberts *et al.*, 1973). Maize roots incubated with 0.1 M *myo*-inositol were found to have a reduced ability to convert [6-^{14}C]Glc to ^{14}C-labelled GalA polysaccharide residues. This was also shown to occur when *Lilium longiflorum* pollen was germinated in the presence of [1-^{14}C]Glc in 5.6 mM or 28 mM inositol-enriched medium (Maiti *et al.*, 1978). The increase in intracellular *myo*-inositol concentration was thought to dilute any ^{14}C-labelled compounds formed via the *myo*-inositol pathway and cause a reduction in ^{14}C incorporation into GalA residues. However, an alternative explanation may be that the cells were originally synthesising UDP-GlcA by UDP-Glc dehydrogenase and that the addition of excess *myo*-inositol provided an alternative substrate. The results obtained by Roberts *et al.* (1973) and Maiti *et al.* (1978) are clear evidence that cells are able to convert *myo*-inositol to UDP-GlcA when exogenous inositol is provided. The results prove the existence of a pathway that has the potential to contribute to plant cell wall synthesis. However, the experiments do not distinguish whether the pathway simply acts as a 'scavenger' under abnormal conditions of excess inositol.

The addition of dGlc to cultured soybean cells reduces the intracellular concentration of *myo*-inositol (Biffen *et al.*, 1990). Biffen *et al.* (1991) manipulated the intracellular concentration of inositol by the addition of dGlc or exogenous inositol to soybean cells. After 5 d of treatment the soybean cells were incubated with *myo*-[^{3}H]inositol. Biffen *et al.* (1991) showed that a high intracellular *myo*-inositol concentration resulted in a proportionately higher incorporation of ^{3}H into the pectin fraction. It was also shown that the amount of ^{3}H incorporated into the pectin fraction decreased with reduced intracellular concentrations of *myo*-inositol. Despite this the final amount of uronic acid residues from pectin remained the same. The authors concluded that the intracellular concentrations of *myo*-inositol in soybean callus cells were not necessary to sustain *myo*-inositol conversion into pectin residues, but a method to eliminate excess *myo*-inositol. However, the alteration of intracellular *myo*-inositol concentrations may be counteracted by the enhancement/repression of the pathway that involves UDP-Glc dehydrogenase. Indeed, if the *myo*-inositol pathway were the predominant pathway of UDP-GlcA formation the reduced intracellular level of *myo*-inositol may enhance the UDP-Glc dehydrogenase pathway to give rise to 'normal' final amounts of uronic acid residues in pectin.

In initial demonstrations of the *myo*-inositol pathway, radiolabelled *myo*-inositol was supplied to excised plant tissue (Loewus *et al.*, 1962; Roberts *et al.*, 1973). Penetrating plant tissues in order to deliver radiolabelled *myo*-inositol to plant cells perturbs cellular conditions and may cause a cellular response such as a wound response. Sasaki *et al.* (1984) overcame this by imbibing French bean seeds in a solution containing *myo*-[2-^{3}H]inositol. When the plant cell wall fraction of the

hypocotyl and root was analysed it was shown that the ^{3}H had been incorporated into uronic acid, Ara and Xyl residues of polysaccharides, demonstrating the *myo*-inositol pathway. The extent of the contribution of the *myo*-inositol pathway to the plant cell wall polysaccharide fraction was not determined.

Studies on lily pollen showed that an inositol oxygenase inhibitor, 2-*O*,C-methylene *myo*-inositol (Fig. 1.6), inhibited the incorporation of ^{3}H from *myo*-[^{3}H]inositol into GalA and pentose units. In addition to this, germination and elongation of the pollen tubes was inhibited but, with the addition of *myo*-inositol, the pollen could be briefly rescued (Chen *et al.*, 1977). This suggested that *myo*-inositol was an important precursor in cell wall biosynthesis as prevention of *myo*-inositol synthesis results in a blockage of cell wall elongation and that the pollen could not be rescued by the UDP-Glc dehydrogenase pathway. However, effects caused by 2-*O*,C-methylene *myo*-inositol may not be specifically related to the inhibition of inositol oxidation (Biffen *et al.*, 1991).

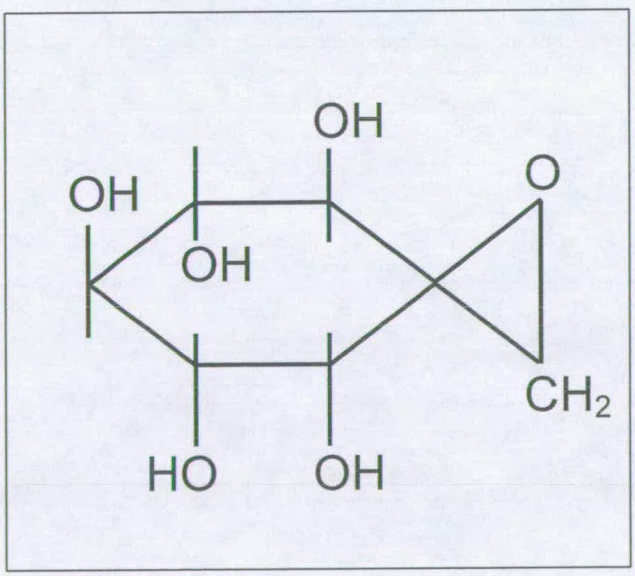

Figure 1.6 Structure of 2-O,C-methylene *myo*-inositol

Asamizu *et al.* (1979) fed suspension cultured carrot cells (*Daucus carota*) [U-^{14}C]Glc. In the presence of 0.6 mM *myo*-inositol, the carrot cells incorporated ^{14}C into neutral hexose residues but with very limited ability into GlcA or GalA. The specific activity of the uronic acid residues (2590 kBq/mol) was 42 times lower than the originally supplied [^{14}C]Glc. When the carrot cells were incubated with *myo*-[^{3}H]inositol, the uronic acid residues were radiolabelled but not the neutral residues were not. In this case the specific activity of the acidic sugars was only 18 times lower than that of *myo*-[^{3}H]inositol. This was an indication that the *myo*-inositol pathway was of greater importance in the formation of UDP-GlcA than the oxidation of UDP-Glc. However, this does not confirm that cells do utilise endogenous *myo*-inositol but only that they can utilise exogenous *myo*-inositol.

When *Fraxinus pennsylvanica* cultures were provided with exogenous *myo*-[U-^{14}C]inositol for 10 weeks, the specific activity of GalA residues in the cell wall was less than 1% of the specific activity in the original *myo*-[U-^{14}C]inositol (Jung *et al.*, 1972). This suggested a greater role of UDP-Glc dehydrogenase in the formation of UDP-GlcA.

Squash (*Cucurbita maxima*) hypocotyl segments were bathed in medium that contained either [1-^{14}C]Glc or *myo*-[2-^{3}H]inositol (Wakabayashi *et al.*, 1989). After incubation the segments were washed and the cell walls were fractionated. As the percentage of ^{14}C incorporation into the cell wall residues was much higher than that of ^{3}H, the authors proposed that the *myo*-inositol pathway contribution to cell wall residues is minimal. Indeed, as *myo*-[^{3}H]inositol can only proceed via the *myo*-inositol pathway to form plant cell wall residues, the fact that so little of the total incorporated ^{3}H was located in plant cell wall polysaccharides may

suggest it has a minor role in the contribution to plant cell wall residues. However, an important additional experimental control would be to determine how well *myo*-[^{3}H]inositol gets through the plasma membrane.

Verma *et al.* (1979), like Asamizu *et al.* (1979), also attempted to assay the relative contributions made by UDP-Glc dehydrogenase and the *myo*-inositol pathway to plant cell wall precursors in carrot cell-suspension cultures. The researchers fed carrot cell-suspension cultures *myo*-[^{3}H]inositol and [^{14}C]Glc. The study relied on the uptake of *myo*-[^{3}H]inositol and the entry of this radiolabelled compound into the *myo*-inositol pathway alone. The addition of [^{14}C]Glc introduced a different radiolabel that could be detected separately from ^{3}H and could, potentially, feed into either the *myo*-inositol pathway or the UDP-Glc dehydrogenase pathway. Analysis of the ^{3}H:^{14}C ratios of compounds known to stem from UDP-GlcA would be indicative of the pathway they arose from. Indeed, the ^{3}H could only have arisen from the *myo*-inositol pathway. The ^{3}H:^{14}C ratios of cellular *myo*-inositol and cell-wall Ara, Xyl and GalA residues were investigated. The cellular *myo*-inositol ^{3}H:^{14}C ratio was > 10-fold higher than that of cell-wall residues. Verma *et al.* (1979) concluded that the contribution of the *myo*-inositol pathway to pentose and uronic acid residues in the cell wall was minor and that the UDP-Glc dehydrogenase pathway predominates in the formation of UDP-GlcA utilised for cell wall synthesis. Verma *et al.* (1979) clearly showed that ^{3}H from *myo*-[^{3}H]inositol could be detected in Ara, Xyl and GalA cell-wall residues. This indicates that the *myo*-inositol pathway is in operation. However, the authors are unable to distinguish if more than one pool of *myo*-inositol exists. If one of these pools was supplied from Glc and directed towards plant cell wall synthesis the ^{3}H:^{14}C ratios of Ara, Xyl and GalA

residues, in the Verma *et al.* (1979) protocol, would be expected to be lower than the cellular *myo*-[^{3}H]inositol.

Although UDP-Glc dehydrogenase has been purified from lily pollen (Davies *et al.*, 1972) a *myo*-inositol pathway has also been shown to exist in lily pollen. A hydrogen isotope-effect may occur when there is a slightly lower chance that an enzyme will catalyse a reaction with a compound that is tritiated at a specific locant. This is known to occur when [5-^{3}H]Glc 6-P is converted to *myo*-[2-^{3}H]inositol 1-P by the action of *myo*-inositol 1-phosphate synthase (Loewus, 1977). If germinating lily pollen, fed [5-^{3}H, 1-^{14}C]Glc, formed polysaccharide precursors via the *myo*-inositol pathway, the hydrogen isotope-effect would result in a lower amount of ^{3}H incorporation into the precursors than [1-^{3}H, 1-^{14}C]Glc. When investigated, the GalA and Glc ^{3}H:^{14}C ratios from the polysaccharide fraction were compared to control samples where the germinating pollen, fed [1-^{3}H, 1-^{14}C]Glc, was not expected to undergo the hydrogen isotope-effect (Loewus *et al.*, 1980). The ^{3}H:^{14}C ratios of GalA residues, in comparison to Glc residues, were lower in pollen fed [5-^{3}H, 1-^{14}C]Glc than in polled fed [1-^{3}H, 1-^{14}C]Glc. Although this demonstrated the presence of a functioning *myo*-inositol pathway without the reliance of exogenous inositol, the study was unable to report the quantitative importance of this pathway in the contribution to plant cell wall polymers.

Kanter *et al.* (2005) created mutants in the *myo*-inositol pathway to determine its importance and claimed that the inositol oxygenase gene family of *Arabidopsis* is involved in the formation of plant cell wall residue precursors. Four putative *myo*-inositol oxygenase-like proteins were identified in *Arabidopsis* that were highly similar to the yeast (*Cryptococcus lactativorus*) *myo*-inositol oxygenase amino acid

sequence. T-DNA insertion lines in each of the three isoforms were isolated. It was shown that wild-type *Arabidopsis* can incorporate ^{3}H from exogenous [^{3}H]inositol into plant cell wall polymers. Two of the *myo*-inositol oxygenase mutants (ΔMIOX1, ΔMIOX2), in comparison to the wild-type plants, had a much reduced incorporation level of ^{3}H from [^{3}H]inositol into plant cell wall residues. The authors stated that this was 'strong evidence' that the gene that had been mutated in each case was involved in a functional *myo*-inositol oxygenase pathway that contributed to plant cell wall residue formation. However, the homozygous knockouts each mutated in one of the *myo*-inositol oxygenase isoforms each had a wild-type phenotype and wild-type cell wall composition. If *myo*-inositol oxygenase were as important as the authors state, one might expect the mutants to exhibit a reduction in cell wall residues formed by the *myo*-inositol pathway. The data show that the isoforms that were mutated were not needed to form phenotypically wild-type plants with wild-type cell wall composition. Indeed, one might even suggest that the *myo*-inositol pathway only occurs when the cells are presented with [^{3}H]inositol as the *myo*-inositol pathway was not required to contribute to the formation of cell wall residues in the mutants formed by Kanter *et al.* (2005). The data presented by Kanter *et al.* (2005) suggest that the pentoses and uronic acids involved in plant cell wall residue synthesis in the mutant plants are either formed by other *myo*-inositol oxygenase isoforms and/or the UDP-Glc dehydrogenase pathway.

Seeds are known to have a store of *myo*-inositol hexaphosphate (phytate). When phytate is present as an insoluble salt bound to metal ions it is known as phytin. The action of phytase on phytin produces phosphate, associated cations and *myo*-inositol. *myo*-Inositol produced in this manner is thought to be

utilised by the developing seedling to form precursors of hemicellulose and pectin (Bewley *et al.*, 1994). Phytate is of interest to researchers involved in the improvement of commercial animal feed because the phosphate contained within phytate is largely inaccessible to monogastric animals. As phytate is considered to be antinutritional, seed phytate levels are a target for manipulation. Hitz *et al.* (2002) attempted to reduce phytate levels that represent 50–70% of the total seed phosphate in wild-type soybean seeds. A single base change in the *myo*-inositol 1-P synthase gene caused a 90% decrease in the specific activity of the enzyme in the soybean seeds. An approximate two-fold reduction in phytate and 15–35-fold increase in inorganic phosphate did not affect seed viability. Although the results suggest that the *myo*-inositol pathway is crucial in phytate formation, a 50% reduction in the normal level of phytate is not lethal. This was also concluded by Wilcox *et al.* (2000) who isolated *low phytic acid* soybean seed mutants that also had a 50% decrease in phytate levels and an approximate 50% increase in inorganic phosphate. Other authors have also concluded that phytate is not crucial for seed function in maize (Raboy et al., 2000). As lethality is not conferred on the mutant seeds reduced in phytate content, the importance of phytate utilised via the *myo*-inositol pathway for growth and development that is, undoubtedly, accompanied by plant cell wall synthesis, is questionable.

1.2.2 Formation of UDP-GalA

Solms *et al.* (1957) and Neufeld *et al.* (1961) utilised 10.5 kg and 5 kg, respectively, of etiolated mung beans (*Phaseolus aureus*) to demonstrate the existence of UDP-GalA in a higher plant. UDP-GalA is a vital precursor of the backbone of rhamnogalacturonan I, rhamnogalacturonan II and homogalacturonan. UDP-GalA

may be reversibly formed from UDP-GlcA by the enzyme UDP-GlcA 4-epimerase (Fig 1.3). As previously detailed the formation of UDP-GlcA may occur via UDP-Glc dehydrogenase action on UDP-Glc or through the *myo*-inositol pathway. Therefore, in relation to the formation of UDP-GalA by UDP-GlcA 4-epimerase, the competing pathways of UDP-GlcA synthesis (section 1.2.1) also hold true for the synthesis of UDP-GalA.

A less well established reaction that could theoretically result in the formation of UDP-GalA would involve the action of a UDP-Gal dehydrogenase on UDP-Gal (Fig 1.3).

1.2.2.1 Epimerisation of UDP-GlcA to UDP-GalA

Early experimentation demonstrated that ^{14}C from exogenous GalA and GlcA are incorporated into pectin and hemicellulose by mung bean seedlings (Kessler *et al.*, 1961) and that UDP-GlcA 4-epimerase, the enzyme able to form UDP-GalA from UDP-GlcA, was present in mung bean seedlings (Feingold *et al.*, 1960). Feingold *et al.* (1960) subjected different ratios of radiolabelled UDP-GlcA and radiolabelled UDP-GalA to enzyme particulate and soluble fractions prepared from mung beans. The UDP-GlcA to UDP-GalA ratio obtained was the same regardless of the starting ratio, suggesting that equilibrium had been attained. When radiolabelled UDP-GlcA and UDP-GalA were individually incubated with the particulate and soluble enzyme fractions, both UDP-GalA and UDP-GlcA were detected. This demonstrated the ability of each fraction to form UDP-GlcA from UDP-GalA and vise versa, presumably by UDP-GlcA 4-epimerase. Enzymic synthesis of UDP-[^{14}C]GalA from commercially obtained UDP-[^{14}C]GlcA, for experimental purposes, was detailed by Liljebjelke *et al.* (1995). The technique utilised a particulate preparation

of radish (*Raphanus sativus*) roots as a source of UDP-GalA 4-epimerase. This illustrates the ease of extraction of UDP-GalA 4-epimerase in comparison to UDP-Gal dehydrogenase (section 1.2.2.2) that could be involved in the formation of UDP-GalA.

The conversion of UDP-GlcA to UDP-GalA is freely reversible and thought to proceed through UDP-4-keto-GalA (Stroud *et al.*, 1964). However, the keto compound is not released from the enzyme and the same hydrogen that was removed from C4 is reattached. If this did not take place it would be possible to demonstrate UDP-GlcA 4-epimerase activity by the loss of ^{3}H from UDP-[4-^{3}H]GlcA.

The *cap1J* gene from *Streptococcus pneumoniae* was cloned and found to encode a UDP-GlcA 4-epimerase (Muñoz *et al.*, 1999). The *Arabidopsis* genome contains six predicted coding regions (*GAE1–GAE6*) with a high degree of sequence similarity to the *S. pneumoniae* UDP-GlcA 4-epimerase gene (Reiter *et al*, 2001). Various isoforms of UDP-GlcA 4-epimerase from *Arabidopsis* have now been characterised (Usadel *et al.*, 2004; Mølhøj *et al.*, 2004; Gu *et al.*, 2004). Recombinant *GAE6* (Usadel *et al.*, 2004) and *GAE1* (Mølhøj *et al.*, 2004) were each heterologously expressed in *Pichia pastoris*. Extracts from transformed *P. pastoris*, as well as controls that were transformed with an empty vector, were incubated with UDP-[^{14}C]GlcA. Only the extract of *P. pastoris* that contained either GAE6 or GAE1 and had not been boiled produced UDP-[^{14}C]GalA. This demonstrated that *GAE1* and *GAE6* cloned from the genomic DNA encoded UDP-GlcA 4-epimerases.

A UDP-GlcA 4-epimerase gene (*GAE1*) with high sequence similarity to, but distinct from, those described by Usadel *et al.* (2004) and Mølhøj *et al.* (2004) was cloned and characterised by Gu *et al.* (2004). The recombinant *GAE1* was only

successfully expressed and produced a viable enzyme in *E. coli* when it lacked the putative transmembrane domain. The protein was presented with UDP-GlcA. The reaction product was analysed by HPLC and subsequent ^{1}H-NMR and confirmed to be UDP-GalA. When the reverse reaction was tested UDP-GlcA was detected. Gu *et al.* (2004) determined that the equilibrium constant for the *Arabidopsis* UDP-GlcA 4-epimerase (1.9) favoured the formation of UDP-GalA. This agreed with the equilibrium constant obtained for the partially purified UDP-GalA 4-epimerase from the blue-green alga (*Anabaena flos-aquae*) (2.6) (Gaunt *et al.*, 1973). The molecular subunit mass of the GAE1 protein (M_r 43500) was smaller than the blue-green alga UDP-GlcA 4-epimerase (M_r 54000) (Gaunt *et al.*, 1973). The activity profile of the GAE1 on gel permeation chromatography gave a peak of activity that corresponded to M_r 88000 and, as with the prokaryote *S. pneumoniae* UDP-GalA 4-epimerase *cap1J*, indicated that the enzyme was active as a dimer.

In contrast to the bacterial UDP-GalA 4-epimerase, the isoforms of UDP-GalA 4-epimerase in *Arabidopsis* are predicted to be type II membrane proteins. Indeed, it was reported that in *Arabidopsis* UDP-GlcA 4-epimerase activity was located in the microsome fraction alone (Mølhøj *et al.*, 2004). This agrees with data provided for membrane preparations of other plant species (Feingold *et al.*, 1960; Liljebjelke *et al.*, 1995). Mung beans were found to have both soluble and membrane-located UDP-GlcA 4-epimerase activities (Feingold *et al.*, 1960). This may be a result of differential target sites of the isoform(s) or a result of the method of preparation that may have released the enzyme, with undamaged activity, from the membrane.

Not all researchers have detected UDP-GlcA 4-epimerase activity in the membrane. Edison *et al.* (1996) studied UDP-GalA metabolism by UDP-GlcA 4-epimerase in an attempt to maximise cell-free polygalaturonate 4-α-galacturonosyltransferase activity. The authors could not detect any UDP-GlcA 4-epimerase activity in either membrane or detergent-solubilised preparations of tobacco. This indicated that tobacco membranes may not have UDP-GlcA 4-epimerase activity or that the reaction conditions optimised for the assay of polygalacturonate 4-α-galacturonosyltransferase denatured the UDP-GlcA 4-epimerase.

1.2.2.2 Dehydrogenase action on UDP-Gal

UDP-Gal can be oxidised to UDP-GalA *in vitro* in the presence of both Pt and O_2 (Stroud *et al.*, 1964). Although the occurrence of UDP-Gal dehydrogenase is not widely documented in plants this does not rule out the possibility that this reation takes place. Carpita and McCann (2000) mention the enzyme 'UDP-Gal dehydrogenase' in the formation of UDP-GalA and curiously do not mention the alternative pathway that proceeds via UDP-GlcA acid 4-epimerase. Carpita and McCann (2000) also fail to cite a reference for the illustrated reaction proposed to involve UDP-Gal dehydrogenase. UDP-Gal dehydrogenase activity has been detected in *Corynebacterium glutamicum* CCTCC M201005, which produces a novel polygalacturonic bioflocculant known as REA-11 (Li *et al.*, 2003). The main structural unit of REA-11 is GalA residues, which are formed from UDP-Gal via UDP-Gal dehydrogenase.

It is of interest to note that UDP-Glc dehydrogenase purified from soybean nodules was capable of utilising UDP-Gal as a substrate (Stewart *et al.*, 1998). UDP-

Gal in this case is a less effective substrate than UDP-Glc. It is not clear, however, whether the enzyme was a *Rhizobium* enzyme.

UDP-Glc dehydrogenase purified from germinating lily pollen was also able to utilise UDP-Gal as a substrate but, again, less efficiently than UDP-Glc (Davies *et al.*, 1972). In this case the originally fed UDP-Gal was noted to be free from UDP-Glc. The purified UDP-Glc dehydrogenase enzyme preparation was free from UDP-Glc 4-epimerase. This is important as it could result in the conversion of UDP-Gal to UDP-Glc and subsequently yield UDP-GalA via UDP-Glc dehydrogenase and UDP-GlcA 4-epimerase. However, direct evidence for UDP-GalA production was not obtained.

It is not always the case that UDP-Glc dehydrogenase is able to utilise UDP-Gal as a substrate. Indeed, previous experiments have shown that UDP-Glc dehydrogenase, purified from pea seedlings, was unable to utilise UDP-Gal as a substrate in the presence of NAD^+ (Strominger *et al.*, 1957).

1.2.3 Formation of GDP-Man

The first demonstration of GDP-Man isolation was conducted by Cabib *et al.* (1954) who utilised bakers' yeast.

GDP-Man is a precursor of mannose-containing plant cell wall polysaccharides such as mannans, glucomannans, galactomannans and glucuronomannans. GDP-Man may also provide the Man residues that are incorporated into glycoproteins. In addition to this, GDP-Man is utilised to form other NDP-sugar precursors such as GDP-L-Fuc and GDP-L-Gal and proposed to have a role in ascorbate synthesis.

Evidence suggests that GDP-Man may be formed through the action of GDP-Man pyrophosphorylase (E.C. 2.7.7.22) on the substrate Man 1-phospate (Fig. 1.4). There is also evidence that GDP-Man is reversibly formed when GDP-Man 2-epimerase acts upon GDP-Glc (Fig. 1.4).

1.2.3.1 Epimerisation of GDP-Man

Experiments carried out by Elbein *et al.* (1966) showed that particulate fractions of mung bean seedlings incorporated ^{14}C from GDP-[^{14}C]Glc into a water- and alkali-insoluble plant cell wall polymer. The addition of GDP-Man to the incubation mixture increased the incorporation of ^{14}C into the polymer. The enhanced utilisation of an NDP-sugar by the presence of another has also been shown to occur in the synthesis of the lipopolysaccharide component of bacterial cell walls (Edstrom *et al.*, 1967). Addition of GDP-[^{14}C]Man to the particulate fraction gave rise to ^{14}C-labelled Glc water- and alkali-insoluble polymer residues. This presented evidence that GDP-Man was epimerised to GDP-Glc via GDP-Man 2-epimerase. However, in this case the addition of GDP-Glc to the incubation mixture inhibited the incorporation of ^{14}C into the polymer from GDP-[^{14}C]Man. When the polymer was partially hydrolysed the products were distinguishable from cellulose (Elbein, 1969). Analysis revealed that the polymer was a glucomannan. It was found that GDP-[^{14}C]Man and GDP-[^{14}C]Glc could not be replaced by different potential mannosyl (TDP-[^{14}C]Man, [^{14}C]Man 6-phosphate, [^{14}C]Man 1-phosphate and [^{14}C]Man) and glucosyl (UDP-[^{14}C]Glc, TDP-[^{14}C]Glc, CDP-[^{14}C]Glc and ADP-[^{14}C]Glc) donors for glucomannan synthesis.

Published articles on GDP-Man 2-epimerase have been sparse. It was noted by Loewus *et al.* (1980) that between 1969 and 1980 no information was published

on GDP-Man 2-epimerase. Dalessandro *et al.* (1986) have since published information suggesting that GDP-Man 2-epimerase operates in the formation of the glucomannan precursors GDP-Man and GDP-Glc in *Pinus sylvestris*. Membrane systems from *P. sylvestris* were capable of incorporating ^{14}C from GDP-[U-^{14}C]Man into Glc residues of glucomannan. Paper electrophoresis and paper chromatography were used to demonstrate that approximately 10–15% of the GDP-Man was epimerised to GDP-glucose for 10 nmol of substrate. The synthesis of the glucomannan from GDP-Man was, as indicated by Elbein (1966), also found to be inhibited by GDP-Glc.

1.2.3.2 Pyrophosphorylase action on Man 1-phosphate

The formation of GDP-Man may occur by the action of GDP-Man pyrophosphorylase on the substrate Man 1-phosphate. Deletion of the GDP-Man pyrophosphorylase gene has been shown to be lethal in both *Candida* and *Saccharomyces cerevisiae* (Warit *et al.*, 2000). Davis *et al.* (2004) investigated the properties of GDP-Man pyrophosphorylase in *Leishmania* parasites and determined that deletion of this gene did not compromise viability but led to a loss of virulence. In the *Yersinia enterocolitica* pathogen, the GDP-Man pyrophosphorylase gene is involved in a cluster that forms lipopolysaccharide O-antigen, which is known to be a major virulence factor (Zhang *et al.*, 1997). In both *Leishmania* and *Y. enterocolitica* GDP-Man biosynthesis is an excellent target for treatment of infected humans.

Reports of GDP-Man pyrophosphorylase from pig liver indicate the presence an α and β subunit with M_r of 43000 and 37000, respectively (Szumilo *et al.*, 1993; Ning *et al.*, 2000). It appears that GDP-Man pyrophosphorylase is conserved among species. Sequence alignments of the GDP-Man pyrophosphorylase gene indicate that

the pig GDP-Man pyrophosphorylase shares 98% similarity to human GDP-Man pyrophosphorylase. The amino-acid sequence similarity between a plant (*Solanum tuberosum*) GDP-Man pyrophosphorylase and pig liver GDP-Man pyrophosphorylase is 76% (Szumilo *et al.*, 2000). In addition, the gene for the GDP-Man pyrophosphorylase has been identified in *Sulfolobus solfataricus*, a hyperthermophilic member of the Archea, and has a high similarity (32%) to the predicted Man pyrophosphorylase genes in *Sacharomyces cerevisiae* and *Arabidopsis* (Sacchetti *et al.*, 2004).

The first report of GDP-Man pyrophosphorylase in plants was by DeAsura *et al.* (1966) who demonstrated the activity of this enzyme in *Gleditschia macracantha* seeds. Recent investigations into GDP-Man pyrophosphorylase in plants have stemmed from the proposal that GDP-Man is the first compound in the ascorbic acid biosynthesis pathway (Wheeler *et al.*, 1998). As GDP-Man is thought to be involved in the biosynthesis of ascorbate, GDP-L-Fuc, glycoproteins and plant cell wall polysaccharides, any disruption in GDP-Man pyrophosphorylase activity in a plant are suggested to have potential pleiotropic effects (Wolucka *et al.*, 2001). Keller *et al.* (1999) altered GDP-Man pyrophosphorylase activity in tomato (*Solanum tuberosum*) plants. Initially a full-length cDNA encoding GDP-Man pyrophosphorylase was isolated. Transgenic tomato plants were created by introducing the cDNA of GDP-Man pyrophosphorylase in an antisense orientation to the promoter. Transformants, selected on the basis of reduced GDP-Man pyrophosphorylase activity, had 41–72% of the GDP-Man pyrophosphorylase activity of wild-type plants. Cell-suspension cultures of the transformants could not be distinguished from those of wild-type by phenotype. Transformant plants grown

on soil showed dark spots on the stems and leaves 10 weeks after they had been transferred onto soil. After three months the aerial parts of the soil grown transformant plants were dead. The parts of the transformant plants that died corresponded to the areas of the plant that had the strongest reduction in GDP-Man pyrophosphorylase. This was attributed to the reduced ascorbate levels caused by a decrease in GDP-Man formation. It was determined that the Man content of the transformant plant cell walls was significantly reduced to 30–50% of the levels found in the leaves of wild-type plants. The reduction in Man content suggests that mannosyltransferase action is limited by the concentration of GDP-Man that had been formed by GDP-Man pyrophosphorylase. The correlation between the reduction in GDP-Man pyrophosphorylase acitivty and the reduction in plant cell wall mannose content suggests that GDP-Man pyrophosphorylase is important in GDP-Man formation in tomato.

Conklin *et al.* (1999) identified *Arabidopsis* GDP-Man pyrophosphorylase mutants (*vtc1-1*) by selecting ascorbate deficient plants. Leaves from wild-type and mutant plants were removed and fed [U-^{14}C]Man: 6.6% and ≈2.6% of the total radioactivity was present as ascorbate in the wild-type and *vtc1-1* mutant, respectively. The blockage in the converstion of Man to ascorbate indicated that one of the genes involved in the conversion of Man to ascorbate was mutated. When crude GDP-Man pyrophosphorylase extract was assayed for the ability to catalyse the formation of [^{14}C]Man 1-P from GDP-[U-^{14}C]Man and PP_i, it was found that extracts from *vtc1-1* yielded ≈35% less [^{14}C]Man 1-P than wild-type extracts. This suggested that *vtc1-1* mutant was mutated in the enzyme GDP-Man pyrophosphorylase. In addition, a transgene that encoded wild-type GDP-Man pyrophosphorylase was

formed and, with the use of *Agrobacterium tumefaciens*, transferred into the *vtc1-1* mutant. The isolation of transgenic *vtc1-1* plants that contained wild-type ascorbate concentrations suggested that a mutation in the GDP-Man pyrophosphorylase gene had been responsible for the phenotype of the *vtc1-1* mutant plants and that complementation had occurred. Although this is evidence that a functional GDP-Man pyrophosphorylase operates in *Arabidopsis* plants, the contribution of GDP-Man to plant cell wall formation via this pathway was not investigated.

1.2.4 Predominating precursor of cellulose — GDP-Glc or UDP-Glc?

Cellulose is the most abundant organic compound on earth. It is estimated that 180 billion tons are produced annually in nature (Perrin, 2001). Despite this the cellulose biosynthesis pathway in higher plants is proving difficult to elucidate. To date there are still questions regarding the mechanism of cellulose synthesis. It is unclear whether plants utilise UDP-Glc and/or GDP-Glc as the substrate for cellulose (Brett, 1981). There is, however, a general assumption that UDP-Glc is the main substrate for cellulose synthesis.

Initial experimentation involved particulate preparations from plant material. Addition of UDP-[^{14}C]Glc to particulate fractions from *P. aureus* and *Lupinus albus* resulted in the formation of β-(1→3)-glucan (Flowers *et al.*, 1968). This was most likely callose. Callose formation may have been promoted by the disruption caused to the cells when the enzyme particulate fraction was formed as the cellulose synthase rosette is very fragile. The failure of UDP-[^{14}C]Glc to yield ^{14}C-labelled β-(1→4)-Glc residues was an indication that GDP-Glc may be the substrate for cellulose synthesis. GDP-[^{14}C]Glc was capable of forming a ^{14}C-labelled β-(1→4)-glucan assumed to be cellulose (Flowers *et al.*, 1969). However, it was also noted

that [^{14}C]Man residues were formed. Indeed, it is likely that the product formed that was termed cellulose was actually a glucomannan and that GDP-[^{14}C]Glc was epimerised to GDP-[^{14}C]Man by the action of GDP-Man 2-epimerase. Furthermore, some early batches of commercial GDP-[^{14}C]Glc were in fact GDP-[^{14}C]Man (G. A. MacLachlan, personal communication).

Brett (1981) fed radiolabelled GDP-Glc to living pea stem slices. When 1 μM GDP-[^{14}C]Glc was fed to the stem slices analysis of the cell wall polymers indicated the predominant formation of a glucomannan and not cellulose. However, this does not rule out the possibility that GDP-Glc is a substrate for cellulose synthesis in certain tissues.

Cotton 'fibre' development of *Gossypium hirsutum* L. involves the deposition of a cellulosic secondary cell wall. Investigations into the NDP-sugar concentrations during cotton 'fibre' formation revealed that UDP-Glc predominated and GDP-sugars were present in very low amounts (Carpita *et al.*, 1980). Carpita *et al.* (1980) also demonstrated that the labelling kinetics and turnover of UDP-Glc (but not GDP-Glc) *in vivo* were able to account for the synthesis rates of sterylglucosides, sucrose, β-1,3-glucan and cellulose. In this case it is suggested that UDP-Glc is the precursor to cellulose in the secondary cell walls of *G. hirsutum* fibres.

Additional evidence that UDP-Glc is a precursor of cellulose has arisen from the recent isolation of cellulose biosynthesis genes (*CesA*) in plants. With the use of cotton 'fibre' membranes Peng *et al.* (2002) have demonstrated the synthesis of sitosterol-cellodextrins from a sitosterol-β-glucoside primer and UDP-Glc. It is suggested that a membrane bound sucrose-synthase provides the UDP-Glc for this process (Kimura *et al.*, 2002).

1.3 Project aim

Section 1.1.2 – section 1.1.3 have detailed the evidence that UDP-GlcA, UDP-GalA and GDP-Man may be formed by more than one biochemical pathway. In addition to this the incomplete evidence that conclusively demonstrates that UDP-Glc is the cellulosic precursor has also been outlined. The aim of this project is to determine the predominant pathway(s) involved in the formation of UDP-GlcA, UDP-GalA, GDP-Man and the cellulosic precursor.

1.4 Potential methods to distinguish the NDP-sugars that predominate in the competing pathways of plant cell wall biosynthesis

Various approaches have been taken to study the competing pathways of NDP-sugar metabolism and the contribution that each pathway makes to the final cell wall polysaccharide content.

Many early experiments detailed the existence of extractable enzymes involved in the various competing pathways. Modern day techniques have enabled researchers to demonstrate that organisms contain the genes required to synthesise certain (putative) enzymes. Positive results in these experiments illustrate that the organism has the capability to form an enzyme but there are problems with these approaches. Studies that demonstrate functional enzyme activity do not give conclusive evidence that the enzyme in question catalyses a reaction in a living cell. Indeed, it is possible that an enzyme may only operate under certain conditions. For example an enzyme may be present but may not function if, under cellular conditions, there is a presence or absence of an effector. Enzyme function may be restricted by compartmentalisation. If the enzyme is in a different compartment from

its substrate(s), the reaction will not proceed. Another complication is that the enzyme may not be detected because it is highly unstable and gets denatured during extraction. The use of the 'modern-day' approach may show that a gene is present. However, to show that a gene functions in a particular pathway within a cell it is also necessary to show that:

1. The gene has been transcribed into mRNA
2. The mRNA is translated into a protein
3. The protein has undergone the necessary post-translational modifications

There is also an added complication that both pathways may operate simultaneously to different extents under various conditions.

It is a difficult task to assess the predominant competing pathway that contributes to plant cell wall synthesis *in vivo*. The introduction of specific precursors to trace a pathway simply demonstrates that the particular pathway in question is operational. If a precursor is fed to an organism in amounts that are greater than trace level there is potential to elevate the metabolite pools to abnormally high concentrations. The pathways that are studied under such conditions may reflect an artificial response that would not otherwise occur such as a 'salvage' pathway.

Another approach to study the importance of the competing pathways in plant cell wall synthesis is the isolation of specific mutants. The difficulty with the interpretation of data obtained from mutant specimens is that many enzymes have a number of isoforms. To obtain plants that are mutant for each isoform is, at present, not an easy feat. The elimination of one functional isoform may stimulate not only the formation of alternative isoforms but also the alternative competing pathway.

Under these circumstances the pathways that function *in vivo* do not represent a true reflection of 'normal' cellular activity.

The research conducted in this project utilises a method that has the potential to determine the predominant pathway involved in UDP-GalA, UDP-GlcA and GDP-Man synthesis, at the same time, *in vivo*, without disruption to 'normal' cellular metabolism.

1.5 Experimental outline used to elucidate the pathways that predominate in the competing pathways of plant cell wall biosynthesis

A single experimental outline has been designed to assess each of the competing pathways (section 1.2.1 – section 1.2.4) simultaneously *in vivo*. The experiment is intended to resolve the predominant pathway(s) involved in plant cell wall synthesis without disruption of 'normal' cell metabolism.

Arabidopsis cell-suspension culture has been selected as the experimental system. The use of a cell-suspension ensures a rapid uptake of radioactivity and that the pathways studied relate to one cell type as the cells used are uniform. An aseptic technique is used to maintain the cells. This is beneficial as the pathways that are studied are known to relate to *Arabidopsis* cell metabolism and not the metabolism of potential microbial contaminants. However, the use of *Arabidopsis* cell-suspension culture has its limitations as it does not reflect an intact plant system that has different developmental stages and differentiated tissues.

The *Arabidopsis* cell-supsension culture is maintained on glycerol for two reasons:

- Glycerol is a less preferential carbon source than hexoses, and thus ensures the rapid uptake of [1-^{3}H]Gal, [U-^{14}C]Glc and [U-^{14}C]Fru.
- Glycerol maintains the net flux of carbon from Fru 6-P to UDP-Gal (Fig. 1.7)

In Fig. 1.7 a group of interconverting compounds is designated as the 'core' metabolites. Where more than one biochemical pathway exists to form a given NDP-sugar, the pathways involved in the formation of that particular NDP-sugar each stem from a different 'core' metabolite. The cells are fed trace levels of [1-^{3}H]Gal, [U-^{14}C]Fru or [U-^{14}C]Glc. The ^{14}C enters the 'core' metabolites and, amongst the 'core' metabolites themselves, flows in the direction of the net flux of carbon. The ^{3}H from [1-^{3}H]Gal enters the 'core' metabolites at the opposite end from the ^{14}C. The flow of ^{3}H through the 'core' metabolites occurs against the net flux of carbon and is predicted to form a ^{3}H:^{14}C ratio gradient within the 'core' metabolites. A metabolite is classed as a 'core' metabolite because the ^{3}H and ^{14}C are received by that metabolite from different 'directions' (Fig. 1.7). Metabolites that stem from 'core' metabolites receive ^{3}H and ^{14}C from the same source. The NDP-sugars that stem from the 'core' metabolites are expected to acquire the same ^{3}H:^{14}C ratio as their parent 'core' metabolite.

The loss of ^{14}C during pentose formation will be taken into account. No loss of ^{3}H from C1 is expected in the pathways shown in Fig. 1.7. In this way measurement of the ^{3}H:^{14}C ratio of intermediates of the competing pathways, or of the monosaccharide residues of the polysaccharides is expected to indicate the pathway that dominates.

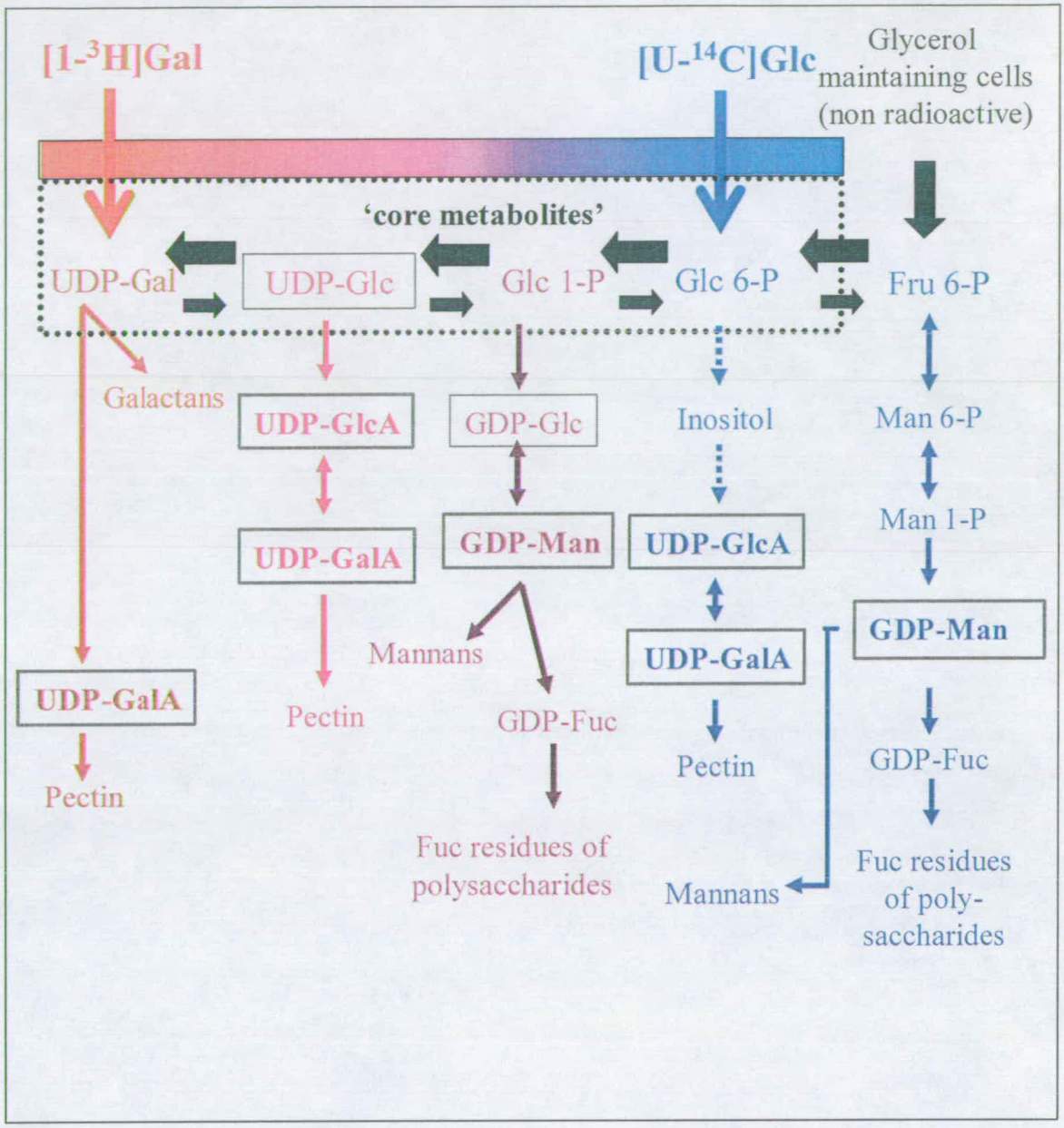

Figure 1.7 Summary of competing pathways of sugar nucleotide interconversion and proposed dual labelling experiment.

[1-^{3}H]Gal and [U-^{14}C]Glc feed into opposite ends of the 'core' metabolite pathway. The colours of the compounds represent the ^{3}H:^{14}C ratio that each compound is expected to have. Compounds are expected to have the same ^{3}H:^{14}C ratio as the 'core' metabolite they stemmed from. UDP-Gal is expected to have the highest ^{3}H:^{14}C ratio shown in red as it is closest to the source of ^{3}H. A decline in the ^{3}H:^{14}C ratio of the 'core' metabolites is expected between UDP-Gal and Glc-6-P as glycerol maintains the flux in a right to left direction in the 'core' metabolites (as written). The metabolites shown in a grey box are the metabolites involved in the competing pathways mentioned in section 1.2.1 - 1.2.4

2. Materials and Methods

2.1 Chemicals

The chemicals used throughout were purchased from BDH AnalaR Chemicals Ltd. (Poole, United Kingdom), Sigma-Aldrich (Poole, United Kingdom) or Fisher Chemicals (Fisher Scientific, Loughborough, United Kingdom).

D-[1-^{3}H]Gal (SA 1.8 × 10^{14} Bq/mol) and L-[1-^{3}H]Ara (SA 1.48 × 10^{8} Bq/mol) were custom synthesised by Amersham using the TL7 technique outlined by Evans *et al.* (1974). To purify the D-[1-^{3}H]Gal the stock solution was streaked onto Schleicher & Schuell 2045 B paper, run in EPW (8:2:1, 96 h), autoradiographed and eluted with H_2O. D-[U-^{14}C]Glc (SA 1.147 × 10^{13} Bq/mol) and [4-^{3}H]toluene (SA 79.9 kBq/g) were obtained from Amersham Pharmacia Biotech, Buckinghamshire, UK. D-[U-^{14}C]Fru (SA 1.05 × 10^{7} Bq/mol), L-[1-^{14}C]Ara (SA 2 × 10^{6} Bq/mol) were obtained from the American Radiolabeled Chemicals Inc., St. Louis, MO.

2.2 Plant culture maintenance

2.2.1 *Arabidopsis thaliana* culture medium

Murashige *et al.* (1962) basal salt with minimal organics (4.4 g/l, Sigma number M-6899) was combined with α-naphthaleneacetic acid (0.05 mg/l), kinetin (0.05 mg/l) and a carbon source (2% w/v). The solution was adjusted to pH 5.8 with 1 M KOH. The culture medium (100 ml/flask) was dispensed into 250-ml conical flasks. The flasks were loosely capped at the neck with a foam bung, covered with two layers of aluminium foil and autoclaved (121°C, 15 min).

2.2.2 Sub-culturing of cell-suspension cultures

Cells were shaken at 25°C under a continuous source of moderate artificial light. *Arabidopsis* cell-suspension culture was subcultured every 5 d into fresh medium (1:10 v/v old culture:fresh medium).

2.3 Electrophoretic and chromatographic separation of compounds

2.3.1 Paper electrophoresis

Samples were loaded onto Whatman 3MM paper. The paper was wetted with a buffer that was either pH 2 (FAW, 1:35:355 by vol.), pH 3.5 (PyAW, 1:10:189 by vol.) or pH 6.5 (PyAW, 33:1:300 by vol.). The paper was placed into a glass tank and hung from a trough situated at the top of the tank that contained the buffer the paper had been wetted with. The bottom of the tank contained the same buffer to immerse the opposite end of the paper. The tank was filled with an immiscible coolant (for electrophoresis at pH 2 and pH 3.5, white spirit was used; for electrophoresis at pH 6.5, toluene was used). A voltage (2.5 kV) was then applied through the buffer for a set period of time (1.0 – 1.5 h) in order to separate the compounds based on their charge:mass ratios.

2.3.2 Descending paper chromatography

Samples were dispensed onto Whatman 3MM paper, Whatman no. 1 or Schleicher and Schuell 2045 B paper. The paper was then placed into a glass tank and hung from a trough situated at the top of the tank that contained a solvent (Table 2.1). The

tank was then sealed with a glass lid and the chromatogram removed after the appropriate time.

Table 2.1 Solvent systems used for descending paper chromatography

Solvent system	Ratios used (by vol.)	Main uses
Acetone/water	85:15	Isolation of inositol
Butan-1-one/acetic acid/saturated boric acid (BAB)	9:1:1	Isolation of Api, Rha and Rib
Butanol/acetic acid/water (BAW)	12:3:5	Initial general separation of monosaccharide mixture
Ethyl acetate/acetic acid/water + 0.25% (w/v) phenylboronic acid	10:5:6	Isolation of Api
Ethyl acetate/pyridine/water	8:2:1; 10:4:3; 9:3:2	Separation of Glc from Gal
Propan-2-ol:acetic acid/water	15:2:3	Isolation of inositol
Phenol:water	4:1 (w/w)	Separation of Fuc from Xyl

2.3.3 Thin-layer chromatography

The samples were loaded onto a TLC plate (MERK, non-fluorescent, silica gel 60, 20 × 20 cm^2) and placed into a glass tank containing 100 ml BAW (2:1:1). The tank was sealed with a glass lid and the plate was removed when the solvent front was approximately 2 cm from the top of the plate.

2.4 Detection of marker compounds and radiolabelled compounds

2.4.1 Aniline hydrogen-phthalate stain

A stock solution of acetone:diethylether:water (49:49:2 by vol.) containing phthalic acid (1.6% w/v) was formed. Prior to use, aniline (0.5 ml/100 ml of stock) was

added to the stock solution. The paper was dipped through the solution, dried and placed in an oven at 105°C for 5 to 10 min.

2.4.2 Silver nitrate stain

The paper was dipped through three solutions (a – c). The paper was dried for 15 min each time before it was dipped through the next solution.

(a) $AgNO_3$ (5 mM in acetone; H_2O was used to redissolve any precipitate).

(b) NaOH (0.125 mM in 96% ethanol). This dip was repeated.

(c) $Na_2S_2O_3$ (10% w/v in water).

The paper was immediately transferred to a basin of water to wash for 1 h and dried.

2.4.3 Thymol stain

A 0.53% (w/v) thymol solution was prepared in ethanol. Concentrated H_2SO_4 (5.3% v/v) was slowly added to the solution. The TLC plate was quickly dipped through this solution, dried and then placed in an oven (120°C, 5 min).

2.4.4 Molybdate stain

Concentrated HCl (3 ml) was added dropwise with rapid stirring to 17 ml of an 11.8% (w/v) ammonium molybdate solution. Perchloric acid (6 ml, 60% v/v) was added dropwise to the solution and the precipitate stirred until it dissolved. Acetone (180 ml) was added. The paper was dipped through this solution, dried and the spots that appeared were marked. The paper was exposed to 366-nm UV radiation or direct sunlight for 10 min and any newly formed spots were marked. The paper was wrapped in aluminium foil and heated at 100°C for 2 min to reveal additional spots.

2.4.5 Autoradiography

^{14}C-Labelled compounds that had been subjected to paper chromatography, paper electrophoresis or TLC were detected by autoradiography on Kodak BioMax MR-1 film. The film was exposed for 1 – 28 d.

2.4.6 Quantitative assay of radiolabelled compounds by scintillation counting

Radioactivity was assayed in a Beckman LS 6500 multi-purpose scintillation counter. Aqueous samples were assayed using a 10:1 (v/v) ratio of 'OptiPhase HiSafe' scintillation fluid (Wallac, Milton Keynes, Bucks, UK) to aqueous sample. Paper samples that were not required for further experimental work were shaken overnight with H_2O (1 ml) and 'OptiPhase HiSafe' (9 ml) was then added. In cases where samples on paper were required for further experimental work, 2 ml of 'OptiScint Hisafe 3' scintillation fluid was added to the dry paper. Prior to additional work on the latter samples the paper was washed in toluene to remove the scintillation fluid.

2.4.7 Elution of samples from paper

The section of paper that contained the sample was cut out, rolled up and placed in the barrel of a 5-ml syringe. The barrel was placed into a 15-ml centrifuge tube and the paper was wetted with water. The tube was then centrifuged (3000 rpm, 10 min). The elution process was repeated five to six times (Eshdat and Mirelman 1972).

2.5 Driselase purification

Unless otherwise stated the Driselase purification procedure and all chemicals involved were maintained in a coldroom (3°C). Driselase (10 g) was stirred rapidly for 15 min in 100 ml buffer (50 mM acetic acid, pH 5.0 Na^+) and centrifuged (10 min, 4000 rpm). $(NH_4)_2SO_4$ (26 g/50 ml supernatant) was dissolved in the supernatant with rapid stirring, left to stand for 15 min at 0°C and centrifuged (10 min, 4000 rpm). The pellet that remained after centrifugation was resuspended in 100 ml $(NH_4)_2SO_4$ (52% w/v) and centrifuged (10 min, 4000 rpm). The pellet was dissolved in 20 ml H_2O and loaded onto a Sephadex G-25 column (1500-ml bed volume, washed with 0.5% CB). The fast-eluting brown material (100 – 150 ml) was collected, frozen (–80°C), freeze dried and stored in a freezer (–20°C).

2.6 Attempts to remove starch from the AIR

2.6.1 Potassium iodide stain — starch detection

A solution containing I_2 (0.33% w/v) and KI (0.67% w/v) was added to samples. The presence of starch was noted if, under microscopic examination, blue–black staining was observed.

2.6.2 AIR treatment with DMSO

Arabidopsis AIR suspension (100 µl) in 80% v/v ethanol was rinsed with DMSO and left to shake gently for 15 d in DMSO (45 ml, 90% v/v). The AIR suspension was centrifuged (1500 rpm, 30 min) and the supernatant was removed to give a final volume of 2.5 ml. A portion (50 µl) of suspension was washed with H_2O (1 ml) and tested for the presence of starch with potassium iodide.

2.6.3 AIR treatment with human salivary amylase

Pre-boiled and un-boiled samples of *Arabidopsis* AIR suspension (100 µl) were treated with human saliva (1 ml, author's saliva in 0.5% CB). The AIR suspensions were incubated (37°C, 3 d). The digest solution was run on a TLC and stained with thymol.

2.6.4 Porcine pancreatic α-amylase activity on soluble potato starch as a substrate

Porcine pancreatic α-amylase (Sigma, type VI-B) solution (1.5%, w/v) was prepared in 0.06% (v/v) pyridine (pH 5.6). The solution was gently shaken for 1 h at 24°C and then centrifuged (1500 – 1700 rpm, 5 min). The supernatant was utilised.

Samples of soluble potato starch (5% w/v in PyAW, 1:1:198, pH 4.7) were boiled or left at room temperature prior to porcine pancreatic α-amylase treatment. Control samples were also treated in the same manner but did not receive amylase. Each sample was incubated at 37°C for 15 d. The digests were loaded onto a TLC plate and run in BAW (2:1:1, 6 h) and the TLC plates were stained with thymol.

2.6.5 Termamyl® 120L activity on soluble potato starch

Termamyl® 120L (Novo Nordisk) is a heat-stable endoamylase that hydrolyses 1,4-α-glucosidic linkages. It is expressed in and produced by a genetically modified strain of *Bacillus licheniformis*.

Soluble potato starch (0.5%, w/v) was dissolved in MES buffer (50 mM in 0.5% CB w/v; Na^+). As per instructions given by the enzyme supplier the pH of the buffer depended on the temperature that was used (25°C, 37°C, pH 6.0; 60°C, pH 5.6; 90°C, pH 7.0).

The starch samples were treated with Termamyl® 120L at room temperature, 37°C, 60°C or 90°C. Samples were monitored for digestion products over a period of 24 h.

2.6.6 Termamyl® 120L activity on AIR

Arabidopsis AIR was washed thoroughly with MES buffer (50 mM, pH 7, Na^+) and the AIR (100 µl) suspension was treated with Termamyl® solution at either 60°C or 90°C as per section 2.6.5.

2.7 Percentage of ^{14}C detected as ^{3}H and standard quench curves

When ^{3}H and ^{14}C are counted together in the same vial with a scintillation counter, the reported ^{3}H value is inflated with a percentage of ^{14}C. This is the result of a slight overlap of the ^{3}H and ^{14}C energy channels utilised by the scintillation counter. To account for this the percentage of ^{14}C detected as ^{3}H was determined. In addition to this quench curves were provided to determine the counting efficiency of the scintillation counter.

A known weight of [4-^{3}H]toluene or [^{14}C]toluene was added to scintillation vials containing 10 ml 'HiSafe OptiPhase' and assayed for radioactivity on a dual ^{3}H and ^{14}C channel. The H# was also documented. A small amount of acetone was added to each vial to quench the sample and the count rate and H# was recorded. This process was repeated until the scintillation vial was full. The diminished ^{3}H and ^{14}C count rates noted at each acetone concentration allowed the counting efficiencies for each isotope to be calculated based on the radioactivity levels known to be present in the vials. The counting efficiencies were plotted against the H# (appendix 1, appendix 2).

Although [^{3}H]toluene is not present in the [^{14}C]toluene sample, ^{3}H is reported by the scintillation counter on a dual isotope counting channel. The percentage of the cpm from a [^{14}C]toluene sample reported as 'false' ^{3}H was calculated and graphed against the H# (appendix 3).

2.8 Calculation used to derive ^{3}H:^{14}C ratio and associated error

A worked example of this calculation is provided (worked example 1, section 2.8.1). The isolated radioactive monosaccharide, and a background sample, were each assayed twice in a scintillation counter (5 – 30 min) for both ^{3}H and ^{14}C. The number (N_S) of counts in the sample apparently due to each isotope was recorded and the error of each value was expressed as 2σ, i.e. $2\sqrt{N_S}$. The background count (N_B) for each isotope was deducted from N_S and the combined error was calculated (formula 1).

Formula 1. Combining errors of two values (N_S and N_B) that are subtracted from one another

$$\text{Combined error} = \sqrt{((2\sqrt{N_B})^2 + (2\sqrt{N_S})^2)}$$

The H# of the radioactive monosaccharide sample enabled the percentage of ^{14}C falsely detected as ^{3}H to be determined with a standard curve (section 2.7, appendix 3). The number of ^{14}C counts falsely detected as ^{3}H was deducted from the machine-reported total ^{3}H count to give the true ^{3}H count and the combined error was calculated (formula 1). The H# also allowed the counting efficiency both for true ^{3}H and for ^{14}C to be obtained when read from a standard curve (section 2.7, appendix 1, appendix 2). The ^{14}C and true ^{3}H counts and their associated errors were

adjusted based on the counting efficiency of each isotope to convert counts to disintegrations. The disintegrations were calculated per second to give a value in Bq and the ^{3}H:^{14}C ratio (Bq/Bq) was calculated. The ^{3}H:^{14}C ratio error was also calculated (formula 2).

Formula 2. Combining errors of two values that are used to form a ratio

Error in ^{3}H:^{14}C ratio $= (\sqrt{((^{3}H \text{ error}/^{3}H)^2 + (^{14}C \text{ error}/^{14}C)^2)}) \times (^{3}H/^{14}C)$

NB: ^{3}H = Bq of ^{3}H ^{14}C = Bq of ^{14}C

^{3}H error = error in Bq of ^{3}H ^{14}C error = error in Bq of ^{14}C

The originally fed [^{14}C]Glc or [^{14}C]Fru was uniformly labelled with ^{14}C. Owing to this each carbon atom in metabolites formed by subsequent biochemical steps had an equal chance of being ^{14}C. However, the originally fed [1-^{3}H]Gal was only labelled at C1.

It was expected that when a [1-^{3}H,U-^{14}C]hexose residue was conerted to a [1-^{3}H,U-^{14}C]pentose residue, 1/6 of the ^{14}C would be lost but all the ^{3}H would be retained. Therefore, the ^{3}H:^{14}C (Bq/Bq) ratio of a five-carbon metabolite would be inflated in comparison to a six-carbon metabolite because of the loss of one ^{14}C atom. In order to compare the ^{3}H:^{14}C (Bq/Bq) ratio of a five-carbon metabolite to that of a six-carbon one, it was therefore appropriate to multiply the measured ^{3}H:^{14}C ratio of the five-carbon metabolite and associated error by 5/6.

2.8.1 Worked example

Calculation used to derive ^{3}H:^{14}C ratio and associated error of a sample of Xyl isolated from UDP-Xyl

- *Uncorrected data*

UDP-Xyl	^{3}H	(a)	60.8 cpm	(b)	63.5 cpm
	^{14}C	(a)	53.5 cpm	(b)	54.6 cpm
Background	^{3}H	(a)	27.4 cpm	(b)	27.5 cpm
	^{14}C	(a)	36.8 cpm	(b)	33.6 cpm

a, b are replicate assays on same sample, counted for 30 min. The sample data is shown in appendix 9 and relate to a sample of Xyl isolated from UDP-Xyl at t = 1 min.

- *Apparent machine-reported ^{3}H — counts registered in total*

UDP-Xyl

^{3}H : (30 min × 60.8 cpm) + (30 min × 63.5 cpm) = **3729** counts

^{14}C : (30 min × 53.5 cpm) + (30 min × 54.6 cpm) = **3243** counts

Background

^{3}H : (30 min × 27.4 cpm) + (30 min × 27.5 cpm) = **1648** counts

^{14}C : (30 min × 36.8 cpm) + (30 min × 33.6 cpm) = **2112** counts

- *Error (2σ)of machine-reported counts*

UDP-Xyl

^{3}H : $2 \times \sqrt{\mathbf{3729}}$ counts = ± **122** counts

^{14}C : $2 \times \sqrt{\mathbf{3243}}$ counts = ± **114** counts

Background

^{3}H : $2 \times \sqrt{\mathbf{1648}}$ counts = ± **81** counts

^{14}C : $2 \times \sqrt{\mathbf{2112}}$ counts = ± **92** counts

- *Deduct background counts from UDP-Xyl counts*

^{3}H : 3729 – 1648 = **2081** counts

^{14}C : 3243 – 2112 = **1131** counts

- *Error in background corrected counts*

^{3}H : $\sqrt{((81)^2 + (122)^2)}$ = ± **146**

^{14}C : $\sqrt{((92)^2 + (114)^2)}$ = ± **146**

- *True ^{3}H counts*

H# = 74, therefore 45% of ^{14}C was falsely recorded as ^{3}H (appendix 3)

Therefore true ^{3}H = **2081** – ((45/100) × **1131**)

= **1572** counts

- *Error associated with true ^{3}H counts*

= $\sqrt{((146)^2 + (146)^2)}$

= ± **206**

- *True ^{3}H (disintegrations)*

H# number = 74, therefore the counting efficiency for ^{3}H was 26.5% (appendix 2)

Therefore true ^{3}H disintegrations = **1572** × (100/26.5)

Counting time was 3600 s

Therefore disintegrations per second (Bq) = (**1572**/3600) × (100/26.5)

= **1.65** Bq

- *Error associated with ^{3}H (Bq)*

(**206**/3600) × (100/26.5)

= ± **0.22** Bq

- *^{14}C disintegrations*

H# number = 74, therefore counting efficiency for ^{14}C was 60% (appendix 1)

Therefore ^{14}C disintegrations = (**1131**) × (100/60)

Counting time was 3600 s

Therefore disintegrations per second (Bq) = (**1131**/3600) × (100/60)

= **0.52** Bq

- *Error associated with ^{14}C (Bq)*

(**206**/3600) × (100/60)

= ± **0.07** Bq

- *$^{3}H/^{14}C$ ratio*

= 1.6/0.5

= **3.2** Bq/Bq

- *Error in the $^{3}H/^{14}C$ ratio*

The error due to the formation of a ratio is:
Error in the $^{3}H/^{14}C$ ratio $= (\sqrt{((\Delta^{3}H/^{3}H)^2 + (\Delta^{14}C/^{14}C)^2)}) \times (^{3}H/^{14}C)$
Where $\Delta^{3}H$ is the error associated with ^{3}H (Bq) and $\Delta^{14}C$ is the error associated with ^{14}C (Bq)

Error in the $^{3}H/^{14}C$ ratio $= \sqrt{((0.2/1.65)^2 + (0.07/0.5)^2)} \times (3.19)$
$= \mathbf{0.57}$

- *Correction factor for C_5 compounds*

To compare the $^{3}H/^{14}C$ ratio of a (U-^{14}C)-labelled C_5 compound to a (U-^{14}C)-labelled C_6 compound it is necessary to multiply the isotope ratio and associated error of a C_5 compound by 5/6.

$5/6 \times (\mathbf{3.19 \pm 0.57})$
$= \mathbf{2.66 \pm 0.48}$

2.9 Calculation required to determine the factor applied to the $^{3}H:^{14}C$ ratio of monosaccharides obtained from ^{3}H-labelled AIR that was combined with ^{14}C-labelled AIR

A worked example of this calculation is provided (worked example 2, section 2.9.1). The counting efficiency of ^{3}H, a weak β-emitter, is greater when the ^{3}H is present in a solution than in a particulate state such as the AIR. Therefore, a portion of each AIR sample was first solubilised with Driselase and then assayed for radioactivity (appendix 6). Based on these assays the volume of undigested ^{3}H-labelled and ^{14}C-labelled AIR suspensions needed to form a 5:1 (or in some cases 3:1) $^{3}H:^{14}C$ (Bq/Bq) ratio was dispensed into separate scintillation vials and assayed for radioactivity (still as a suspension of particulates). Although the ^{3}H and ^{14}C counts thus obtained did not represent the $^{3}H:^{14}C$ (Bq/Bq) ratio (because the counting efficiencies were unknown), the counts obtained for the particulate suspension ensured that the error incurred owing to the dispensation of a suspension could be accounted for.

As each parent AIR suspension was divided into six replicate portions, the average cpm per portion was calculated (appendix 7). When this was compared to the intended dpm value determined in the Driselase digest, the counting efficiency for ^{3}H-labelled AIR (22.5%) and ^{14}C-labelled AIR (90%) was determined. The 'intended' dpm was multiplied by the average counting efficiency to give the 'intended' cpm. The 'intended' cpm was divided by the cpm recorded for each portion of AIR to give a unique correction factor that would take into account whether too much or too little AIR particulate matter had been dispensed into the portion in question. When the correction factor for the ^{14}C-labelled AIR was divided by the correction factor for the partnered ^{3}H-labelled AIR, the ^{3}H:^{14}C correction factor for that particular portion was established.

2.9.1 Worked example

Approach employed to account for the dispensation of a suspension and the ratios that were formed on a 3:1 ^{3}H:^{14}C (Bq/Bq) basis rather than a 5:1 ^{3}H:^{14}C (Bq/Bq) ratio. This enabled all the final isotope ratios obtained in Fig. 3.38 to be compared whether they originally had a ^{3}H:^{14}C of 3:1 (Bq/Bq) or 5:1 (Bq/Bq).

Part 1. Sample D (Appendix 6). Alteration of a 3:1 ^{3}H:^{14}C (Bq/Bq) ratio to be comparible to a 5:1 ^{3}H:^{14}C (Bq/Bq) ratio

In this case a ratio was formed based on a 3:1 ^{3}H:^{14}C (Bq/Bq) ratio.

- 100 µl ^{3}H-labelled AIR digested with Driselase contained: **32453** dpm
  Therefore, 300 µl of **^{3}H-labelled AIR suspension** should contain:
  3 × 32453 dpm
  = **97359** dpm
- Number of dpm of ^{14}C-labelled AIR digested with Driselase required to form 3:1 3H:14C (Bq/Bq) ratio: **32453** dpm
  As a 5:1 ^{3}H:^{14}C (Bq/Bq) ratio had been intended, the dpm required to form this with 300 µl of ^{3}H-labelled AIR would be:
  97359/5
  ^{14}C = **19472** dpm

However, as a 3:1 ^{3}H:^{14}C ratio was formed the sample should contain:

^{14}C = 97359/3 = **32453** dpm

Part 2. Sample D (Appendix 7). Correction factor applied to the isotope ratios to correct for the dispensation of a suspension

The ^{3}H- and ^{14}C-labelled AIR suspensions were each divided into six nominally equal portions that should each contain 32453 dpm ^{14}C and 97359 dpm ^{3}H (specified in Appendix 6). Each of the twelve portions of AIR suspension were assayed for radioactivity:

Portion No.	^{14}C (cpm)	^{3}H (cpm)
1	37777	25465
2	31716	20459
3	23529	21954
4	23388	20812
5	26018	20454
6	27551	19352
Average (samples 1–6)	**28330**	**21416**

As the intended Bq had been calculated from the Driselase-digested ^{3}H- and ^{14}C-labelled AIR portions of sample D, it was possible to deduce the counting efficiency of the undigested AIR suspension (formula 3).

Counting efficiency of undigested AIR = $\frac{\text{Average cpm of six values}}{(\text{Intended Bq} \times 60)}$

Formula 3

	^{14}C	^{3}H
Intended dpm per portion for a ^{3}H:^{14}C (Bq/Bq) ratio (in this case) of **3:1**	541 × 60 (Part 1. Intended Bq × 60) = **32453** dpm	1623 × 60 (Part 1. Intended Bq × 60) = **97359** dpm
Counting efficiency of undigested AIR	(28330/32453) × 100 = **87%**	(21416/97359) × 100 = **22%**

The average counting efficiency for undigested AIR was determined for all eight independently radiolabelled samples A – H. In order to compare the intended radioactivity (dpm) with the undigested AIR cpm values, the averaged counting efficiency of 'solid' AIR (samples A – H; **90.0%** for ^{14}C; **22.5%** for ^{3}H) was used to calculate the cpm of the Driselse-digested ^{3}H- and ^{14}C-labelled AIR portions as if they had been a undigested AIR sample:

	^{14}C	^{3}H
Intended cpm (based on undigested AIR counting efficiency) if this sample had been based on a ^{3}H:^{14}C (Bq/Bq) ratio of **5:1**	19472 × 0.900 = **17525** cpm	97359 × 0.225 = **21906** cpm

As the number of cpm that were intended to be contained in each sample were known, a correction factor could be associated with each portion to ensure that any deviation from the desired 5:1 ^{3}H:^{14}C (Bq/Bq) ratio due to the dispensation of a suspension was accounted for (formula 4)

Deviation from intended cpm = $\frac{\text{Intended cpm}}{\text{cpm registered for sample}}$

Formula 4

	Deviation from intended cpm	
Portion No.	^{14}C	^{3}H
1	17525/37777 = **0.46**	21906/25465 = **0.86**
2	17525/31716 = **0.55**	21906/20459 = **1.07**
3	17525/23529 = **0.74**	21906/21954 = **1.00**
4	17525/23388 = **0.75**	21906/20812 = **1.05**
5	17525/26018 = **0.67**	21906/20454 = **1.07**
6	17525/27551 = **0.64**	21906/19352 = **1.13**

The ^{3}H:^{14}C (Bq/Bq) correction factor due to the dispensation of a suspension was calculated as per formula 5.

^{3}H:^{14}C (Bq/Bq) correction factor due to dispensation of a suspension Formula 5 =	$\frac{^{3}H \text{ deviation from intended cpm}}{^{14}C \text{ deviation from intended cpm}}$

Portion No.	^{3}H:^{14}C (Bq/Bq) correction factor due to dispensation of a suspension
1	0.86/0.46 = **1.85**
2	1.07/0.55 = **1.94**
3	1.00/0.74 = **1.34**
4	1.05/0.75 = **1.40**
5	0.67/1.07 = **1.59**
6	1.13/0.64 = **1.78**

In order to make the final ratio values comparable they were multiplied by their corresponding ^{3}H:^{14}C correction factor due to dispensation of a suspension.

2.10 ^{3}H:^{14}C Ratios of monosaccharides obtained from the AIR of *Arabidopsis* cell-suspension culture fed [1-^{3}H]Gal and [U-^{14}C]Glc

This experiment was designed to obtain and compare ^{3}H:^{14}C ratios of cell wall monosaccharides to determine the predominant competing pathway that each monosaccharide arose from. An outline of the experimental protocol for this section is detailed in Fig. 2.1.

Glycerol-maintained *Arabidopsis* cell-suspension culture, aged 2 d, was filtered through muslin and the fine cell-suspension (filtrate) adjusted to 10% SCV. This was dispensed into six glass vials (0.5 ml/vial) and the cells were gently shaken for 30 min. Purified [1-^{3}H]Gal (5 MBq in 50 µl H_2O) was added to each of three vials and [U-^{14}C]Glc (1 MBq in 50 µl H_2O) was added to each of the remaining vials. At selected time points 20 µl of cell-free medium was assayed for non-volatile radioactivity.

At 480 min 2 ml ethanol was added to each vial to give a final conc. of 80% (v/v) and shaken for 3 d. Each suspension was transferred into a 15-ml graduated centrifuge tube and the cells were washed in 20 × 14 ml of 80% (v/v) ethanol.

An AIR–ethanol suspension (2 ml) was formed in each centrifuge tube and 1 ml of each suspension was dispensed into a screw-cap Sarstedt tube of known weight. The Sarstedt tubes were centrifuged (13000 rpm, 10 min) and 750 µl of supernatant was removed. Acetone (1 ml) was added to each tube. The Sarstedt tubes were centrifuged (13000 rpm, 10 min), the supernatant was removed and the samples were left overnight to dry. TFA (2 M, 1 ml) was added to each Sarstedt tube

and the tubes were re-weighed. The samples were heated at 120°C for 1 h and the

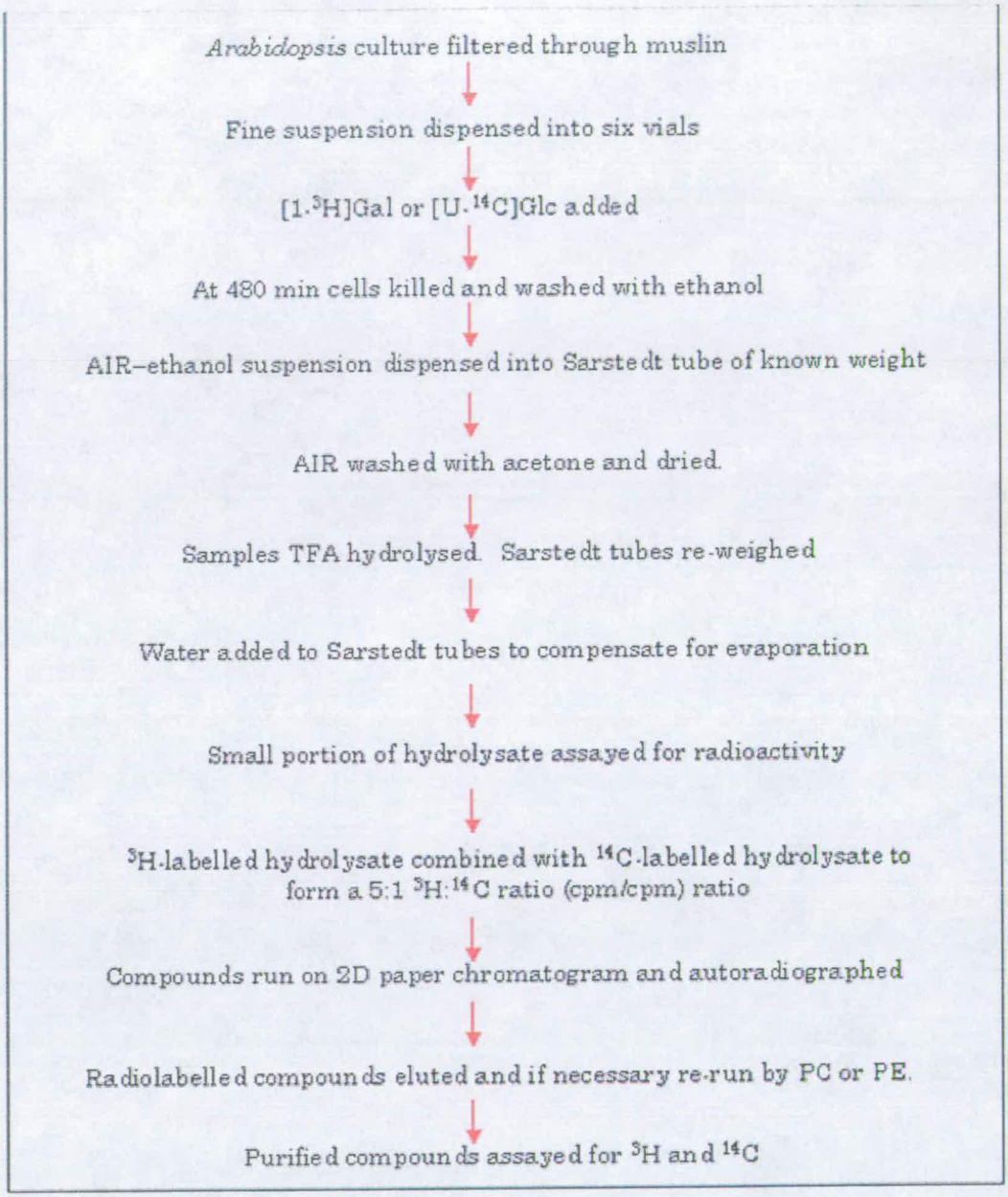

Figure 2.1 Overview of the protocol used to determine the ^{3}H:^{14}C ratios of monosaccharides from the AIR of *Arabidopsis* cell-suspension culture fed [1-^{3}H]Gal and [U-^{14}C]Glc

tubes were weighed. To compensate for any evaporation that occurred during heating, H_2O was added to each Sarstedt tube to increase its weight to that noted prior to heating. A 10-µl portion of each sample solution was assayed for radioactivity.

Each ^{3}H-labelled hydrolysate was combined with a ^{14}C-labelled hydrolysate to form a 5:1 ^{3}H:^{14}C (cpm/cpm) ratio. The compounds in each sample were separated by paper chromatography and visualised with autoradiography. The radiolabelled compounds were eluted and dried in a SpeedVac. Compounds that required further purification (Fig. 3.15) were redissolved in 100 µl H_2O and subjected to either paper chromatography or paper electrophoresis.

The purified compounds were autoradiographed, eluted, dried in a SpeedVac, redissolved in 2 ml H_2O and assayed for ^{3}H and ^{14}C.

2.11 ^{3}H:^{14}C Ratios of monosaccharides obtained by different methods from *Arabidopsis* cell-suspension culture fed [1-^{3}H]Gal and either [U-^{14}C]Glc or [U-^{14}C]Fru

This experiment was designed to obtain and compare ^{3}H:^{14}C ratios of cell wall monosaccharides that had been derived from different known polysaccharide sources. This was carried out to determine if the pathway used to form a particular monosaccharide was dependent on the polysaccharide it is used to form. An outline of the experimental protocol for this section is shown in Fig. 2.2.

Arabidopsis cell-suspension culture was transferred from a Glc to a glycerol medium and after 3 d was filtered through muslin. The fine cell-suspension (filtrate) was adjusted to 10% SCV, dispensed into sixteen glass vials (500 µl/vial) and gently shaken for 30 min at 25°C. To each of eight vials [1-^{3}H]Gal (1 MBq in 50 µl H_2O) was added. [U-^{14}C]Glc (0.2 MBq in 50 µl H_2O) or [U-^{14}C]Fru (0.05 MBq in 50 µl H_2O) was added the remaining vials. At selected time points 20 µl of cell-less medium was sampled from each vial. Samples containing ^{14}C were dispensed directly into a scintillation vial and assayed for radioactivity. Samples containing ^{3}H were dried onto 2 × 2 cm^2 Whatman 3MM paper and assayed for non-volatile radioactivity.

At 480 min 3.67 ml CM (1:1) was added to each vial to extract phosphatidylinositol to form a single phase with composition CMW 10:10:3 (the water component was regarded as the medium and cell sap). The vials were gently shaken for 24 h. The contents of each vial were transferred into a 15-ml centrifuge tube and an equal volume of water was added. The tubes were centrifuged (3200

rpm, 15 min) and the lipid-rich lower (chloroform-rich) phase was removed and

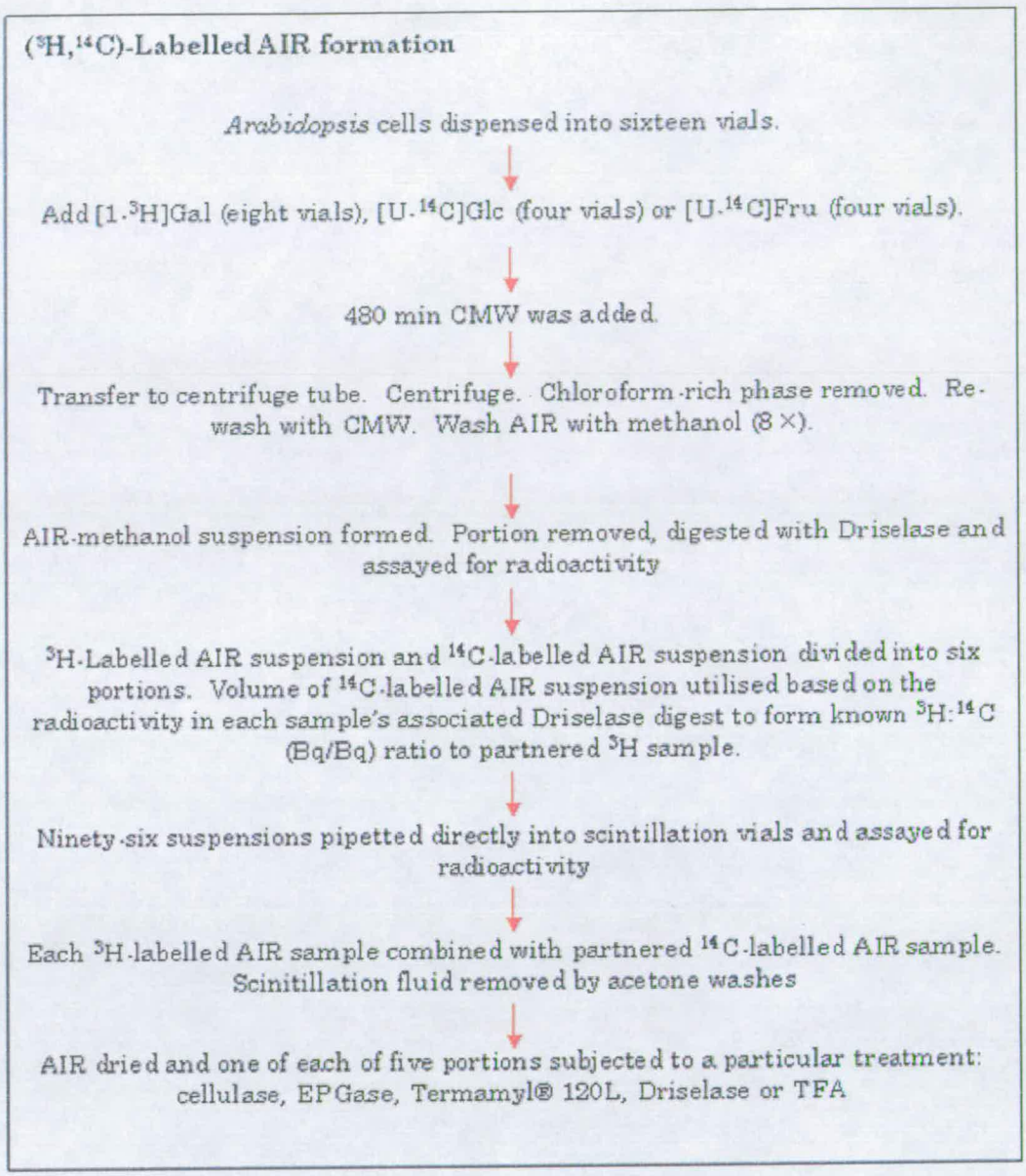

Figure 2.2 Overview of protocol used to determine the $^{3}H:^{14}C$ ratios of monosaccharides obtained by different methods from *Arabidopsis* cell-suspension culture fed [1-^{3}H]Gal and [U-^{14}C]Glc or [U-^{14}C]Fru

Continued overleaf

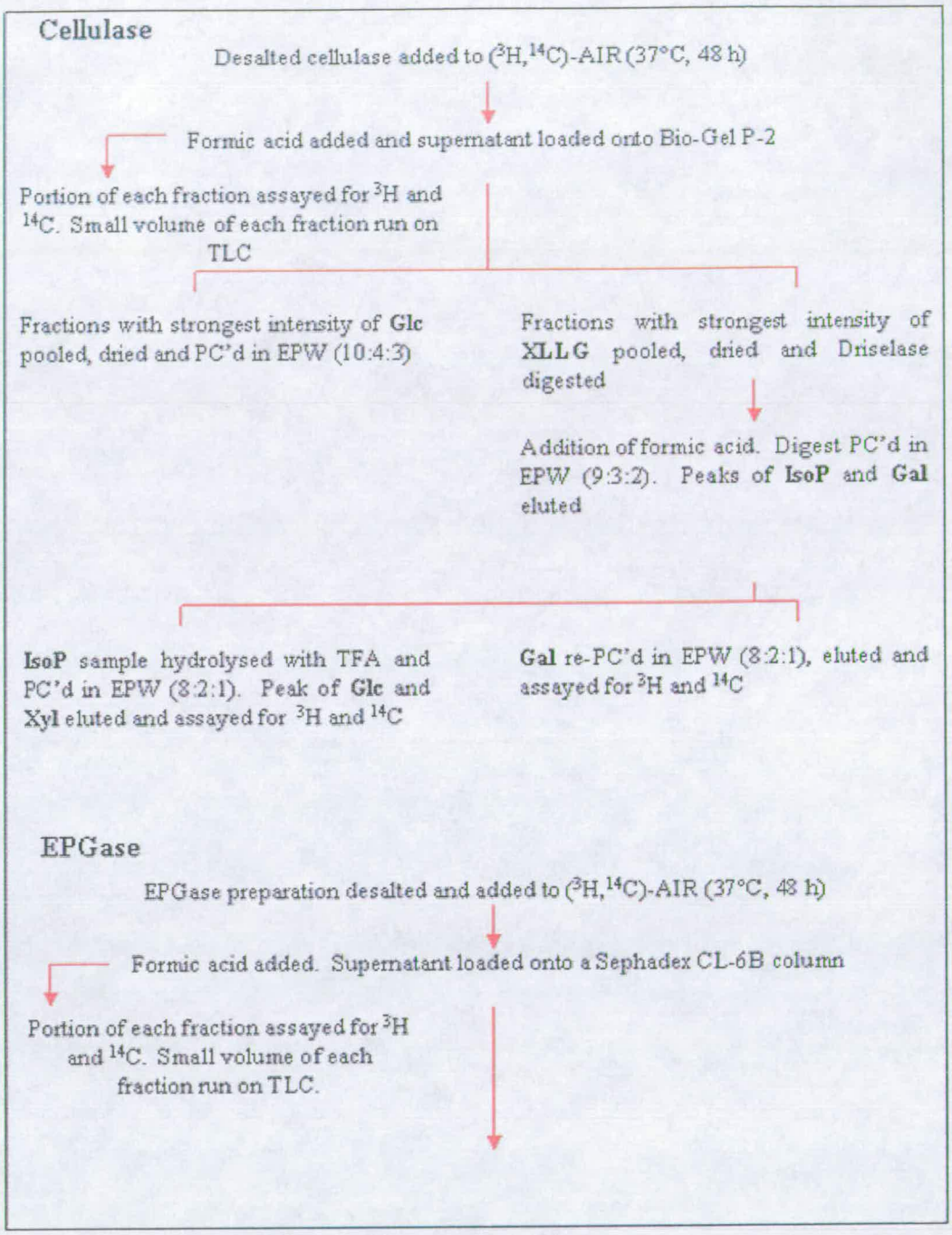

Figure 2.2 Continued

Continued overleaf

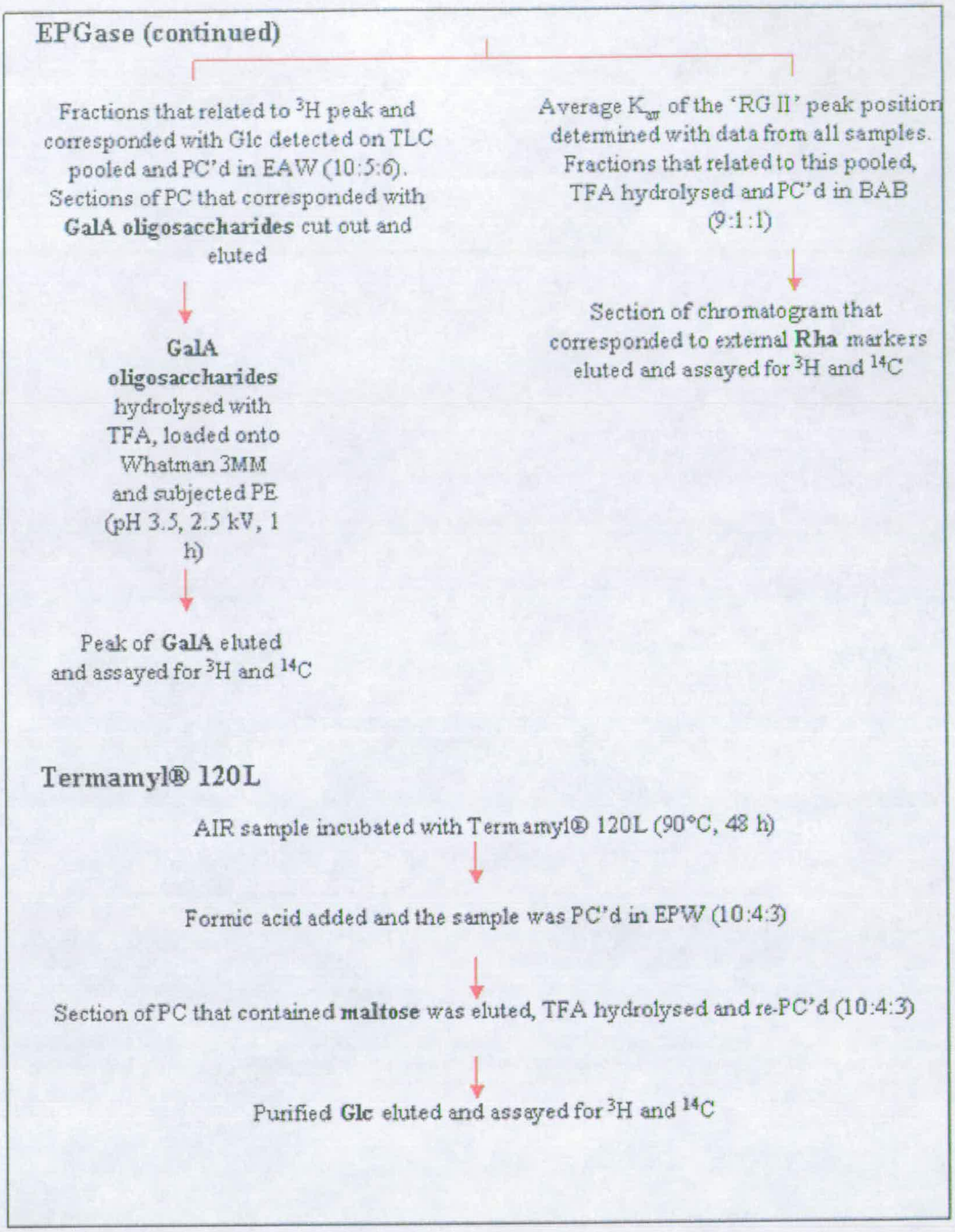

Figure 2.2 Continued

Continued overleaf

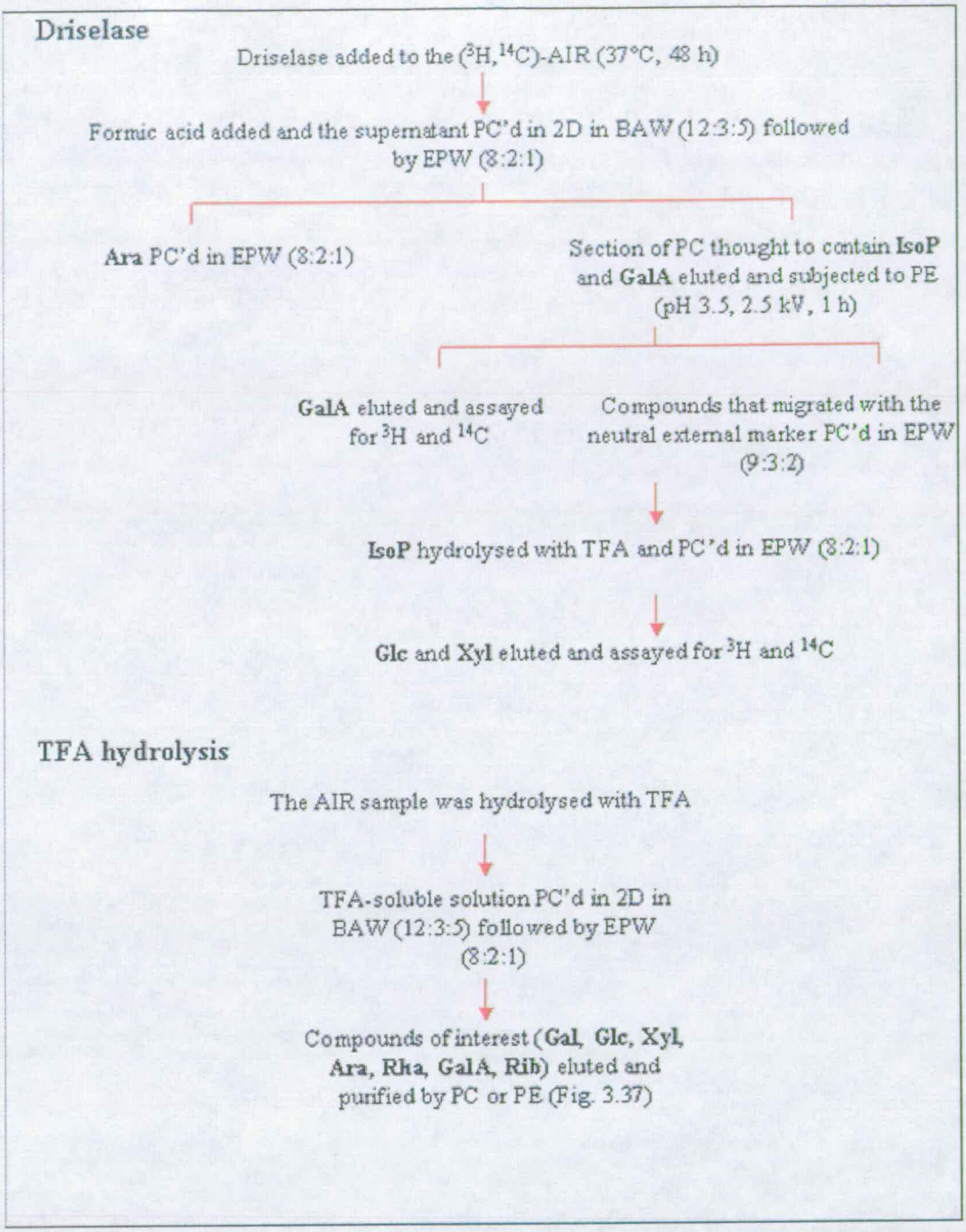

Figure 2.2 Continued

refrigerated. CMW was added to the aqueous phase and thoroughly mixed. The tubes were centrifuged (3200 rpm, 15 min). The lower phase was again removed and pooled with the previous extraction. Methanol (80% v/v) was used to form and wash the AIR. Methanol (80% v,v) was added to each tube to make a single phase with a final volume of 9 ml. The tubes were shaken and centrifuged (3200 rpm, 10 min) to pellet the AIR. A portion (5 ml) of the supernatant was removed and stored. More methanol (80% v/v, 5 ml) was added to each tube and the contents were thoroughly suspended. The tubes were centrifuged (3200 rpm, 10 min). A portion (5 ml) of the supernatant was removed and combined with the previously removed supernatant. The methanol wash process was repeated six more times using 10 ml of methanol and removing 10 ml of supernatant each time. In the final wash, enough supernatant was removed to leave 2 ml in each tube. An AIR–methanol suspension was formed in each tube. A 100-µl portion of each suspension was dispensed into a screw-cap Sarstedt tube and left to dry. A Driselase solution (1 ml, 0.5% w/v, PyAW 1:1:98 with 0.5% CB) was added to each Sarstedt tube and gently shaken at 37°C for 72 h. Formic acid was added to each tube to a final conc. 15% (v/v) and the contents of each tube were dispensed into a scintillation vial. The volume of sample was increased to 2 ml with water and 'Hisafe OptiPhase' (20 ml) was added. The radioactivity was assayed to determine the radioactivity present in each parent sample (Worked example 2.9.1, part 1). With this information the volume of AIR suspension required to form a 5:1 ^{3}H:^{14}C (Bq/Bq) ratio could be calculated.

Each of the ^{3}H-labelled AIR suspension samples were subdivided into five × 300-µl portions that were directly pipetted into scintillation vials. The ^{14}C-labelled AIR suspension samples were also divided into five portions but in this case the

volume of ^{14}C sample used was based on the radioactivity contained in each sample's associated Driselase digest. The volume of ^{14}C sample dispensed into a scintillation vial was judged so as to form an approximately known ^{3}H:^{14}C ratio to a partnered ^{3}H sample. The volume in each scintillation vial was increased to 1 ml with H_2O. 'Hisafe OptiPhase' was added and the radioactivity was assayed. The same sample was later transferred from the scintillation vial into a centrifuge tube to combine each ^{14}C-labelled sample with its partnered ^{3}H-labelled sample. The AIR samples were washed with a total of 75 ml (6 × 15 ml) acetone to remove the scintillation fluid. Care was taken not to remove any AIR.

The acetone was removed and the AIR was dried. The five portions containing a known ^{3}H:^{14}C were exposed to one of each of the following treatments: cellulase (section 2.11.1), endopolygalacturonase (section 2.11.2), Termamyl® 120L (section 2.11.3), Driselase (section 2.11.4) or TFA hydrolysis (section 2.11.5).

2.11.1 Cellulase treatment

A 250-µl aliquot of a suspension of *endo*-1,4-β-D-glucanase preparation (EC 3.2.1.4) from *Trichoderma longibrachiatum* (Megazyme, 53 U/mg) was dissolved in 2.25 ml PyAW (1:1:98 in 0.5% w/v CB). Ammonium sulphate was removed with a PD-10 column (Sephadex G-25M; bed volume 9 ml; Pharmacia) which had been washed with PyAW (25 ml, 1:1:98 in 0.5% w/v CB). The cellulase solution (2.5 ml) was added to the column and 2.5 ml of eluent was rejected. PyAW (3.5 ml, 1:1:98 in 0.5% w/v CB) was added to the column and 3.5 ml of eluent (desalted enzyme) was collected.

The de-salted enzyme preparation (420 µl) was added to each AIR sample, gently shaken at 37°C for 2 d and frozen. Portions (10 µl) of each sample solution

were assayed for radioactivity. Formic acid (final conc. 15% w/v) and markers were added to the samples that remained and each sample was loaded onto a Bio-Gel P-2 column (150-ml bed volume, washed with PyAW 1:1:98 in 0.5% CB). A portion (5 μl) of each fraction was spotted onto a silica-gel TLC plate, run in BAW (2:1:1, 8 h) and stained with thymol. Fractions that showed the strongest intensity of Glc were run on Schleicher and Schuell 2045 B paper in EPW (10:4:3, 130 h). The chromatogram was cut into strips, which were assayed for radioactivity. The sections of chromatogram that corresponded with a peak of radioactivity and external Glc marker were pooled, washed with toluene and eluted. The Glc was further purified by paper chromatography (Whatman 3MM, EPW 8:2:1, 28 h) and the radioactive Glc detected as in the previous chromatogram. The strips of paper that corresponded with a peak of radioactive Glc were washed in toluene. The Glc was eluted, dried, redissolved (2 ml H_2O) and assayed for ^{3}H and ^{14}C.

Bio-Gel P-2 fractions that eluted approximately with the internal marker (XLLG) were pooled, dried and digested with Driselase (200 μl, 0.5% in w/v PyAW with 0.5% w/v CB, 37°C, 48 h). The samples were each treated with formic acid (final conc. 15% v/v), loaded onto Whatman no. 1 and run in EPW (9:3:2, 21 h). The chromatogram was cut into strips, which were assayed for radioactivity. Strips that corresponded with IsoP and Gal were washed with toluene; the sugar was eluted, dried, redissolved (100 μl H_2O) and treated as in Table 2.2.

Table 2.2 Treatment of monosaccharides and disaccharides obtained from digested xyloglucan oligosaccharides

Compound	Treatment
IsoP	Hydrolysed with TFA (2 M, 120°C, 1 h), run on Whatman no. 1 in EPW (9:3:2, 21 h)
Gal	Run on Schleicher and Schuell 2045 B in EPW (8:2:1, 120 h)

Each chromatogram was cut and assayed for radioactivity. The strips that corresponded with both the relevant markers and peaks of radioactivity were washed with toluene. The sugars were eluted, dried and redissolved in 2 ml of H_2O and assayed for ^{3}H and ^{14}C.

2.11.2 EPGase treatment

EPGase was used to obtain a ^{3}H:^{14}C ratio of RG-II-derived Rha.

The EPGase preparation (EC 3.2.1.15, 1440 U/mg protein; Sigma) was desalted as per section 2.11.1. To discourage lactone ring formation of GlcA NaOH (100 µl, 0.1 M) was added to each AIR sample (25°C, overnight) followed by acetic acid (100 µl, 0.25 M in 0.5% w/v CB). The desalted EPGase solution (375 µl) was added to each AIR sample and gently shaken at 37°C for 48 h. A small portion (10 µl) of each solution was assayed for radioactivity. Formic acid (final conc. 15% w/v), Glc (400 µg) and blue dextran (250 µg) were added and the mixture was loaded onto a Sepharose CL-6B column (150-ml bed volume, washed with PyAW 1:1:98 in 0.5% CB). A portion (2 µl) of each fraction was run by TLC in BAW (2:1:1) and stained with thymol. A further portion of each fraction (100 µl) was assayed for radioactivity. Fractions that related to a ^{3}H peak and corresponded with a monosaccharide marker detected on the TLC plate were pooled, dried, redissolved

(100 µl H_2O) and loaded run on Schleicher & Schuell 2045 B paper in EPW (10:5:6, 52 h). The section of sample track that corresponded with the GalA oligosaccharides was cut out, eluted and dried. The GalA oligosaccharide sample was TFA hydrolysed (2 M, 120°C, 1 h). The hydrolysate was run on Whatman 3MM paper by electrophoresis (pH 3.5, 2.5 kV, 1 h). The electrophoretogram was cut into strips, which were assayed for radioactivity. Strips that related to a peak of radioactivity that corresponded with an external GalA marker were pooled and washed with toluene; the sugar was eluted, dried, redissolved in 2 ml H_2O and assayed for ^{3}H and ^{14}C.

The K_{av} of the 'RG-II' peak position, recognised as the peak that eluted before the internal monosaccharide marker, was determined for each of the eight sample repeats and an average K_{av} value was taken. The fraction that related to the average K_{av} was pooled with four fractions on either side and the five combined fractions were dried, TFA hydrolysed (100 µl, 2 M, 120°C, 1 h) and run on Schleicher and Schuell 2045 B paper in BAB (9:1:1, 16 h). Each sample track area that corresponded with an external Rha marker was eluted, dried and redissolved in 2 ml H_2O. Each RG-II-derived Rha sample was assayed for ^{3}H and ^{14}C.

2.11.3 Termamyl® 120L

In order to obtain starch-derived Glc, Termamyl® 120L preparation (50 µl) was diluted in MES buffer (4.5 ml, 50 mM, pH 6.0, Na^{+}) and 0.5 ml was added to each AIR sample, incubated (90°C, 48 h) and frozen. The samples were centrifuged (2500 rpm, 20 min) and 10 µl of the supernatant was assayed for radioactivity. A portion (250 µl solution) of each Termamyl® 120L-digested sample was dried in a

SpeedVac and redissolved in 100 µl H_2O. Formic acid was added at a final conc. of 15% v/v. The samples were run on Schleicher and Schuell 2045 B paper in EPW (10:4:3, 24 h). The chromatogram was autoradiographed and the section of paper that related to radiolabelled maltose was eluted. The eluted maltose was dried and TFA hydrolysed (1 ml, 2 M, 120°C, 1 h). The hydrolysate was run on Schleicher and Schuell 2045 B paper in the same solvent system as before for 50 h. The chromatogram was cut into strips and assayed for radioactivity. The strips of paper that corresponded with an external Glc marker and a peak of radioactivity were pooled, eluted, dried, redissolved in 2 ml H_2O and assayed for ^{3}H and ^{14}C.

2.11.4 Driselase digestion

Driselase was utilised to obtain Ara from the cell wall and xyloglucan-derived Glc and Xyl.

To each AIR sample 150 µl of Driselase 0.5% (w/v) in PyAW (1:1:98 in 0.5% w/v CB) was added. The sample was incubated at 37°C whilst gently shaking for 48 h and frozen. A sample (10 µl) of the digest solution was assayed for radioactivity. Formic acid was added (final concentration 15% v/v) and the samples were paper chromatographed (BAW 12:3:5 followed by EPW 8:2:1) in 1D. The chromatogram was autoradiographed and the radiolabelled compounds were identified with external markers, eluted, dried and redissolved (50 µl, H_2O). The neutral monosaccharides were purified by a second paper chromatography system (Fig. 3.34), then eluted, dried, redissolved in 2 ml H_2O and assayed for ^{3}H and ^{14}C.

The eluted sample thought to contain radiolabelled uronic acids and isoprimeverose was subjected to paper electrophoresis (pH 3.5, 2.5 kV, 1.5 h). The purified GalA was eluted, dried, redissolved in 2 ml H_2O and assayed for ^{3}H and ^{14}C.

The neutral compounds on the electrophoretogram were eluted, dried, redissolved in 100 µl H_2O and run on Schleicher and Schuell paper 2045 B in EPW (10:4:3, 130 h). The chromatogram was cut into strips which were assayed for radioactivity. The strips that showed a peak of radioactivity and corresponded with an external IsoP marker were pooled and washed with toluene. The IsoP sample was eluted, dried and TFA hydrolysed (2 M, 120°C, 1 h). The hydrolysate was run on Schleicher and Schuell 2045 B in EPW (8:2:1, 48 h). The chromatogram was cut into strips and the sections of paper that contained radiolabelled Glc or Xyl were washed with toluene and eluted. The eluted monosaccharides were dried, redissolved in 2 ml H_2O, and assayed for ^{3}H and ^{14}C.

2.11.5 TFA hydrolysis

TFA hydrolysis was used to obtain total Gal, Xyl, Ara, GalA, Rha, Rib and Glc that was derived from starch and the cell wall. In addition to this the TFA-insoluble material enabled cellulosic Glc to be obtained. TFA (2 M, 1 ml) was added to each AIR pellet, heated (120°C, 1 h) and centrifuged (3000 rpm, 10 min). A sample (10 µl) of TFA-soluble material was assayed for radioactivity. A further portion of the supernatant (550 µl) was dispensed into a screw-cap Sarstedt tube, dried and redissolved in H_2O (50 µl). The monosaccharides were purified by paper chromatography and paper electrophoresis (Fig. 3.37). The purified samples were eluted from the paper and ^{3}H and ^{14}C were assayed.

2.12 Analysis of the ^{3}H:^{14}C ratios of intermediary metabolites and incorporated monosaccharide residues over time

In this experiment the extraction of intermediary metabolites, over time, was used to identify the sequence of labelling in the metabolites to potentially identify the predominant pathway in each of the competing pathways of sugar nucleotide synthesis. An outline of the experimental protocol for this section is given in Fig. 2.3.

Arabidopsis cell-suspension culture was transferred from Glc medium to glycerol medium. After 3 d the cells were filtered through three layers of muslin. The fine cell-suspension (filtrate) was adjusted to a 10% SCV and 400 µl was dispensed into each of thirty glass flat-bottomed screw-cap vials. A stock solution that contained both [U-^{14}C]Fru (240 kBq) and [1-^{3}H]Gal (490 kBq) in 20 µl H_2O was added to each vial. The cells were incubated for various lengths of time and then killed with 1.6 ml of a solution of ethanol:formic acid (7:1) and allowed to shake gently over night at room temperature. The insoluble material was allowed to sediment and 1.5 ml of supernatant was transferred into a screw-cap Sarstedt tube, dried and redissolved in 100 µl H_2O. The samples were stored at –80°C. Selected samples were thawed and subjected to paper electrophoresis (pH 2.0, 1.5 kV, 1 h) on Whatman 3MM paper. External markers were stained with molybdate and the sample tracks were autoradiographed. The electrophoretograms were subdivided into four zones (section 2.12.1 – 2.12.2), which were eluted and dried.

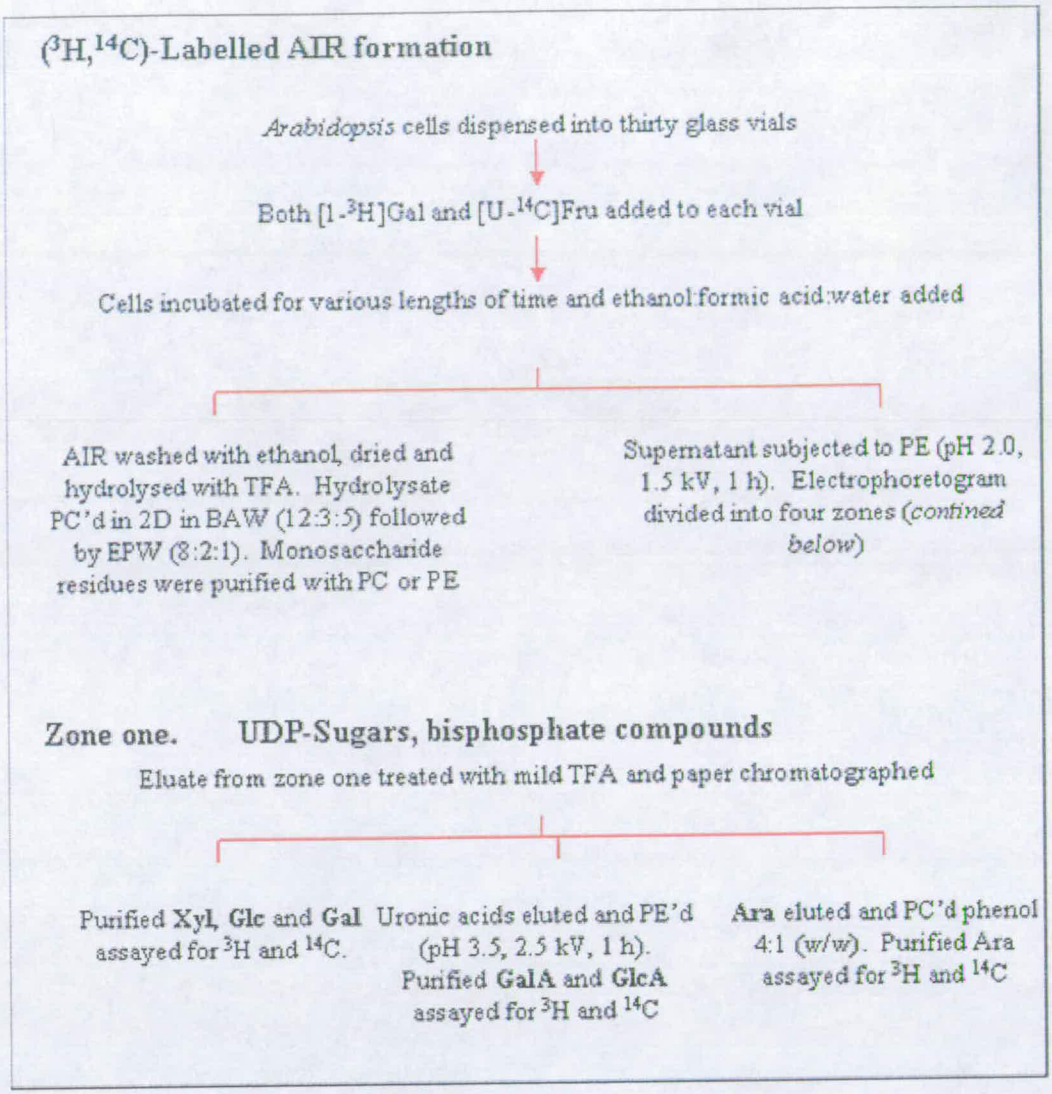

Figure 2.3 Overview of protocol used to determine the ^{3}H:^{14}C ratios of intermediary monosaccharides and incorporated monosaccharides over time
Continued overleaf

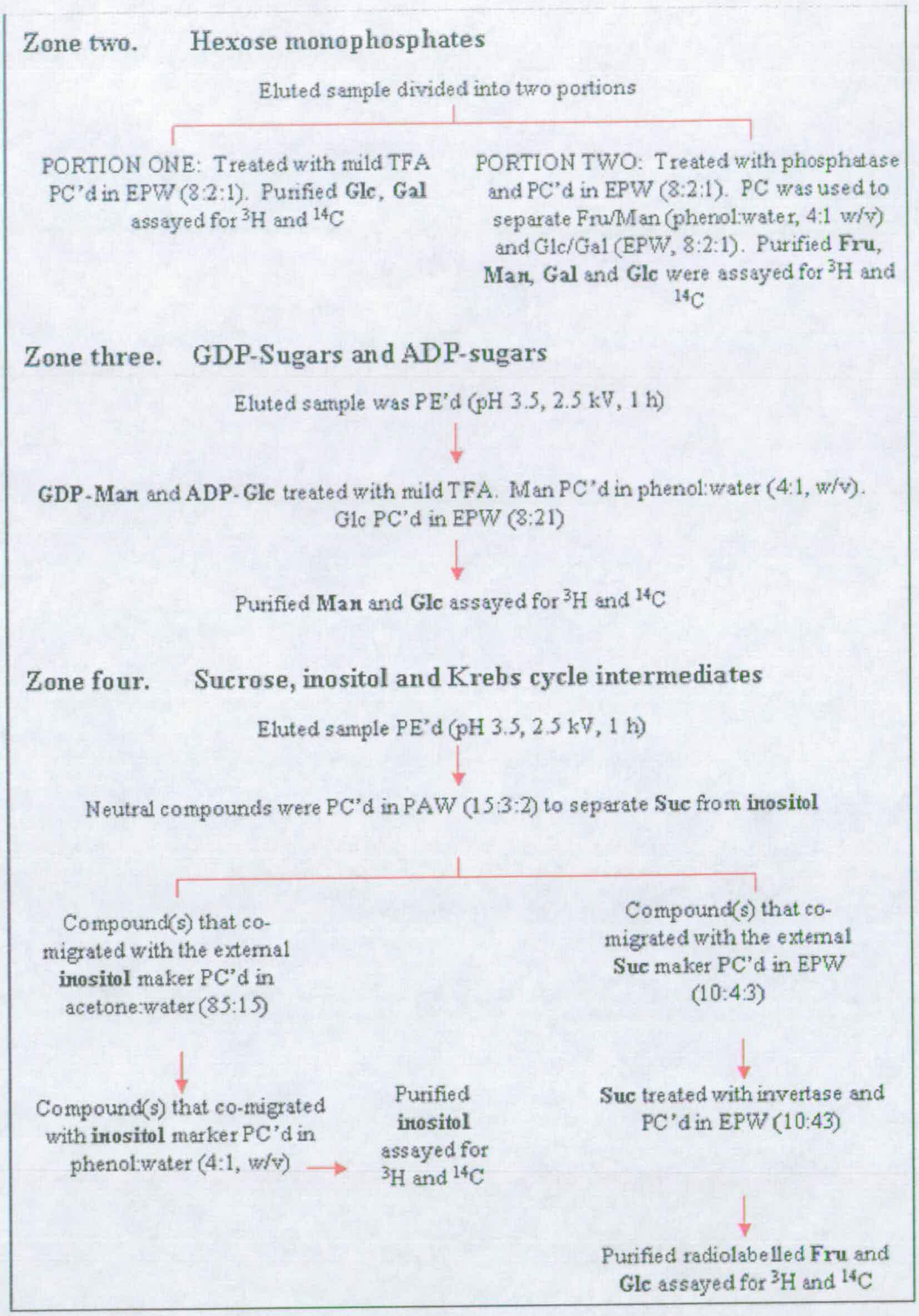

Figure 2.3 Continued

2.12.1 Zone 1 — Bisphosphate compounds and UDP-sugars

Each sample was TFA hydrolysed (50 µl, 0.1 M, 100°C, 25 min) in order to release the monosaccharide of interest from the UDP. The samples were run on Whatman 3MM paper in BAW (12:3:5, 17 h) followed by EPW (8:2:1,17 h) and the chromatograms were autoradiographed. The purified radiolabelled sugars were eluted, dried, redissolved in 2 ml H_2O and assayed for ^{3}H and ^{14}C. The sections of paper that contained sugars that were thought to be radiochemically impure (uronic acids and Ara) were eluted and dried. The eluted sugars were redissolved in 50 µl H_2O. The uronic acids were purified by paper electrophoresis (pH 3.5, 2.5 kV, 1.5 h) and Ara was purified by paper chromatography (phenol:water, 4:1 w/w). The sample tracks were cut into sections and assayed for radioactivity. Strips that contained radioactivity that had co-migrated with a relevant external marker were pooled. The sections of paper were washed with toluene, dried and eluted. The eluted sugars were redissolved in 2 ml H_2O and assayed for ^{3}H and ^{14}C.

2.12.2 Zone 2 — Monophosphate compounds

Each sample was redissolved in 100 µl H_2O and divided into two portions.

One portion was treated with mild TFA (900 µl, 0.1 M final conc., 100°C, 25 min), dried, redissolved (50 µl H_2O) and paper chromatographed (EPW, 8:2:1). The Glc and Gal separated compounds were eluted, dried, redissolved in 2 ml H_2O and assayed for ^{3}H and ^{14}C.

The remaining portion was dried in a SpeedVac, digested with acid phosphatase (EC 3.1.3.2) (100 µl, 1% w/v in PyAW 1:1:98 with 0.5% CB w/v) and the compounds were separated with paper chromatography (EPW, 8:2:1). Fru and

Glc were eluted, dried, redissolved and further purified with paper chromatography (phenol:water, 4:1 w/w; EPW, 8:2:1, respectively). The purified compounds were eluted, dried, redissolved in 2 ml H_2O and assayed for ^{3}H and ^{14}C.

2.12.3 Zone 3 — GDP-sugars and ADP-sugars

At pH 6 both GDP-sugars and ADP-sugars have a similar net charge and cannot be separated. The samples were redissolved in 50 µl H_2O and subjected to paper electrophoresis (pH 3.5, 2.5 kV 1 h). At pH 3.5 guanosine has a greater electrophoretic mobility than adenine that enables both compounds to be separated from one another. The radiolabelled compounds that co-migrated with GDP-Man or ADP-Glc were each cut out, eluted, dried and hydrolysed with TFA (900 µl, 0.1 M final conc., 100°C, 25 min). The samples were dried, redissolved in 50 µl H_2O and separated by paper chromatography (phenol:water, 4:1 w/w; EPW, 8:2:1, respectively). The sample tracks were cut into sections and assayed for radioactivity. The pieces of paper that contained radiolabelled Man and Glc were washed with toluene. The radiolabelled Man and Glc were eluted and dried. The eluted sugars were redissolved in 2 ml H_2O and assayed for ^{3}H and ^{14}C.

2.12.4 Zone 4 — Neutral compounds

In addition to the neutral compounds isolated from the initial separation procedure, compounds that did not migrate but were ionised at pH 2 were also contained in the 'neutral' zone. To separate the neutral compounds from the compounds with ionisable groups, the samples were redissolved in 50 µl H_2O and subjected to paper electrophoresis (pH 3.5, 2.5 kV, 1.5 h) at a higher pH. The neutral band was eluted, dried, redissolved in 50 µl H_2O and the compounds separated with paper

chromatography (PAW 15:3:2). Radiolabelled Suc and inositol were eluted, dried and redissolved (50 µl H_2O). The inositol was purified in two separate paper chromatography solvent systems (acetone:water, 85:15; phenol:water, 4:1 w/w). The Suc was paper chromatographed (EPW, 10:4:3), eluted, dried and redissolved in 1 ml MOPS (50 mM, Na^+ in 0.5% CB w/v) that contained 10 µl of an invertase preparation (Biochemical, BDH, 3000 U/ml). The digest was dried and paper chromatographed (EPW, 10:4:3). Fru was eluted from the chromatogram and the Glc purified further with paper chromatography and eluted (EPW, 10:4:3). The Fru and Glc samples were dried, redissolved in 2 ml H_2O and assayed for ^3H and ^{14}C.

3. Results

3.1 Development of experimental protocol

3.1.1 [1-^{3}H]Gal stock solution purity and specific activity

The purity of the [1-^{3}H]Gal stock solution was investigated by paper chromatography with two different solvent systems (Fig. 3.1). Unlike the BAW solvent front, the EPW solvent front was allowed to run off the end of the paper. The lower number of total cpm detected on chromatogram B (Fig. 3.1) was possibly a result of radiolabelled contaminants that had dripped off the end of the chromatogram. The ^{3}H cpm that co-migrated with an external Gal marker on chromatogram B accounted for only 37% of the total cpm detected on chromatogram A. This indicated a high proportion of contamination in the [^{3}H]Gal stock that could not be attributed to ^3H_2O as the [^{3}H]Gal was originally dried onto the paper. For this reason the [1-^{3}H]Gal stock solution was purified by preparative paper chromatography.

For determination of the SA of the [1-^{3}H]Gal stock solution, [^{3}H]Gal (1480 kBq) and serial dilutions of Gal were chromatographed on Schleicher and Schuell paper in EPW (8:2:1, 48 h) and stained with silver nitrate. The staining intensity of the [^{3}H]Gal track was compared to spots of Gal of known weight. The staining intensity of the [^{3}H]Gal stock solution indicated that it had a specific activity of 1.8×10^{14} Bq/mol.

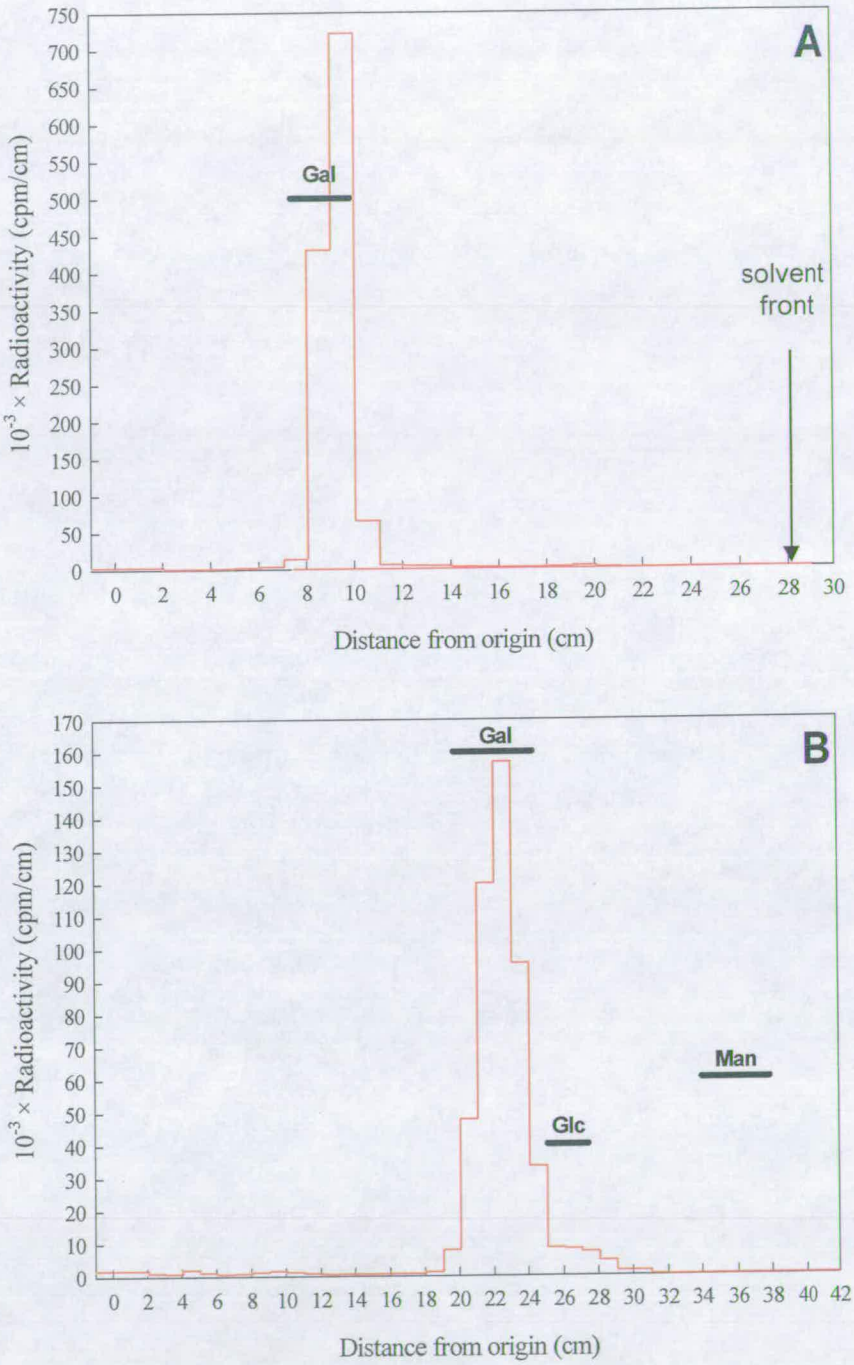

Figure 3.1 Determination of [1-^{3}H]Gal stock purity

[1-^{3}H]Gal stock solution was chromatographed on Whatman 3MM in (**A**) BAW (12:3:5, 7 h) or (**B**) EPW (8:2:1, 48 h). External markers (—) were stained with aniline hydrogen-phthalate.

3.1.2 [1-^{3}H]Gal, [U-^{14}C]Glc and [U-^{14}C]Fru uptake and radiolabel incorporation into the AIR by *Arabidopsis* cell-suspension culture

The model organism *Arabidopsis*, in cell-suspension culture, was chosen for experiments used throughout this project. Glycerol was selected as the carbon source to maintain the cells as it is less preferred than the radiolabelled monosaccharides that were fed to the cells. The use of glycerol optimises the uptake of trace [1-^{3}H]Gal, [U-^{14}C]Glc and [U-^{14}C]Fru and the incorporation of ^{14}C and ^{3}H into cell wall components. A rapid uptake allows a transient higher specific activity of radiolabel entry into the NDP-sugar intermediates. This eases their detection and isolation.

Glycerol-maintained *Arabidopsis* cell-suspension culture was fed [1-^{3}H]Gal or [U-^{14}C]Glc and the disappearance of each isotope from the medium was monitored. The majority of [^{14}C]Glc and [^{3}H]Gal was taken up in 1 h (Fig. 3.2). The cells had taken up 88% of the total ^{14}C and 48% (net) of the ^{3}H by 7.5 h. The cells did not take up 100% of the radioactivity, probably because the majority of the radioactivity that 'remained' in the medium was not in the original chemical form. The radioactivity detected is thought to consist of radiolabelled polysaccharides and metabolites that diffused or were sloughed into the medium. Indeed, at 7.5 h, 77% of the detected ^{3}H could be attributed to volatile ^{3}H-compounds thought to be predominantly $^{3}H_2O$.

Approximately 30% of ^{14}C and 23% of ^{3}H had been incorporated into the AIR at 7.5 h.

The kinetics of radiolabel incorporation into the AIR and disappearance from the ASF of glycerol-maintained *Arabidopsis* cell-suspension culture was investigated. *Arabidopsis* cell-suspension culture that was fed [U-^{14}C]Glc reached a

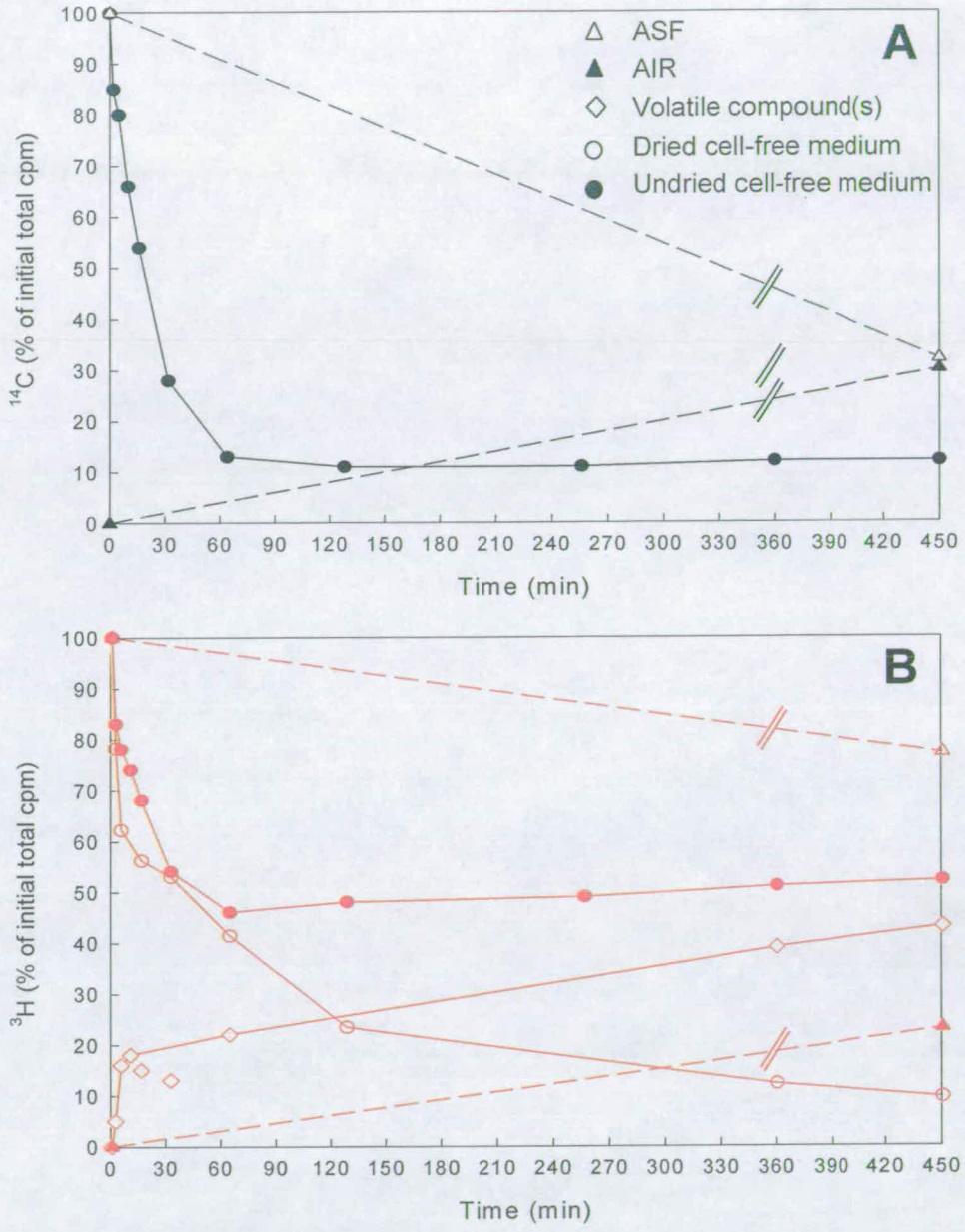

Figure 3.2 Net uptake of ^{14}C and ^{3}H by *Arabidopsis* cell-suspension culture

Glycerol-maintained *Arabidopsis* cell suspension culture (5 ml/pot, fine cell suspension, 10% SCV) aged 2 d was dispensed into Sterilin pots and shaken (1 h). [U-^{14}C]Glc (42 kBq, 100 µl in H_2O) (**A**) or [1-^{3}H]Gal (37 kBq, 100 µl in H_2O) (**B**) was added to each culture at t=0 and at intervals two 50-µl samples of cell-free medium were taken. One sample was dried. Both of the samples were assayed for radioactivity. Ethanol (22 ml, 80% v/v) was added to each pot at 450 min. The AIR was washed with ethanol (500 ml, 80% v/v). A sample (1 ml) of the ASF was assayed for radioactivity. A 2-ml AIR suspension was formed and 50 µl of suspension assayed for radioactivity. The cell-free medium is included in the ASF. In **A** the radioactivity attributed to (◊) volatile compound(s) was calculated as the radioactivity that could not be accounted for by the AIR and ASF. In **B** the level of radioactivity obtained for the dried cell-free medium sample was deducted from that of the cell-free medium sample that had not been dried. This was used to calculate the radioactivity attributed to (◊) volatile compound(s).

plateau of net radiolabel uptake and radiolabel incorporation into the AIR at 4 h (Fig. 3.3). At this point the cells had incorporated 24% of the ^{14}C into the AIR with 20% ^{14}C 'remaining' in the medium. At 8 h, only 64% of the total radioactivity was accounted for in AIR and ASF of the [^{14}C]Glc fed sample. The 36% that remained unaccounted for was presumed to be $^{14}CO_2$ produced by the cells owing to respiration.

[^{3}H]Gal was not taken up as rapidly as [^{14}C]Glc (Fig. 3.3). A plateau of ^{3}H uptake and radiolabel incorporation into the AIR was witnessed after 6 h. At the plateau 18% of the ^{3}H had been incorporated into the AIR.

In the initial experiment (Fig. 3.2) both isotopes were taken up within 1 h but in the subsequent one [^{3}H]Gal and [^{14}C]Glc were taken up within 4 h and 6 h respectively (Fig. 3.3). Every effort was made to ensure that the cultures were maintained under consistent conditions. However, variability can occur in a biological system without an obvious reason. Although uptake rate was variable, the maximum extent of uptake and incorporation had always been reached by 8 h. For this reason all subsequent feeding experiments were conducted over 8 h.

Cultures were monitored for their ability to take up and incorporate ^{14}C from [U-^{14}C]Fru. Fig. 3.4 shows that the cells had taken up the maximum ^{14}C from [^{14}C]Fru by 2 – 3 h. This was slower than the uptake of [^{14}C]Glc, whose maximum uptake was achieved by 30 min. The incorporation of ^{14}C from [^{14}C]Glc and [^{14}C]Fru into the AIR was 17%.

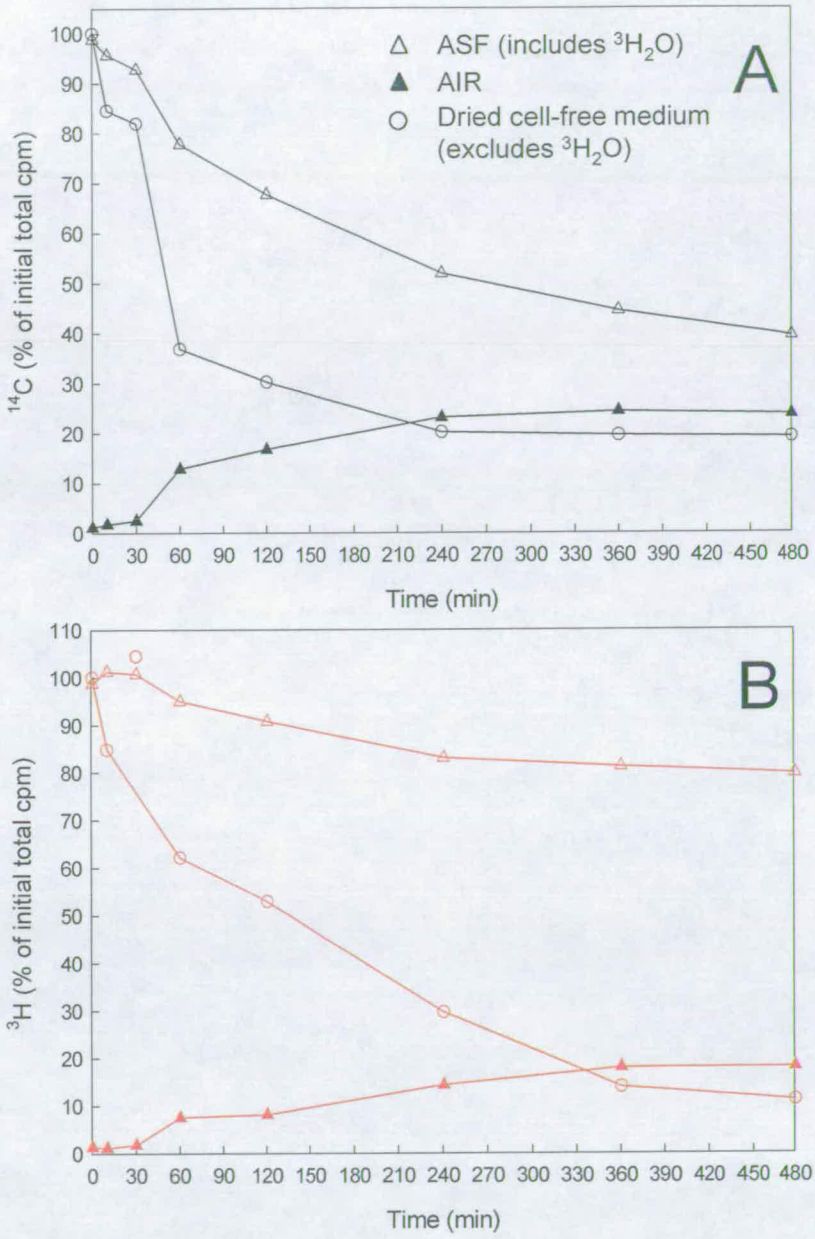

Figure 3.3 Kinetics of net ^{14}C and ^3H uptake and incorporation into the AIR by *Arabidopsis* cell-suspension culture

Glycerol-maintained *Arabidopsis* cell suspension culture (0.5 ml, fine cell suspension, 10% SCV) aged 2 d was fed (**A**) [U-^{14}C]Glc (37 kBq, 50 µl) or (**B**) [1-^3H]Gal (37 kBq, 50 µl) at t=0. A sample (20 µl) of cell-less medium was taken from each culture at t=0 and at intervals a second sample (20 µl) was removed from one ^{14}C vial and one ^3H vial and assayed for non-volatile radioactivity. Ethanol (2 ml, 80% v/v) was immediately added to the whole remaining culture after the second sample had been taken. The AIR was washed with ethanol (48 ml, 80% v/v) and the AIR fraction and ASF were both assayed for radioactivity. The radioactivity in the cell-free medium that was not incorporated into a polymer is included in the ASF.

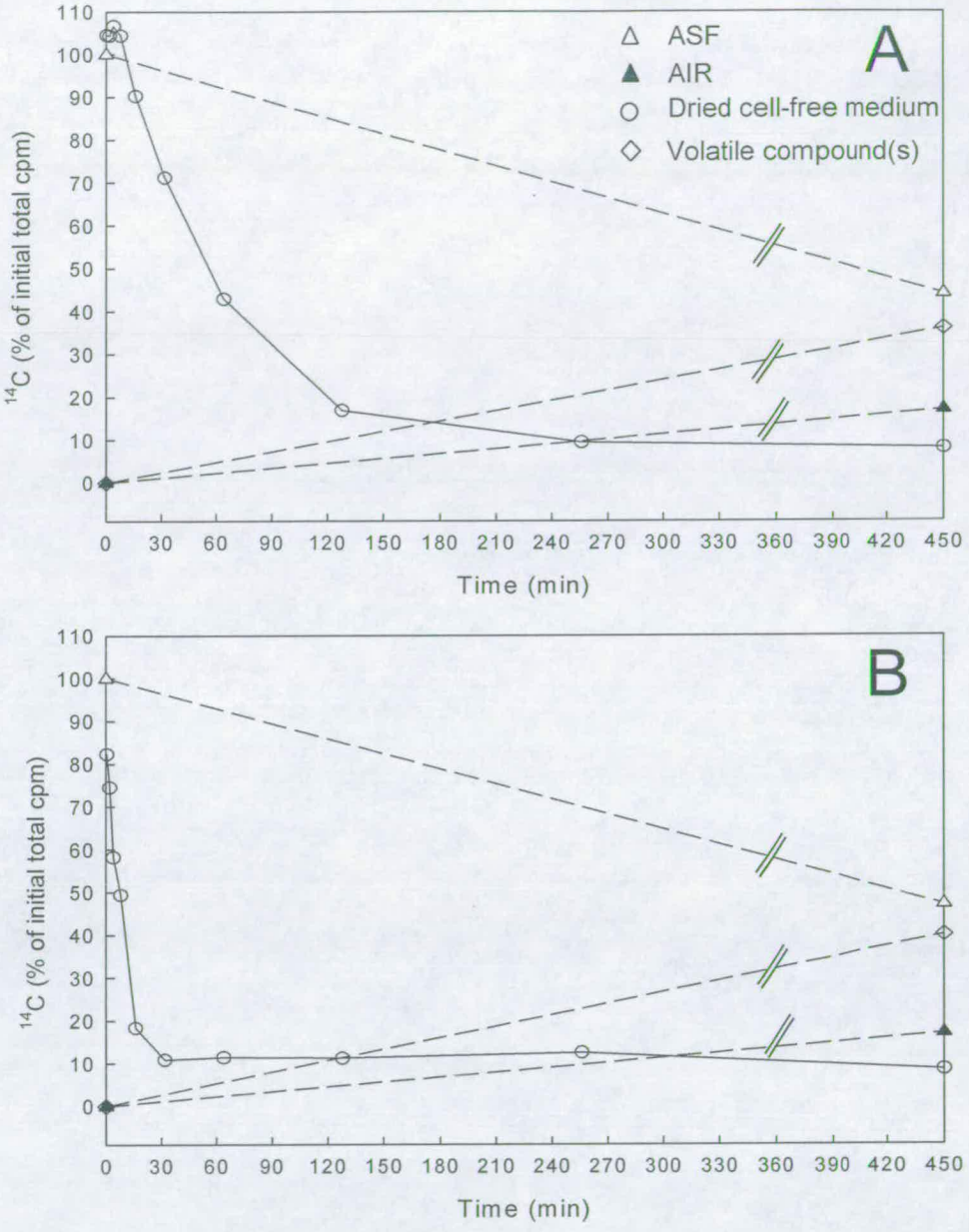

Figure 3.4 Uptake of [U-^{14}C]Fru or [U-^{14}C]Glc and incorporation by *Arabidopsis* cell-suspension culture

Arabidopsis cell-suspension culture (5 ml, fine cell suspension, 10% SCV), 3 d old, newly transferred from Glc to glycerol medium was fed (**A**)[U-^{14}C]Fru (37 kBq in 100 µl H_2O) or (**B**) [U-^{14}C]Glc (37 kBq in 100 µl H_2O). Cell-less medium (50 µl) was sampled from each culture and assayed for radioactivity. At 450 min 20 ml ethanol (80% v/v) was added to each culture and the AIR was washed with 500 ml ethanol (80% v/v). Portions of the AIR (200 µl suspension) and ASF (1 ml) were assayed for radioactivity. The radioactivity attributed to (◇) volatile compound(s) was calculated as the radioactivity that could not be accounted for by the AIR and ASF.

3.1.3 Attempt to increase radiolabel incorporation into AIR

The *Arabidopsis* cell-suspension culture grown on glycerol was originally maintained on Glc. Through continuous subculturing on glycerol, the cells might have adapted to glycerol. This could explain why the exogenous [1-^{3}H]Gal or [U-^{14}C]Glc was not taken up as readily in Fig 3.4 as in Fig 3.3. To counteract this the cells that were maintained on Glc were transferred to glycerol medium 3 d prior to experimentation and fed [1-^{3}H]Gal or [U-^{14}C]Glc.

The time taken to achieve maximum uptake was independent of whether the cells had been continuously subcultured on glycerol or newly transferred from Glc to glycerol medium (Fig. 3.5) and was similar to Fig. 3.4. This suggested that adaptation to glycerol was not an explanation for the slow uptake found in Fig. 3.4.

The total extent of ^{3}H incorporation (17%) into the AIR in both methods was comparable to that determined in Fig. 3.3. A 3% increase in ^{14}C incorporation into the AIR was found when cells were newly transferred onto glycerol medium from Glc medium. Therefore, cells were subsequently transferred from Glc medium to glycerol medium 3 d prior to experimentation.

3.1.4 Summary of radiolabel uptake and incorporation into the AIR by *Arabidopsis* cell-suspension culture

The results show that 9 – 12% and 10 – 15% of the radioactivity fed as [1-^{3}H]Gal or [U-^{14}C]Glc, respectively, was located in the culture medium at 7.5 – 8.0 h. By this time, 17 – 23% of the ^{3}H and 17 – 30% of the ^{14}C had been incorporated into the AIR. When cells were fed [U-^{14}C]Fru for 8 h, the cell-free medium contained 10% of the radioactivity and 17% had been incorporated into the AIR.

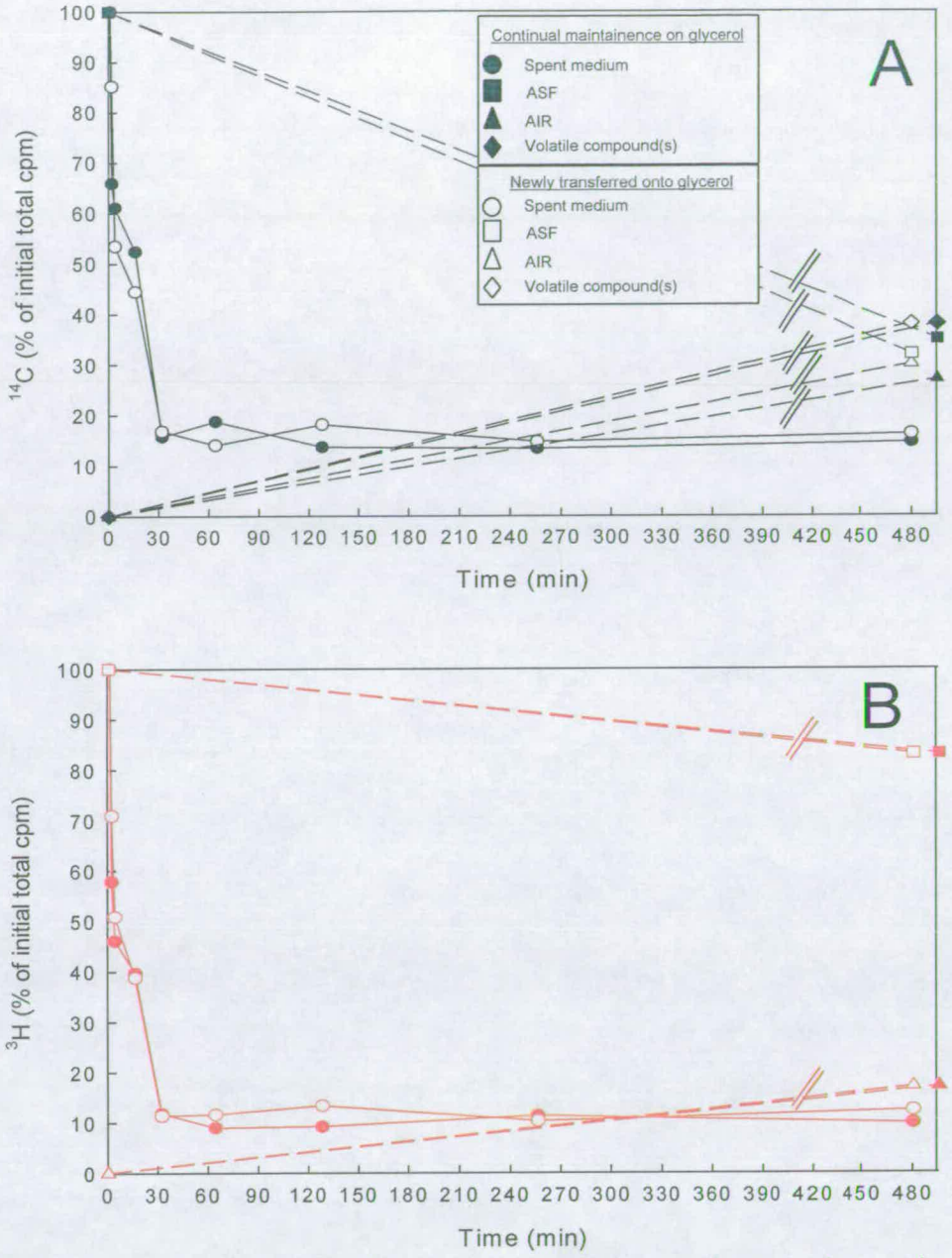

Figure 3.5 Effect of glycerol adaptation on the uptake and incorporation of [1-^{3}H]Gal or [U-^{14}C]Glc by *Arabidopsis* cell-suspension culture

Glc-maintained *Arabidopsis* cell suspension culture, aged 3 d, was subcultured onto glycerol medium. A line of *Arabidopsis* cell suspension culture that had been continually maintained on glycerol medium was also utilized. The cultures, aged 3 d, were adjusted to form a 10% SCV. The cells were transferred into four Sterilin pots (5 ml/pot) and gently shaken for 30 min. (**A**) [U-^{14}C]Glc (37 kBq in 100 µl H_2O) or (**B**) [1-^{3}H]Gal (37 kBq in 100 µl H_2O) was added. After selected time intervals cell-less medium was removed from each pot and assayed for non-volatile radioactivity. The level of radioactivity in the AIR was assayed at 480 min.

3.1.5 Apparent K_m values for Glc and Gal uptake systems

In order to estimate the maximum concentration of [1-^{3}H]Gal and [U-^{14}C]Glc which would be profitable to feed *Arabidopsis* cell-suspension cultures, it was necessary to determine the apparent K_m values for exogenous Gal and Glc uptake. The experiment was used to determine a concentration of radioisotope where the maximum radioactivity could be fed to a small number of cells that would take up as much radioisotope precursor as possible. The maximum radioactivity makes the detection of compounds much easier. As the major techniques utilised throughout this project were paper chromatography and paper electrophoresis, the use of a small number of cells minimises the potential to overload chromatograms and electrophoretograms.

Glycerol-maintained *Arabidopsis* cell-suspension cultures were incubated with different concentrations of either [1-^{3}H]Gal or [U-^{14}C]Glc. The apparent K_m values could be calculated from information on the uptake rates. Figure 3.6 (A) shows that the uptake rate of exogenous Glc was proportional to the Glc concentration within the range of 10 to 373 μM. The uptake rate at 373 μM was 0.5 μmol Glc/h/ml suspension.

A Lineweaver–Burke plot (Fig. 3.7) for uptake of exogenous Gal showed a K_m of approximately 240 μM and V_{max} of approximately 0.4 μmol Gal/ h/ ml suspension. This indicates that the maximum concentration at which it would be profitable to feed [1-^{3}H]Gal to *Arabidopsis* cell-suspension culture is less than 240 μM to ensure the ^{3}H fed to the cells is taken up in a short space of time.

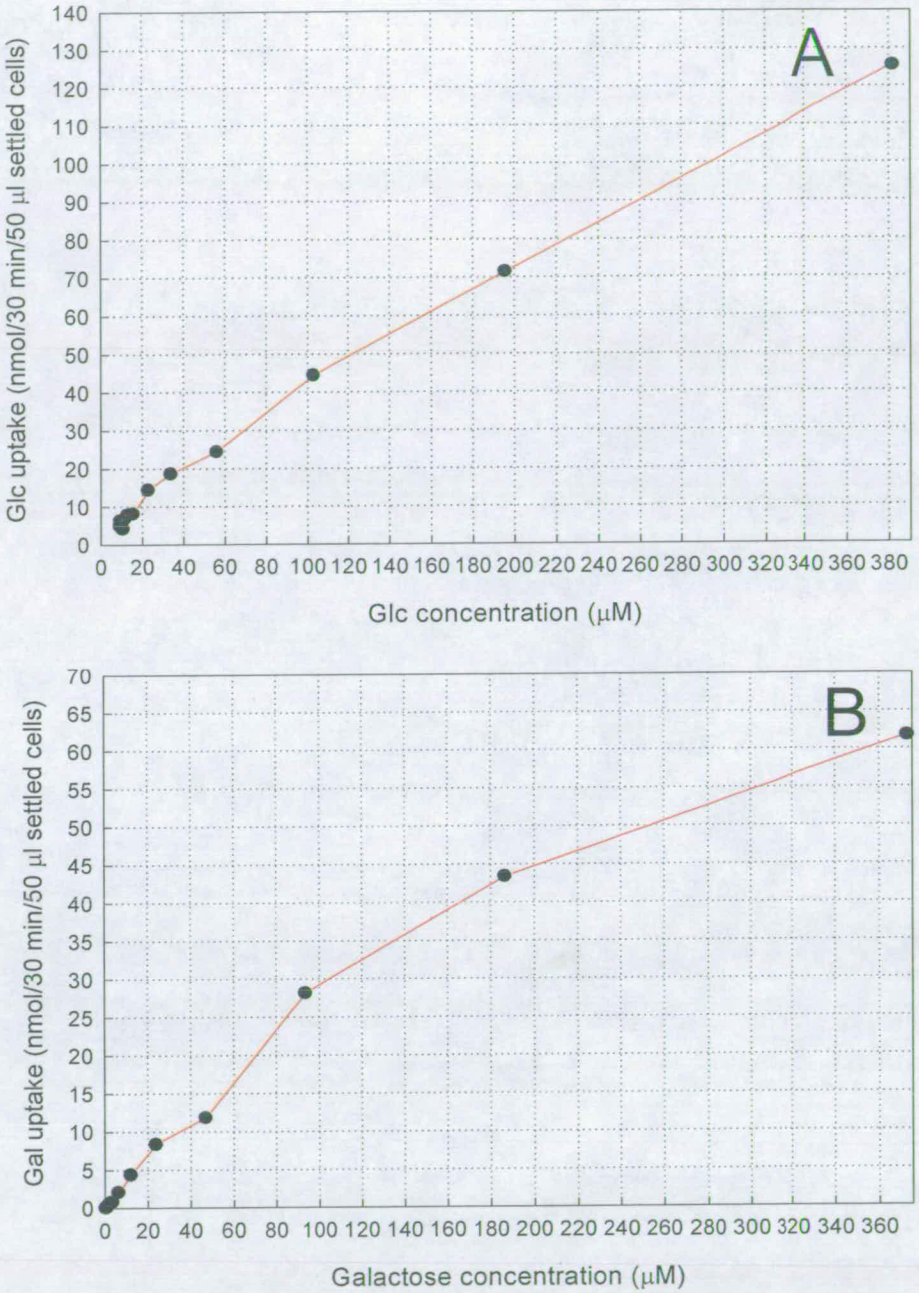

Figure 3.6 Effect of concentration on uptake rate of Glc and Gal in *Arabidopsis* cell-suspension culture maintained on glycerol

Glycerol-maintained *Arabidopsis* cell suspension culture, aged 2 d, was dispensed into glass vials (500 µl/vial, 10% SCV) and gently shaken (1 h). Dried [1-^{3}H]Gal (27 kBq/aliquot) samples were redissolved in a series of non-radioactive Gal concentrations (50 µl of 4 to 4096 µM) and dispensed into the glass vials. At time intervals cell-less medium was assayed for non-volatile radioactivity. This procedure was repeated using [U-^{14}C]Glc and serial dilutions of non-radioactive Glc. The rate of (**A**) Glc and (**B**) Gal uptake was calculated.

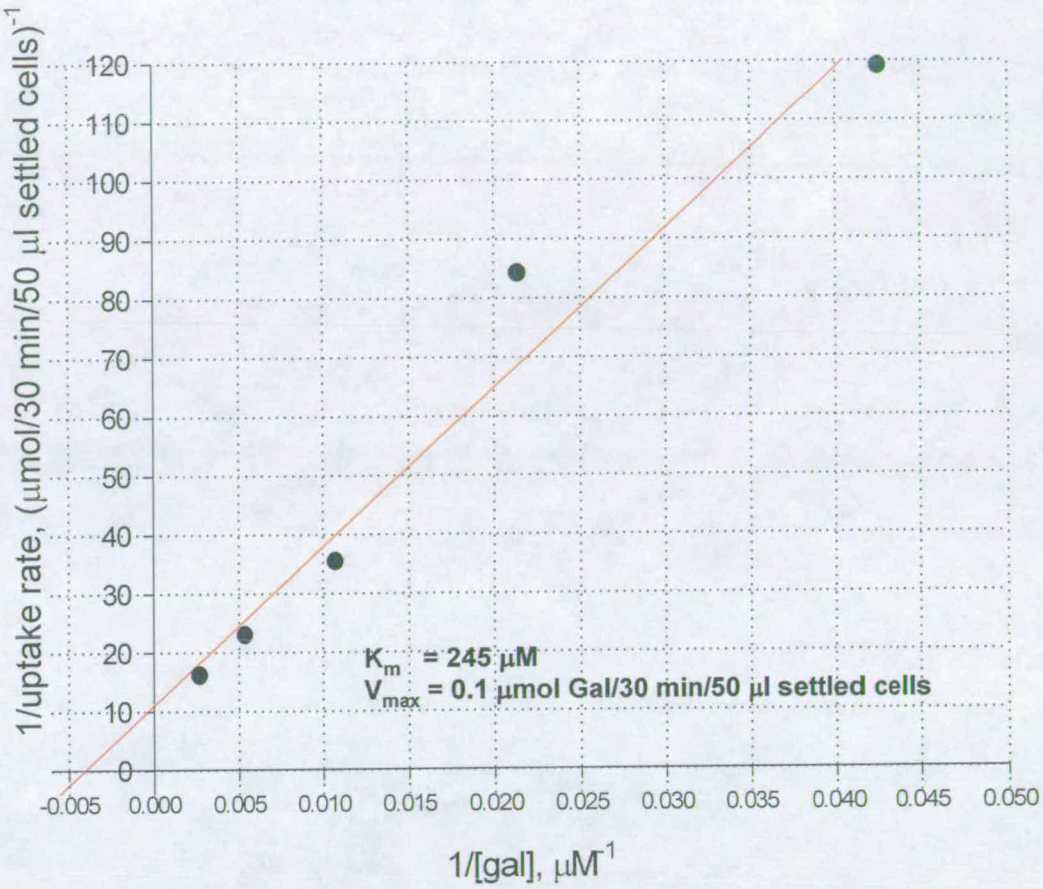

Figure 3.7 Lineweaver–Burke plot of exogenous Gal uptake in glycerol-maintained *Arabidopsis* cell-suspension culture

3.1.6 Potential loss of ^{3}H from (1-^{3}H)-labelled monosaccharides during acid treatment or incorporation into polysaccharides

The experimental outline (section 1.5) relies on the incorporation of ^{3}H into AIR polysaccharides to enable a ^{3}H:^{14}C ratio to be calculated. If there was loss of ^{3}H during chemical treatment of ^{3}H-monosaccharides or during their incorporation into polysaccharides the results obtained would not permit a true indication of the pathways involved.

3.1.6.1 Effect of prolonged exposure to TFA on various (^{3}H,^{14}C)-labelled monosaccharides

The lability of ^{3}H from (^{3}H,^{14}C)-labelled monosaccharides that had been isolated from the AIR with hot acid was investigated. TFA was added to a solution of a monosaccharide (Ara, Xyl, GalA, Rha, Glc and Rib) with a known ^{3}H:^{14}C ratio. The solution was heated and at intervals samples were paper chromatographed. The section of the chromatogram that contained the monosaccharide of interest was cut out and assayed for ^{3}H and ^{14}C. The results (Fig. 3.8) show that, in all cases, the both ^{3}H and ^{14}C in the parent monosaccharide decreased over 8 h. This indicates that the sugars are unstable in hot acid. Despite this, the ^{3}H:^{14}C (Bq/Bq) ratios (Fig. 3.8) remained at the value of the untreated control for a minimum of 4 h. Often at timepoints greater than 4 h, the radioactivity became too low for the ratio to be credible. However, the results from this experiment validated the protocol used to obtain the ^{3}H:^{14}C ratios of the component monosaccharides of AIR which never used more than 1 h in TFA.

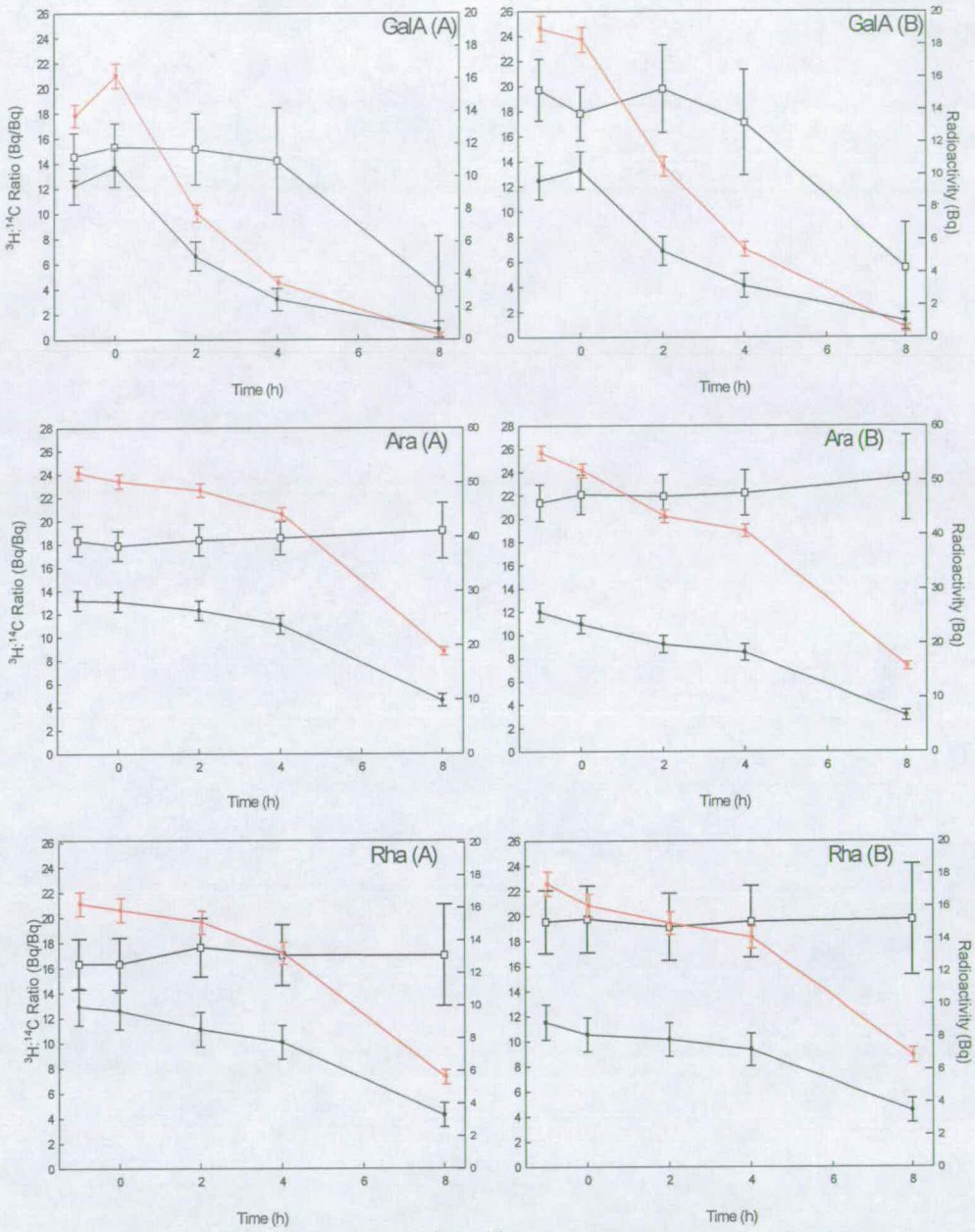

Figure 3.8 Effect of TFA on (^{3}H, ^{14}C)-labelled monosaccharides

[^{3}H,^{14}C]Monosaccharides, purified from the AIR of *Arabidopsis* cell suspension culture fed [U-^{14}C]Glc and [1-^{3}H]Gal (as in the experiment described in section 3.2.1), were subjected to TFA (500 µl, 2 M, 120°C) and re-purified by 1D paper chromatography (BAW 12:3:5, 16 h; EPW 8:2:1, 16 h on Whatman 3MM), eluted and assayed for ^{3}H and ^{14}C. The points shown at −1 h are values prior to the addition of TFA. The points shown at 0 h are values at room temperature after TFA addition. The level of ^{3}H (—) and ^{14}C (—) and the ^{3}H:^{14}C (Bq/Bq) ratio (—□—) are shown. The ^{14}C (Bq) values are inflated × 10. The error bars are unique to each timepoint and relate to the counting error of the detection method (section 2.8). A, B, C and D are repeats.

Continued overleaf

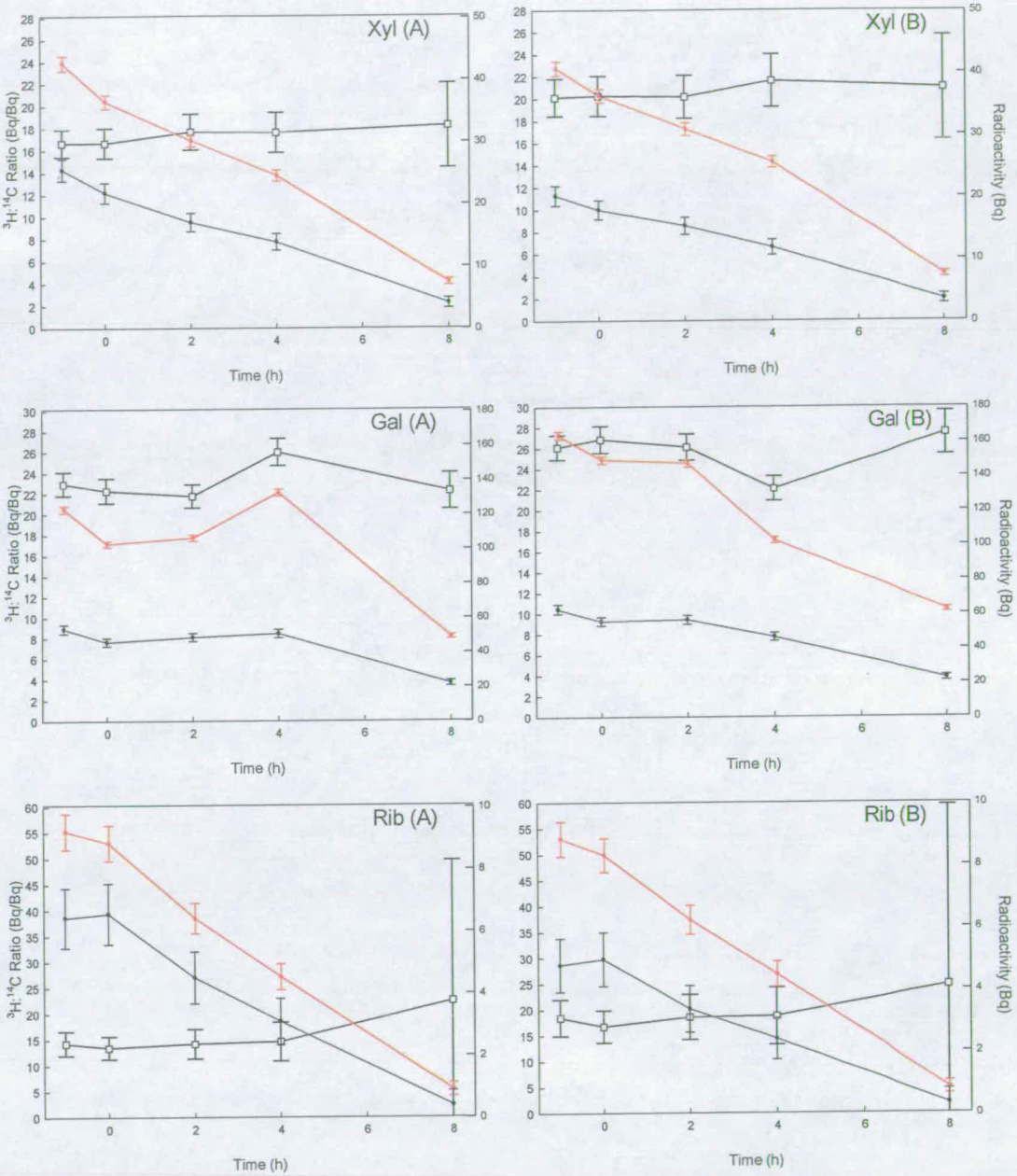

Figure 3.8 Continued

Continued overleaf

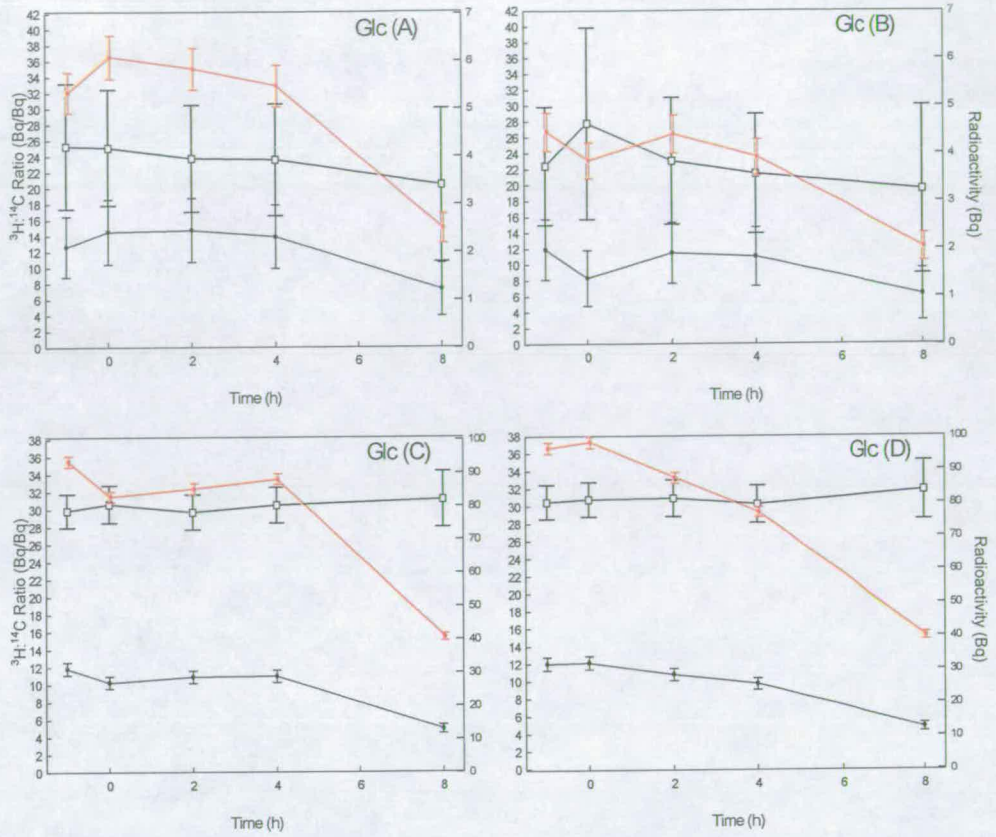

Figure 3.8 Continued

3.1.6.2 Lability of ^{3}H from NDP-[1-^{3}H]monosaccharides during transglycosylation in vivo

If NDP-[1-^{3}H]monosaccharides lost ^{3}H during transglycosylation (Fig. 3.9) the ^{3}H:^{14}C ratio of polysaccharide sugar residues would differ from that of their NDP-sugar precursors.

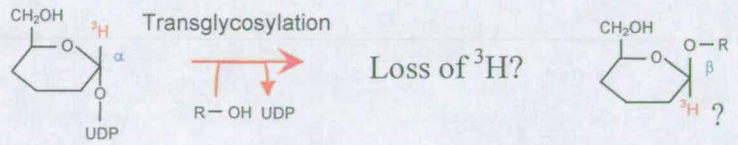

Figure 3.9 Potential loss of ^{3}H from position 1 due to transglycosylation

[1-^{3}H, 1-^{14}C]Ara was fed to *Arabidopsis* cell-suspension cultures. Ara was selected as it was thought to feed into a small, confined branch of the sugar-nucleotide interconversion pathway (Fig 3.10). If ^{3}H was lost during transglycosylation the Ara released from the AIR would have a lower ^{3}H:^{14}C ratio than the [^{3}H,^{14}C]Ara originally fed to the cells. However, this was not found to be the case. Both Ara and Xyl obtained from AIR were radioactive (Fig. 3.11) and had the same ^{3}H:^{14}C (Bq/Bq) ratio as the stock [^{3}H, ^{14}C]Ara (Fig. 3.12). This indicated that ^{3}H was not lost from position 1 during phosphorylation by arabinokinase, epimerisation, or transglycosylation.

The AIR was expected to yield radiolabelled Ara and Xyl. However, it also gave rise to small quantities of radiolabelled Glc and Gal (Fig 3.11). This suggests that the Xyl residue of UDP-Xyl could enter the pentose phosphate pathway and hence glycolytic intermediates could be radiolabelled (Fig. 3.10). The ^{3}H:^{14}C ratio of Glc and Gal are very similar to those of Xyl and Ara. Fig. 3.23 shows [1-^{3}H, 5-^{3}H]xylulose 5-P. The ^{3}H at C1 is highlighted in red. When the ^{3}H is traced in the

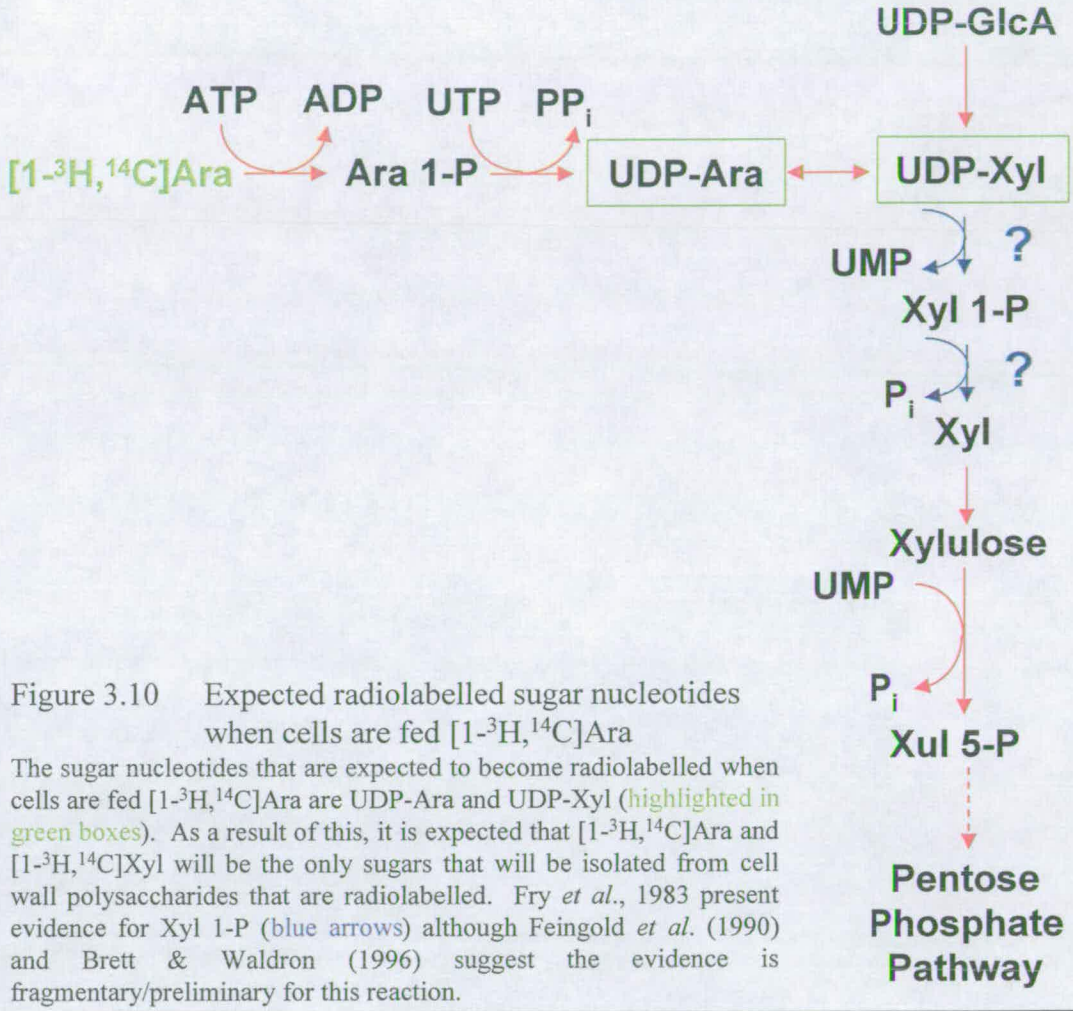

Figure 3.10 Expected radiolabelled sugar nucleotides when cells are fed [1-^{3}H,^{14}C]Ara

The sugar nucleotides that are expected to become radiolabelled when cells are fed [1-^{3}H,^{14}C]Ara are UDP-Ara and UDP-Xyl (highlighted in green boxes). As a result of this, it is expected that [1-^{3}H,^{14}C]Ara and [1-^{3}H,^{14}C]Xyl will be the only sugars that will be isolated from cell wall polysaccharides that are radiolabelled. Fry *et al.*, 1983 present evidence for Xyl 1-P (blue arrows) although Feingold *et al.* (1990) and Brett & Waldron (1996) suggest the evidence is fragmentary/preliminary for this reaction.

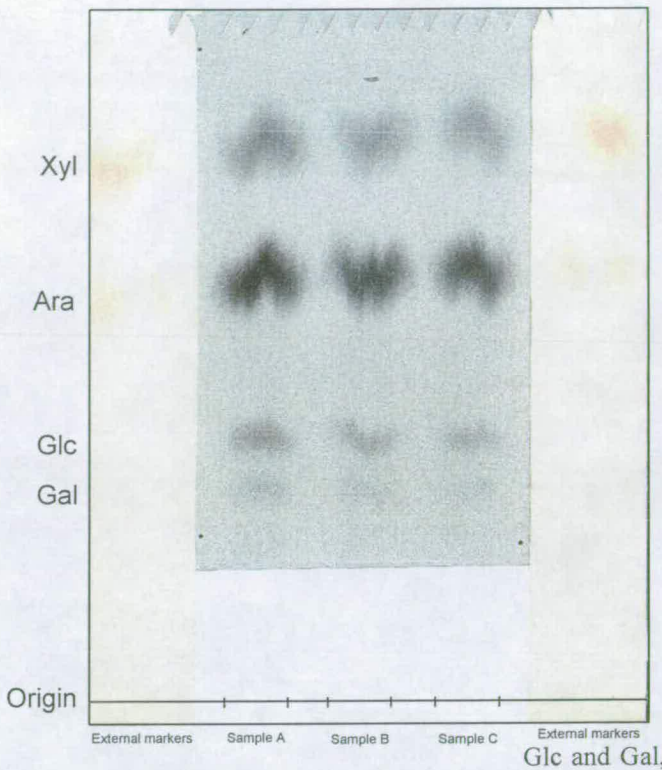

Figure 3.11 Autoradiogram of a paper chromatogram of isolated cell-wall monosaccharides from *Arabidopsis* cell-suspension culture fed [1-^{3}H,1-^{14}C]Ara

The AIR of *Arabidopsis* cell-suspension culture (400 µl, 3 d old, 10% SCV) fed [1-^{14}C,1-^{3}H]Ara was acid hydrolysed (TFA, 2 M, 120°C, 1 h). The hydrolysate was separated with 1D paper chromatography on Whatman 3MM (EPW, 8:2:1, 16 h followed by BAW, 12:3:5, 16 h). Radiolabelled replicate samples A – C were detected with autoradiography. The external markers that border samples A – C were stained with aniline-hydrogen-phthalate. Although no external markers are present for Glc and Gal, the position on the chromatogram in this solvent system relative to Xyl and Ara strongly suggests they are Glc and Gal.

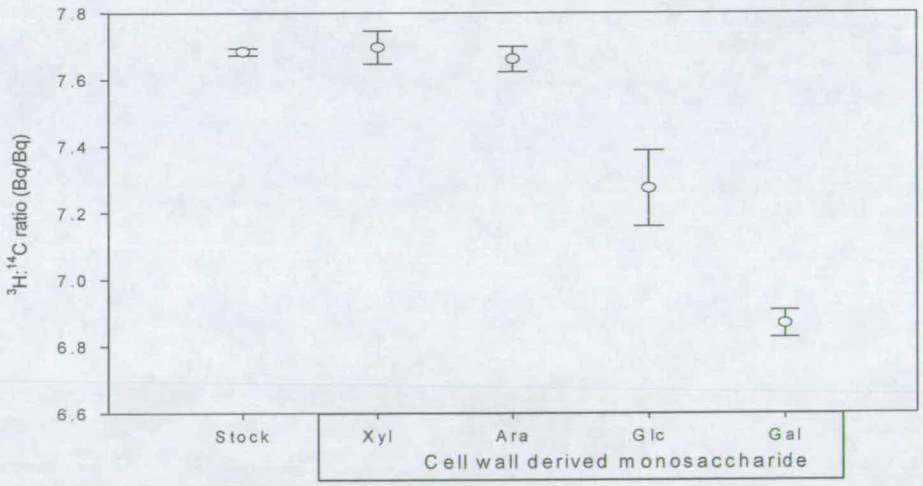

Figure 3.12 ^{3}H:^{14}C Ratios of isolated cell-wall monosaccharides from *Arabidopsis* cell-supsension culture fed [1-^{14}C, 1-^{3}H]Ara

The level of ^{3}H and ^{14}C in the cell wall derived monosaccharides obtained from Fig. 3.11 were assayed and the ^{3}H:^{14}C ratios compared to the ratio obtained for the original [1-^{14}C, 1-^{3}H]Ara stock solution. Error bars indicate SE of three replicates.

3.1.7 Attempts to remove the starch component of the AIR

The synthesis of starch occurs in the plastids. The major NDP-sugar utilised in starch formation is ADP-Glc (Preiss, 1991), whereas wall matrix glucans are synthesised from UDP-Glc or possibly GDP-Glc in Golgi bodies. Analysing the ^{3}H:^{14}C ratio of Glc from polysaccharides in the AIR would include Glc from both starch and wall matrix glucans. Attempts were therefore made to remove starch from AIR. For a reliable ratio of total Glc from wall matrix glucans all the starch would need to be eliminated from the sample. In addition to this it was necessary to obtain conditions of starch solubilisation that would minimise any pectin solubilisation.

DMSO has previously been used to remove starch from the AIR (Carpita *et al.*, 1987). However, when *Arabidopsis* AIR suspension was treated with DMSO for 15 d, washed with H_2O and stained with iodine, microscopic investigation revealed the presence of starch granules. This was similar to the control that had been treated with a chlorobutanol (0.5%, w/v) solution instead of DMSO.

Attempts were made to digest pre-boiled and un-boiled samples of *Arabidopsis* AIR suspension with human saliva. Starch breakdown products could not be detected by TLC (data not shown).

Arabidopsis AIR and soluble potato starch were either boiled (to gelatinise starch) or left at room temperature and subsequently treated with porcine pancreatic α-amylase. The α-amylase yielded Glc when gelatinised starch was the substrate. When AIR was treated in the same manner as the soluble potato starch no starch breakdown products could be detected by the TLC system (data not shown).

Arabidopsis AIR and soluble potato starch were treated with Termamyl® 120L at various temperatures.

Soluble potato starch digestion products were yielded when samples were maintained at 60°C and 90°C (Fig. 3.13 A – D). Over a period of 24 h the greatest yield of starch digestion products from potato starch (Fig. 3.13 D) and the AIR (Fig. 3.14 B) occurred when the samples were incubated at 90°C.

In conclusion, starch removal from the AIR of *Arabidopsis* cell-suspension culture would only be of use if all the starch was removed and the technique employed to remove the starch did not compromise any of the other AIR components. On this basis treatment of the AIR with DMSO, human salivary amylase, porcine pancreatic α-amylase or Termamyl® was not suitable.

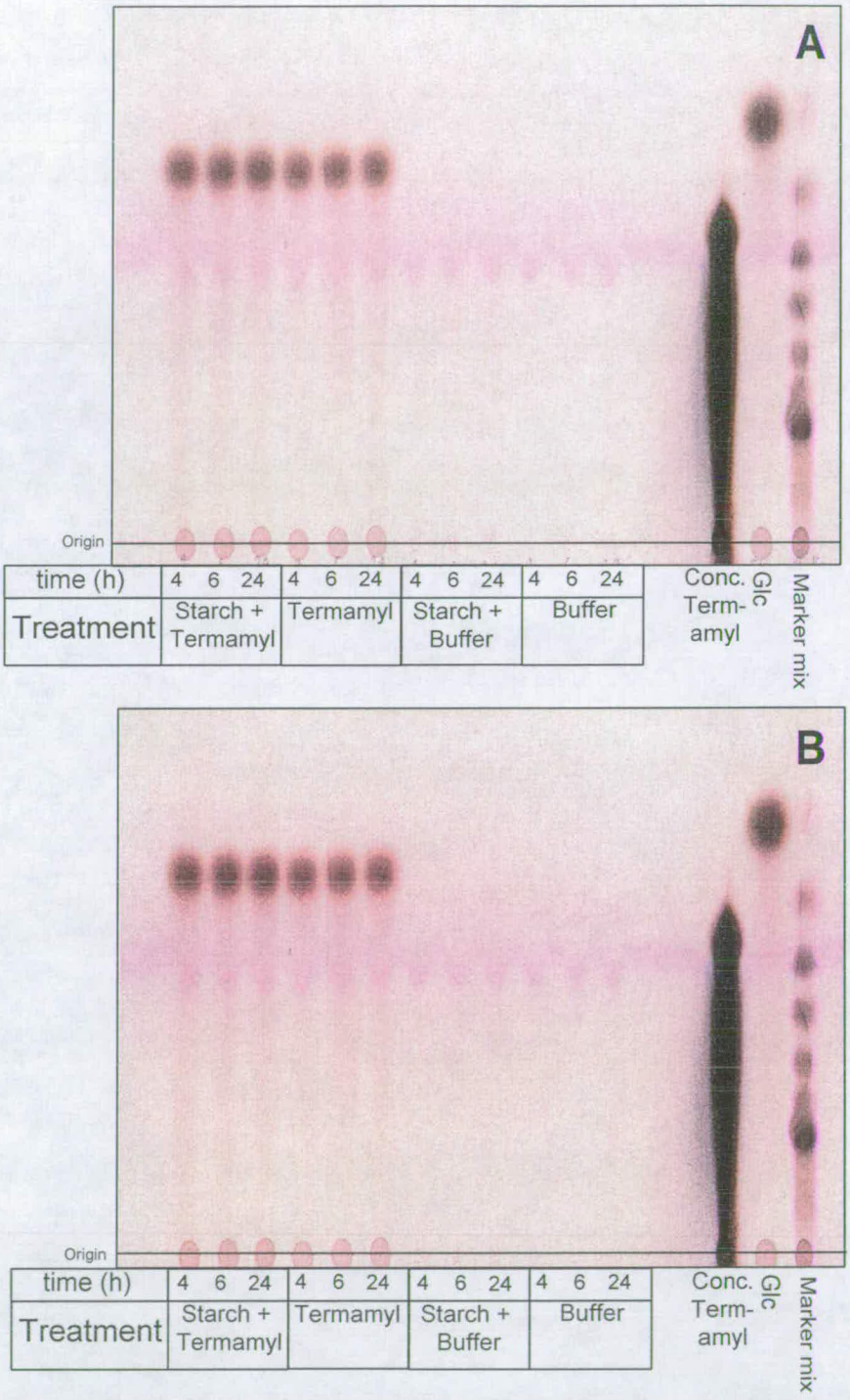

Figure 3.13 Soluble potato starch digestion using Termamyl® 120L

Soluble potato starch samples that had not been pre-gelatinised were incubated at (**A**) room temperature, (**B**) 37°C, (**C**) 60°C and (**D**) 90°C (continued overleaf) and the digest products separated on TLC in BAW (2:1:1, 6 h) . The TLC plate was stained with thymol. In order of fastest migrating compounds the marker mix contains Glc, maltose, maltotriose, maltotetraose, maltopentaose, maltohexaose and maltoheptaose. The intense spot in the Termamyl is a lactose contaminant in the enzyme preparation.

Continued overleaf

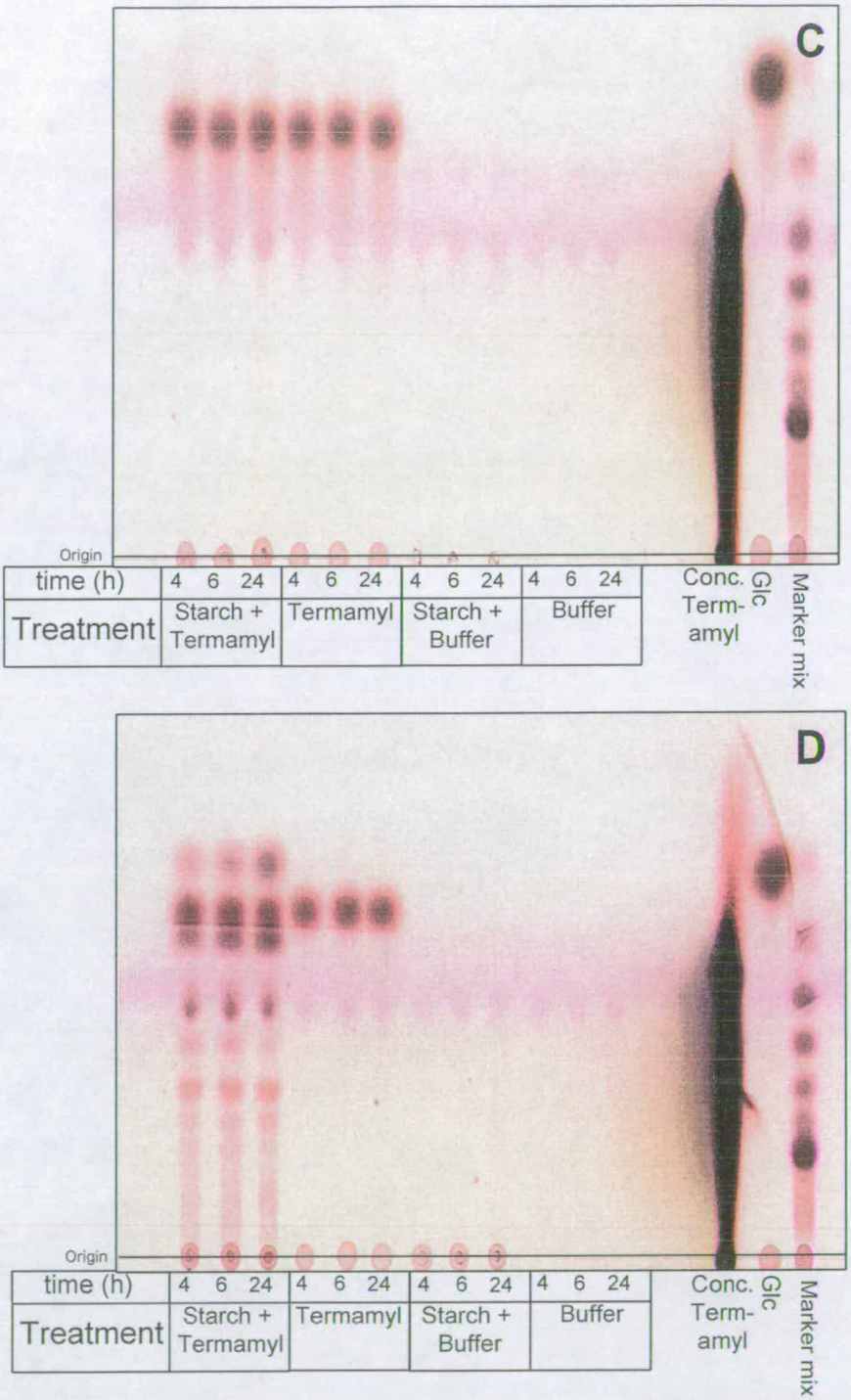

Figure 3.13 Continued

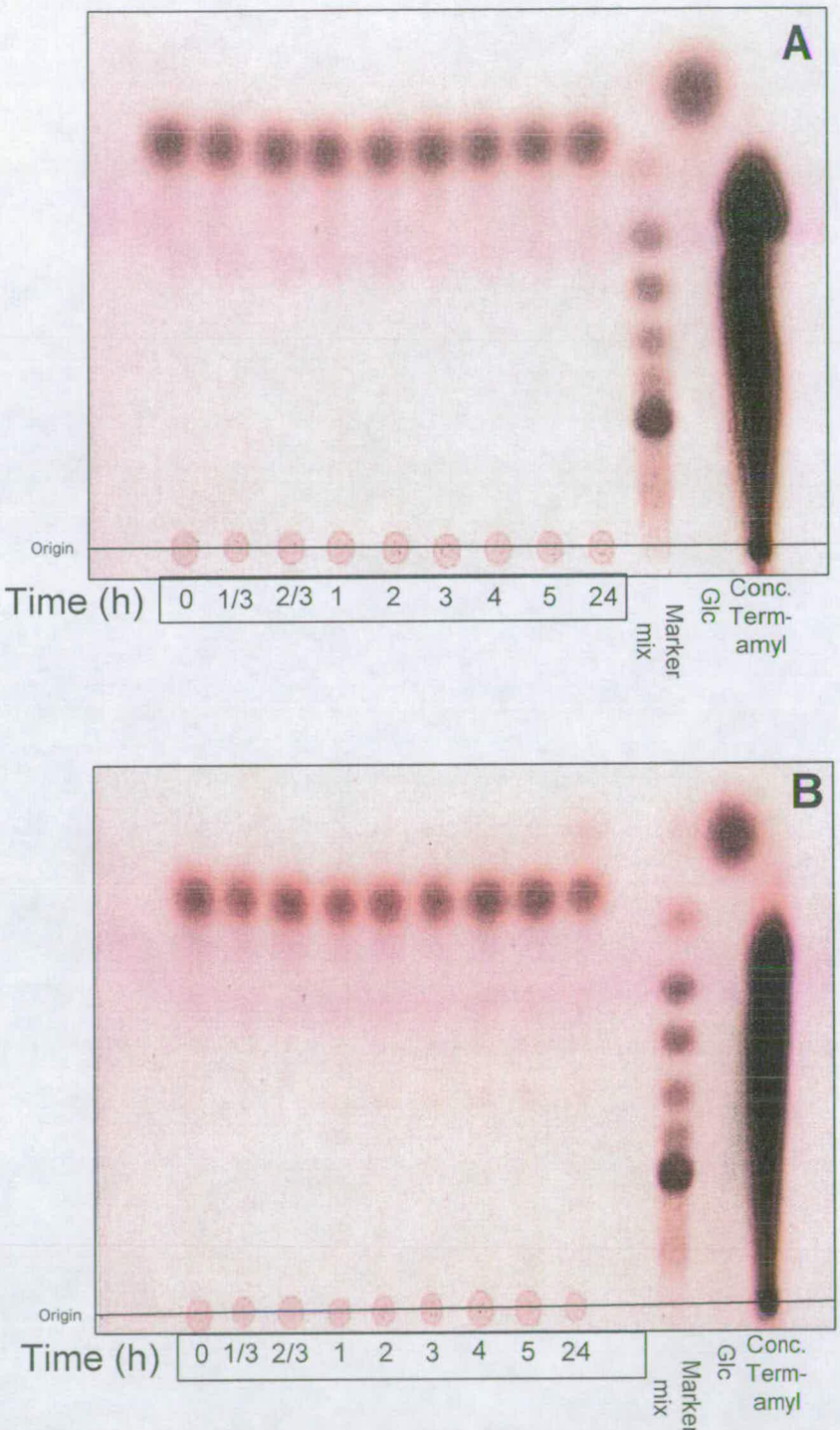

Figure 3.14 *Arabidopsis* alcohol-insoluble residue suspension digested with Termamyl over 24 h

Experiments conducted at (A) 60°C and (B) 90°C. Details as per Fig 3.13.

3.2 Experiments to deduce the predominating pathways in sugar nucleotide metabolism in the biosynthesis of plant cell walls

3.2.1 ^{3}H:^{14}C Ratios of monosaccharides obtained from the AIR of *Arabidopsis* cell-suspension culture fed [1-^{3}H]Gal and [U-^{14}C]Glc

Arabidopsis cell-suspension culture was fed either [1-^{3}H]Gal or [U-^{14}C]Glc. The AIR was hydrolysed with 2 M TFA. The solubilised radioactivity in each hydrolysate was assayed and based on this value each ^{3}H-labelled hydrolysate was combined with a ^{14}C-labelled hydrolysate to from a 5:1 ^{3}H:^{14}C (cpm/cpm) ratio. The first step towards purification of the compounds in the (^{3}H,^{14}C)-hydrolysate was paper chromatography (Fig. 3.15). Fig. 3.15 provides qualitative information about AIR-derived ^{14}C-labelled monosaccharides. From the autoradiogram it is suggested that the order of greatest ^{14}C radiolabel intensity in the isolated compounds is: Glc/Gal>Ara=Xyl>GlcA/GalA>Rha>Rib>Fuc>Man>Api. All of the sugars, except for Glc and Rib, were expected to be obtained from cell wall polysaccharides from the AIR. Glc is only partially derived from the cell wall polysaccharides as it is mixed with Glc residues from starch. Rib is thought to have arisen from RNA.

The radiolabelled compounds were eluted and, where necessary, further purified.

3.2.1.1 Purification of TFA hydrolysate compounds

GalA and GlcA from paper chromatograms such as that shown in Fig. 3.15, were further purified by paper electrophoresis (Fig. 3.16). It is clear from Fig. 3.16 that

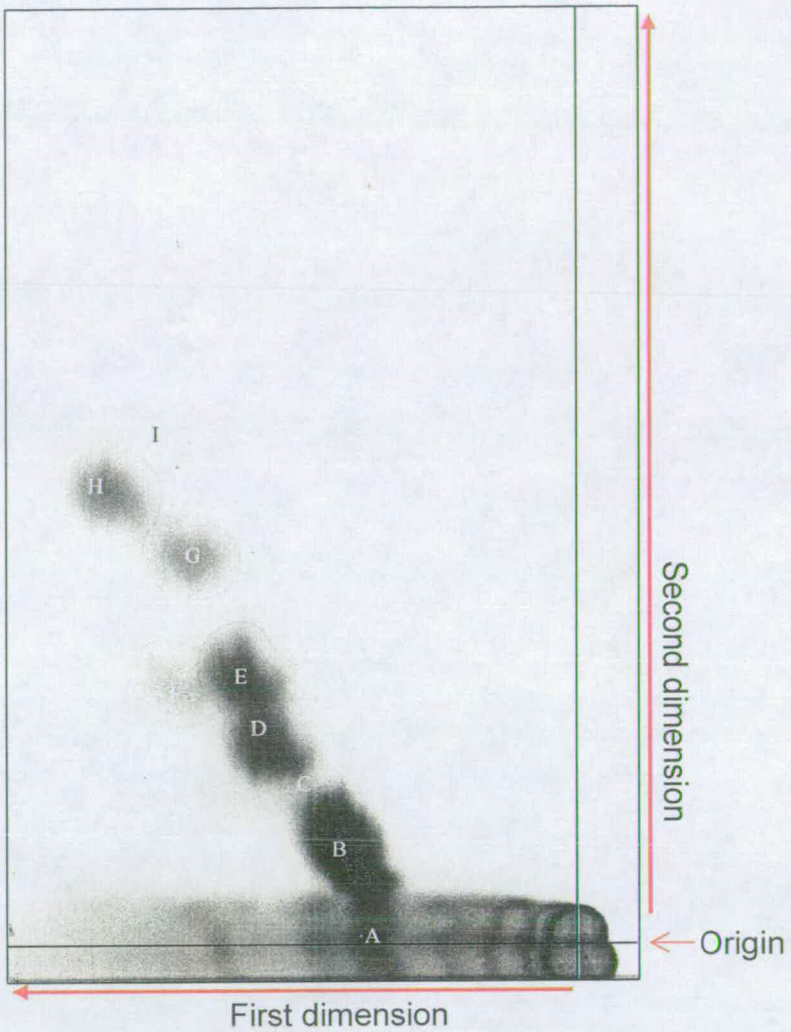

Compounds suggested to be:					
A	GlcA & GalA	**D**	Ara✓	**G**	Rib ✓
B	Glc & Gal	**E**	Xyl ✓	**H**	Rha ✓
C	Man	**F**	Fuc	**I**	Api

Figure 3.15 *Arabidopsis* (^{3}H,^{14}C)-hydrolysate separated by paper chromatography

The sample was dispensed onto Schleicher and Schuell 2045B paper and the chromatogram was run in 2D (BAW 12:3:5, 27 h, followed by EPW 8:2:1, 30 h). The chromatogram was autoradiographed and the compounds were identified by comparison to a chromatogram that had been run by the same method with standard markers and stained with aniline hydrogen-phthalate. The sample shown is representative. The (✓) indicates the compound did not require further purification.

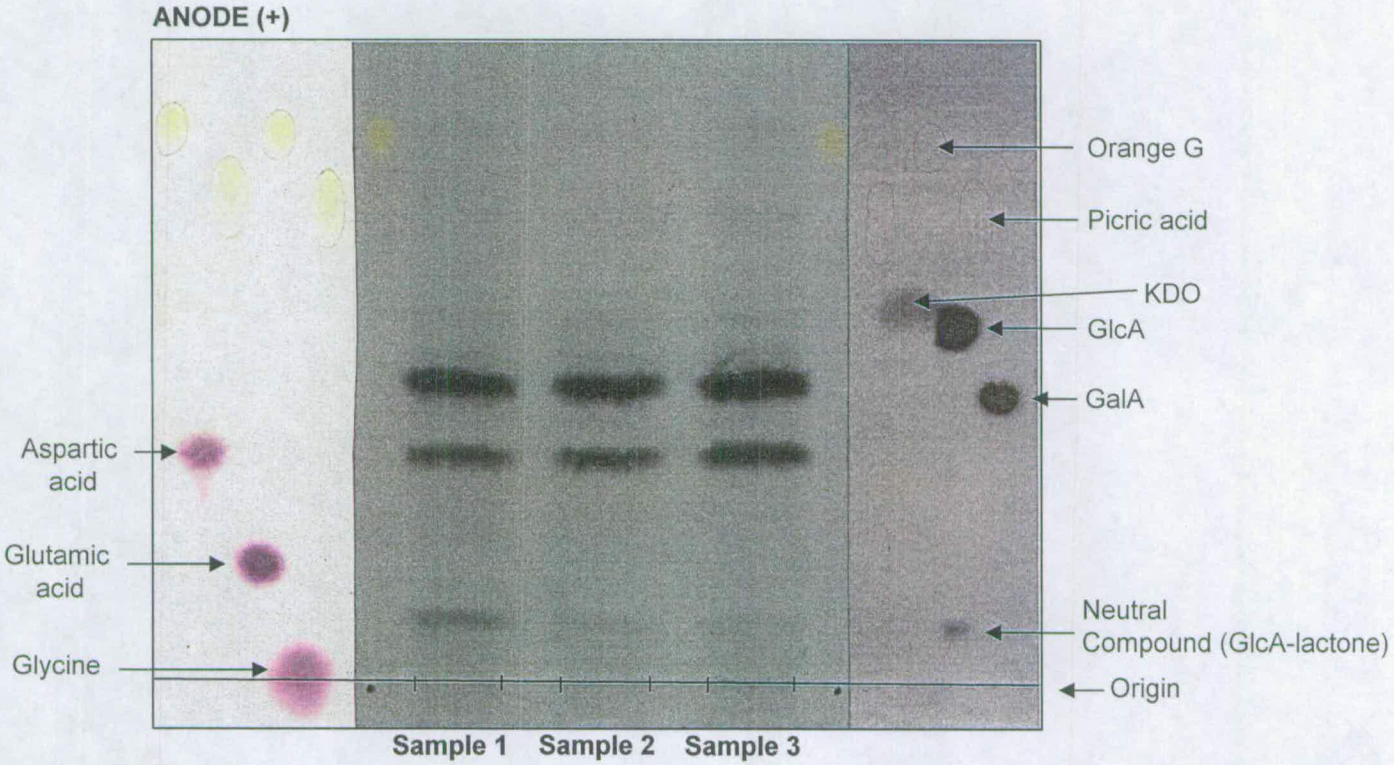

Figure 3.16 (^{3}H,^{14}C)-Labelled uronic acids from *Arabidopsis* TFA hydrolysate further purified by paper electrophoresis

The GlcA and GalA ("A") samples eluted from the paper chromatogram shown in Fig. 3.15 were dried and treated with NaOH (40 µl, 50 mM, 5 min) to cleave the lactone ring of glucuronolactone. The samples were treated with acetic acid acid (60 µl, 50 mM), loaded onto Whatman 3MM paper and subjected to paper electrophoresis (pH 3.5, 2.5 kV, 1 h). Radioactive compounds were autoradiographed. The amino acid external markers (left border) were stained with ninhydrin. The remaining markers (right border) were stained with silver nitrate. Samples 1–3 are replicates.

the ^{14}C detected in GalA is far greater than that in GlcA. This indicates that GalA is far more prevalent in AIR-derived polysaccharides than GlcA. [^{14}C]Asp, thought to have arisen from proteins, was also detected in Fig. 3.16. The [^{14}C]Asp was found to have less ^{14}C than GalA.

Glc, Gal, Man, Fuc, and Api obtained from Fig 3.15 were further purified by paper chromatography (Fig. 3.17 – Fig. 3.20).

The identity of the putative Rib was investigated further. Although Rib has never been shown to be a constituent of plant cell wall polysaccharides, the ^{3}H:^{14}C ratio of Rib is of interest as it provides information about other biochemical pathways that are subjected to the dual labelling system. Rib is very likely to be part of the AIR as a component of RNA. Spot G shown on Fig. 3.15 was in a position that corresponds to Rib. A portion of the eluted sample was subjected to an alternative solvent system (BAB, 9:1:1, 16 h). Fig. 3.21 indicates that the radiolabelled compound co-migrated exactly with the internal Rib markers. This strongly suggests that spot G (Fig. 3.15) was Rib.

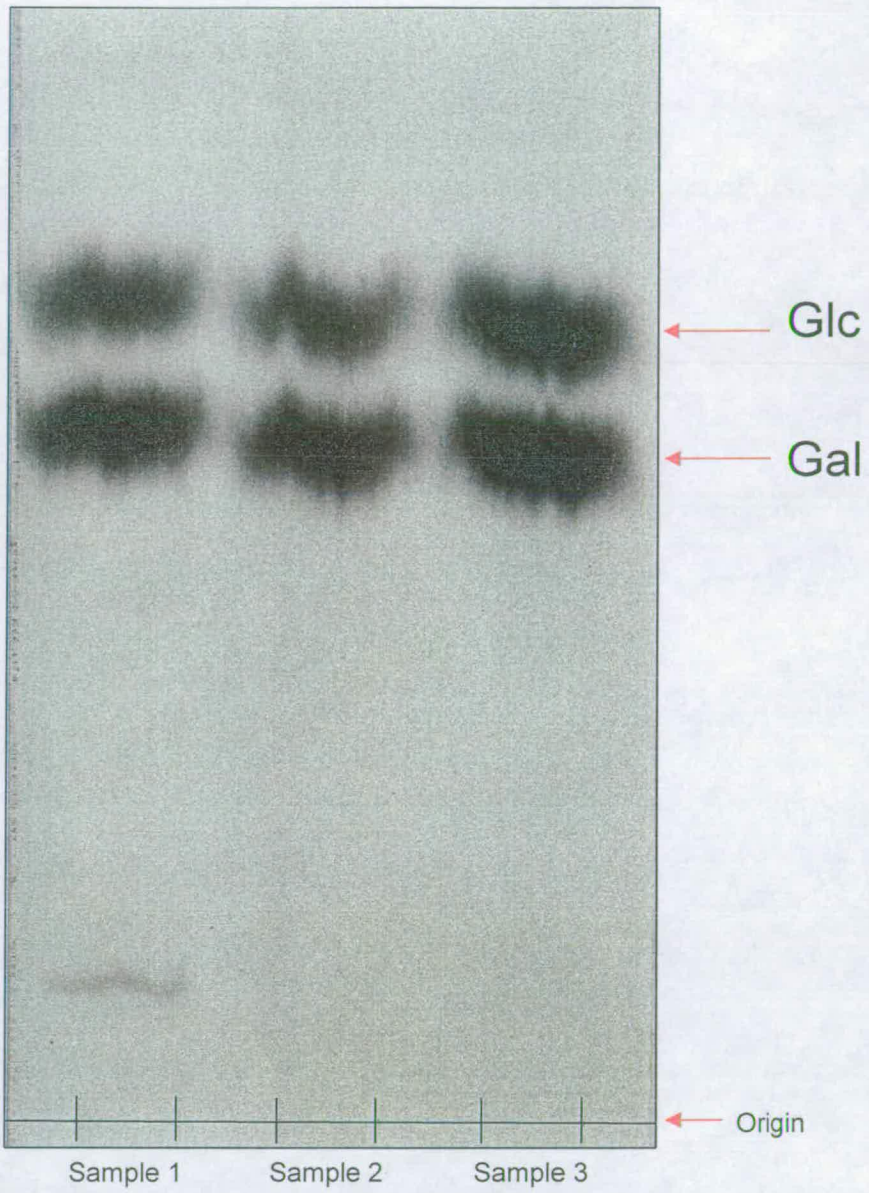

Figure 3.17 [^{3}H,^{14}C]Glc and [^{3}H,^{14}C]Gal from *Arabidopsis* hydrolysate further purified by paper chromatography

The Glc and Gal ("B") samples eluted from the paper chromatogram shown in Fig. 3.15 were loaded onto Schleicher and Schuell 2045B paper, run in EPW (8:2:1, 120 h) and autoradiographed (as shown). The identity of Glc and Gal was determined with external markers (not shown). Samples 1–3 are replicates.

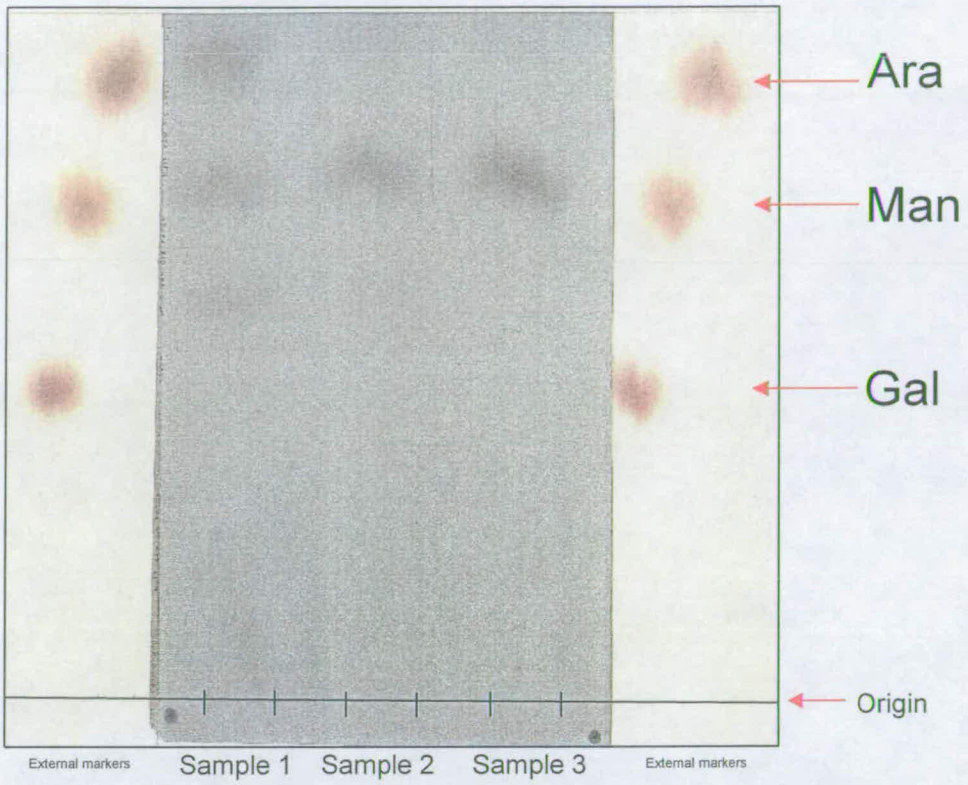

Figure 3.18 [^{3}H,^{14}C]Man from *Arabidopsis* hydrolysate further purified by paper chromatography

The Man ("C") sample eluted from the paper chromatogram shown in Fig. 3.15 was loaded onto Schleicher and Schuell 2045B paper, run in EPW (8:2:1, 100 h) and autoradiographed. The external markers were stained with aniline hydrogen-phthalate. Samples 1–3 are replicates.

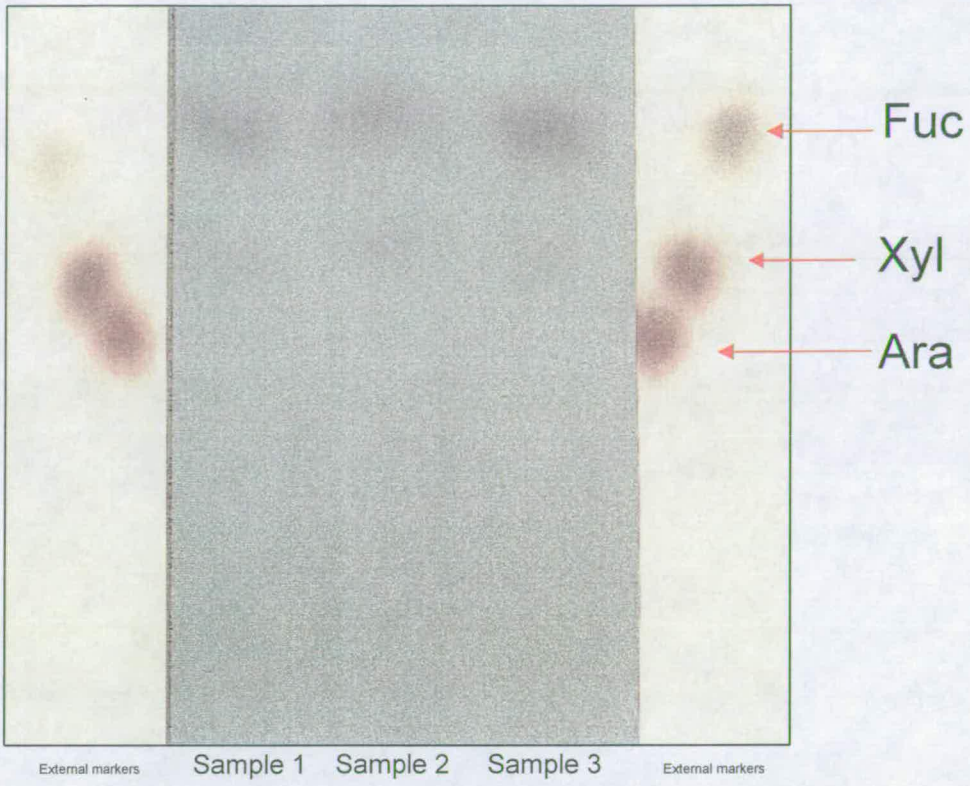

Figure 3.19 [^{3}H,^{14}C]Fuc from *Arabidopsis* hydrolysate further purified by paper chromatography

The Fuc ("F") sample eluted from the paper chromatogram shown in Fig. 3.15 was loaded onto Schleicher and Schuell 2045B paper, in BAW (12:3:5, 100 h) and autoradiographed. No origin is represented as only the upper section of the chromatogram is shown. The external markers were stained with aniline hydrogen-phthalate. Samples 1–3 are replicates.

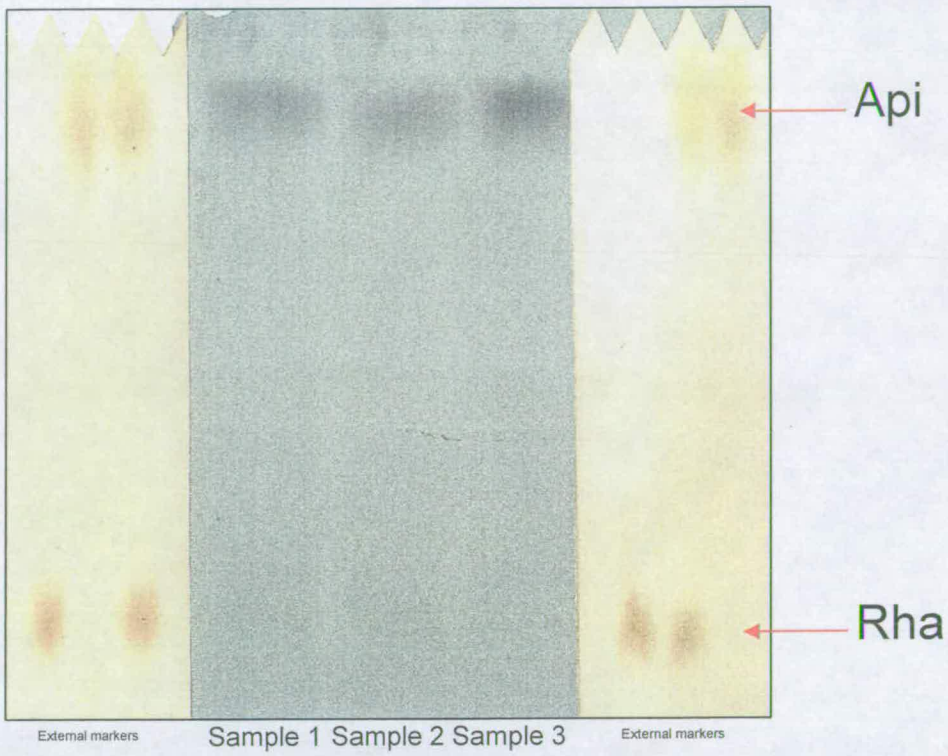

Figure 3.20 [^{3}H,^{14}C]Api from *Arabidopsis* hydrolysate purified by paper chromatography

The Api ("I") sample was eluted from the paper chromatogram shown in Fig. 3.15, loaded onto Schleicher and Schuell 2045B paper, run in Ethyl acetate/acetic acid/water + 0.25% (w/v) phenylboronic acid (10:5:6) and autoradiographed. No origin is represented as only the upper section of the chromatogram is shown. The external markers were stained with aniline hydrogen-phthalate. Samples 1–3 are replicates.

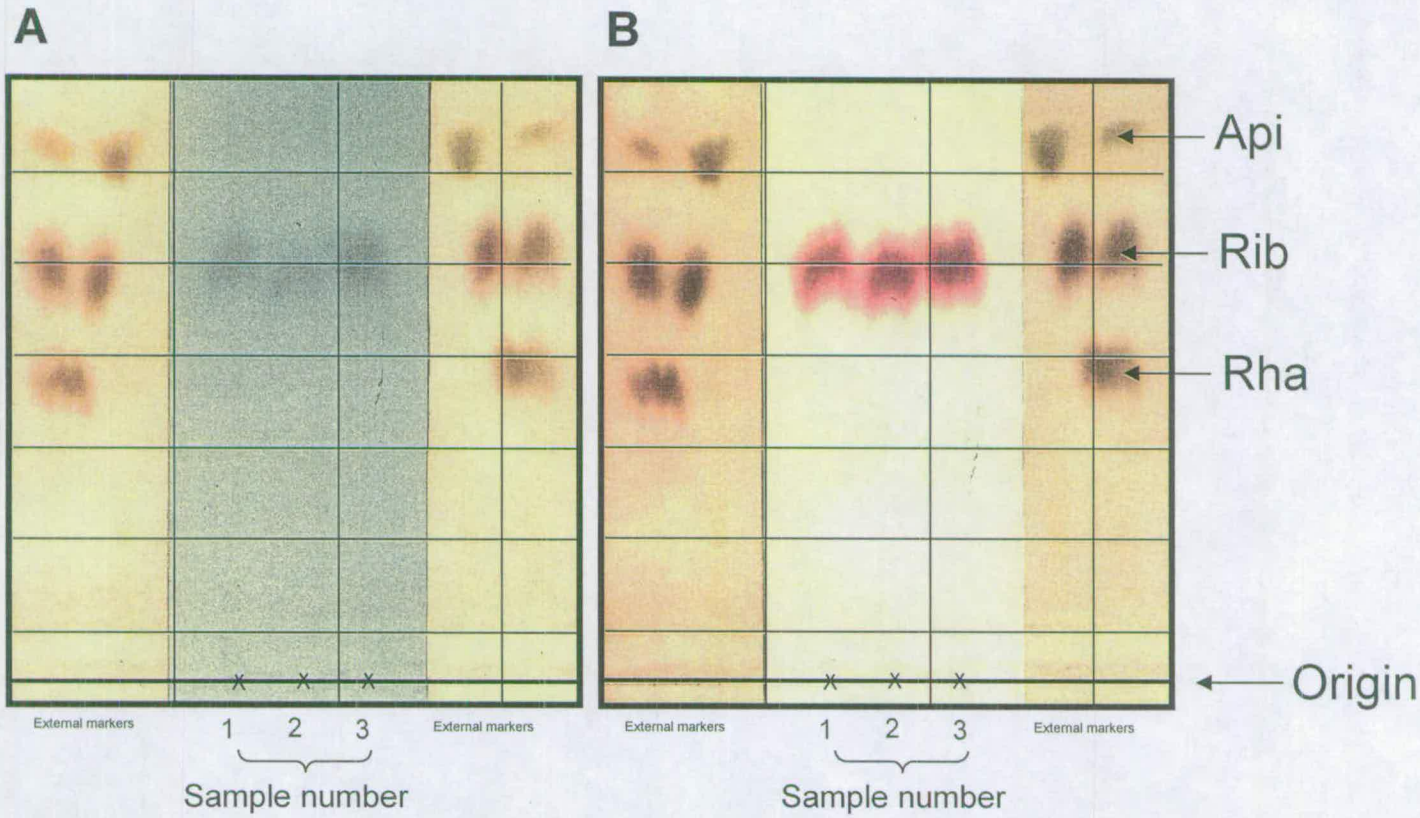

Figure 3.21 Evidence towards the identification of putative [^{3}H,^{14}C]Rib purified from *Arabidopsis* hydrolysate

An internal Rib marker (250 μg) was added to each sample. The samples were chromatographed (BAB, 9:1:1, 16 h) on Whatman 3MM. (**A**) The radioactive samples were autoradiographed. (**B**) The external markers and sample tracks were stained with aniline hydrogen-phthalate. The grid is used to correlate the radiolabelled compounds in A with the internal Rib marker shown in B. Samples 1–3 are replicates.

3.2.1.2 ^{3}H:^{14}C Ratios of monosaccharides derived from the AIR TFA hydrolysate

The purified monosaccharides were assayed for ^{3}H and ^{14}C (Appendix 5). A worked example used to determine the ^{3}H:^{14}C ratios of each of the monosaccharide residues is presented in the Materials and Methods (section 2.8.1). As the cells were originally fed a monosaccharide that had six ^{14}C-labelled atoms, it would not be possible to make direct comparisons between the isotope ratios of C_5 to C_6 compounds. The calculations account for this to enable comparisons between C_5 compounds and those of C_6 compounds. Figure 3.22 shows the calculated ^{3}H:^{14}C ratios. Gal was expected to have the highest ^{3}H:^{14}C ratio as the first point of ^{3}H entry into the 'core' metabolites is at UDP-Gal. The high ^{3}H:^{14}C ratio of Gal gives validity to the experiment as an isotope gradient within the 'core' metabolites, predicted in the experimental outline (section 1.5), was achieved.

Cell-wall derived GalA residues could stem from the parent 'core' metabolites UDP-Gal, Glc 6-P or UDP-Glc (Fig. 1.5). According to the original experimental outline (section 1.5), compounds that are formed from the same 'core' metabolite precursor are expected to have the same ratio. Gal is known to stem from the parent metabolite UDP-Gal. As the ^{3}H:^{14}C ratio of GalA is much lower than the ratio of Gal this suggests that the parent 'core' metabolite that formed UDP-GalA is more 'distanced' from the source of ^{3}H than UDP-Gal. This indicates that Glc 6-P or UDP-Glc are more likely to be the predominant parent 'core' metabolites of UDP-GalA than UDP-Gal.

GDP-Man may be formed from the parent 'core' metabolites Glc 1-P or Glc 6-P. If UDP-GalA were formed via the *myo*-inositol pathway from the 'core'

metabolite Glc 6-P, the ratio of GalA would be expected to be the same or less than that of Man. However, if UDP-GalA were formed from the 'core' metabolite UDP-Glc, the ratio of GalA would be expected to be higher than that of Man. Fig. 3.22 clearly shows that the $^{3}H:^{14}C$ ratio of GalA is higher than those of Man and Fuc (the latter being derived from GDP-Man). This suggests that the parent 'core' metabolite that formed UDP-GalA is closer to the source of ^{3}H than Glc 6-P. This indicates that the *myo*-inositol pathway does not predominantly form UDP-GalA.

UDP-GlcA may act as the direct precursor of UDP-GalA, UDP-Api and UDP-Xyl, which itself can be epimerised to UDP-Ara. Fig. 3.22 shows that the $^{3}H:^{14}C$ ratio of GalA is approximately equal to those of Ara, Xyl and Api and therefore suggests they share a common parent 'core' metabolite.

The precursor for Rha that is incorporated into plant cell wall polysaccharides is presumed to be UDP-Rha. UDP-Rha is thought to be directly formed from the 'core' metabolite UDP-Glc. No alternative to this pathway has been proposed in plants, although if the polysaccharide Rha residue precursor were the same as in bacteria, TDP-Rha, the Rha residues would arise from the 'core' metabolite Glc 1-P. Fig. 3.22 shows that Rha has a similar isotope ratio to GalA, Ara, Xyl and Api. As GalA, Ara, Xyl and Api cannot be formed from Glc 1-P and the cell-wall Rha precursor is thought to be UDP-Rha this suggests that each of the isolated sugars is likely to have been formed from the same 'core' metabolite, UDP-Glc.

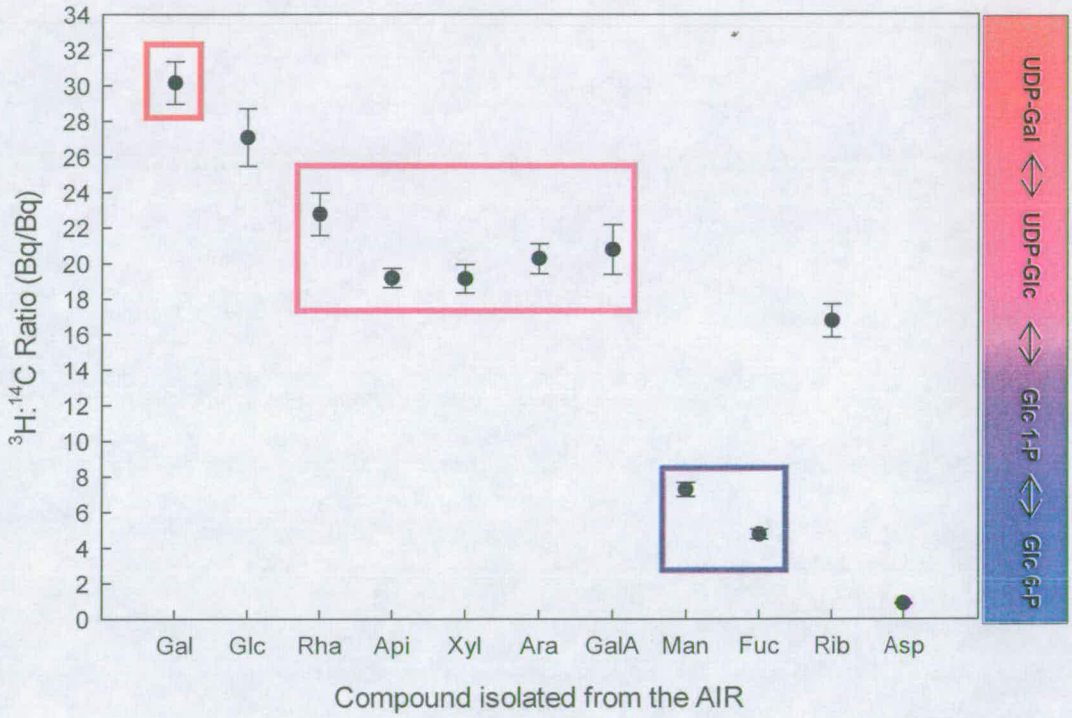

Figure 3.22 Isotope ratios of (^{3}H,^{14}C)-labelled monosaccharides purified from *Arabidopsis* AIR hydrolysate

The colour gradient indicates the 'core' metabolites that each of the cell-wall monosaccharides may have stemmed from. The increased level of red in the colour gradient represents a higher ^{3}H:^{14}C ratio as this is 'closer' to the ^{3}H source. An increased level of blue indicates a lower ^{3}H:^{14}C ratio as this is more 'distanced' from the ^{3}H source. The boxes that surround the compounds isolated from the AIR indicate the area of the colour gradient (and hence 'core' metabolite) that the isolated compounds are most likely to stem from. The error bars are standard error where N=4 (Appendix 5).

The isotope ratio of Rha is similar but slightly higher than those of GalA, Ara, Xyl and Api. This is also true of the isotope ratio of total Glc that is composed of both non-cellulosic cell wall Glc residues and *ex* starch Glc residues. Fig. 3.23 shows that [1-^{3}H]Gal can result in the formation of UDP-[6-^{3}H]Glc. If UDP-[6-^{3}H]Glc was converted to UDP-GlcA the ^{3}H would be lost. This may explain why the GalA, Xyl, Ara and Api have a slightly lower ^{3}H:^{14}C ratio than Glc (total) and Rha that would retain the ^{3}H at C6.

The isotope ratio of GlcA (15.28 $\pm$ 1.38 Bq/Bq; not shown in Fig. 3.22) residues was lower than that of GalA, Ara, Xyl and Api. This was unexpected as GalA, Ara, Xyl and Api residues are derived from UDP-GlcA. However, GlcA is present in the cell wall in very low amounts and the GlcA isolated from acid hydrolysis of the AIR was not very heavily radiolabelled (Fig. 3.16). In addition to this the autoradiogram utilised to isolate GlcA showed a background smear of radioactivity. If the GlcA were contaminated with a radiolabelled compound the ratio could be altered. Therefore the GlcA ratio may be explained by the impurity of the GlcA.

The ratios of Man and Fuc are lower than the ratios of GalA, Ara, Xyl, Api and Rha. This suggests that Man and Fuc were formed from a 'core' metabolite that is more 'distanced' in the metabolic pathway from the source of ^{3}H than the 'core' metabolite that formed GalA, Ara, Xyl, Api and Rha. The 'core' metabolites that could have formed GDP-Man and GDP-Fuc are Glc 1-P (via GDP-Glc) and/or Glc 6-P (via Fru 6-P, Man 6-P, Man 1-P). As no other compounds definitively stem from these 'core' metabolites, there is no way to distinguish whether GDP-Man and GDP-Fuc arose from Glc 1-P or Glc 6-P.

The precursor of Rib in RNA is thought to be Rib 5-P (Horecker, 2002). The formation of Rib 5-P from the 'core' metabolite Glc 6-P via Glc 6-P dehydrogenase would result in the loss of ^{3}H at C1 when Glc 6-P is converted into 6-phosphoglucono-δ-lactone (Fig. 3.23).

Cells fed [1-^{3}H]Gal could form [^{3}H]Rib. Despite the fact that the ^{3}H-labelled precursors for [^{3}H]Rib synthesis are 'distanced' from the ^{3}H source, the purified [^{3}H,^{14}C]Rib has a very high ^{3}H:^{14}C ratio. If formed by the pathways illustrated in Fig. 3.23, Rib would be expected to have a similar or lower ^{3}H:^{14}C ratio than Man or Fuc. This is because Man and Fuc are derived from either Glc 1-P or Glc 6-P. It is unexpected that the ^{3}H:^{14}C ratio of Rib is considerably higher than that of Man and Fuc and may suggest that an alternative pathway is in operation (section 4.4).

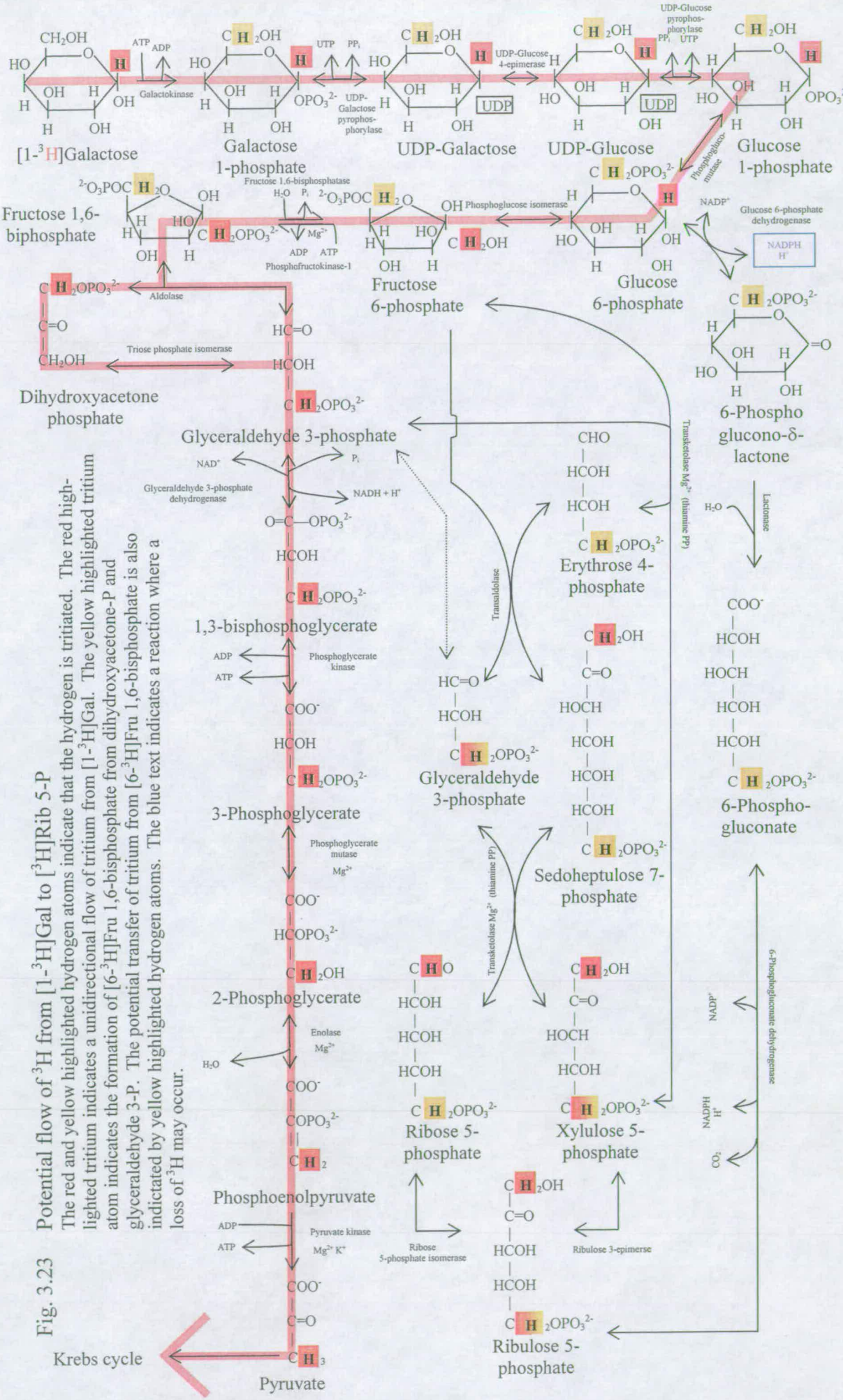

Fig. 3.23 Potential flow of ^3H from [1-^3H]Gal to [^3H]Rib 5-P
The red and yellow highlighted hydrogen atoms indicate that the hydrogen is tritiated. The red highlighted tritium indicates a unidirectional flow of tritium from [1-^3H]Gal. The yellow highlighted tritium atom indicates the formation of [6-^3H]Fru 1,6-bisphosphate from dihydroxyacetone-P and glyceraldehyde 3-P. The potential transfer of tritium from [6-^3H]Fru 1,6-bisphosphate is also indictated by yellow highlighted hydrogen atoms. The blue text indicates a reaction where a loss of ^3H may occur.

3.2.2 ^{3}H:^{14}C Ratios of monosaccharides obtained from different polysaccharide sources in *Arabidopsis* cell-suspension culture fed [1-^{3}H]Gal and either [U-^{14}C]Glc or [U-^{14}C]Fru

In the previous experiment (section 3.2.1) the ^{3}H:^{14}C ratios were formed from a combination of a ^{3}H-labelled and ^{14}C-labelled AIR hydrolysate. This method relied on precision pipetting to obtain reproducible ratio values. To ensure that more reliable results were obtained than with the previous method, a different approach was adopted in this section. In this case the AIR suspension, obtained from *Arabidopsis* cell-suspension culture fed [1-^{3}H]Gal and either [U-^{14}C]Glc or [U-^{14}C]Fru, was subdivided into portions and each portion was assayed for radioactivity. The inclusion of [U-^{14}C]Fru meant that the 'core' metabolite pathway was increased by one additional metabolite (Fru 6-P). This had the potential to distinguish monosaccharides that had been derived from Glc 6-P and Fru 6-P. The AIR was quantitatively retrieved from each scintillation fluid and washed, and each ^{3}H-labelled AIR sample was combined with a ^{14}C-labelled AIR sample. In the previous experiment the artificial ^{3}H:^{14}C ratio that was formed was based on the radioactivity incorporated into polymers that could be hydrolysed with TFA and, for this reason, did not include cellulose. The advantage of this experiment was that it ensured that the entire amount of radioactivity that had been incorporated into the AIR was taken into account. In the previous experiment (section 3.1) the dispensation of too much or too little radioactivity due to pipetting error, could not be accounted for. In this experiment, with the knowledge of the amount of radioactivity contained in each (^{3}H,^{14}C)-labelled AIR sample, any inconsistency in the dispensation of ^{3}H-labelled or ^{14}C-labelled AIR suspension could be accounted for (section 2.9).

Each (^{3}H,^{14}C)-labelled AIR sample was committed to a different treatment designed to isolate a specific monosaccharide or other building block that had arisen from either a variety of polysaccharides or a known polysaccharide.

3.2.2.1 *Cellulase treatment*

Arabidopsis (^{3}H,^{14}C)-labelled AIR samples were incubated with cellulase to produce xyloglucan oligosaccharides. Some monosaccharides were obtained as by-products. The compounds were separated by gel-permeation chromatography (Fig. 3.24). The ^{3}H and ^{14}C profiles (Fig. 3.24) indicate three major peaks. The peaks corresponded with the internal standards blue dextran, XLLG and Glc.

The fractions that corresponded with both a peak of radioactivity and the Glc internal marker were pooled and the radiolabelled Glc was purified by paper chromatography (Fig. 3.25). It is clear from Fig. 3.25 that there is a distinct lack of ^{3}H in the radioactive profile.

The radioactive xyloglucan oligosaccharides, which corresponded approximately with an internal marker of XLLG (Fig. 3.24), were pooled and Driselase-digested to release radiolabelled IsoP and to a lesser extent Gal and Glc, which were separated by paper chromatography (Fig. 3.26, A). The putative Glc and Gal were rechromatographed (Fig. 3.26 B, C). The putative IsoP was eluted from the paper, hydrolysed with acid and paper chromatographed to give a xyloglucan-derived Glc and Xyl.

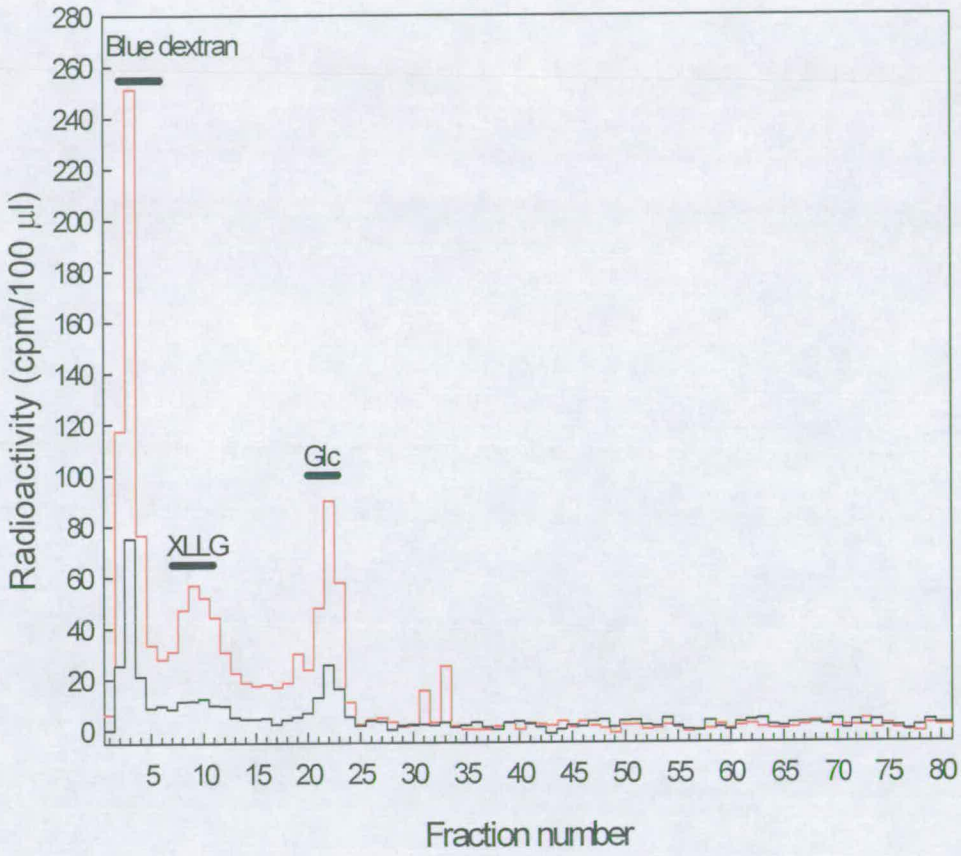

Figure 3.24 Gel permeation chromatography of products from cellulase digestion of (^{3}H,^{14}C)-labelled AIR

Blue dextran (2.5 mg), Glc (4.1 mg) and 0.7 mg of XLLG were added to the 410 µl of cellulase-digested (^{3}H,^{14}C)-labelled AIR sample. The sample was loaded onto a Bio-Gel P-2 column with a 150-ml bed volume and washed through with PyAW (1:1:98 in 0.5% CB). The blue dextran marked the void volume. A portion (5 µl) of each fraction was spotted onto a TLC plate and run in BAW (2:1:1, 8 h). The TLC plate was stained with thymol to determine the fractions that contained XLLG and Glc (marked on the graph). A portion (100 µl) of each fraction was assayed for radioactivity. The sample shown is representative and the values are corrected for the background radioactivity. The (——) represents ^{3}H and the (——) ^{14}C.

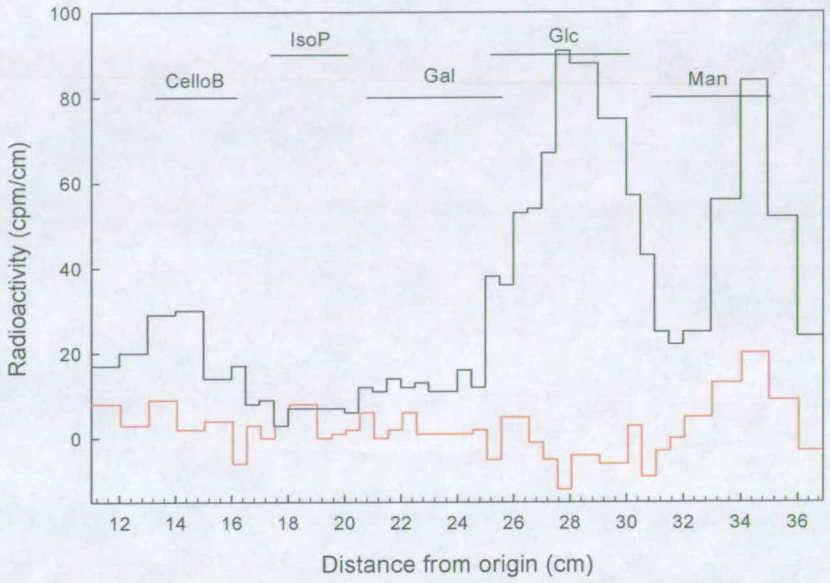

Figure 3.25 Paper chromatography purification of Glc obtained from cellulase digestion of (^{3}H,^{14}C)-labelled AIR

The fractions of radioactivity that eluted with the internal Glc marker on the Bio-Gel P-2 column (see Fig. 3.24) were run on Schleicher and Schuell paper in EPW (10:4:3, 130 h). The chromatogram was cut into strips, which were assayed for radioactivity. The sample shown is typical and the values are corrected for the background radioactivity. The (——) represents ^{3}H and the (——) ^{14}C.

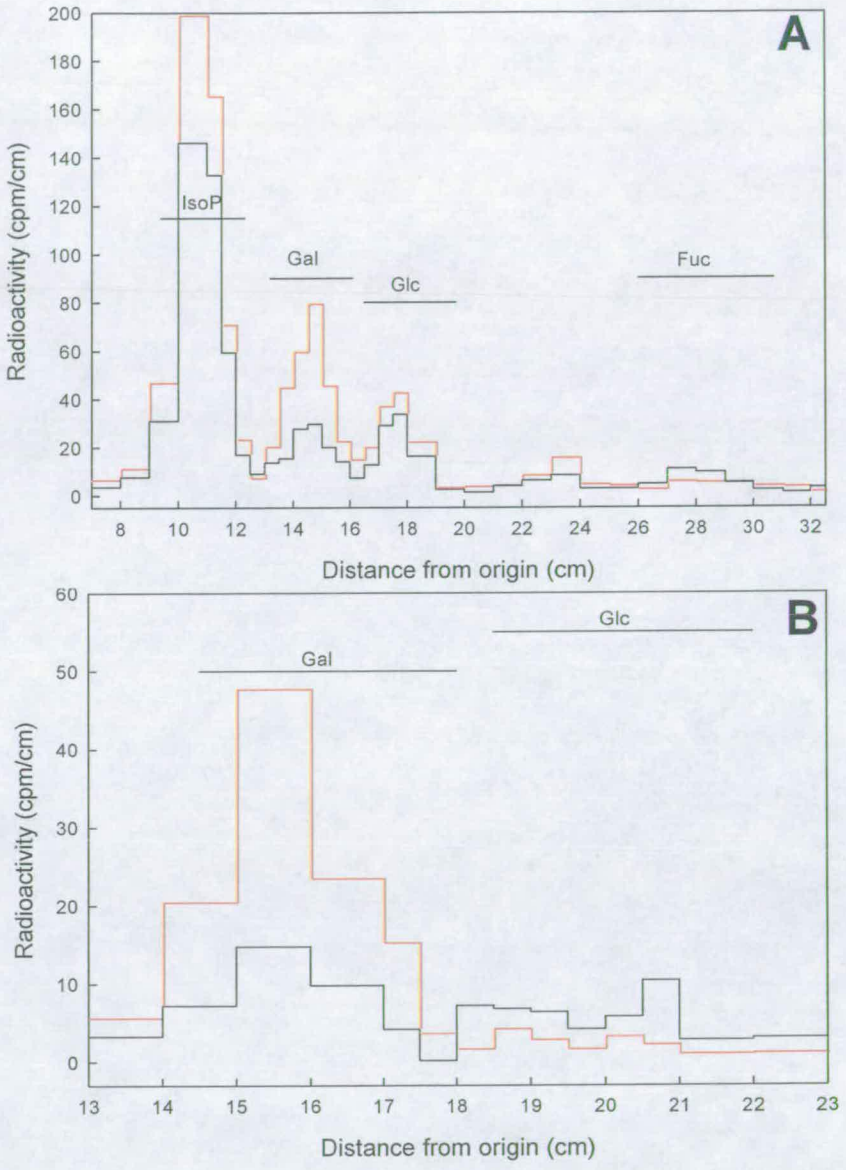

Figure 3.26 Paper chromatogram of sugars obtained from the xyloglucan oligosaccharides produced by cellulase digestion of (^{3}H,^{14}C)-labelled AIR

Bio-Gel P-2 fractions that eluted with the internal XLLG (see Fig. 3.24) were pooled, dried and digested with Driselase (200 µl, 0.5% in w/v PyAW with 0.5% w/v CB, 37°C, 48 h). The samples were each treated with formic acid (final conc. 15% v/v), loaded onto (**A**) Whatman no. 1 and run in EPW (9:3:2, 21 h). The chromatogram was cut into strips and assayed for radioactivity. The peaks of radioactivity that corresponded to the external IsoP, Gal and Glc markers were washed in toluene and eluted. The eluted (**B**) Gal and (**C**) Glc samples were run on Schleicher and Schuell 2045B in EPW (8:2:1, 120 h). The eluted IsoP sample was hydrolysed with TFA (2 M, 120°C, 1 h) and run on (**D**) Schleicher and Schuell paper 2045B EPW (8:2:1, 48 h). The chromatograms were cut into strips and assayed for radioactivity. The (——) represents ^{3}H and the (——) ^{14}C. The samples shown are typical and the values shown are corrected for the background radioactivity.

Continued overleaf

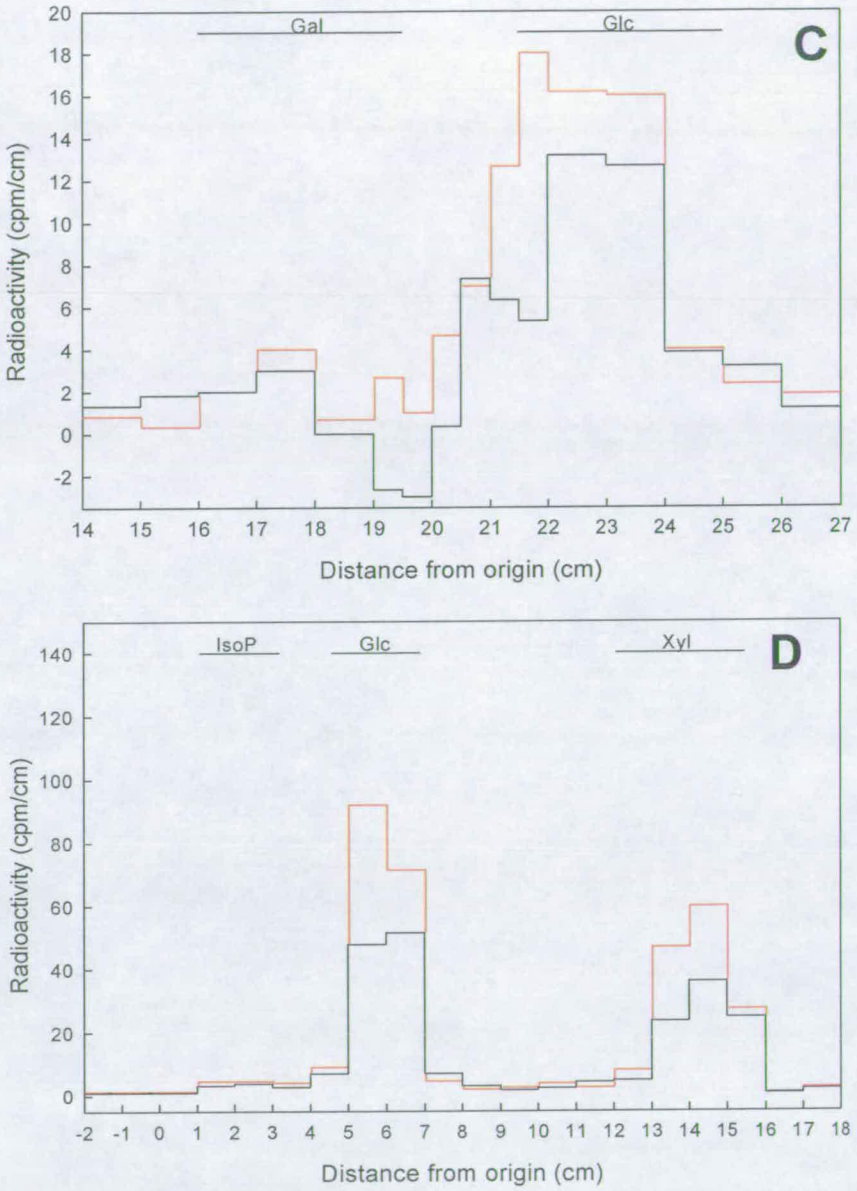

Figure 3.26 Continued

3.2.2.2 EPGase treatment

EPGase was used to digest pectin in the (^{3}H,^{14}C)-labelled AIR. The EPGase digest was initially separated by gel-permeation chromatography (Fig. 3.27). Sepharose CL-6B was used here instead of BioGel P-2 as it has a broad fractionation range. The ^{3}H and ^{14}C profiles (Fig. 3.27) show a dominant peak of radioactivity that corresponds with the internal monosaccharide marker.

The fractions that co-eluted with the internal Glc marker were pooled and paper chromatographed to resolve the GalA oligosaccharides (Fig. 3.28). The GalA oligosaccharides were eluted, TFA hydrolysed and subjected to paper electrophoresis. The paper electrophoretogram was cut into strips and the strips were assayed for radioactivity (Fig. 3.29). Fig. 3.29 shows a distinct peak of GalA.

The elution profile of the EPGase digest on Sephadex CL-6B also shows a small peak of radioactivity in fractions 23 – 31 (Fig. 3.27). Its K_{av} value (~0.56 $\pm$ 0.01; mean $\pm$ SE; N=8) was as expected for RGII. The fractions eluting at K_{av} 0.48–0.64 were pooled, TFA hydrolysed and paper chromatographed (Fig. 3.30), and the purified RG-II-derived Rha was eluted and assayed for ^{3}H and ^{14}C.

3.2.2.3 Termamyl® 120L

The AIR from *Arabidopsis* cell-suspension culture was digested with the α-amylase 'Termamyl® 120L' to obtain maltose (*ex* starch). The digest was paper chromatographed (Fig. 3.31). Maltose was eluted, TFA-hydrolysed and rechromatographed to give rise to a peak of purified radiolabelled Glc (Fig. 3.32).

3.2.2.4 Driselase digestion

Some (^{3}H,^{14}C)-labelled AIR samples were Driselase-digested and the digests

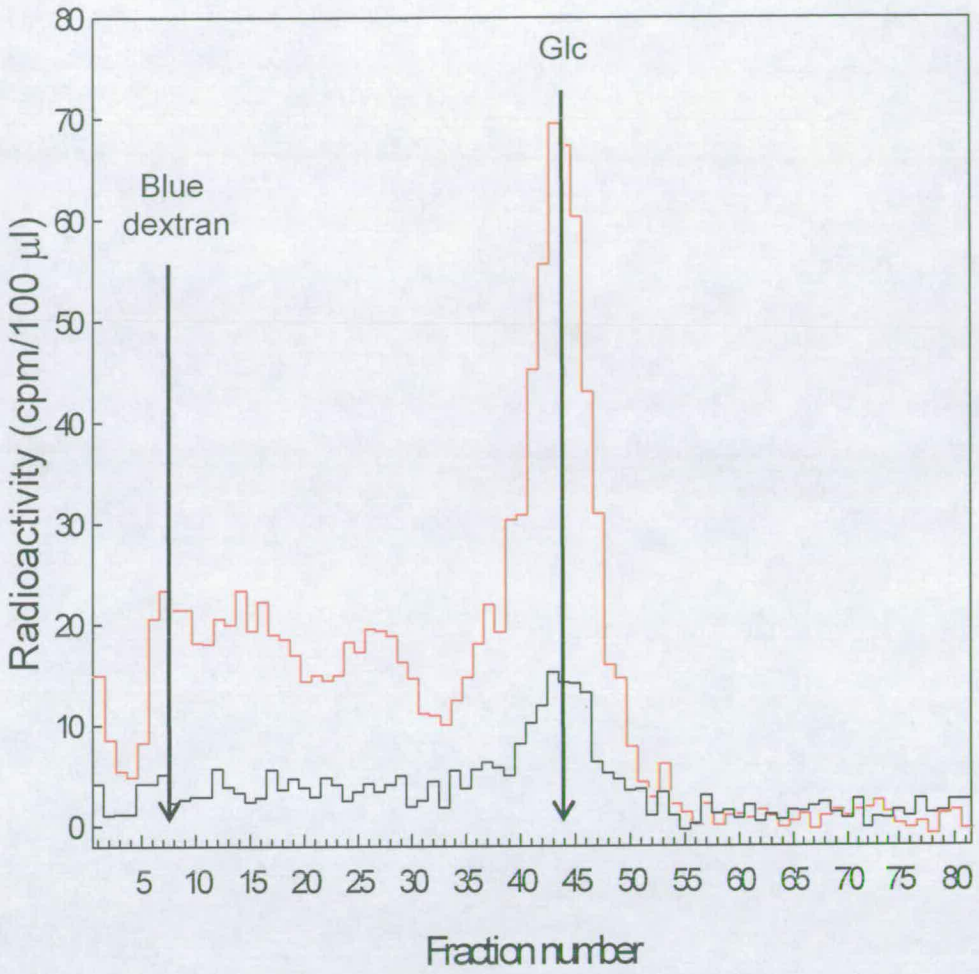

Figure 3.27 Gel-permeation chromatography of products from EPGase digestion of (^{3}H,^{14}C)-labelled AIR

Arabidopsis AIR was digested with EPGase and loaded onto a Sepharose CL-6B column. A portion of the eluted fractions was spotted onto a TLC plate and stained with thymol to detect the internal blue dextran and Glc markers (indicated on the graph with an arrow). A further 100 µl of each fraction was assayed for radioactivity. The (——) represents ^{3}H and the (——) ^{14}C. The sample is typical and the values shown are corrected for the background radioactivity.

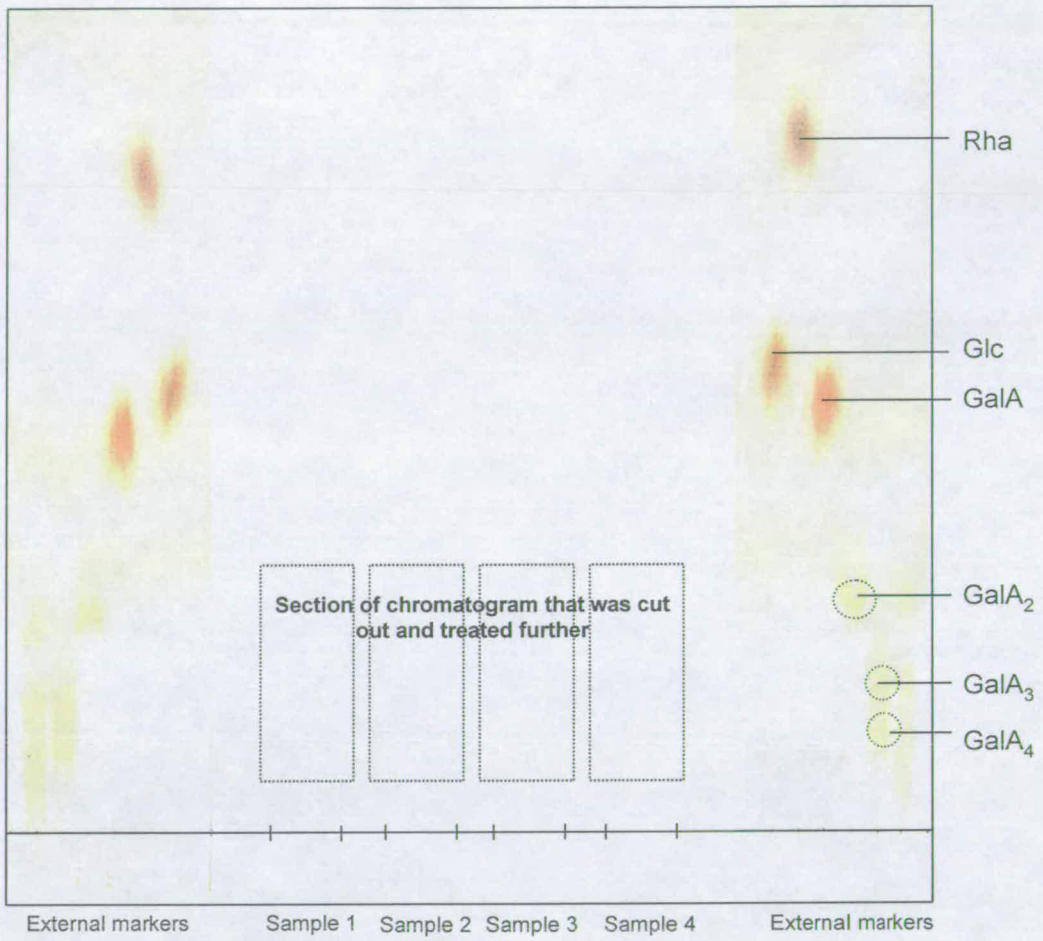

Figure 3.28 Paper chromatography purification of GalA oligosaccharides

The fractions that related to the peak of internal Glc from Fig. 3.28 were pooled and run on Schleicher and Schuell 2045B in EAW (10:5:6, 52 h).

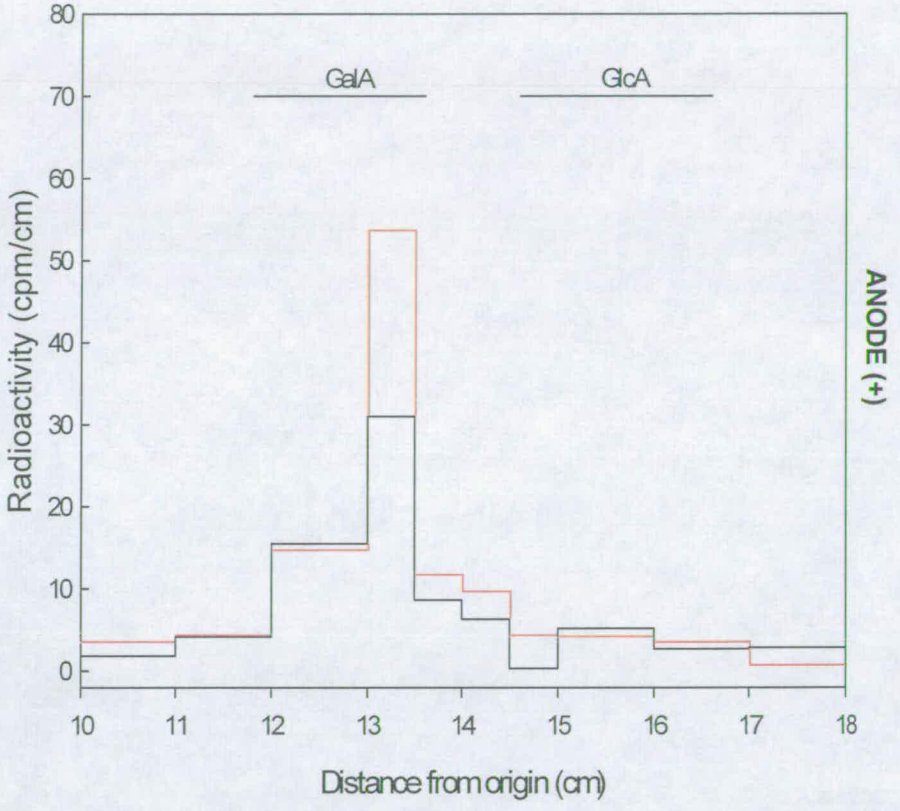

Figure 3.29 Paper electrophoretogram of GalA obtained from EPGase digestion of (^{3}H,^{14}C)-labelled AIR

GalA oligosaccharides were purified from the EPGase digest of (^{3}H,^{14}C)-AIR (Fig. 3.28), TFA hydrolysed (2 M, 120°C, 1 h) and subjected to paper electrophoresis (Whatman 3MM, pH 3.5, 2.5 kV, 1 h). The electrophoretogram was cut into strips and, which were assayed for radioactivity. The (——) represents ^{3}H and the (——) ^{14}C. The sample is typical and the values shown are corrected for the background radioactivity.

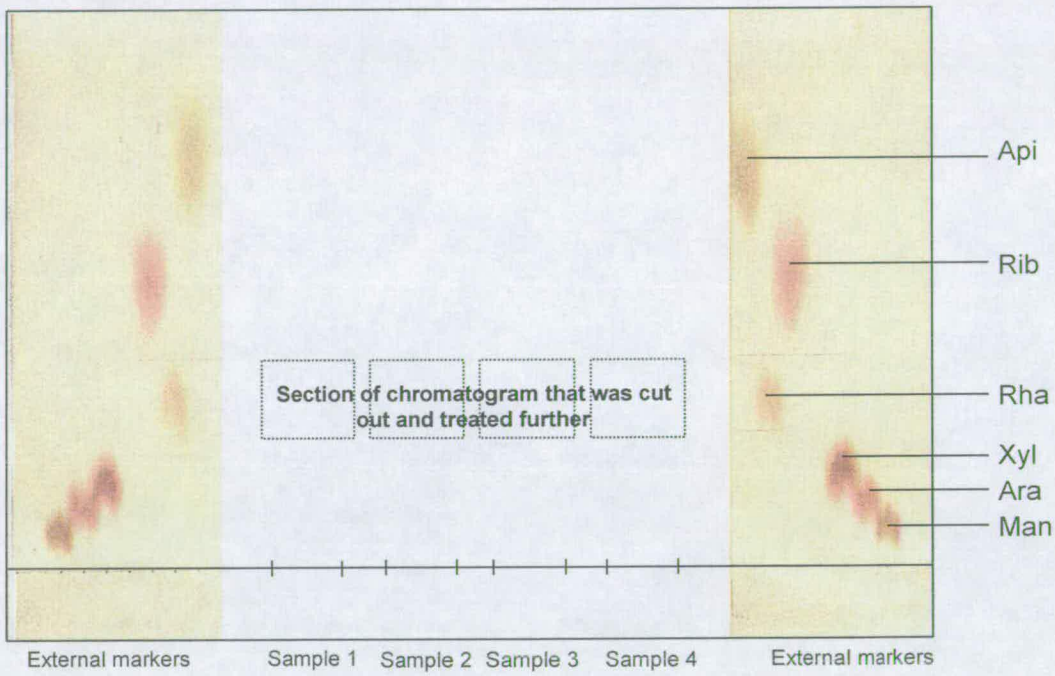

Figure 3.30 Paper chromatography purification of RG-II-derived Rha

The fractions that related to the average 'RG-II' K_{av} were TFA hydrolysed (2 M, 100 µl, 1 h, 120°C) and run on Schleicher and Schuell 2045B in BAB (9:1:1, 16 h).

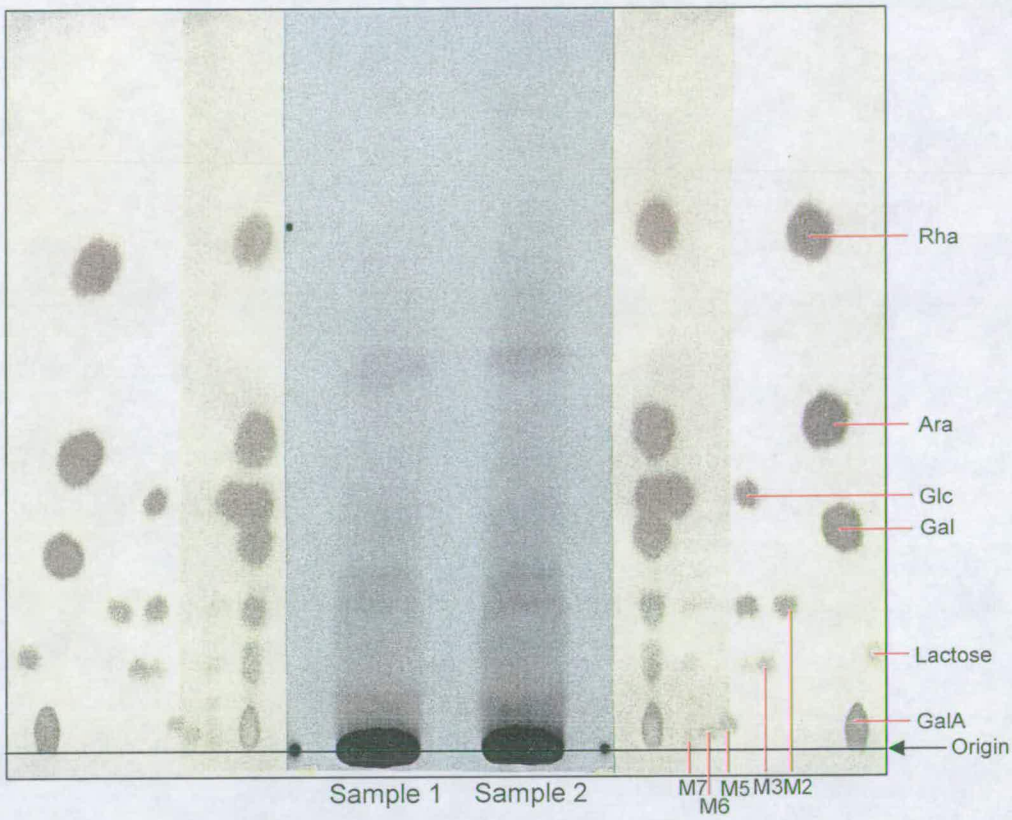

Figure 3.31 Paper chromatography of compounds obtained from Termamyl® 120L digestion of (^{3}H,^{14}C)-labelled AIR

Termamyl 120L AIR digests were run on Schleicher and Schuell 2045B paper in EPW (10:4:3, 50 h). The radiolabelled compounds were autoradiographed (central). The external markers that border the autoradiogram were stained with silver nitrate. The sample shown is typical.

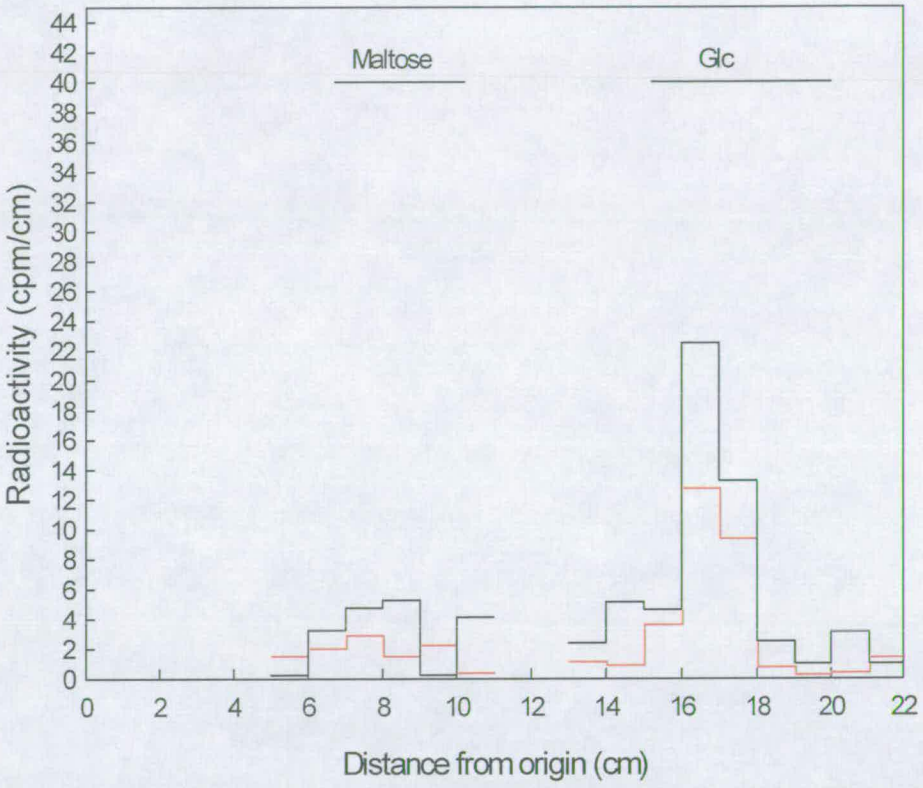

Figure 3.32 Paper chromatography purification of [^{3}H,^{14}C]Glc obtained from acid hydrolysis of maltose

Maltose purified from a Termamyl 120L digest of (^{3}H,^{14}C)-labelled AIR shown in Fig. 3.31 was acid hydrolysed (2 M, 120°C, 1 h) and run on Schleicher and Schuell 2045B paper in EPW (10:4:3, 50 h). The chromatogram was cut into strips, which were assayed for radioactivity. The (——) represents ^{3}H and the (——) ^{14}C. The sample is typical and the values shown are corrected for the background radioactivity.

separated by paper chromatography (Fig. 3.33). The order of greatest ^{14}C radiolabel intensity is Glc>Uronic acids>Gal>IsoP>Ara. The putative Ara and Gal were eluted from the chromatogram shown in Fig. 3.33 and further purified by paper chromatography (Fig. 3.34 A, B). The section of chromatogram shown in Fig. 3.33 that contained radiolabelled uronic acids and IsoP was eluted. The eluted compounds were subjected to paper electrophoresis (Fig. 3.35) to obtain purified [^{3}H,^{14}C]GalA. Fig. 3.35 clearly shows the presence of radiolabelled GalA but not GlcA. The neutral zone on the electrophoretogram, thought to contain IsoP, was eluted and the eluate paper chromatographed (Fig. 3.36 A) to give a single peak that corresponded with an external IsoP marker. The putative IsoP obtained from Fig. 3.36 (A) was hydrolysed with TFA. The hydrolysate was chromatographed to obtain xyloglucan-derived Xyl and Glc (Fig. 3.36 B).

3.2.2.5 TFA hydrolysis

Some (^{3}H,^{14}C)-labelled AIR samples were hydrolysed with TFA (2 M, 120°C, 1 h) and the hydrolysate was paper chromatographed in 2D (as per section 3.2.1, Fig. 3.22). However, unlike in section 3.2.1, Rib was the only compound that did not undergo further purification.

The decreased amount of radioactivity utilised in this experiment in comparison to the first experiment (section 3.2.1) meant that, after further purification of the monosaccharides, autoradiography was not sensitive enough to detect the compounds. Therefore, each paper chromatogram or electrophoretogram was cut into strips and the strips were assayed for radioactivity. This method was

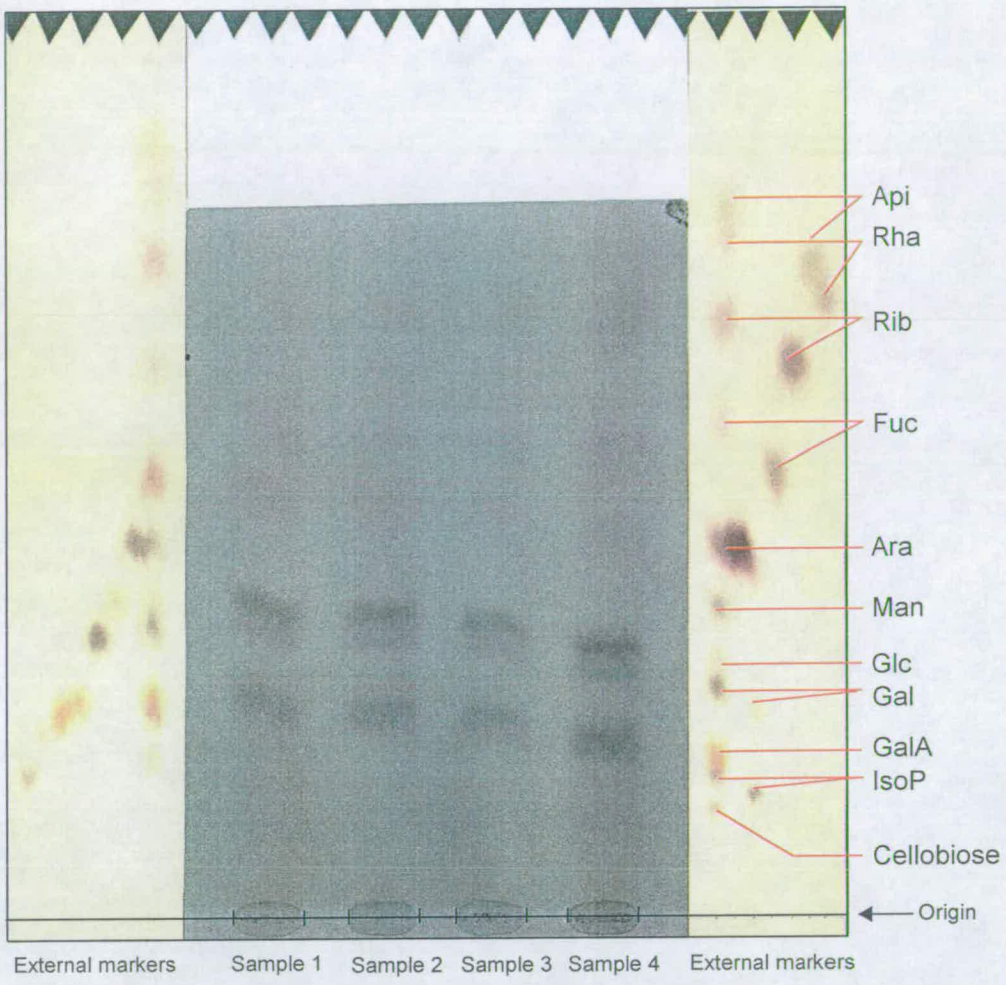

Figure 3.33 Paper chromatography purification of products from Driselase digestion of (^{3}H,^{14}C)-labelled AIR

(^{3}H,^{14}C)-Labelled AIR was digested with Driselase and the products were run on Whatman 3MM in BAW (12:3:5, 17 h) followed by EPW (8:2:1, 17 h) in 1D. The sample is a representative.

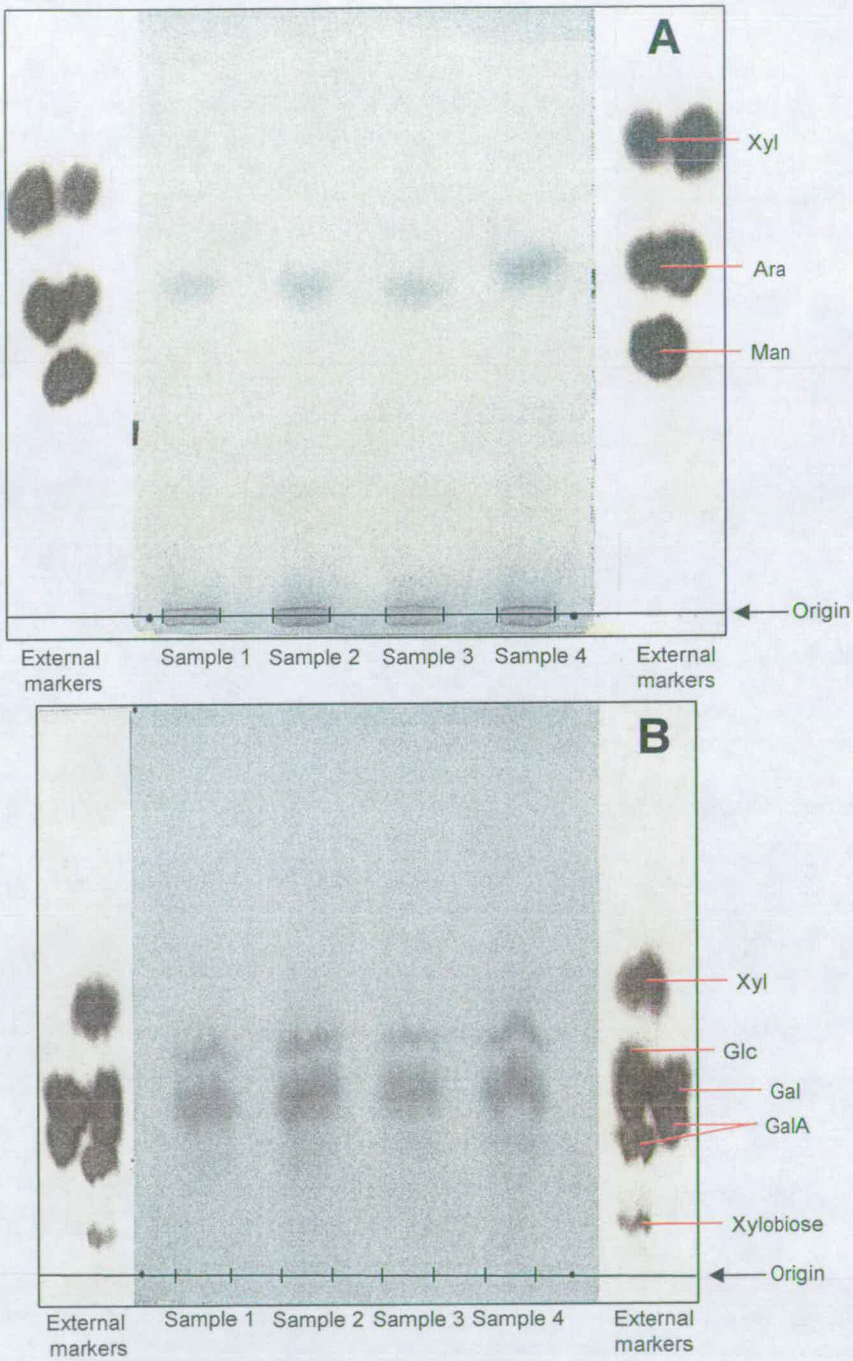

Figure 3.34 Paper chromatography purification of [^{3}H,^{14}C]Ara and [^{3}H,^{14}C]Gal obtained from Driselase digestion of (^{3}H,^{14}C)-labelled AIR

The Ara and Gal eluted from the chromatogram shown in Fig. 3.33 were run on Schleicher and Schuell 2045B paper in (**A**) EPW (8:2:1, 36 h) and (**B**) BAW (12:3:5, 74 h), respectively. In (**B**) the largest spot of radioactivity was eluted as Gal. The radiolabelled compound that migrated faster than the Gal is proposed to be a small amount of Glc. The samples shown are representative.

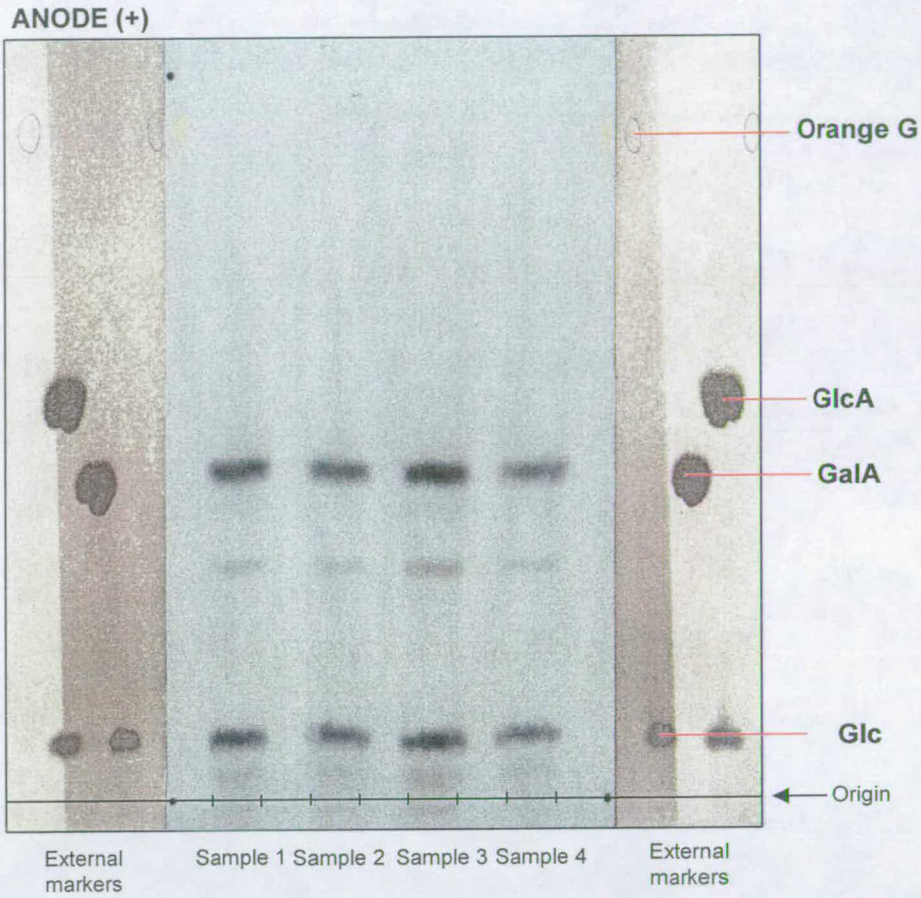

Figure 3.35 Paper electrophoresis separation of [^{3}H,^{14}C]IsoP and (^{3}H,^{14}C)-labelled uronic acids obtained from Driselase digestion of (^{3}H,^{14}C)-labelled AIR

The area of chromatogram that co-migrated with GalA, GlcA and IsoP shown in Fig. 3.33 was eluted and subjected to paper electrophoresis on Whatman 3MM (pH3.5, 2.5 kV, 1.5 h). The external markers were stained with silver nitrate. The sample shown is typical.

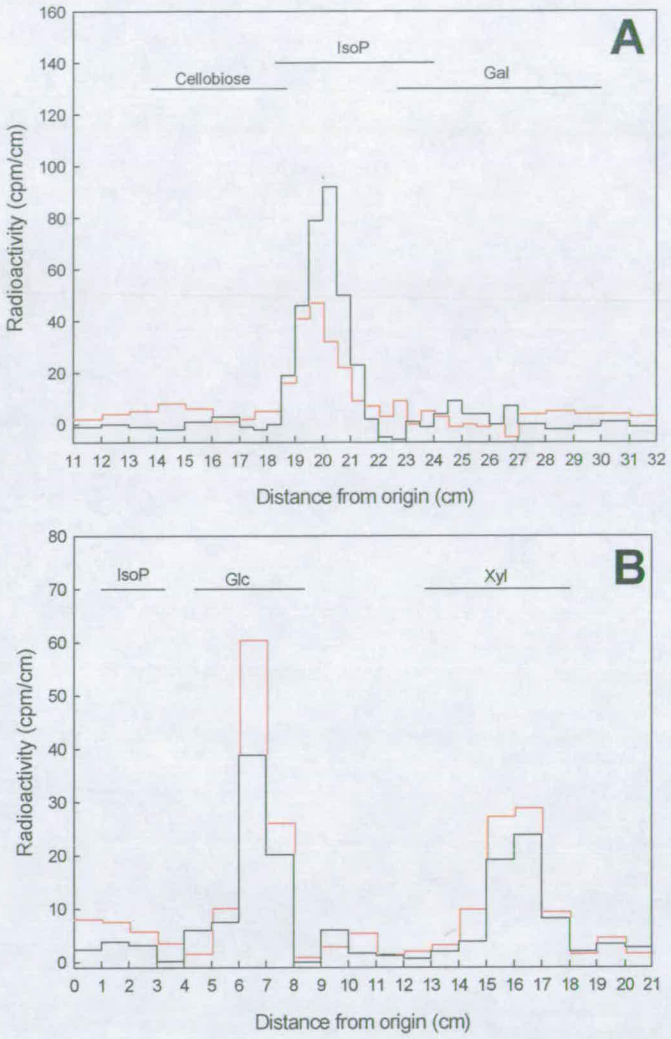

Figure 3.36 Paper chromatography purification of Xyl and Glc obtained from [^{3}H,^{14}C]IsoP originally derived from a Driselase digestion of (^{3}H,^{14}C)-labelled AIR.

The area that corresponded with the neutral zone of the electrophoretogram shown in Fig. 3.35 was run on (**A**) Whatman no. 1 in EPW (9:3:2, 21 h). The chromatogram was cut into strips, which were assayed for radioactivity. The strips of paper that contained the peak of radioactivity that corresponded with IsoP were washed with toluene and eluted. The eluted IsoP was hydrolysed with TFA (2 M, 120°C, 1 h) and the hydrolysate was run on (**B**) Schleicher and Schuell paper 2045B in EPW (8:2:1, 48 h). The chromatogram was cut into strips which were assayed for radioactivity. The (——) represents ^{3}H and the (——) ^{14}C. The samples are representative and the values shown are corrected for the background radioactivity.

utilised to localise purified radiolabelled Gal, Glc, Xyl, Rha, Ara and GalA from the hydrolysate to yield distinct peaks of each monosaccharide (Fig. 3.37).

3.2.2.6 ^{3}H:^{14}C Ratios of monosaccharides derived from the AIR by different methods

In section 3.2.2 the AIR from cells fed either [1-^{3}H]Gal, [U-^{14}C]Glc or [U-^{14}C]Fru was subdivided into portions, which were assayed for radioactivity. The AIR samples were combined so that each ^{3}H-labelled sample was partnered with a ^{14}C-labelled sample to form an individually known ^{3}H:^{14}C ratio. The purified monosaccharides derived from the (^{3}H,^{14}C)-AIR were obtained by different methods and assayed for ^{3}H and ^{14}C.

A worked example of the calculations used to determine the ^{3}H:^{14}C ratio of each of the monosaccharides is presented in the Materials and Methods (section 2.9.1). Some of the ^{3}H:^{14}C ratios were based on a 3:1 ^{3}H:^{14}C ratio and others on a 5:1 ^{3}H:^{14}C ratio. The isotope ratio calculations account for this to make each of the final monosaccharide isotope ratios comparable. Like section 3.2.1.2 the cells were originally fed a monosaccharide that had six ^{14}C-labelled carbon atoms ([U-^{14}C]Glc or [U-^{14}C]Fru). Owing to this it would not be possible to make direct comparisons between the isotope ratios of C_5 to C_6 compounds. The calculations account for this to enable comparisons between C_5 compounds and those of C_6 compounds. Fig. 3.38 shows the calculated ^{3}H:^{14}C ratios (Appendix 8).

The isotope ratio for Gal, whether derived from the AIR of cells originally fed [U-^{14}C]Glc or [U-^{14}C]Fru, and whether derived from total Gal or xyloglucan-derived Gal, had the highest ^{3}H:^{14}C value and confirms the validity of the

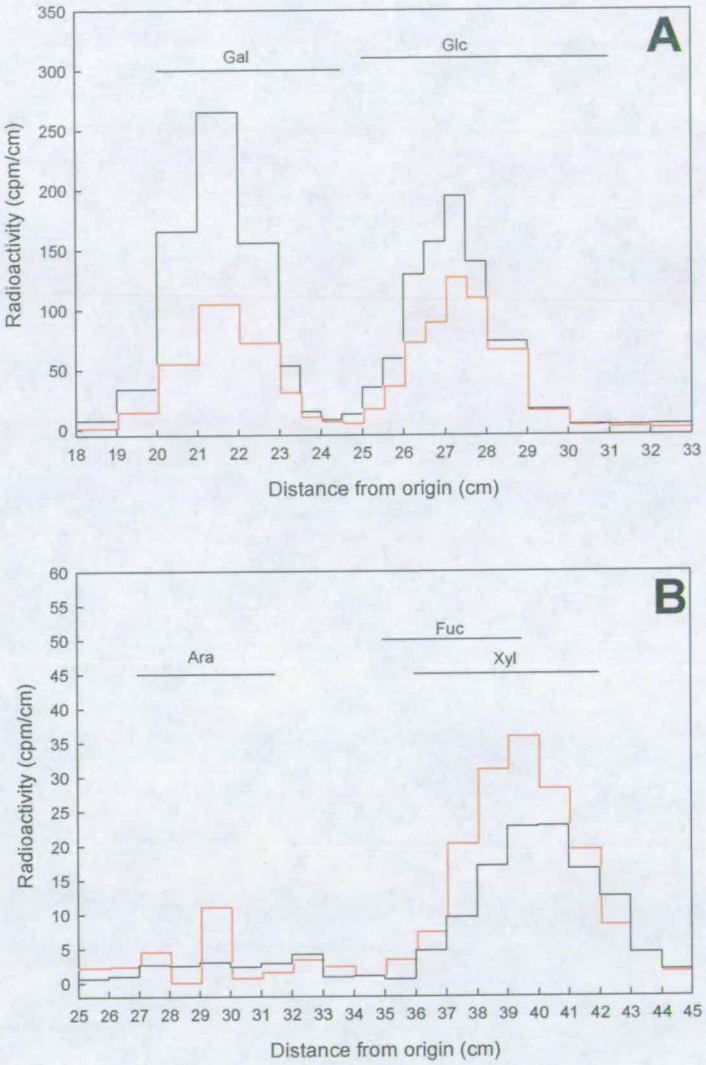

Figure 3.37 Paper chromatography purification of radiolabelled monosaccharides obtained from TFA hydrolysis of (^{3}H,^{14}C)-labelled AIR

The relevant areas of the chromatogram separated as per Fig. 3.22 were eluted and rechromatographed to purify the compounds. The eluted Gal/Glc sample was run on (**A**) Schleicher and Schuell 2045B in EPW (8:2:1, 120 h); Xyl was run on (**B**) Schleicher and Schuell 2045B in EPW (8:2:1, 60 h); Rha was run on (**C**) Schleicher and Schuell 2045B in BAB (9:1:1, 16 h) and Ara was run on (**D**) Schleicher and Schuell 2045B in EPW (8:2:1, 72 h). The GalA sample was loaded onto Whatman 3MM and subjected to paper electrophoresis (pH 3.5, 2.5 kV, 1 h). Each chromatogram and electrophoretogram was cut into strips and assayed for radioactivity. The (——) represents ^{3}H and the (——) ^{14}C. Each sample is representative and the values shown are corrected for background radioactivity.

Continued overleaf

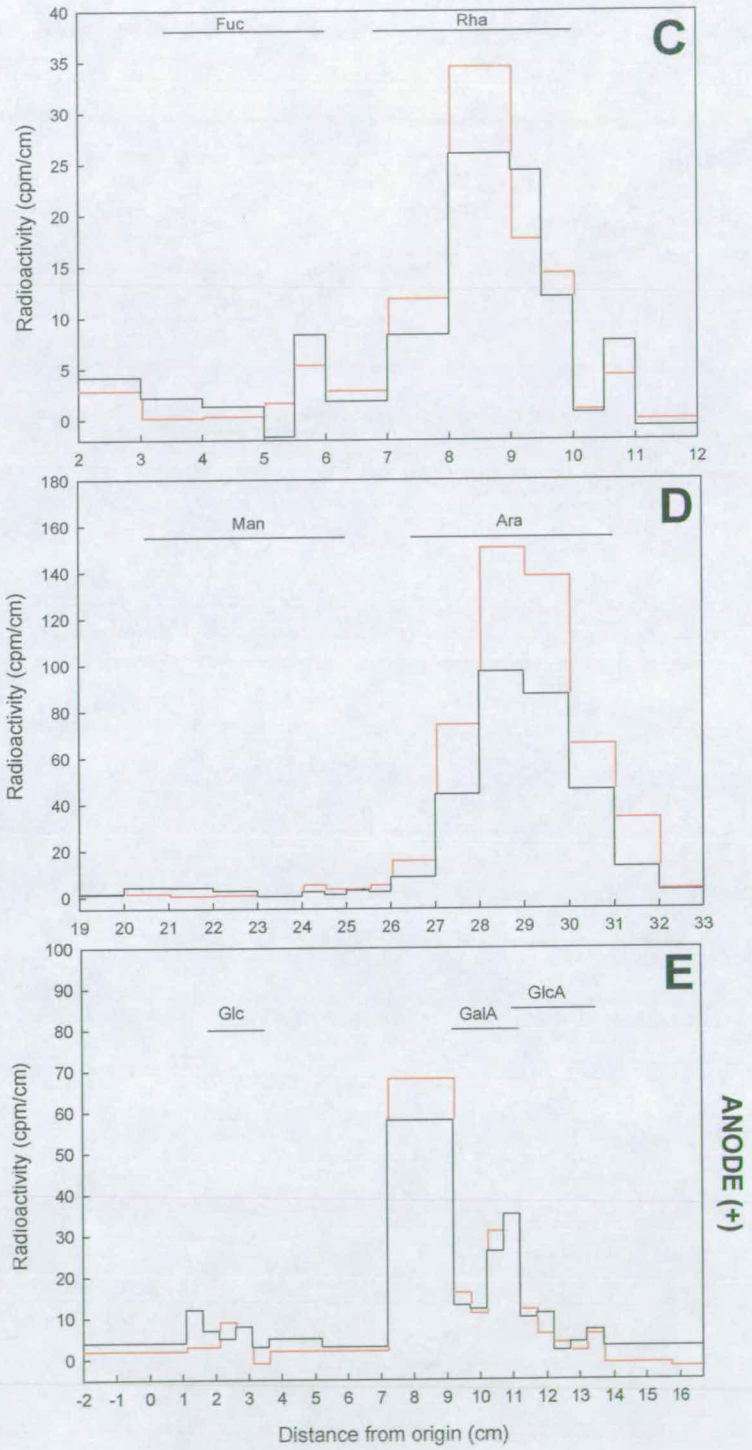

Figure 3.37 Continued.

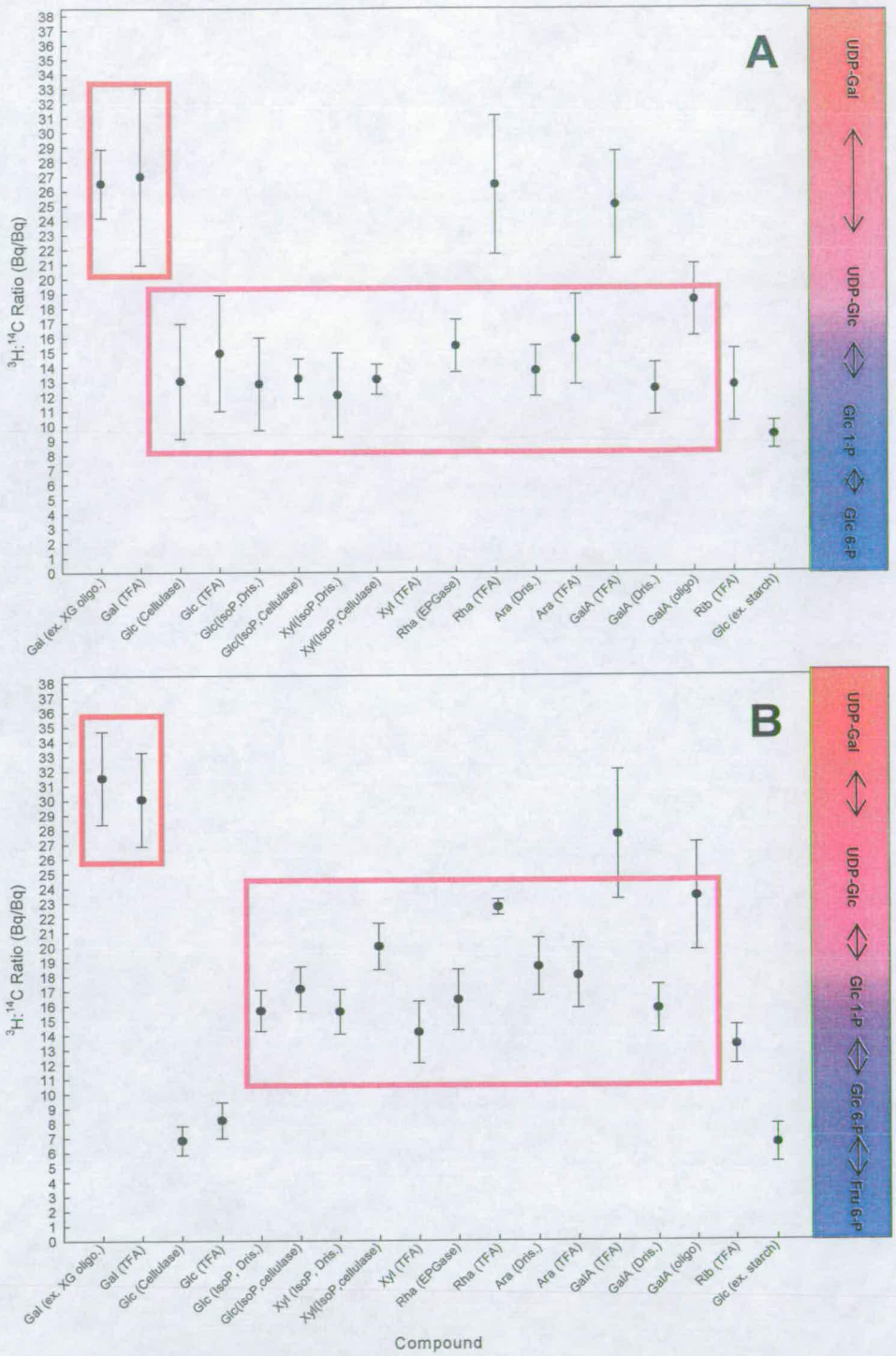

Figure 3.38 Normalised ^{3}H:^{14}C ratios of monosaccharides obtained from the AIR of cells fed [1-^{3}H]Gal combined with the AIR of cells fed (**A**) [U-^{14}C]Glc or (**B**) [U-^{14}C]Fru.

The colour gradient indicates the 'core' metabolites that each of the cell-wall monosaccharides may have stemmed from. The increased level of red in the colour gradient represents a high ^{3}H:^{14}C ratio as this is 'closer' to the ^{3}H source. An increased level of blue indicates a lower ^{3}H:^{14}C ratio as this is more 'distanced' from the ^{3}H source. The error bars shown are standard error where N=4 (Appendix 8).

experimental protocol utilised in both this experiment (section 3.2.1) and the previous experiment (section 3.2.2).

Below the high isotope ratio of Gal lie the ratios of a group of compounds. In the case of [U-^{14}C]Glc-fed cells, these compounds are Glc (cellulosic, *ex* IsoP, total matrix and starch), Xyl (*ex* IsoP), Rha (*ex* RG-II), Ara (total and Driselase-released) and GalA (Driselase-released and pectin oligogalacturonide-derived). Based on their similar ratios, the aforementioned compounds, bar Glc (*ex* starch), are thought to share the same common parent 'core' metabolite, namely UDP-Glc (section 3.2.2.6). Man and Fuc were unable to be obtained in this experiment because the amount of radioactivity used was too low. Despite this the closeness between the pattern of results shown in Fig. 3.38 A and that in the last experiment (Fig. 3.22) suggests that the previous conclusions hold true.

A similar distribution of ^{3}H:^{14}C ratios is witnessed in the monosaccharides derived from [U-^{14}C]Fru-fed cells. Fig. 3.38 B shows that Glc (*ex* IsoP), Xyl (*ex* IsoP and TFA), Rha (EPGase and TFA), Ara (Driselase and TFA) and GalA (Driselase) all have similar isotopic ratios. This again suggests that these compounds have the same parent 'core' metabolite, namely UDP-Glc.

The most obvious difference in the ^{3}H:^{14}C ratios between Fig. 3.38 A and Fig. 3.38 B is that the Glc (*ex* cellulose, TFA and *ex* starch) isotope ratios become distinct from the grouped isotope ratios after [^{14}C]Fru-feeding. The only difference between the [^{14}C]Glc-feeding and [^{14}C]Fru-feeding experiment is addition of Fru 6-P as a 'core' metabolite in the latter experiment. The addition of one more 'core' metabolite is not expected to appreciably change the isotope ratio gradient amongst the 'core' metabolites UDP-Gal, UDP-Glc, Glc 1-P and Glc 6-P. Fru 6-P and its

products would be expected to have a similar ^{3}H:^{14}C ratio to Glc 6-P in the [^{14}C]Glc-feeding experiment but a lower isotope ratio in the [^{14}C]Fru-feeding experiment. It is therefore unexpected that the Glc (*ex* cellulose, TFA and *ex* starch) isotope ratios are much lower than those of the boxed group in the [^{14}C]Fru-feeding experiment.

The precursor of starch is widely thought to be ADP-Glc. The formation of starch in relation to the 'core' metabolites is thought to proceed through Fru 6-P to triose phosphates. The triose phosphates are transported into the plastids where they are converted to ADP-Glc. If this were the case the Glc (*ex* starch) would be predicted to have a similar/lower isotope ratio to Fru 6-P (in [U-^{14}C]Fru fed cells) or Glc 6-P (in [U-^{14}C]Glc fed cells) derivatives. If the cells formed ADP-Glc in the cytosol and directly imported the cytosolic ADP-Glc into the plastids for starch synthesis the 'core' metabolite of ADP-Glc would be Glc 1-P and would be expected to have a higher isotope ratio than Fru 6-P (in [U-^{14}C]Fru fed cells) or Glc 6-P (in [U-^{14}C]Glc fed cells) derivatives. The absence of isotope ratios from compounds known to be derived from 'core' metabolites more metabolically 'distanced' from the ^{3}H source than UDP-Glc does not allow a conclusion to be drawn on these two proposed pathways of starch synthesis.

The similarity between the Glc (total matrix) and Glc (*ex* starch) ^{3}H:^{14}C ratios may be influenced by the quantity of starch synthesised by the cells. If starch formation dominated over cellulose formation the Glc isotope ratio from starch could, potentially, influence the total Glc isotope ratio.

The isotope ratio of Rib is in a similar position to that shown in Fig. 3.22. This is true whether the Rib is obtained from cells fed [^{14}C]Glc or [^{14}C]Fru and reinforces the possibility that the pathways that stem from Fru 6-P and Glc 6-P (Fig.

3.23) may not be the predominant pathways for the synthesis of Rib residues in RNA.

The quantity of radioactivity used in this experiment did not allow for the isolation of Man and Fuc. Despite this there is a similar distribution pattern of isotope ratios witnessed between Fig. 3.38 and Fig. 3.22. The ability to isolate AIR-derived monosaccharides by different methods and obtain a similar ratio in each case suggests that the isotope ratios obtained by different techniques are not an artefact of a particular method that was used.

3.2.3 Analysis of the ^{3}H:^{14}C ratios of intermediary metabolites and incorporated monosaccharide residues over time

In the previous sections (section 3.2.1, section 3.2.2) the [1-^{3}H]Gal and [U-^{14}C]Glc or [U-^{14}C]Fru were fed to the cells and an artificial total ^{3}H:^{14}C ratio was formed by combination of a ^{3}H-AIR hydrolysate with ^{14}C-AIR hydrolysate or ^{3}H-AIR with ^{14}C-AIR. In the following experiment, however, a solution that contained both [1-^{3}H]Gal and [U-^{14}C]Fru was fed to the cells. In this section a study of the kinetics of radiolabel entry into the intermediary metabolites involved in sugar nucleotide formation pathways and end products was conducted. This was carried out to understand more about the order that the metabolites are labelled in. Indeed, a metabolite that is further from the radiolabelled source will not become radiolabelled until after its precursors are radiolabelled. The order of radiolabel entry into intermediary metabolites could suggest which of the sugar nucleotide pathways predominate. In addition to this the AIR was TFA-hydrolysed and the monosaccharides in the hydolysate were purified and assayed for their ^{3}H:^{14}C ratio to enable a kinetic study of radiolabel entry into the end products.

3.2.3.1 Initial separation of intermediary metabolites

Arabidopsis cell-suspension culture was fed [1-^{3}H]Gal and [U-^{14}C]Fru and incubated for various lengths of time, after which the cells were killed with ethanol:formic acid to extract low molecular weight metabolites. The best method of initial separation of the low molecular weight metabolites, based on the separation of standard markers (Fig. 3.39), was paper electrophoresis (pH 2.0, 1.5 KV, 1.0 h). The supernatant was subjected to paper electrophoresis to separate the bulk of the intermediary

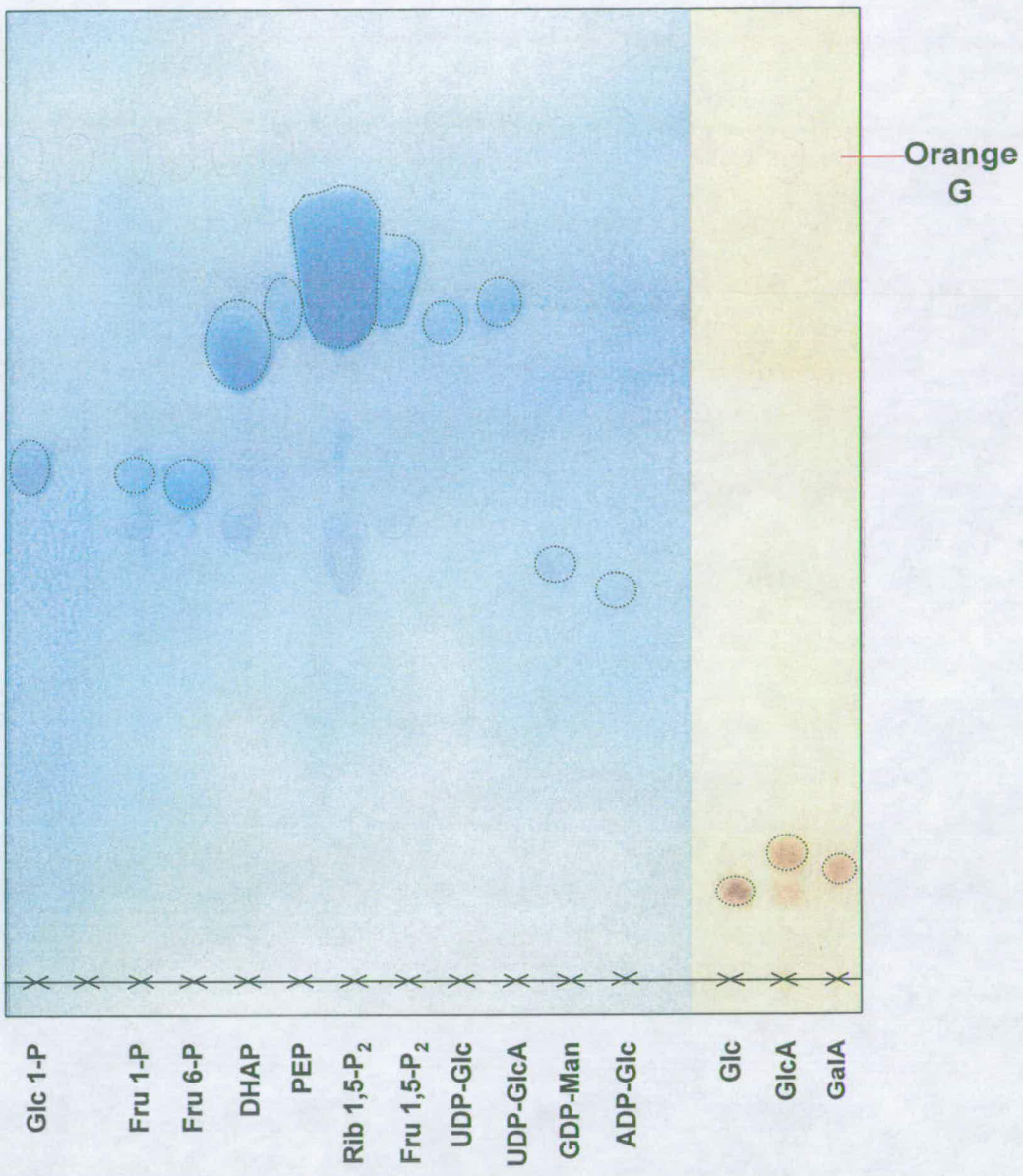

Figure 3.39 Separation of standard markers by paper electrophoresis

Markers (0.5% w/v) were loaded onto Whatman 3MM and subjected to paper electrophoresis (pH 2.0, 1.5 kV, 1.0 h). (1) Stained with molybdate. (2) Stained with aniline hydrogen phthalate. Compounds that are not circled are contaminants.

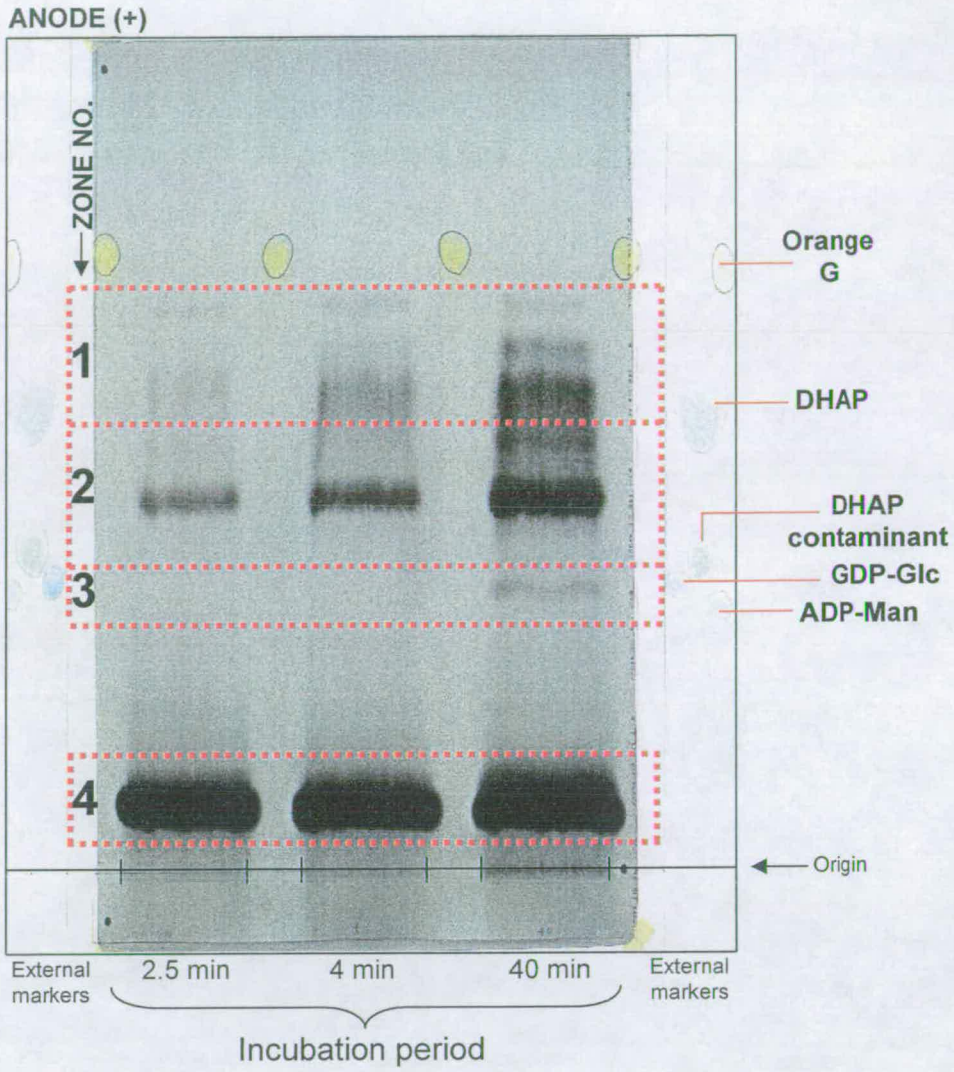

Figure 3.40 Initial separation of (^{3}H,^{14}C)-labelled small molecular weight cellular metabolites

The ethanol:formic acid:water (7:1:2, v/v/v) soluble fraction was loaded onto Whatman 3MM and subjected to paper electrophoresis (pH 2.0, 1.5 kV, 1.0 h). **Zone one** contains the UDP-sugars and bisphosphate compounds. **Zone two** includes most hexose monophosphates. **Zone three** contains the GDP- and ADP-sugars and **zone four** includes neutral sugars and Krebs cycle intermediates. The external markers were stained with molybdate. The radioactive compounds were autoradiographed. The sample shown is representative.

metabolites into four zones (Fig. 3.40), which were eluted and treated further. The zone with the greatest amount of ^{14}C radioactivity at all time points was zone four. This was most likely because it contained unmetabolised [U-^{14}C]Fru. Zone two had the second greatest intensity of ^{14}C followed by zone one and then zone three.

3.2.3.2 Zone one — Bisphosphate compounds, UDP-sugars

The samples from zone one were hydrolysed with mild acid to remove the UDP group from the monosaccharide of interest. Conditions of mild acid would not yield free Glc or Fru from Glc 1,6-P_2 and Fru 1,6-P_2. Therefore the Glc obtained from the mild acid hydrolysate is considered to be *ex* UDP-Glc. The hydrolysates were paper chromatographed and autoradiographed (Fig. 3.41). The monosaccharides of interest included the uronic acids and the compounds that migrated faster than the uronic acids. It was found that UDP-Glc was already radiolabelled by 1.5 min. At each timepoint Glc had the greatest amount of radioactivity followed by Gal, Ara and Xyl. Unfortunately Rha was lost.

^{3}H is a weak β-emitter. The dark spots on the autoradiogram predominantly represent ^{14}C. The autoradiogram in Fig. 3.41 shows that the point of ^{14}C entry into the 'core' metabolite pathway is closer to Glc than Gal. Fig. 3.41 also shows that Ara and Xyl were detected at later timepoints. The radiolabelled Xyl, Glc and Gal spots were eluted and assayed for ^{3}H and ^{14}C.

The uronic acids shown in Fig. 3.41 were eluted and separated by paper electrophoresis (Fig. 3.42). It is clear that, of the time points taken, the maximum radiolabel incorporation into both GalA and GlcA occurs by 40 min. The peak of radiolabel decreased after 120 min and detection of the compounds was lower still after 8 h.

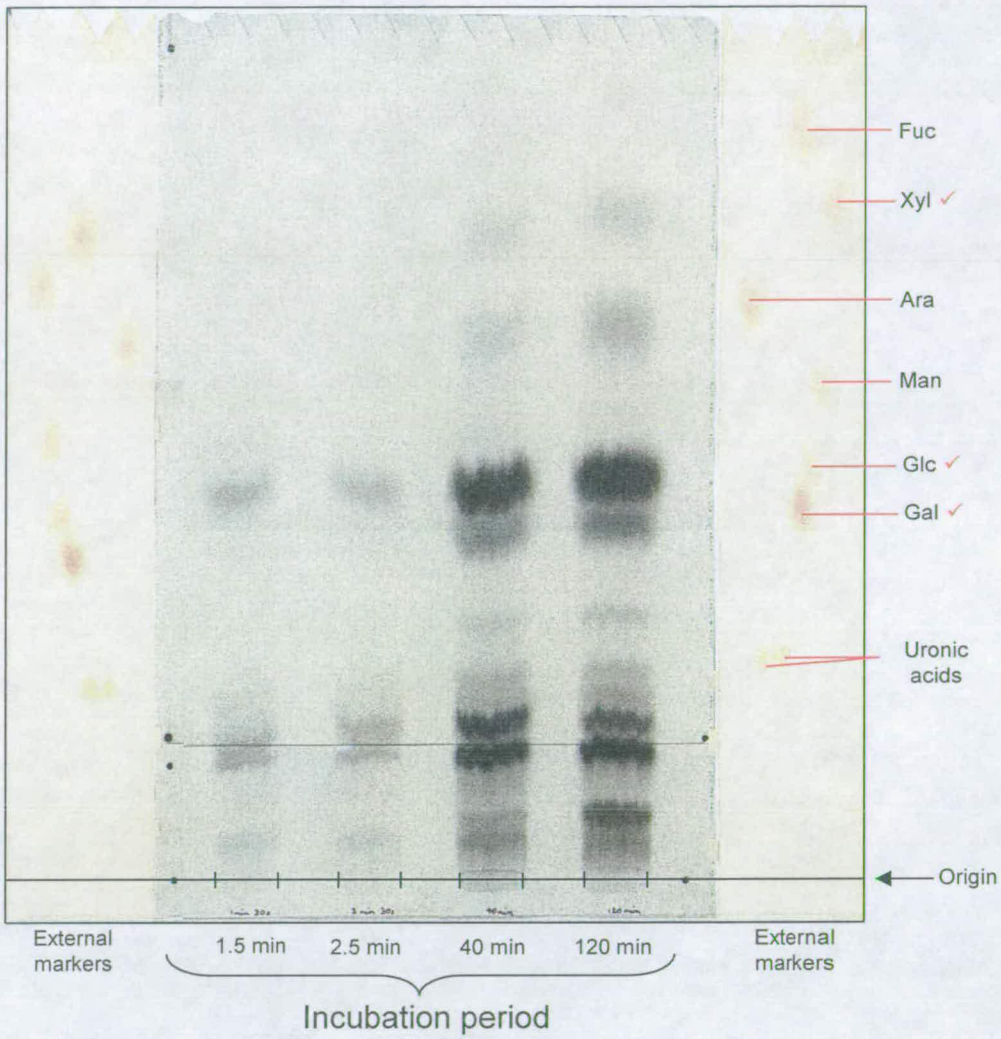

Figure 3.41 Separation of the products obtained by mild acid hydolysis of UDP-[^{3}H,^{14}C]sugars and bisphosphate compounds

Zone one eluted from the electrophoretogram shown in Fig. 3.40 was hydrolysed with mild acid and run on Whatman 3MM in BAW (12:3:5, 17 h) followed by EPW (8:2:1, 17 h). The external markers were stained with aniline hydrogen-phthalate. The radioactive sample compounds were autoradiographed. The chromatogram shown is representative. The (✓) indicates the radioactive compound that corresponded to this marker was deemed not to require further purification. The bands beneath the uronic acids could include acid-resistant monophosphates formed by partial hydrolysis of bisphosphates and, possibly, phosphoglyceric acid.

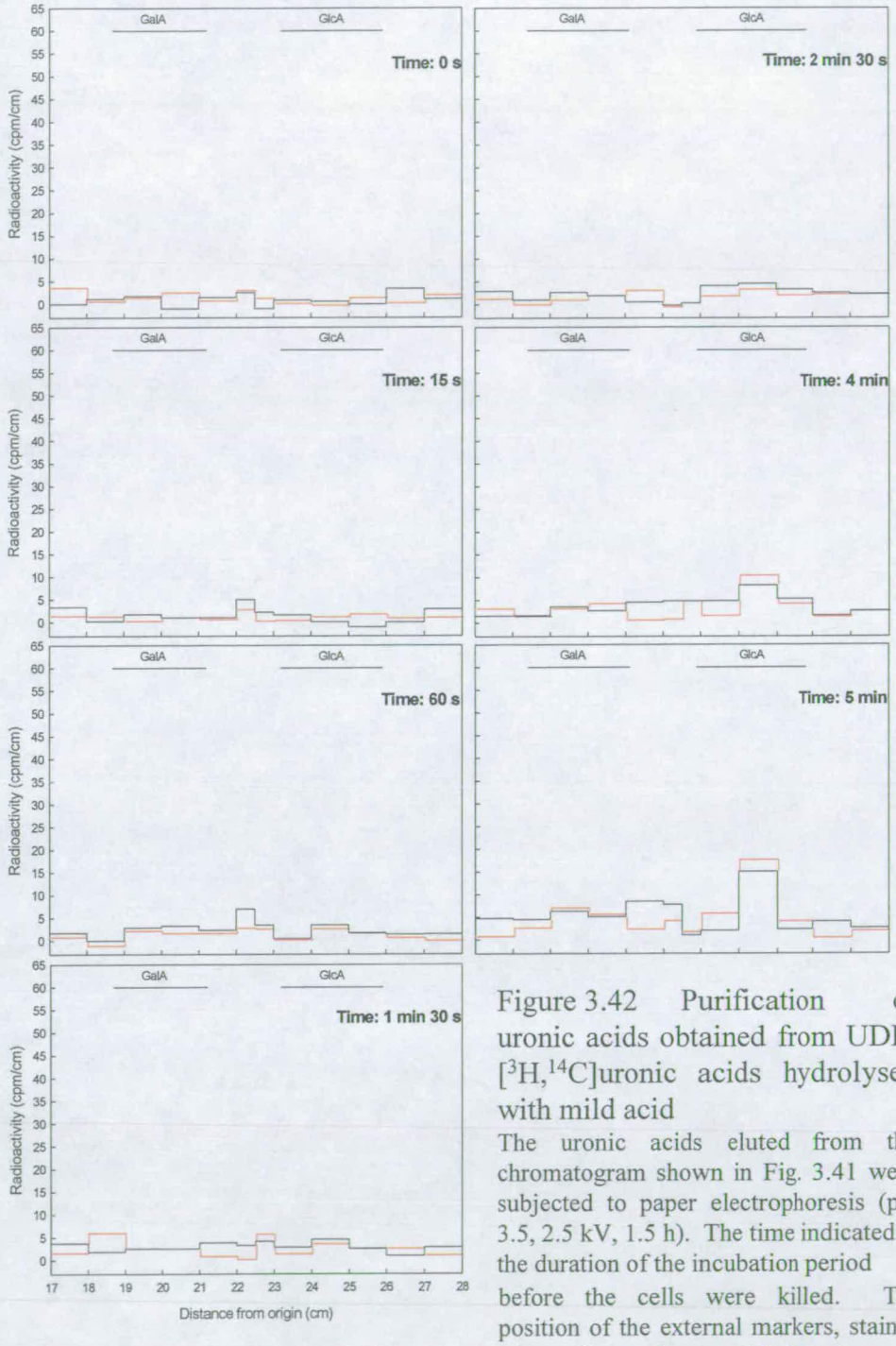

Figure 3.42 Purification of uronic acids obtained from UDP-[^{3}H,^{14}C]uronic acids hydrolysed with mild acid

The uronic acids eluted from the chromatogram shown in Fig. 3.41 were subjected to paper electrophoresis (pH 3.5, 2.5 kV, 1.5 h). The time indicated is the duration of the incubation period before the cells were killed. The position of the external markers, stained with aniline hydrogen-phthalate, is indicated on each graph. The (—) represents ^{3}H and the (⟶) represents ^{14}C.

Continued overleaf

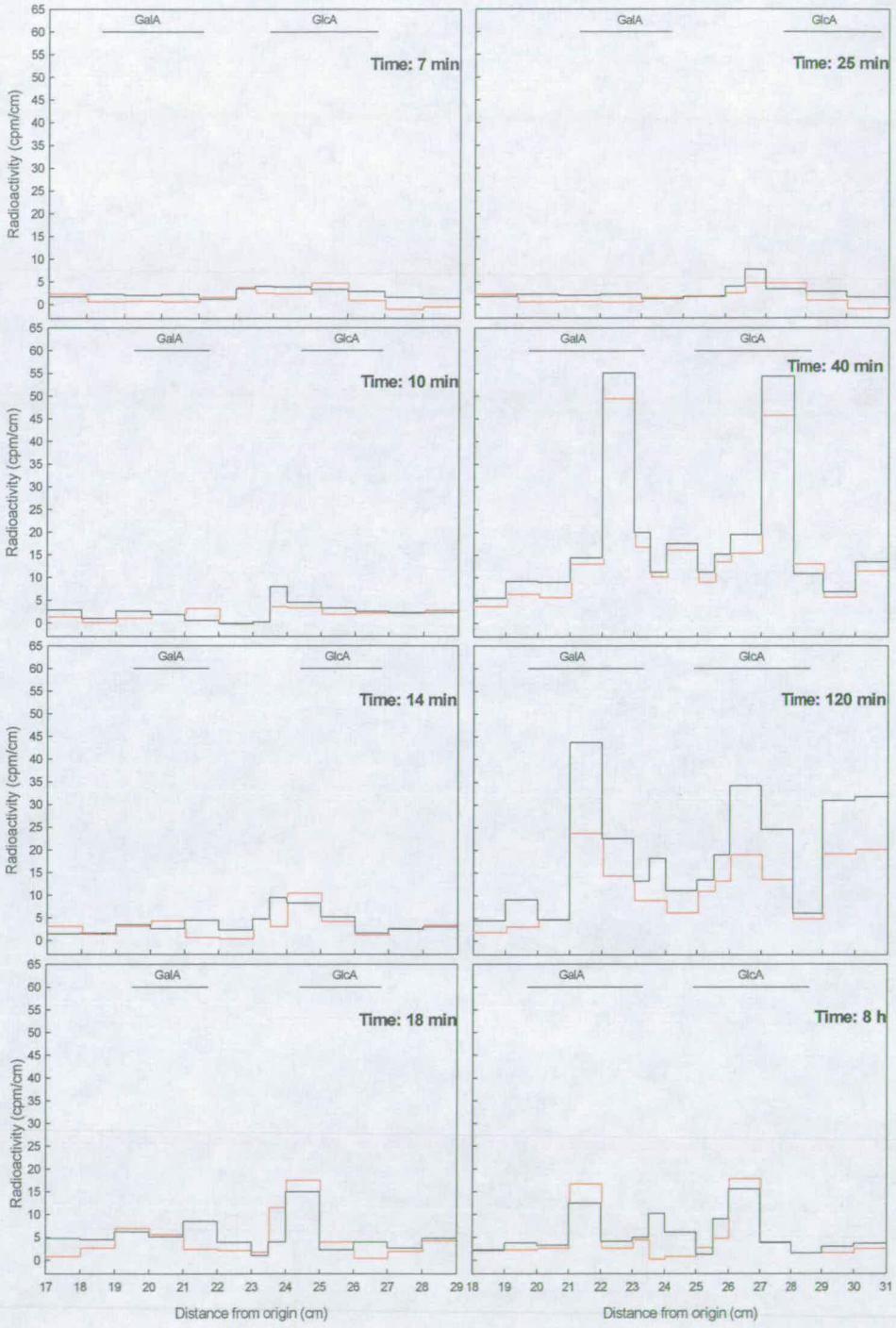

Figure 3.42 Continued

The Ara band eluted from the paper chromatogram shown in Fig. 3.41 was thought to be too wide to contain only a single compound. Therefore the eluted Ara was further purified by paper chromatograpy in phenol (Fig. 3.43). Indeed, the later timepoints that have a peak of Ara show a small peak that migrates slightly faster than Rha. A large peak of radiolabelled Ara is witnessed at 25 min and continues at least until 120 min. At 8 h the radiolabelled Ara peak is still present but to a much lesser extent.

The strips of paper that related to the Ara, GalA and GlcA samples were washed in toluene and eluted.

3.2.3.3 Zone two — Hexose monophosphates

Techniques such as paper electrophoresis and paper chromatography are not readily able to separate a mixture of monophosphorylated monosaccharides that are phosphorylated at different positions. For example Glc 1-P and Glc 6-P are too similar to separate by these methods. In order to assay each of the main monophosphorylated monosaccharides it was necessary to divide each sample obtained from the electrophoretogram shown in Fig. 3.40 (zone two) into two aliquots.

The first aliquot was treated with an acid phosphatase to remove all the phosphate groups and then paper chromatographed (Fig. 3.44). Fig. 3.44 shows the appearance of radiolabelled Glc and Fru by 15 s. Any phosphorylated compounds remain at the origin. As the acid phosphatase treatment leaves very little ^{14}C-labelled material at the origin of the chromatogram (Fig. 3.44) the digestion was successful. Glc is more ^{14}C-labelled than Fru throughout the timecourse even the original ^{14}C-

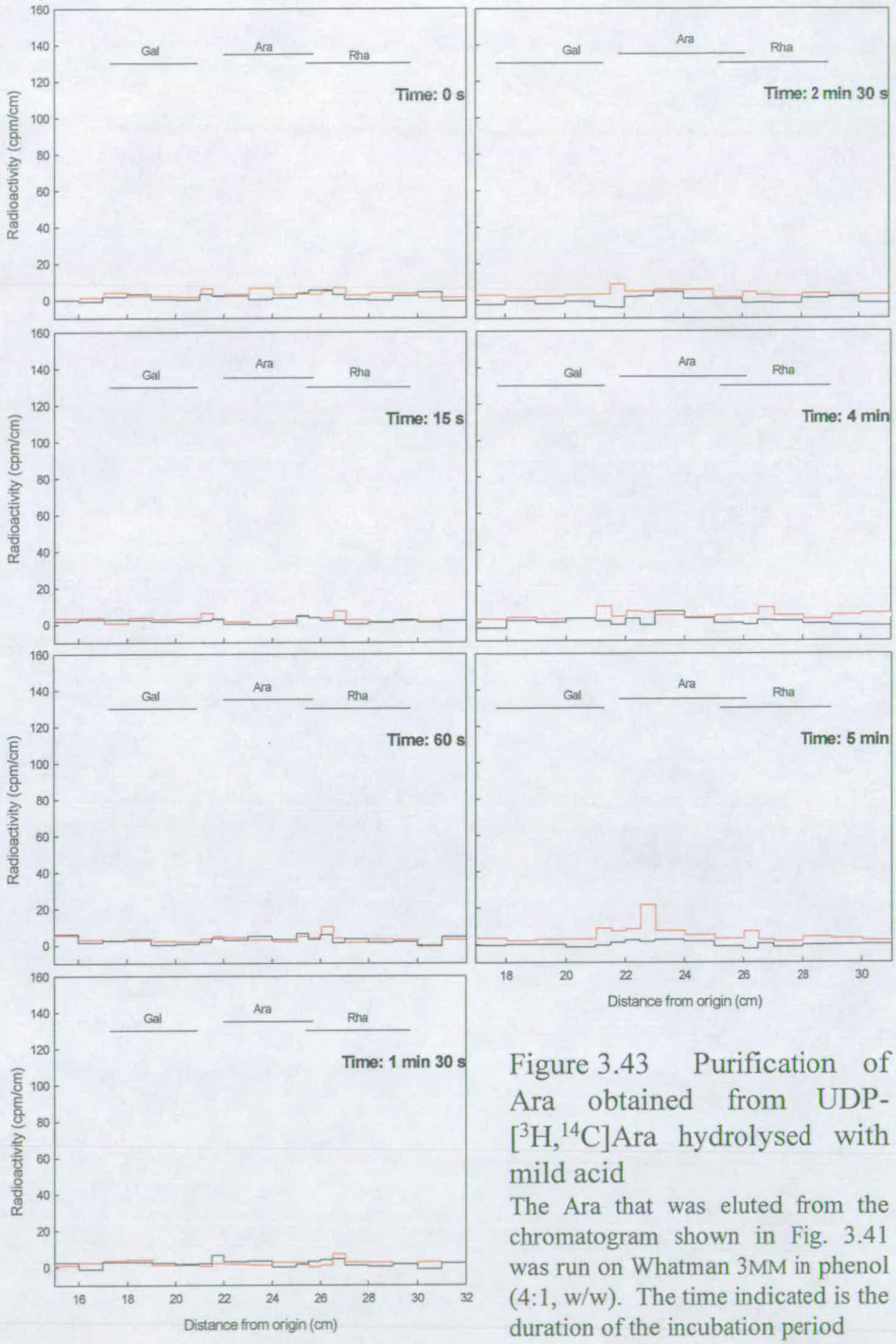

Figure 3.43 Purification of Ara obtained from UDP-[^{3}H,^{14}C]Ara hydrolysed with mild acid

The Ara that was eluted from the chromatogram shown in Fig. 3.41 was run on Whatman 3MM in phenol (4:1, w/w). The time indicated is the duration of the incubation period before the cells were killed. The position of the external markers, stained with aniline hydrogen-phthalate, is indicated on each graph. The (——) represents ^{3}H and the (——) represents ^{14}C. *Continued overleaf*

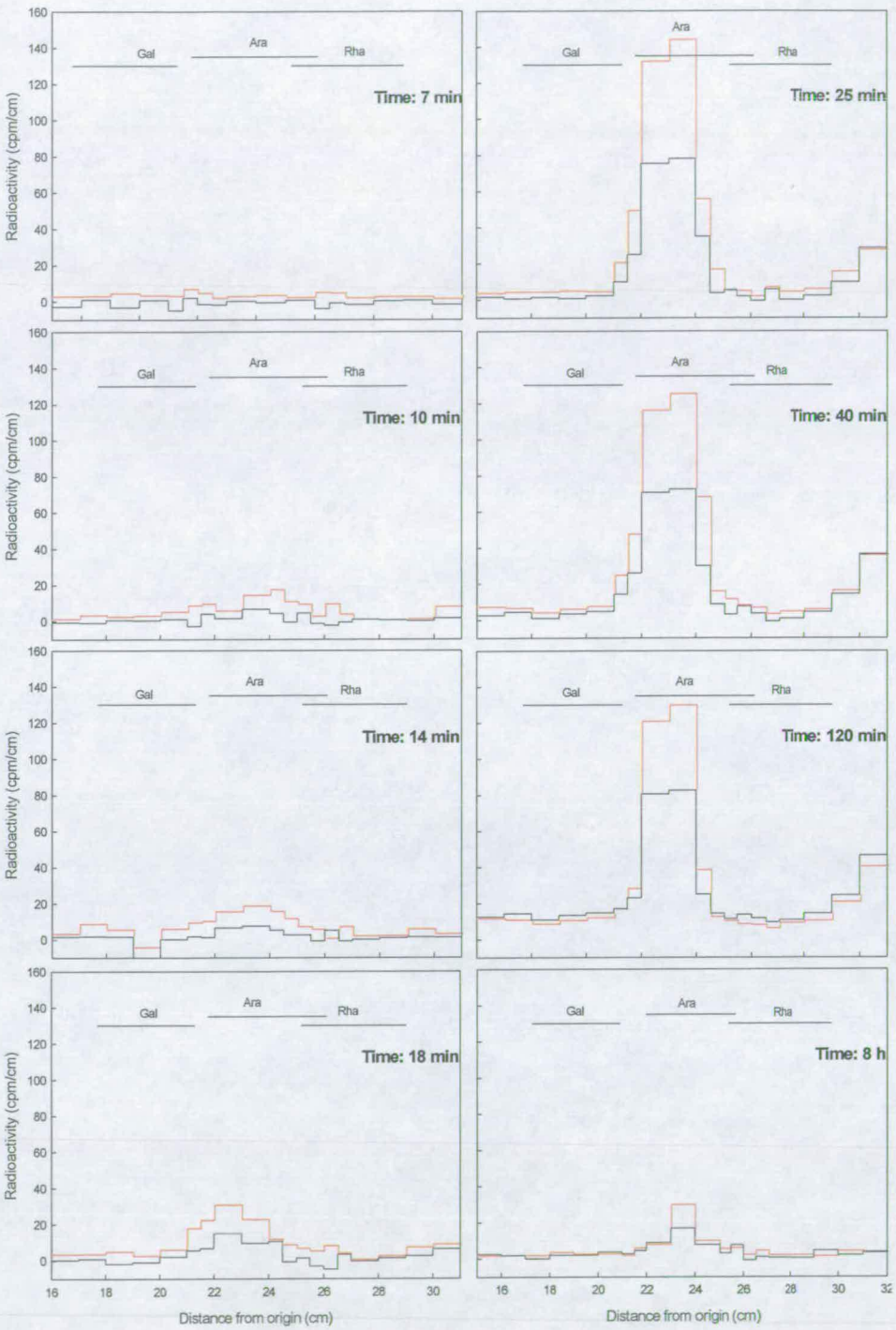

Figure 3.43 Continued

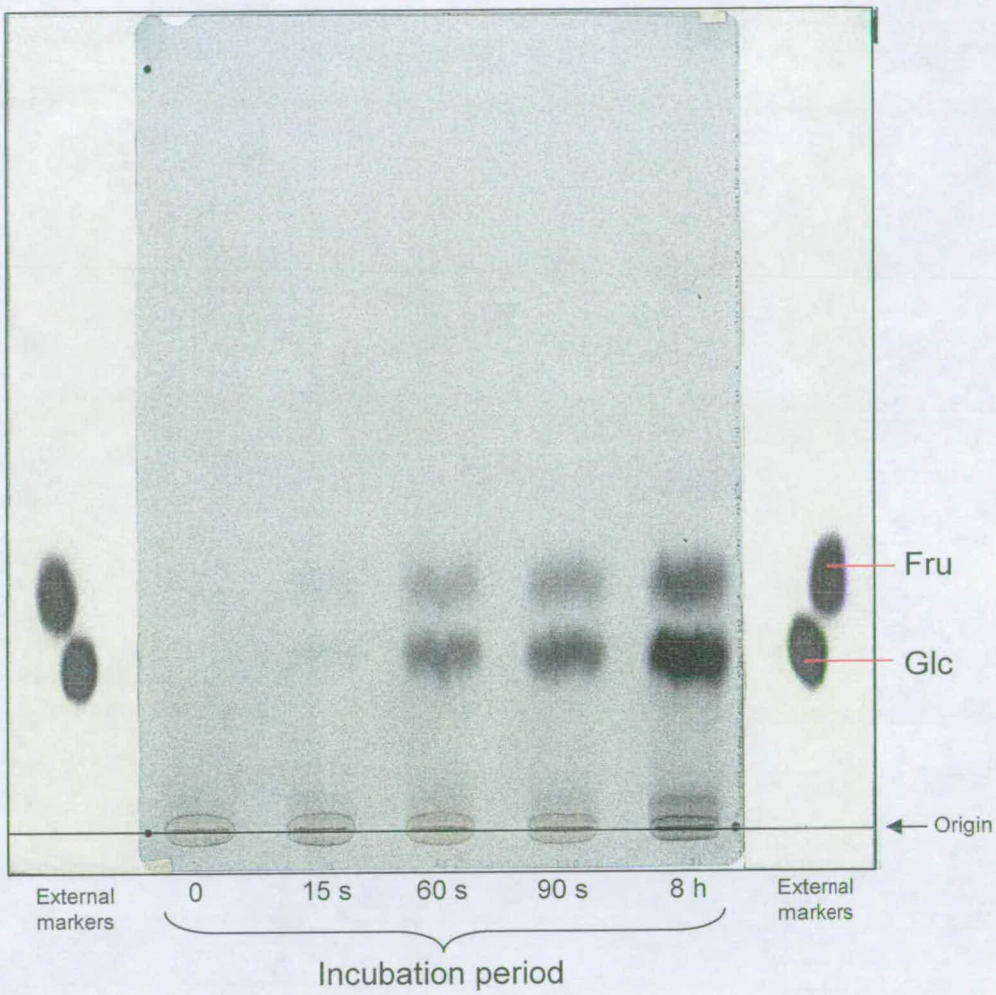

Figure 3.44 Separation of products obtained from monophosphorylated (^{3}H,^{14}C)-compounds treated with acid phosphatase

A portion of the sample eluted from the electrophoretogram shown in Fig. 3.40 (zone two) was treated with an acid phosphatase and run on Whatman 3MM in EPW (8:2:1, 16 h). The external markers were stained with silver nitrate. The samples were autoradiographed. The chromatogram shown is representative. In this system, Man approximately co-migrates with Fru.

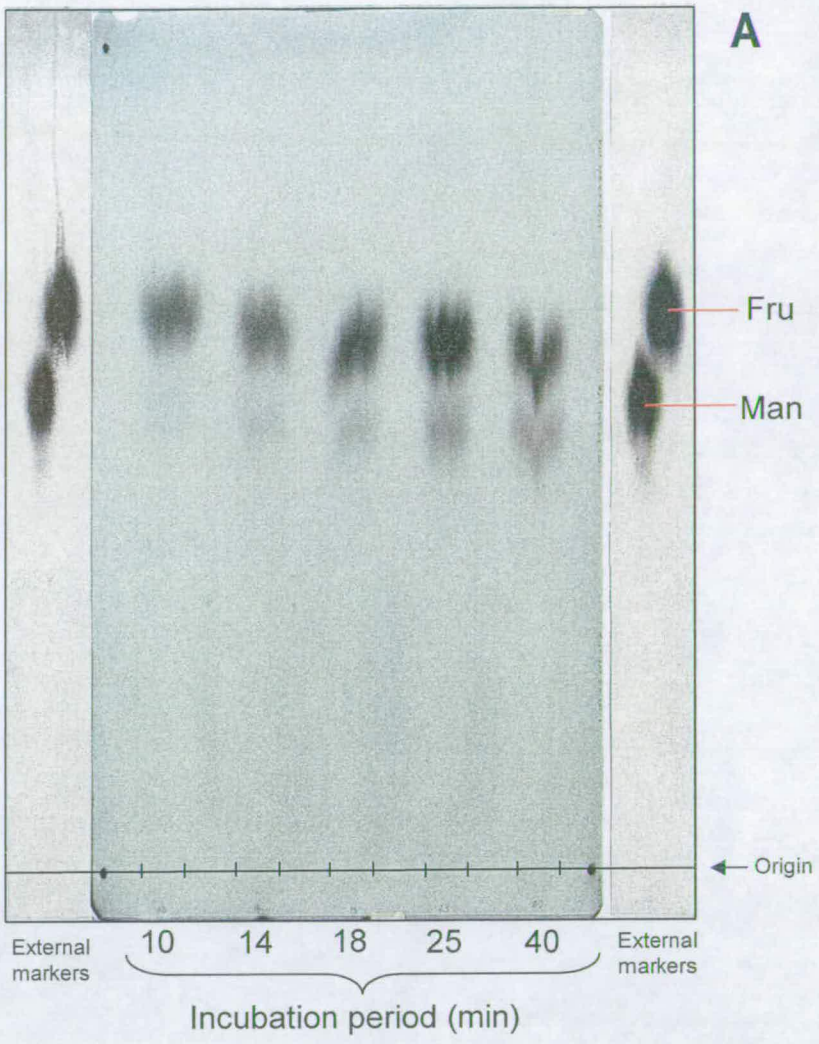

Figure 3.45 Separation of products from monophosphorylated [^{3}H,^{14}C]Fru, [^{3}H,^{14}C]Man and [^{3}H,^{14}C]Glc treated with an acid phosphatase

(**A**) The sample that co-migrated with Fru shown in Fig. 3.44 was eluted and run on Whatman 3MM in phenol/water (4:1 w/w, 20 h). The external markers were stained with silver nitrate (**B**) The sample that co-migrated with Glc shown in Fig. 3.44 was eluted and run on Whatman 3MM in EPW (8:2:1, 40 h). In this case the external markers were stained with aniline hydrogen-phthalate. All of the samples were autoradiographed. The chromatograms shown are representative.

Continued overleaf

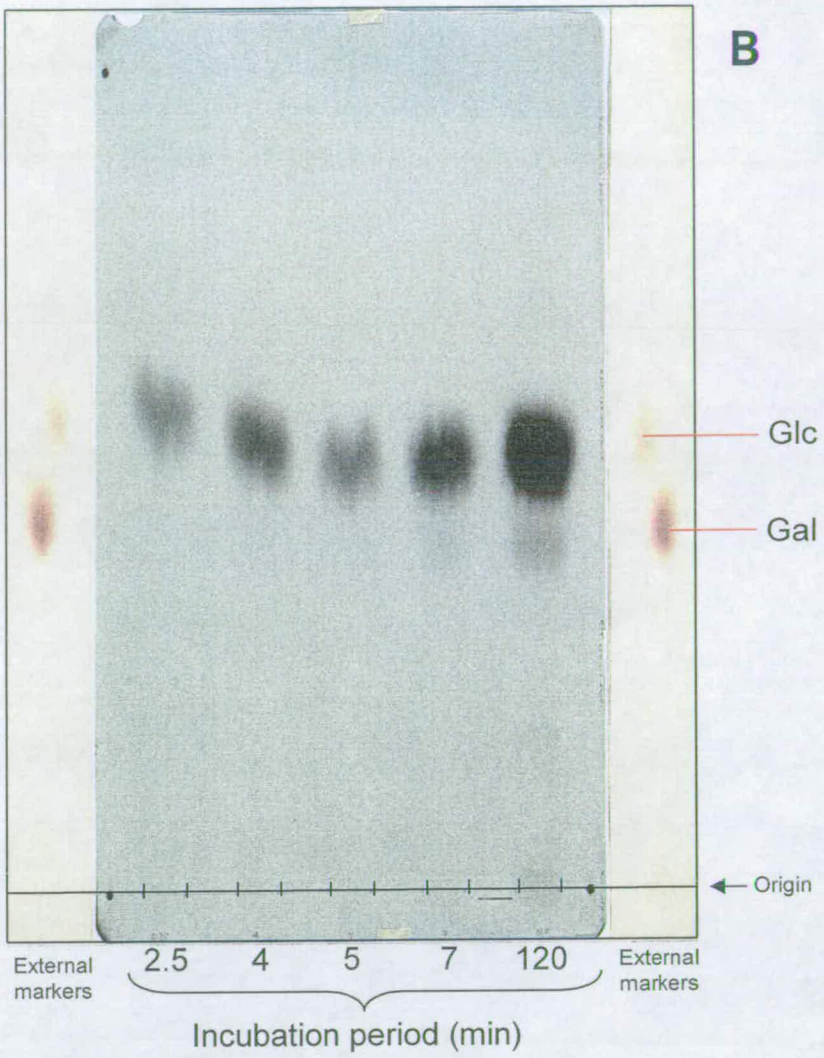

Figure 3.45 Continued

labelled carbon source was [U-^{14}C]Fru. The samples that co-migrated with Glc and Fru were further purified by paper chromatography (Fig. 3.45). This resulted in purified total Glc, Fru and Man that had been monophosphorylated (at any position) prior to the enzyme treatment.

The second aliquot was hydrolysed with mild acid to release the phosphate group from compounds phosphorylated at the anomeric carbon. In conditions of mild hydrolysis, hexoses phosphorylated at C6 retain their phosphate group (Fry, 2000). The compounds that had lost their phosphate group from the anomeric carbon were then separated from the hexose 6-P compounds and any Fru 1-P by paper chromatography (Fig. 3.46). In comparison with Fig. 3.44, which shows the separation of compounds treated with an acid phosphatase, Fig. 3.46 clearly shows that ^{14}C-labelled phosphorylated compounds such as hexose 6-P compounds and Fru 1-P remain at the origin. Radiolabelled Glc and to a slightly lesser extent Gal and possibly Man were detected by this method. The purified Glc and Gal present on the chromatograms, thought to be derived from their respective 1-phosphates, were eluted. When the eluted compounds were assayed for ^{3}H and ^{14}C it was possible to estimate values for the quantity of radioactivity that was contained in the hexose 6-P metabolite pool. The amount of radioactivity obtained for the hexose pool phosphorylated at the anomeric carbon alone was deducted from the combined quantity of radioactivity assayed for the hexoses monophosphorylated at any position. This provided the value of radioactivity for the pool of monosaccharides monophosphorylated at the non-anomeric positions, presumably mainly the 6-position. Fru was purified from the hexose monophosphorylated pool and could be a combination of Fru 6-P and Fru 1-P. However, as Fru 1-P is not thought of as a

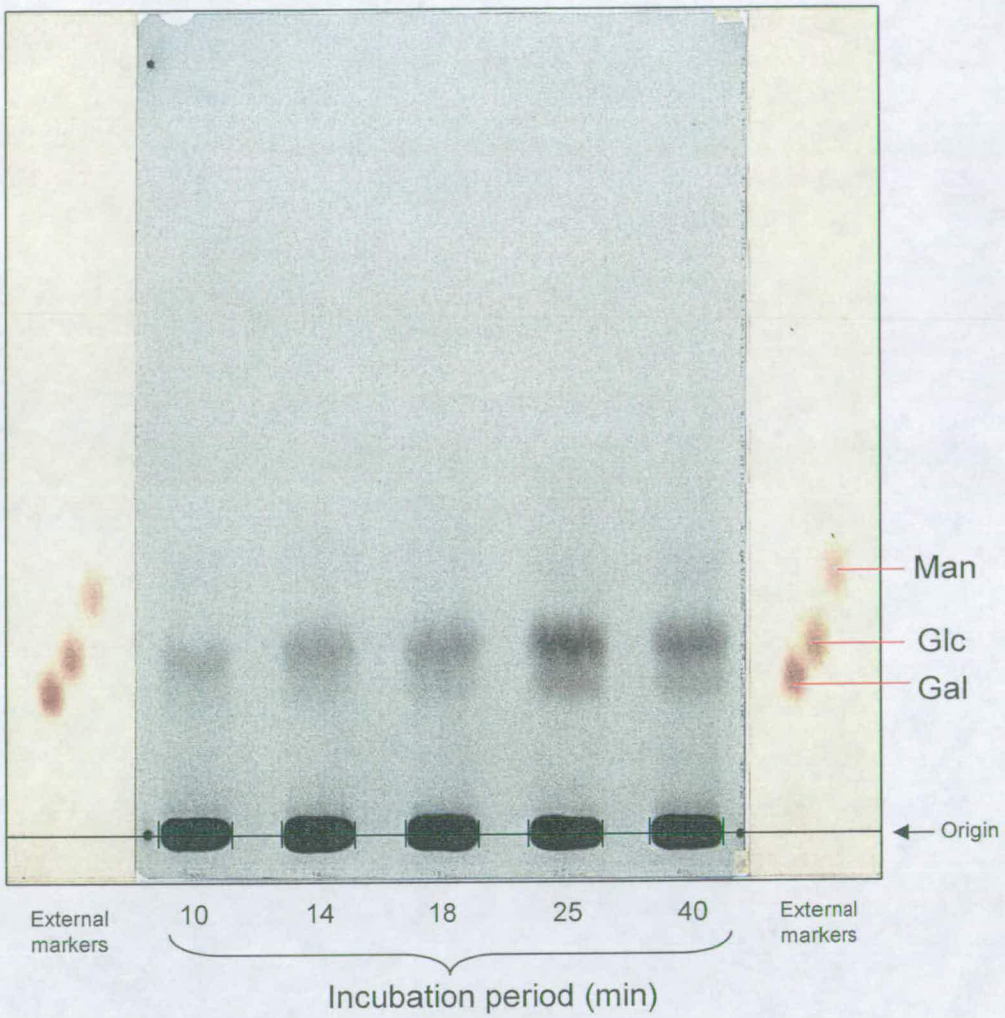

Figure 3.46 Separation of products obtained by mild acid hydrolysis of monophosphorylated (^{3}H,^{14}C)-compounds

A portion of the sample eluted from the electrophoretogram shown in Fig. 3.40 (zone two) was acid hydrolysed (0.1 M, 100°C, 25 min) and run on Whatman 3MM in EPW (8:2:1, 16 h). The external markers were stained with aniline hydrogen-phthalate. The samples were autoradiographed. The chromatogram shown is representative.

major metabolite this was classed as Fru 6-P. It is noted that a small percentage of the Gal 1-P may be L-Gal 1-P (a possible precursor of L-ascorbate), which will stem from a completely different 'core' metabolite.

3.2.3.4 Zone three — GDP- and ADP- sugars

GDP-Man and ADP-Glc were predicted to be in zone three (Fig. 3.40). GDP-sugars were separated from ADP-sugars by further paper electrophoresis at pH 3.5 (Fig. 3.47); both were eluted and hydrolysed with mild acid. The mild acid treatment removed the monosaccharide of interest from its associated nucleotide. The sugars released were purified by paper chromatography (Fig. 3.48 – Fig. 3.49).

Man and Glc were the main sugars released from GDP-sugars and ADP-sugars, respectively. An initial peak of radiolabel in Man that originated from GDP-sugars was witnessed at 18 min that climaxed at 120 min. At 8 h the radioactivity was only marginally higher than that at t=0. Glc from the ADP-sugars was maximally radiolabelled at approximately 40 min and to a lesser extent could still be detected at 8 h.

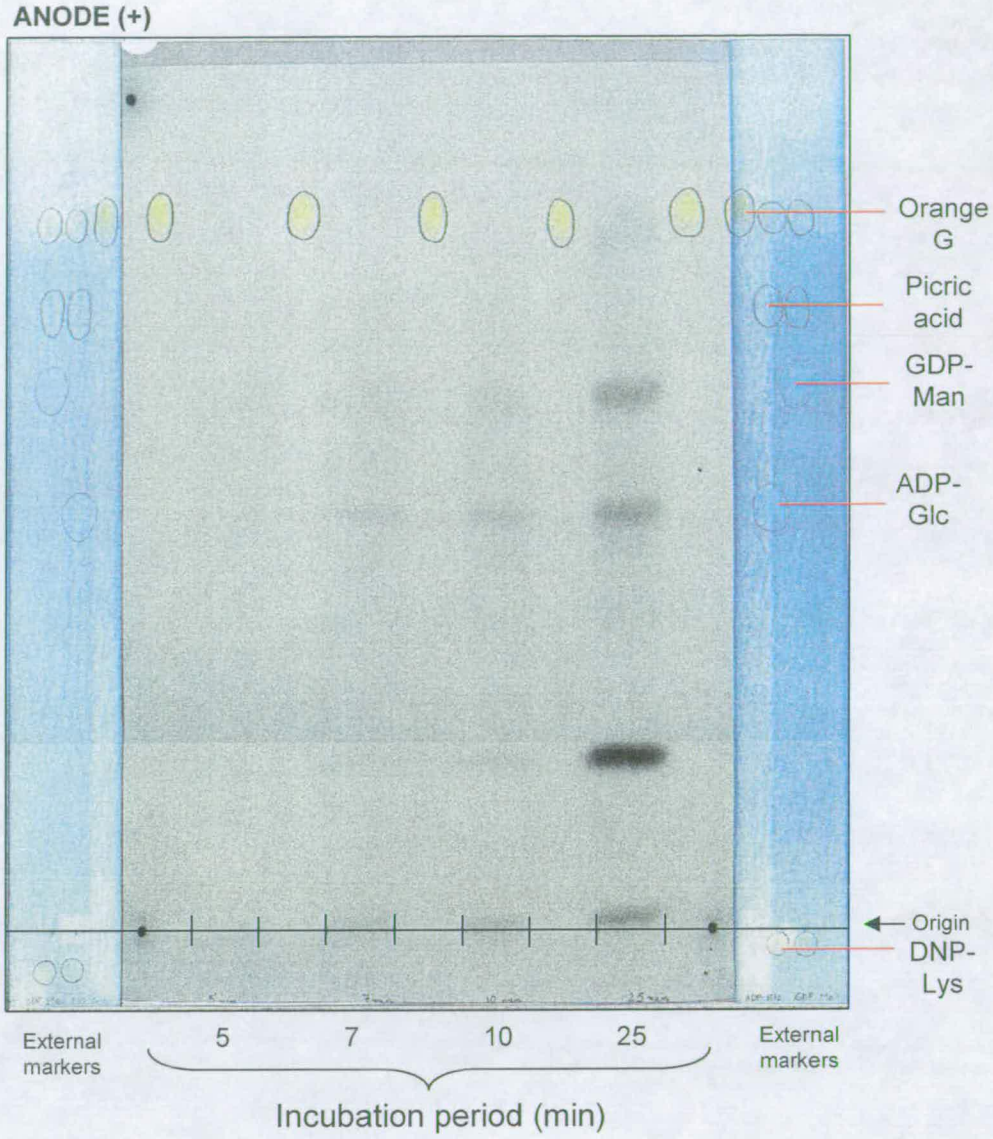

Figure 3.47 Separation of (^{3}H,^{14}C)-labelled GDP- and ADP-sugars

The sample eluted from the electrophoretogram shown in Fig. 3.40 (zone three) was loaded onto Whatman 3MM and subjected to paper electrophoresis (pH 3.5, 2.5 kV, 1 h). The external markers were stained with molybdate. The samples were autoradiographed. The electrophoretogram shown is representative.

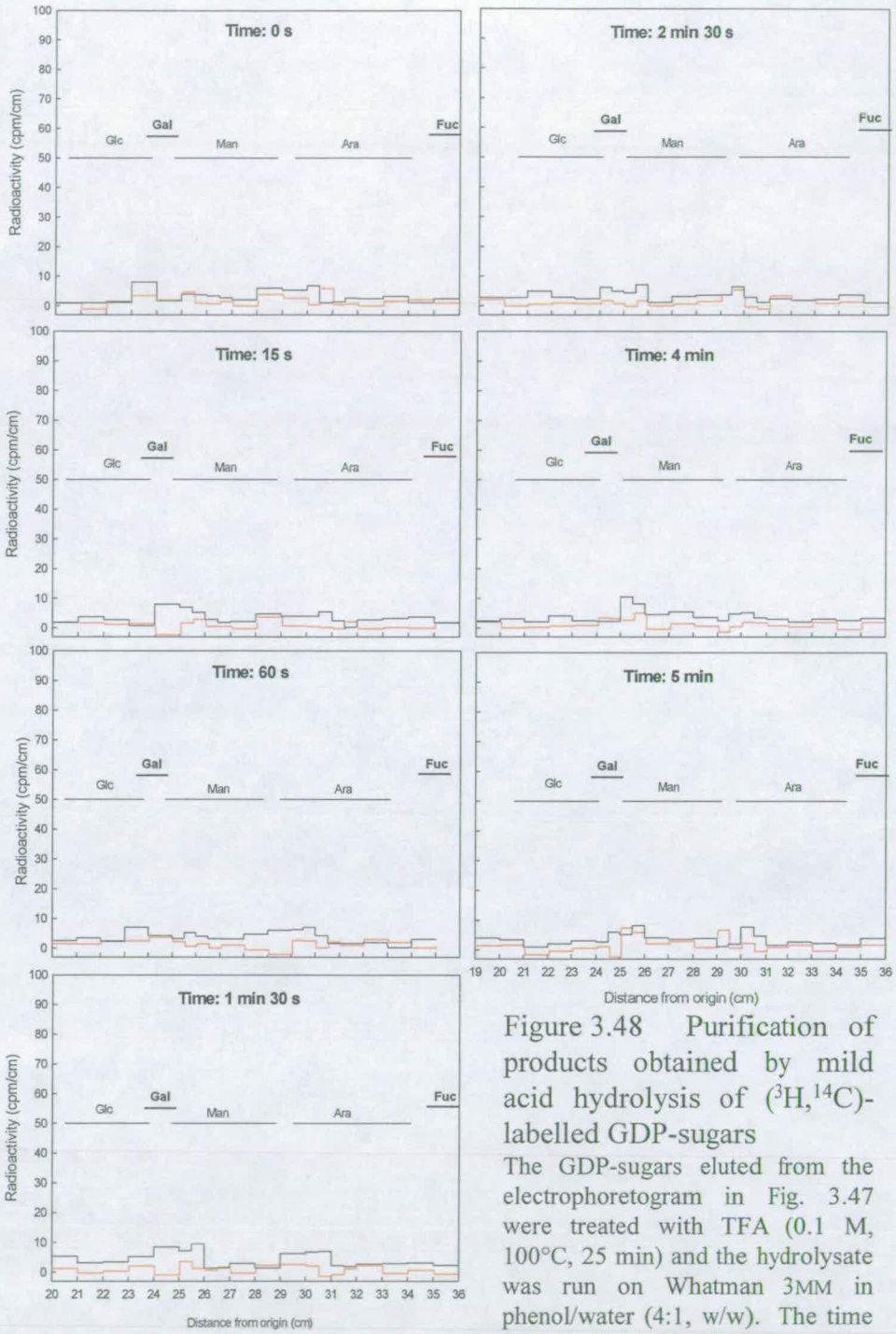

Figure 3.48 Purification of products obtained by mild acid hydrolysis of (^{3}H,^{14}C)-labelled GDP-sugars

The GDP-sugars eluted from the electrophoretogram in Fig. 3.47 were treated with TFA (0.1 M, 100°C, 25 min) and the hydrolysate was run on Whatman 3MM in phenol/water (4:1, w/w). The time indicated is the duration of the incubation period before the cells were killed. The position of the external markers, stained with aniline hydrogen-phthalate, is indicated on each graph. The (——) represents ^{3}H and the (——) represents ^{14}C counted prior to elution.

Continued overleaf

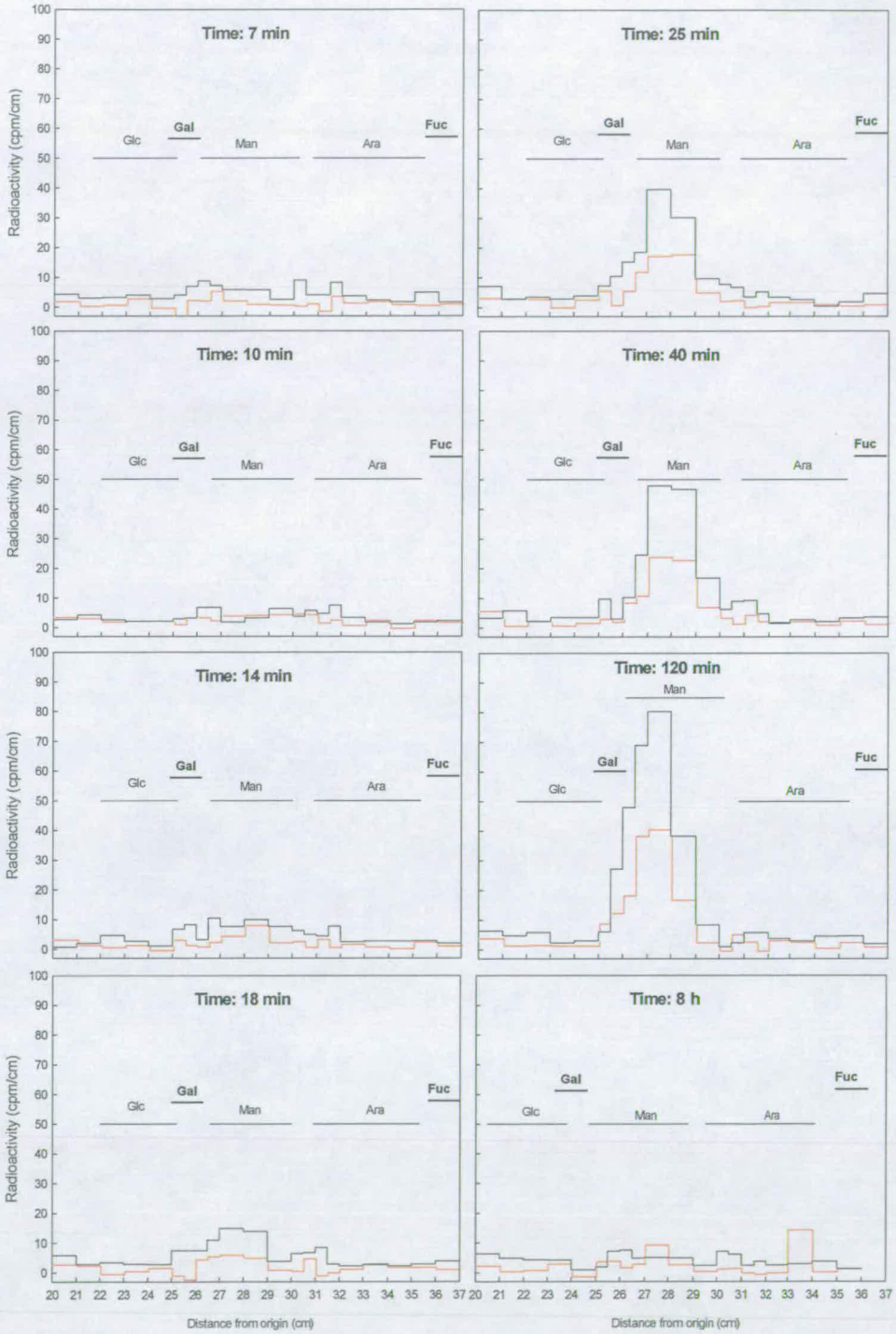

Figure 3.48 Continued

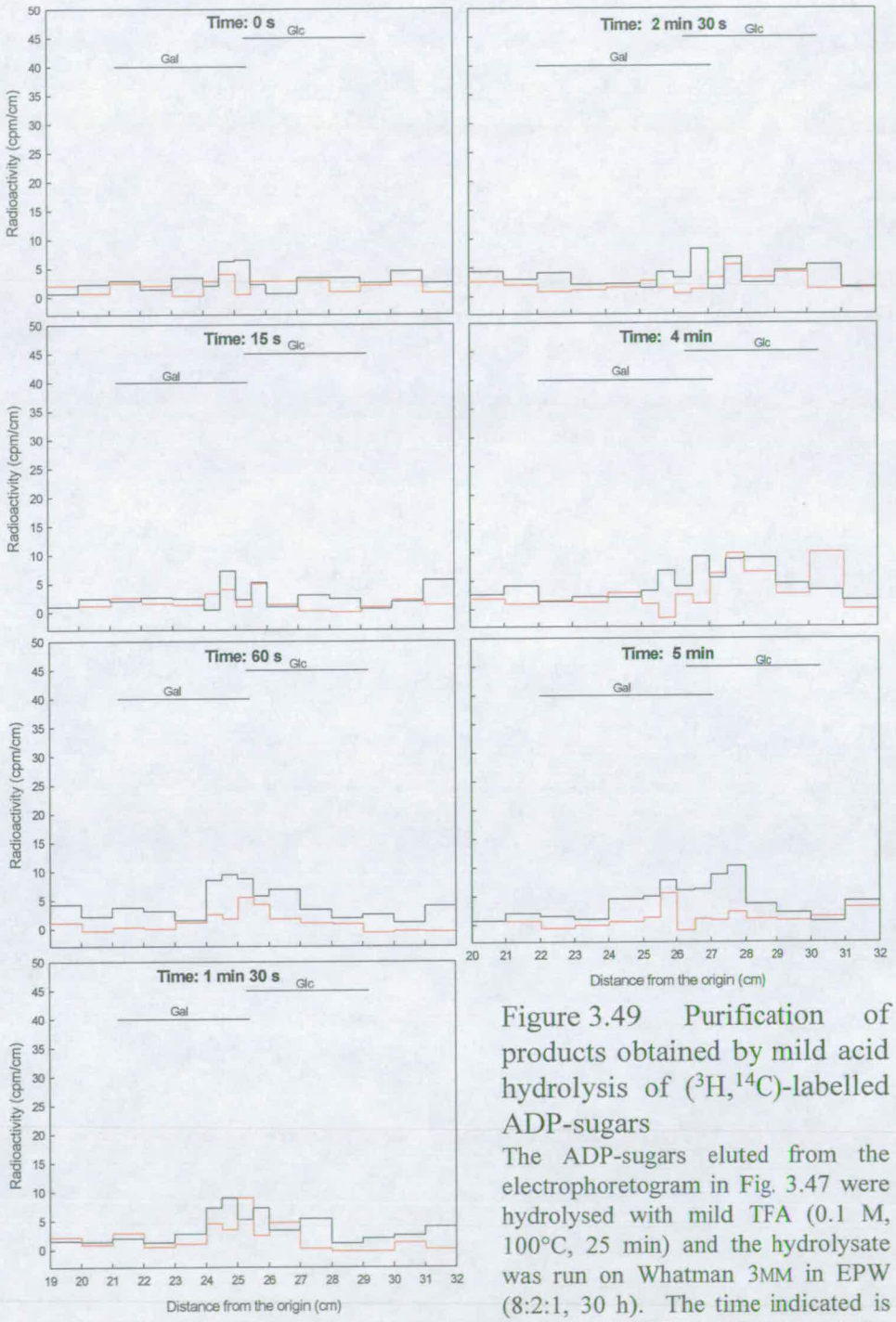

Figure 3.49 Purification of products obtained by mild acid hydrolysis of (^{3}H,^{14}C)-labelled ADP-sugars

The ADP-sugars eluted from the electrophoretogram in Fig. 3.47 were hydrolysed with mild TFA (0.1 M, 100°C, 25 min) and the hydrolysate was run on Whatman 3MM in EPW (8:2:1, 30 h). The time indicated is the duration of the incubation period before the cells were killed. The position of the external markers, stained with aniline hydrogen-phthalate, is indicated on each graph. The (——) represents ^{3}H and the (——) represents ^{14}C. *Continued overleaf*

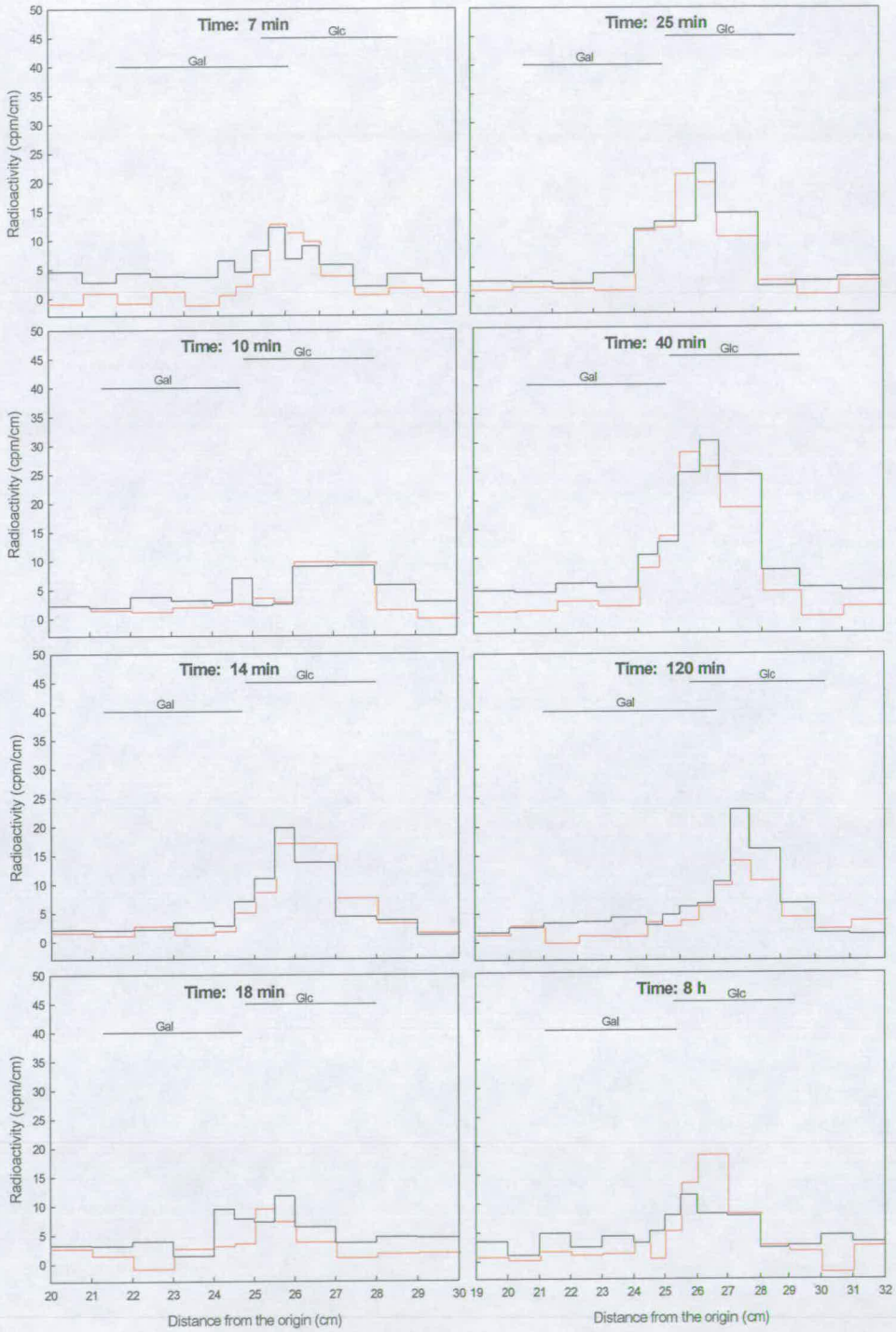

Figure 3.49 Continued

3.2.3.5 Zone 4 — Neutral compounds of interest

The neutral compounds of interest were Suc and inositol. The section of electrophoretogram shown in Fig. 3.40 that contained compounds that co-migrated with a neutral external marker was eluted. The eluted compounds were subjected to paper electrophoresis at pH 3.5 (Fig. 3.50). This step was taken to ensure that charged compounds such as malic acid and citric acid that did not migrate at pH 2.0 but would migrate at pH 3.5, were separated from Suc and *myo*-inositol. The compounds that migrated with the neutral external marker were eluted and paper chromatographed (Fig. 3.50).

The Suc was re-chromatographed (Fig. 3.51), eluted and treated with invertase. The hydrolysed Suc sample was paper chromatographed (Fig. 3.53 A). Fru was eluted from this chromatogram and deemed pure. The section of chromatogram shown in Fig. 3.53 A, that spanned the region that contained both Glc and potentially Suc was eluted and paper chromatographed to purify these compounds (Fig. 3.53 B). The purified Glc that originated from Suc was eluted.

The compound(s) that co-migrated with the external inositol marker in Fig. 3.51, were eluted and paper chromatographed (Fig. 3.54 A). To determine whether the compound was inositol, the spot of radioactivity that correlated with the external *myo*-inositol marker was eluted and paper chromatographed in a different solvent system (Fig. 3.54 B). The co-migration of the radiolabelled compound with *myo*-inositol strongly suggested that it was inositol. However, it was noted that this radiolabelled compound was present at t=0 (Fig. 3.54) and throughout the experiment at a constant level. This suggests that inositol was present as a contaminant in the original [U-^{14}C]Fru stock solution fed to the cells.

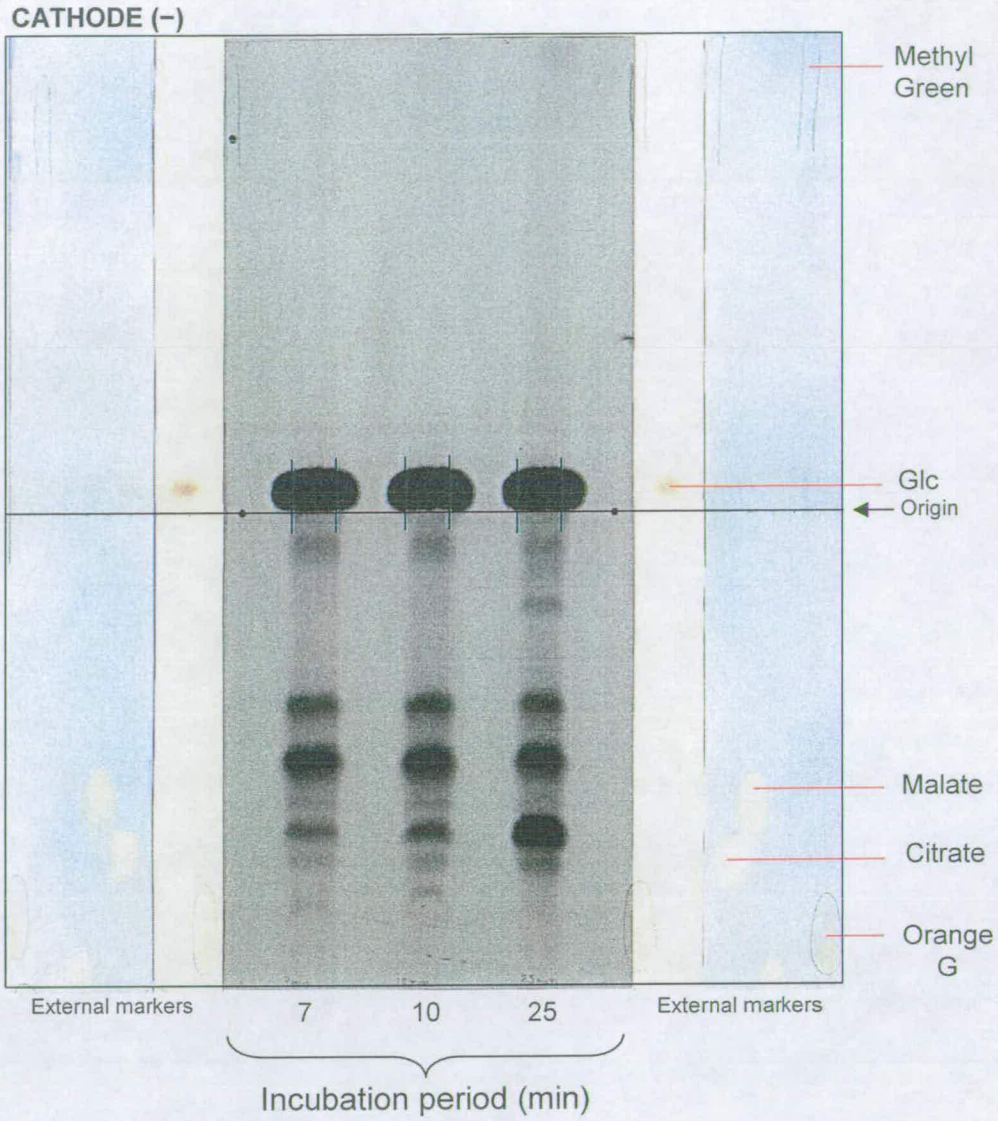

Figure 3.50 Separation of [^{3}H,^{14}C]Suc and [^{3}H,^{14}C]inositol from charged compounds

The section of electrophoretogram shown in Fig. 3.40 that contained the neutral compounds (zone four) was eluted, loaded onto Whatman 3MM and subjected to paper electrophoresis (pH 3.5, 2.5 kV, 1.0 h). The acidic external markers were stained with bromophenol blue. The Glc external marker was stained with aniline hydrogen-phthalate. The samples were autoradiographed. The chromatogram shown is representative.

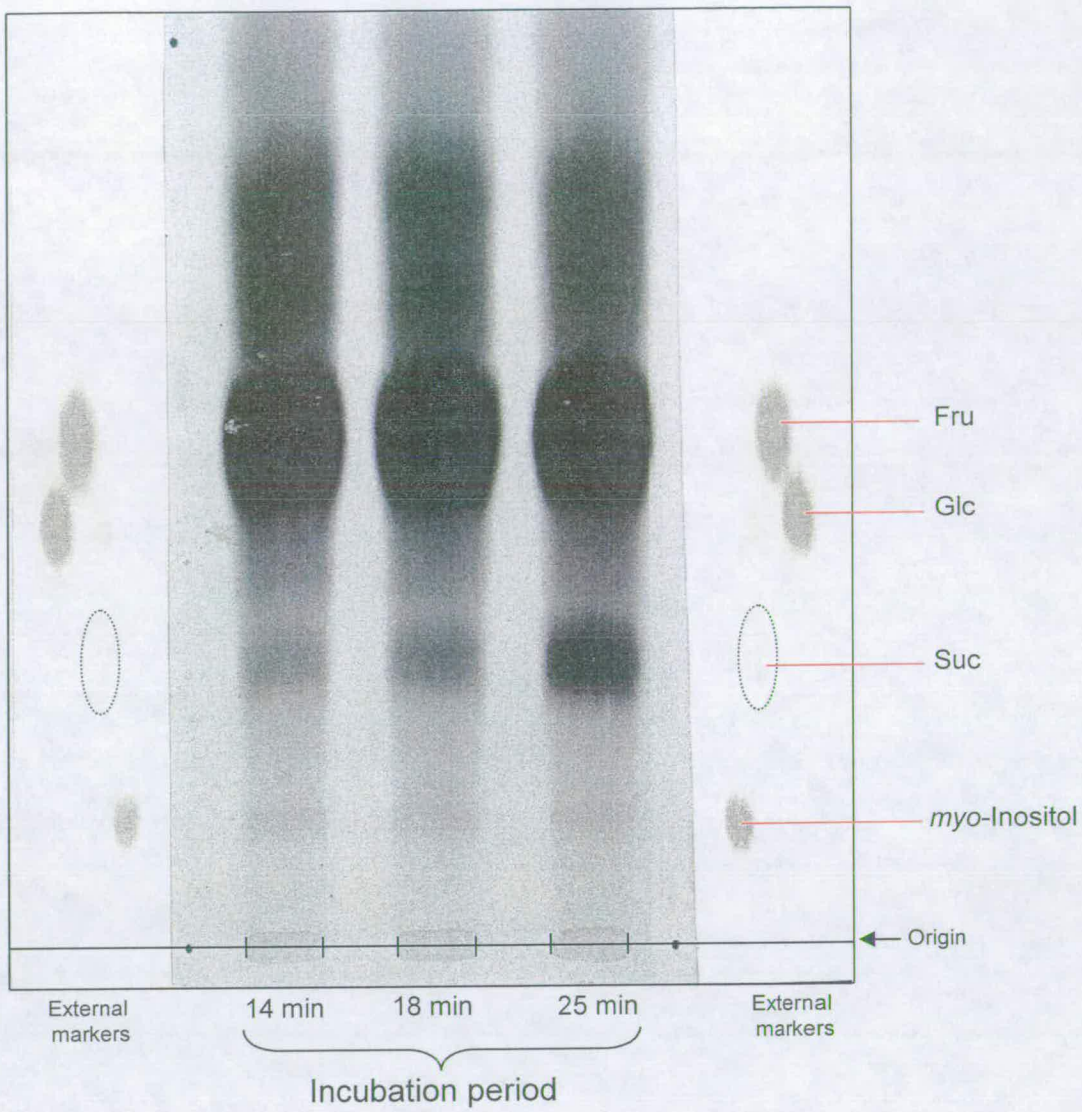

Figure 3.51 Separation of [^{3}H,^{14}C]Suc and [^{3}H,^{14}C]inositol by paper chromatography

The compounds that comigrated with the neutral maker shown on Fig. 3.50 were eluted and run on Whatman 3MM in PAW (15:3:2, 22 h). The external markers were stained with silver nitrate and the samples were autoradiographed. The chromatogram shown is representative.

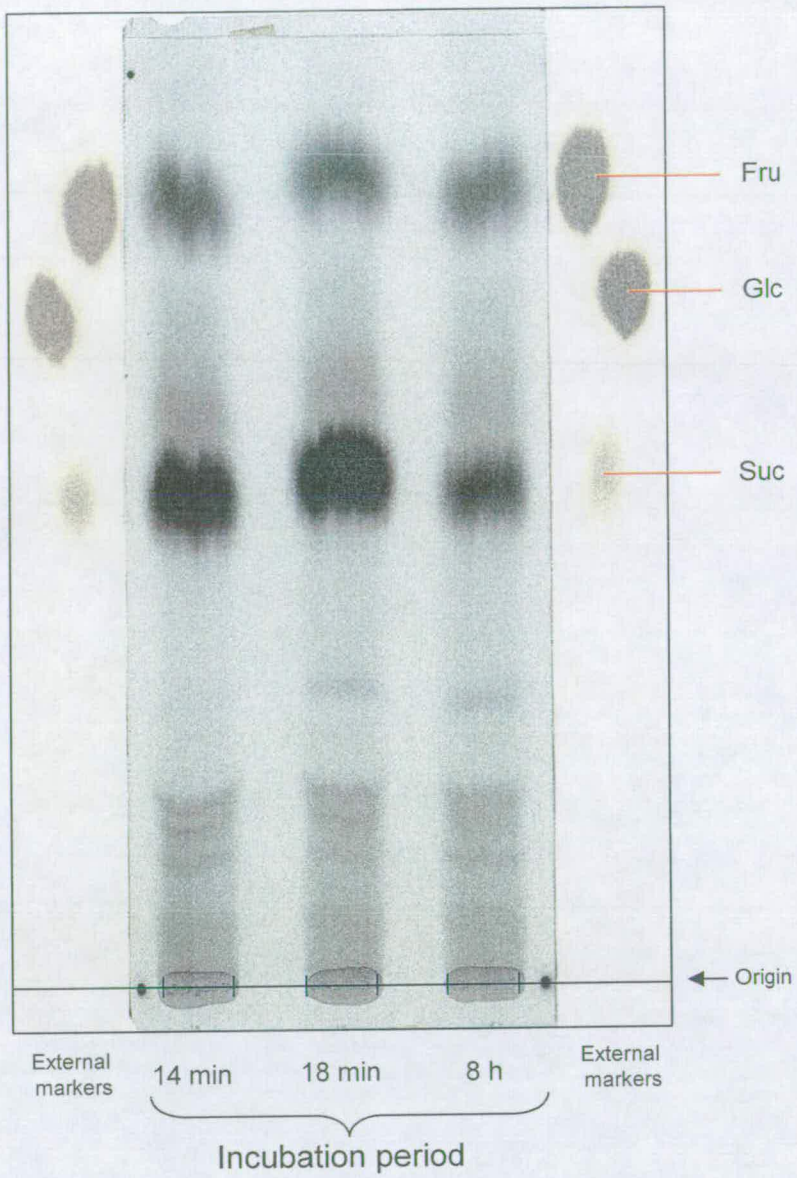

Figure 3.52 [^{3}H,^{14}C]Suc purification by paper chromatography

The compounds that comigrated with Suc shown in Fig. 3.51 were eluted and run on Whatman 3MM in EPW (10:4:3, 16 h). The external markers were stained with silver nitrate and the samples were autoradiographed. The chromatogram shown is representative.

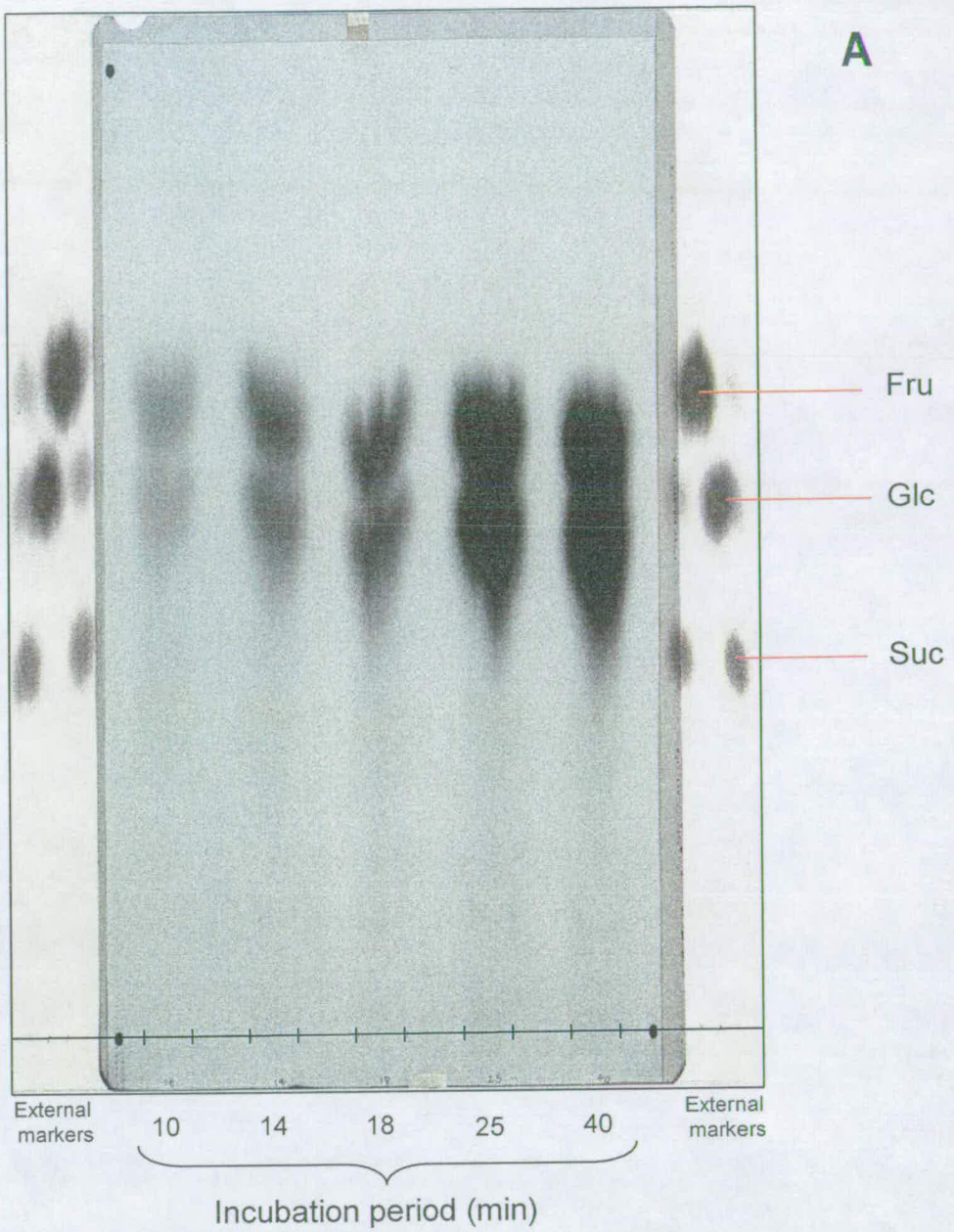

Figure 3.53 Paper chromatography purification of the hydrolysis products of purified [^{3}H,^{14}C]Suc treated with invertase

(**A**) Purified Suc obtained eluted from the chromatogram shown in Fig. 3.52 was treated with invertase. The hydrolysis products were loaded onto Whatman 3MM and run in EPW (10:4:3, 16 h). (**B**) The section of chromatogram, shown in part A, that spanned the region that contained both Glc and Suc was eluted, loaded onto Whatman 3MM and run in EPW (10:4:3, 20 h). All of the external markers were stained with silver nitrate and all of the samples were autoradiographed. The chromatograms shown are representative.

Continued overleaf.

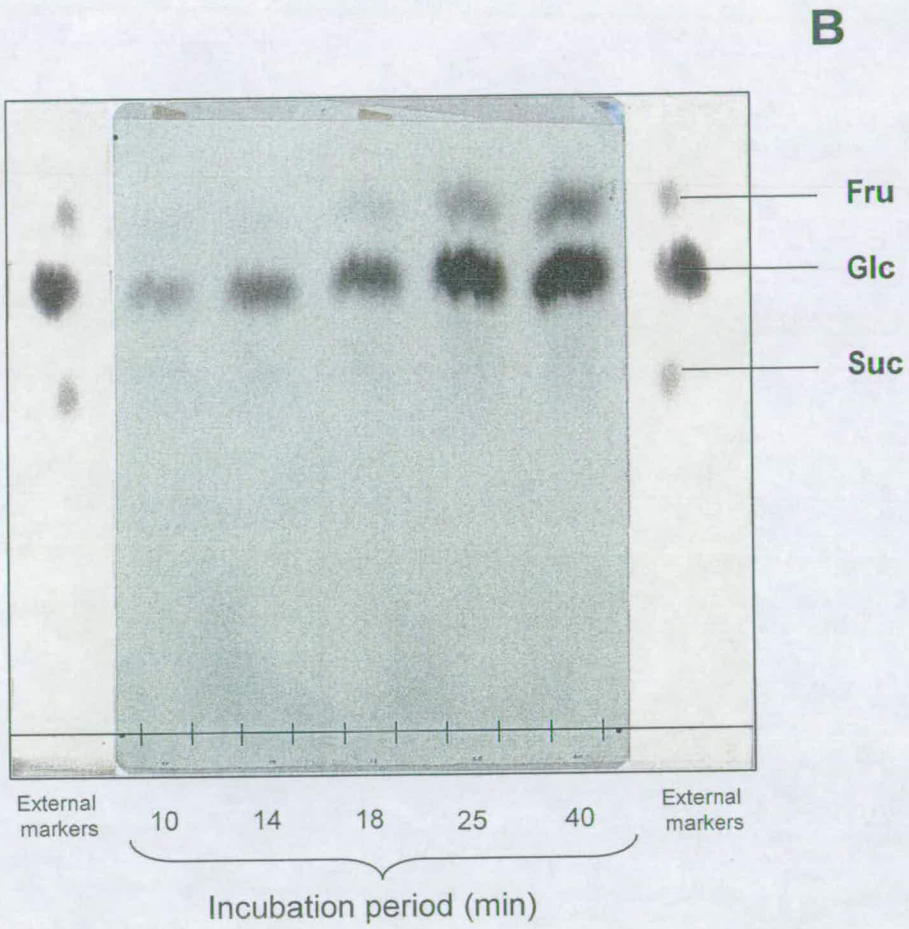

Figure 3.53 Continued

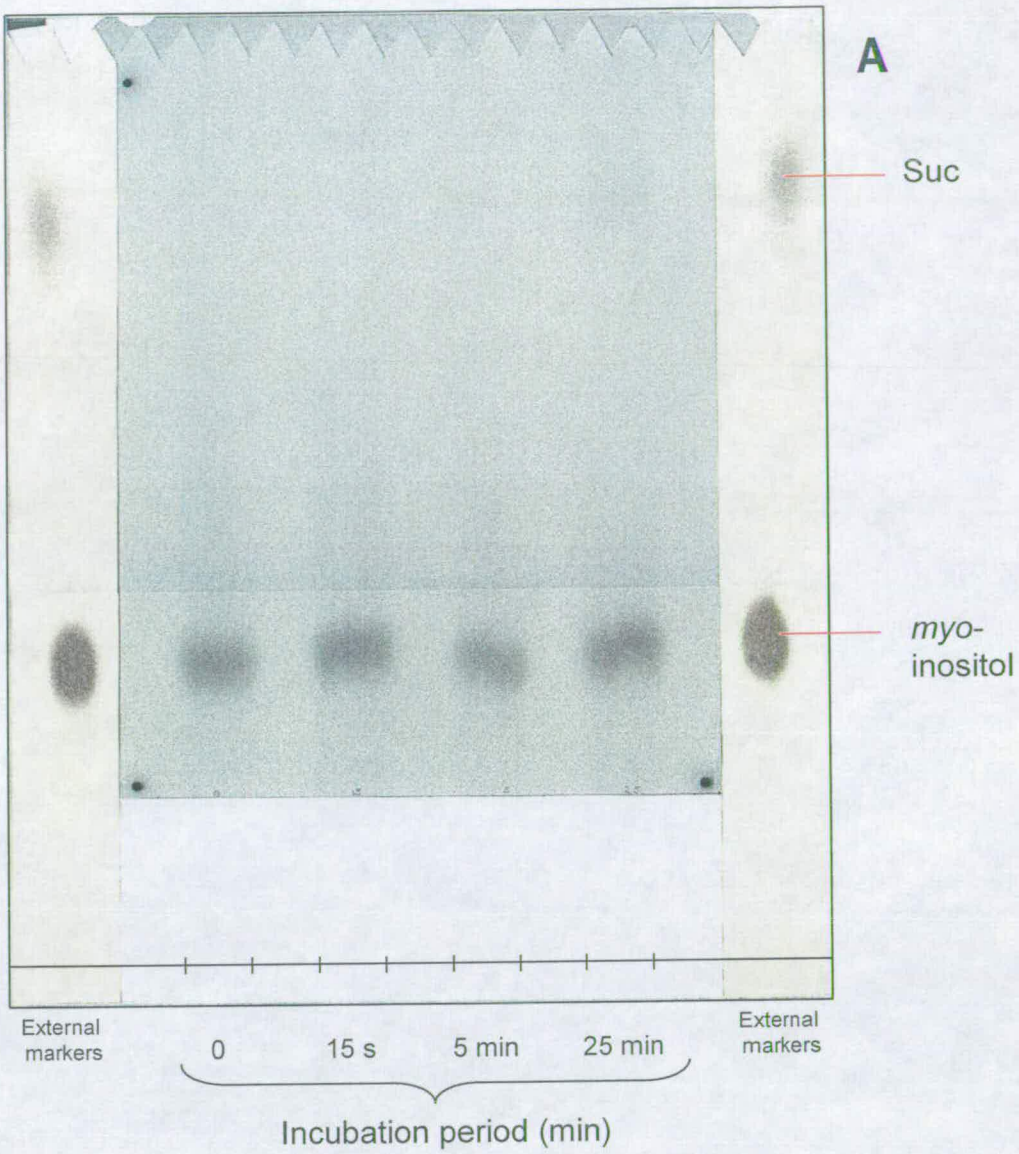

Figure 3.54 Paper chromatography purification of [^{3}H,^{14}C]inositol

(**A**) The inositol sample eluted from the chromatogram shown in Fig. 3.51 was loaded onto Whatman 3MM and run in acetone:water (85:15, 48 h). (**B**) The section of chromatogram that comigrated with the inositol external marker was eluted and run on Whatman 3MM in phenol/water (4:1 w/w, 20 h). The external markers were stained with silver nitrate and the samples were autoradiographed. The chromatograms shown are representative.

Continued overleaf

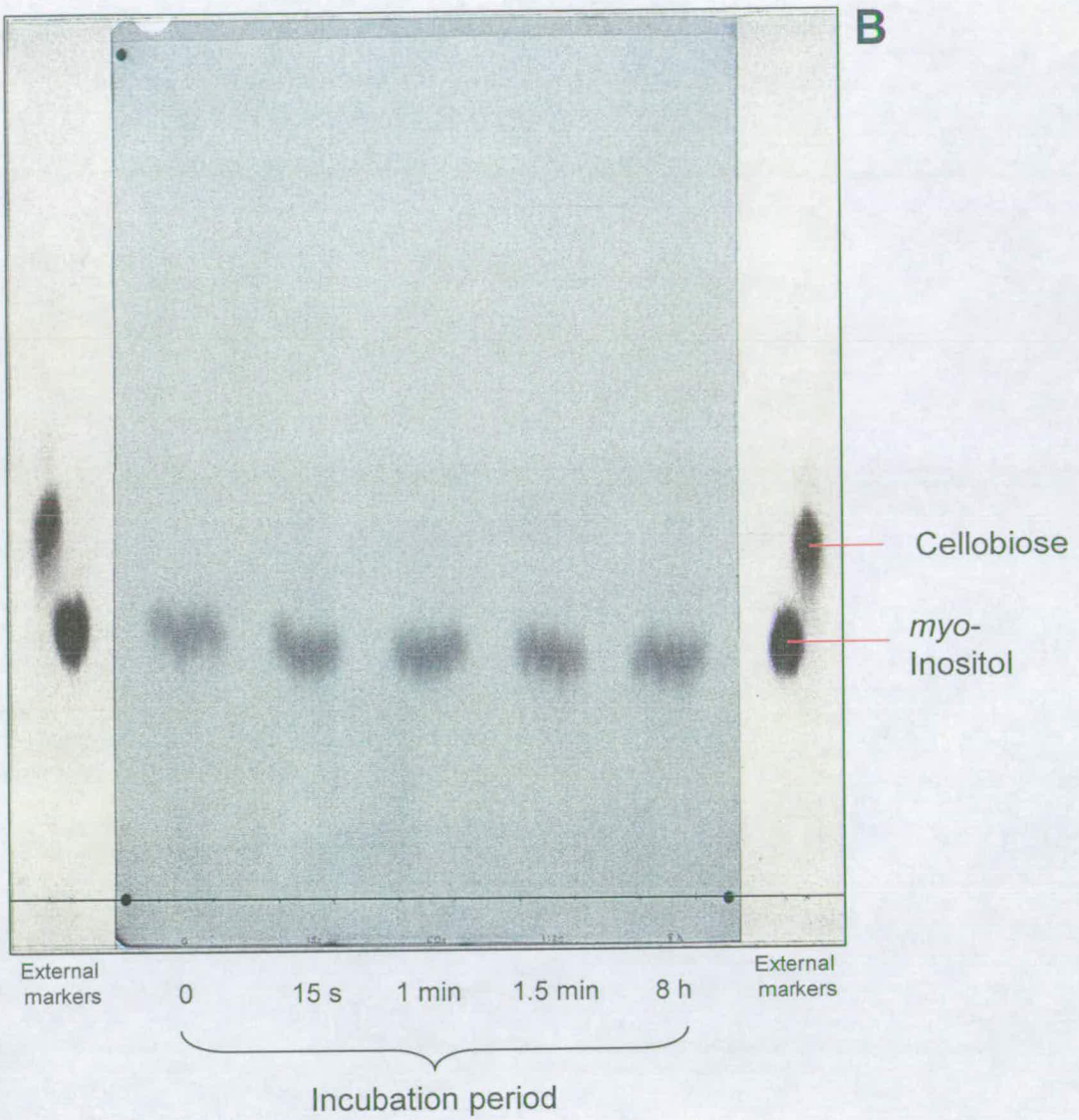

Figure 3.54 Continued

3.2.3.6 *Radiolabel incorporation into the AIR over time*

After the intermediary metabolites had been extracted from the cells the insoluble residue, which contained polysaccharies was washed with ethanol, dried and hydrolysed with TFA. The hydrolysate was paper chromatographed (Fig. 3.55). The Glc isolated in Fig. 3.55 includes Glc from cell wall polysaccharides and starch. Fig. 3.55 shows that monosaccharides that become radiolabelled the fastest are Glc, Gal and Man. There is slight doubt about the identity of Man as this could be contaminated with [U-^{14}C]Fru if the AIR was not washed free of [U-^{14}C]Fru that the cells were originally fed. Glc and Gal are the most heavily radiolabelled compounds of those detected (Fig. 3.55). Ara, Xyl and GalA become labelled after Glc, Gal and "Man". The compounds were purified by paper chromatography (Fig 3.56 A–E).

3.2.3.7 *The quantity of radioactivity in the intermediary metabolites*

As described above, the cells were fed a solution that contained both [1-^{3}H]Gal and [U-^{14}C]Fru, then killed with acidified ethanol and the metabolites were extracted and purified. The total radiolabel entry into each of the metabolites was examined (Fig. 3.57). In order to utilise the [^{3}H]Gal the cells were required to convert it into ^{3}H-labelled Gal 1-P. The Gal 1-P graph indicates that a maximum initial rate of ^{3}H incorporation into Gal 1-P takes place within 1 min. The Gal 1-P pool is maximally radiolabelled with ^{3}H radiolabelled by 20 min. After 20 min a decline in ^{3}H occurs. This is most likely due to the exhaustion of the [^{3}H]Gal source. As there are six metabolic steps required to convert [^{14}C]Fru to ^{14}C-labelled D-Gal 1-P, the maximum initial rate of ^{14}C entry into the Gal 1-P metabolite pool takes slightly longer to achieve than the ^{3}H maximum initial rate and occurs by about 2 min. The ^{14}C in the Gal 1-P pool is also maximally radiolabelled at

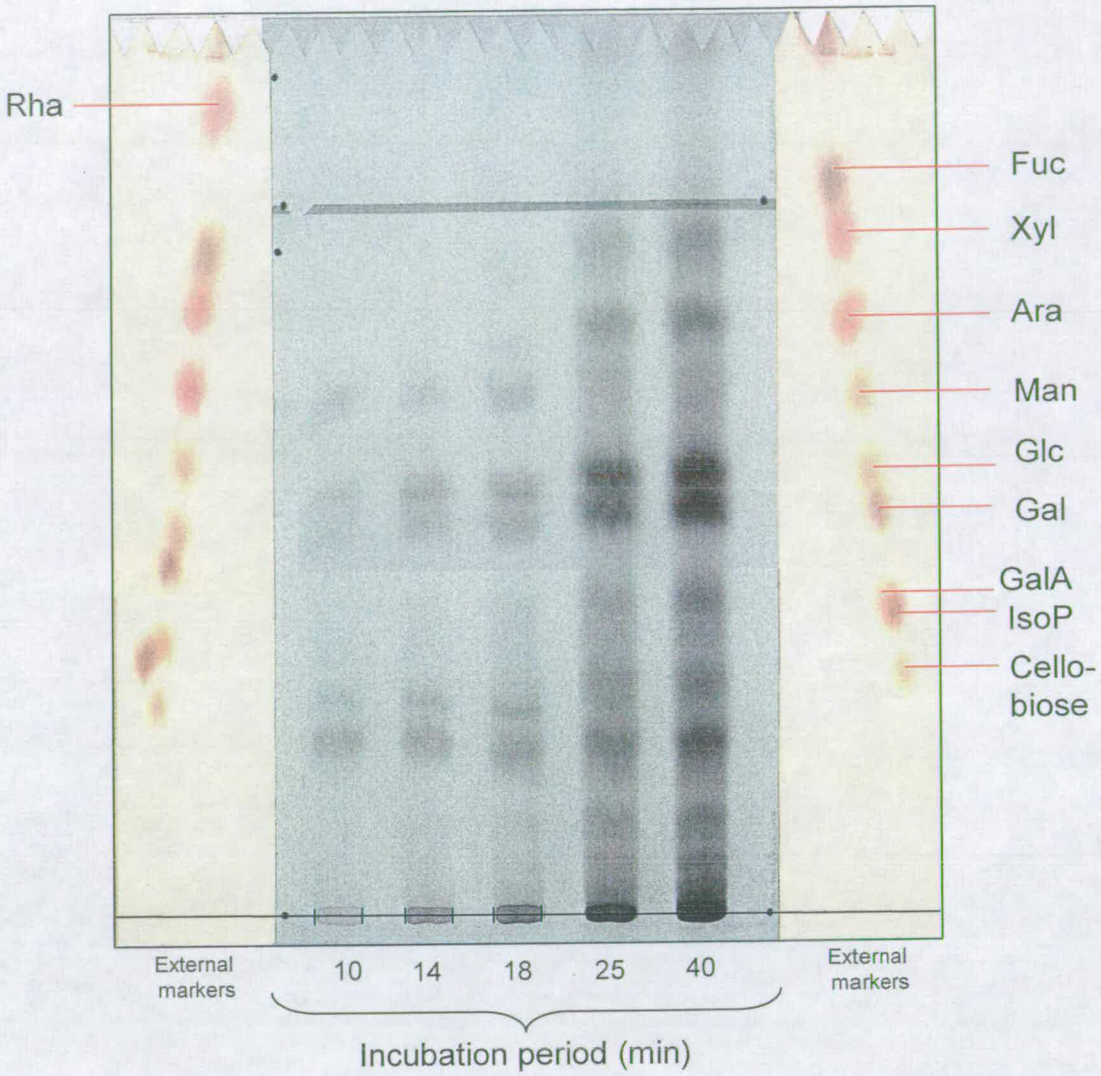

Figure 3.55 *Arabidopsis* (^{3}H,^{14}C)-hydrolysate separated by paper chromatography

(^{3}H,^{14}C)-Labelled AIR was hydrolysed with TFA (2 M, 120°C, 1 h) and run on Whatman 3MM in BAW (12:3:5, 16 h) followed by EPW (10:4:3, 16 h) in 1D. The external markers were stained with aniline hydrogen-phthalate. The samples were autoradiographed. The chromatogram is representative.

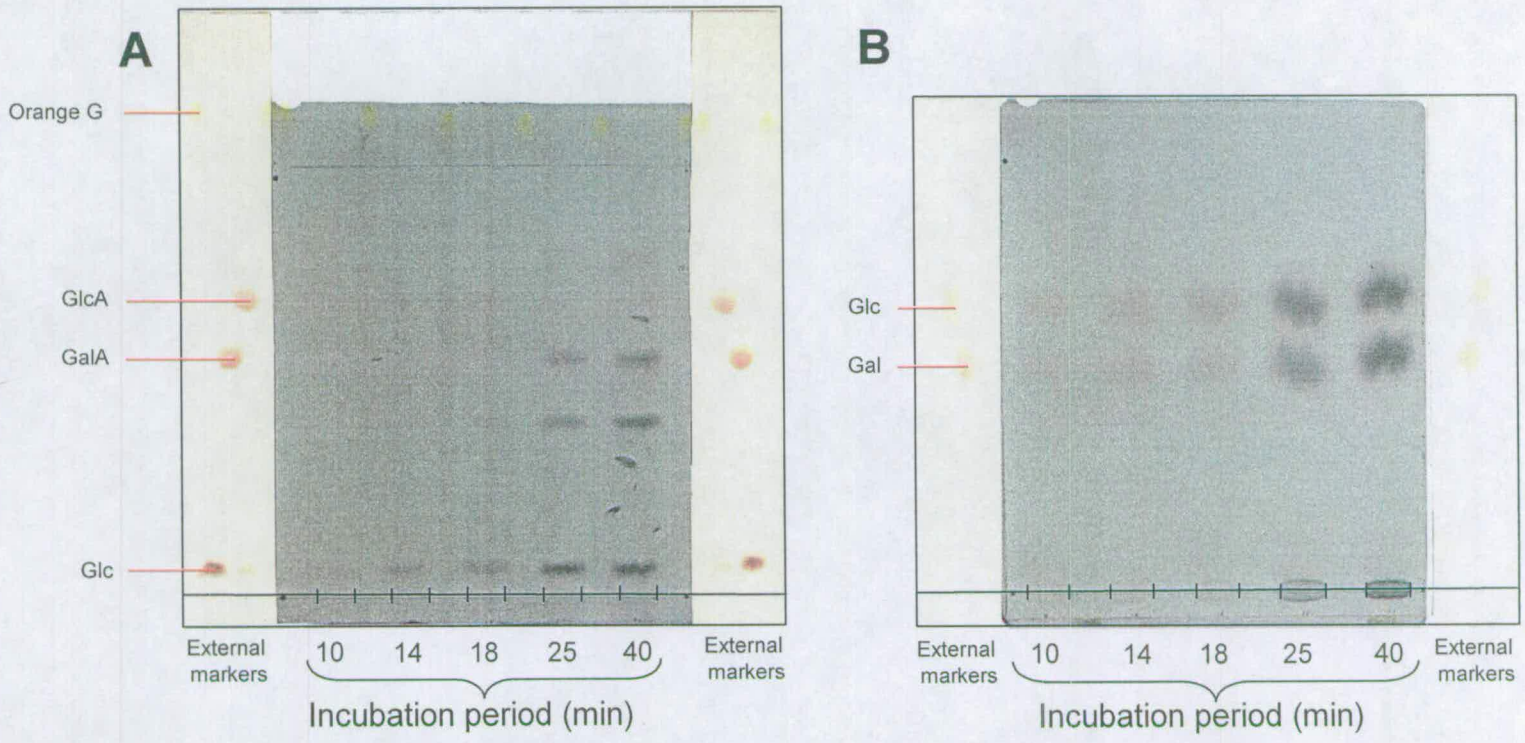

Figure 3.56 Paper electrophoresis purification of [^{3}H,^{14}C]GalA and paper chromatography purification of [^{3}H,^{14}C]Glc, [^{3}H,^{14}C]Gal, [^{3}H,^{14}C]Fuc, [^{3}H,^{14}C]Xyl, [^{3}H,^{14}C]Ara, [^{3}H,^{14}C]Man from *Arabidopsis* AIR hydrolysate

The radiolabelled compounds that required further purification from the paper chromatogram shown in Fig. 3.55 were eluted and loaded onto Whatman 3MM paper. The GalA sample was subjected to (**A**) paper electrophoresis (pH 3.5, 2.5 kV, 1.5 h). The Glc/Gal sample run in (**B**) EPW (8:2:1, 32 h). The Fuc/Xyl sample was run in (**C**) BAW (12:3:5, 26 h). The Ara sample was run in (**D**) phenol/water (4:1, w/w, 20 h). The "Man" sample was run in (**E**) phenol/water (4:1, w/w, 20 h). The external markers were stained with aniline hydrogen-phthalate. The chromatograms and electrophoretogram shown are representative.

Continued overleaf

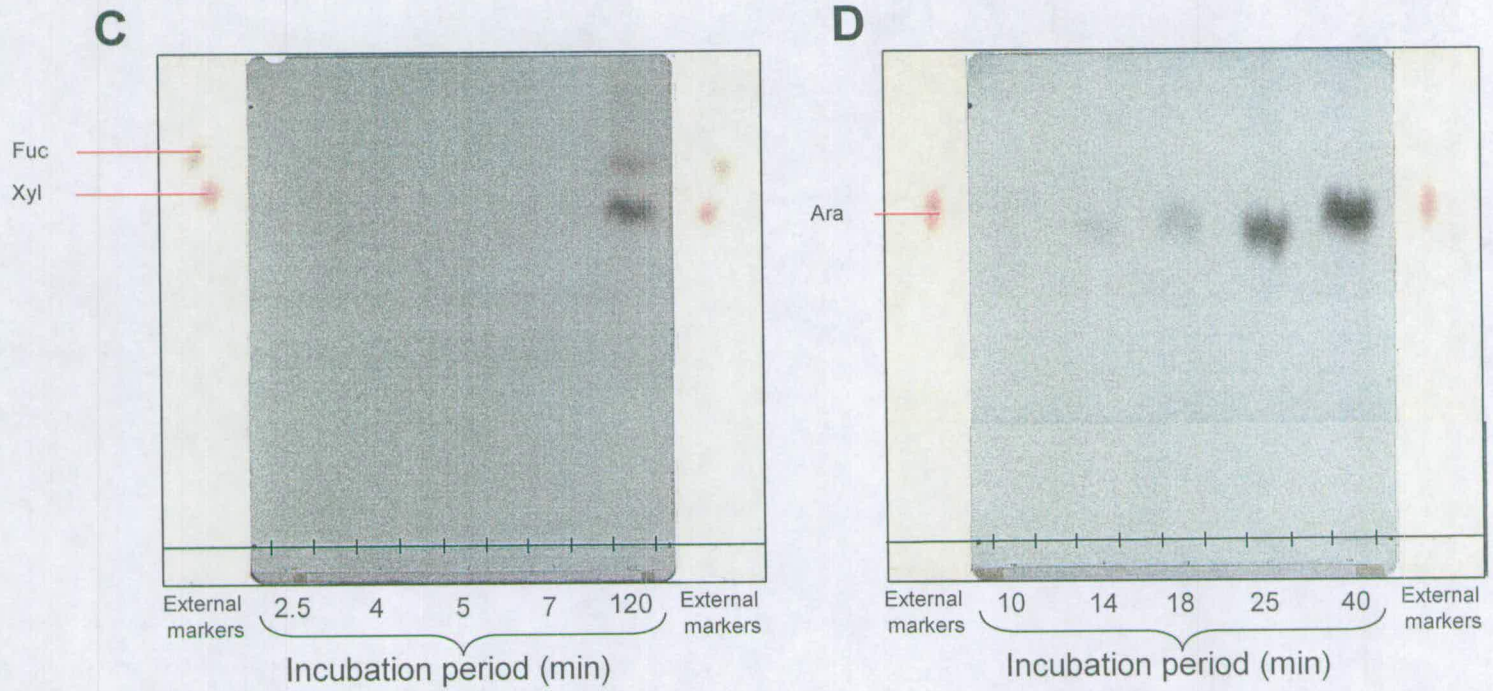

Figure 3.56 Continued

Continued overleaf

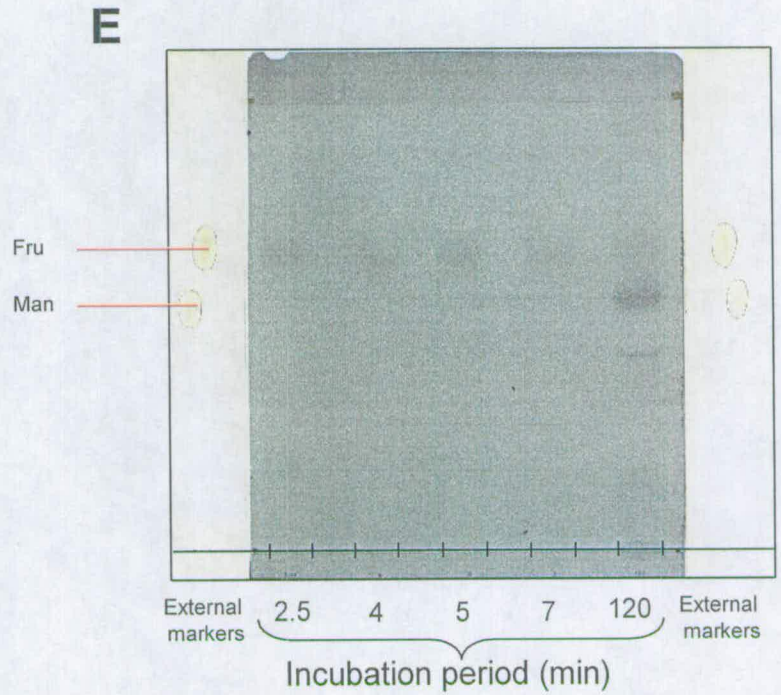

Figure 3.56 Continued

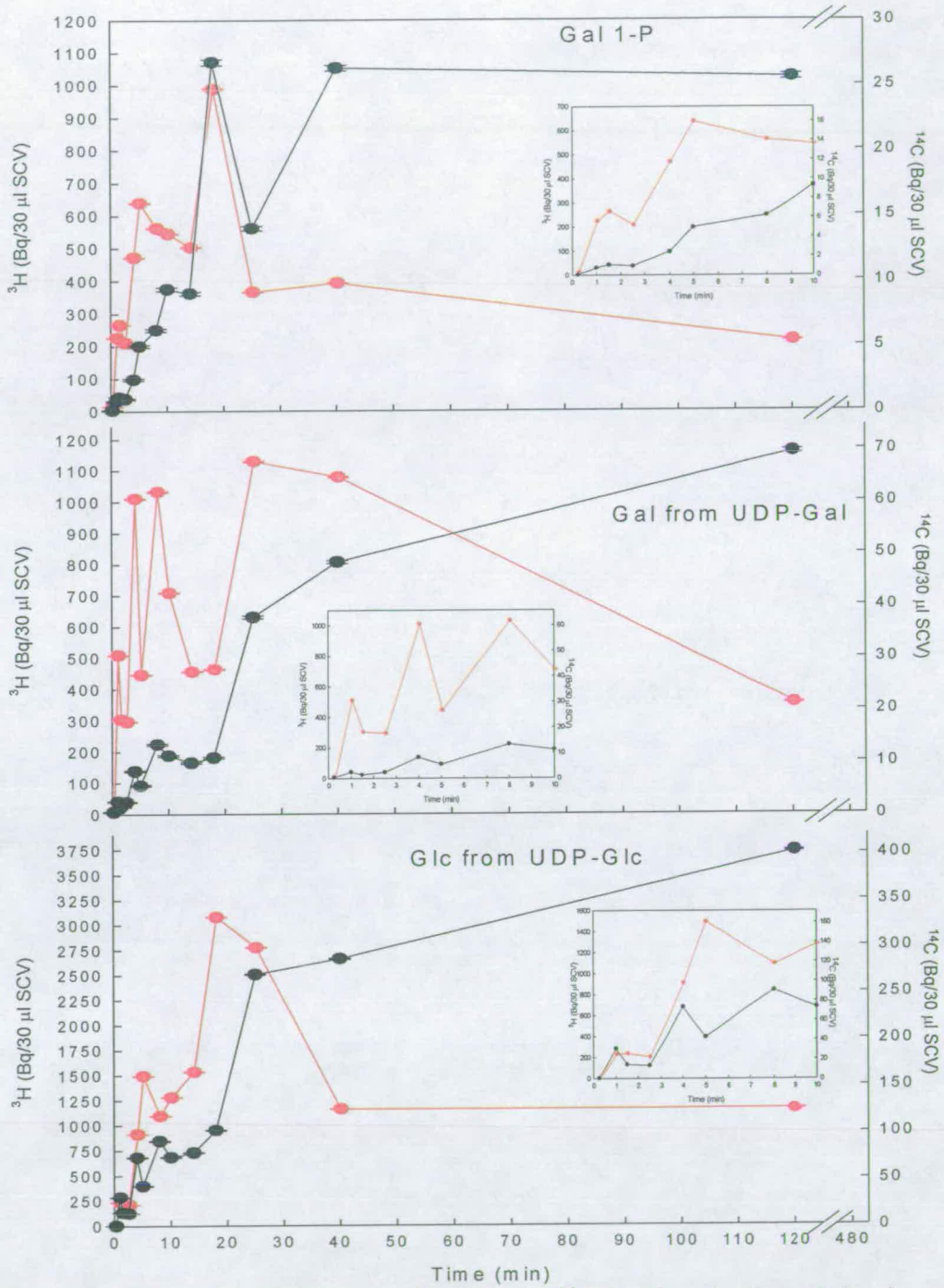

Figure 3.57 Kinetic study of the ^{3}H and ^{14}C levels of radioactivity in the intermediary metabolites purified from *Arabidopsis* cell-suspension culture

The graphs shown inset magnify the initial values. The error bars are unique to each time point and relate to the method used to detect the radiolabelled isotopes. The (—) represents ^{3}H and the (—) represents ^{14}C.

Continued overleaf

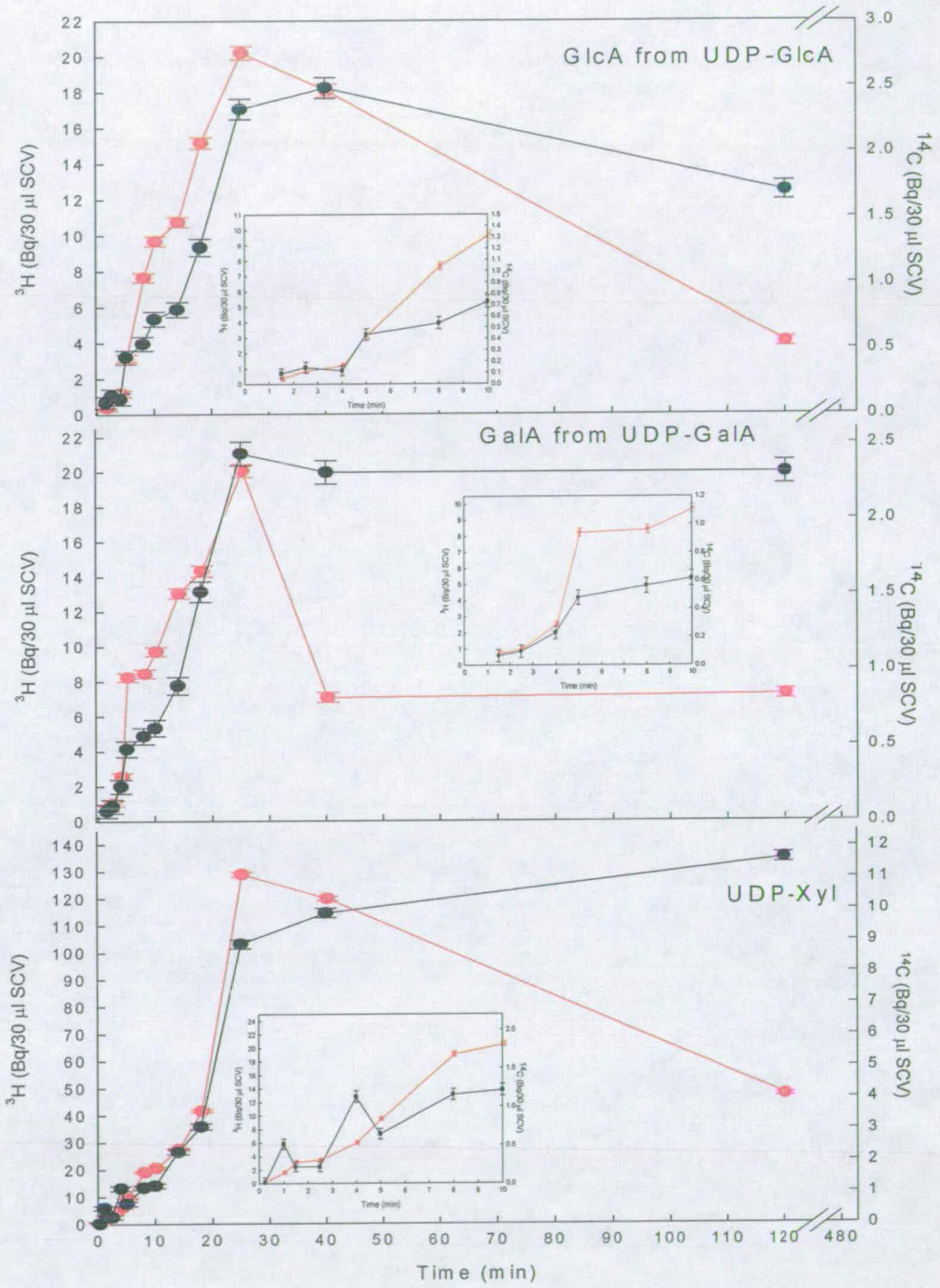

Figure 3.57 Continued.

Continued overleaf

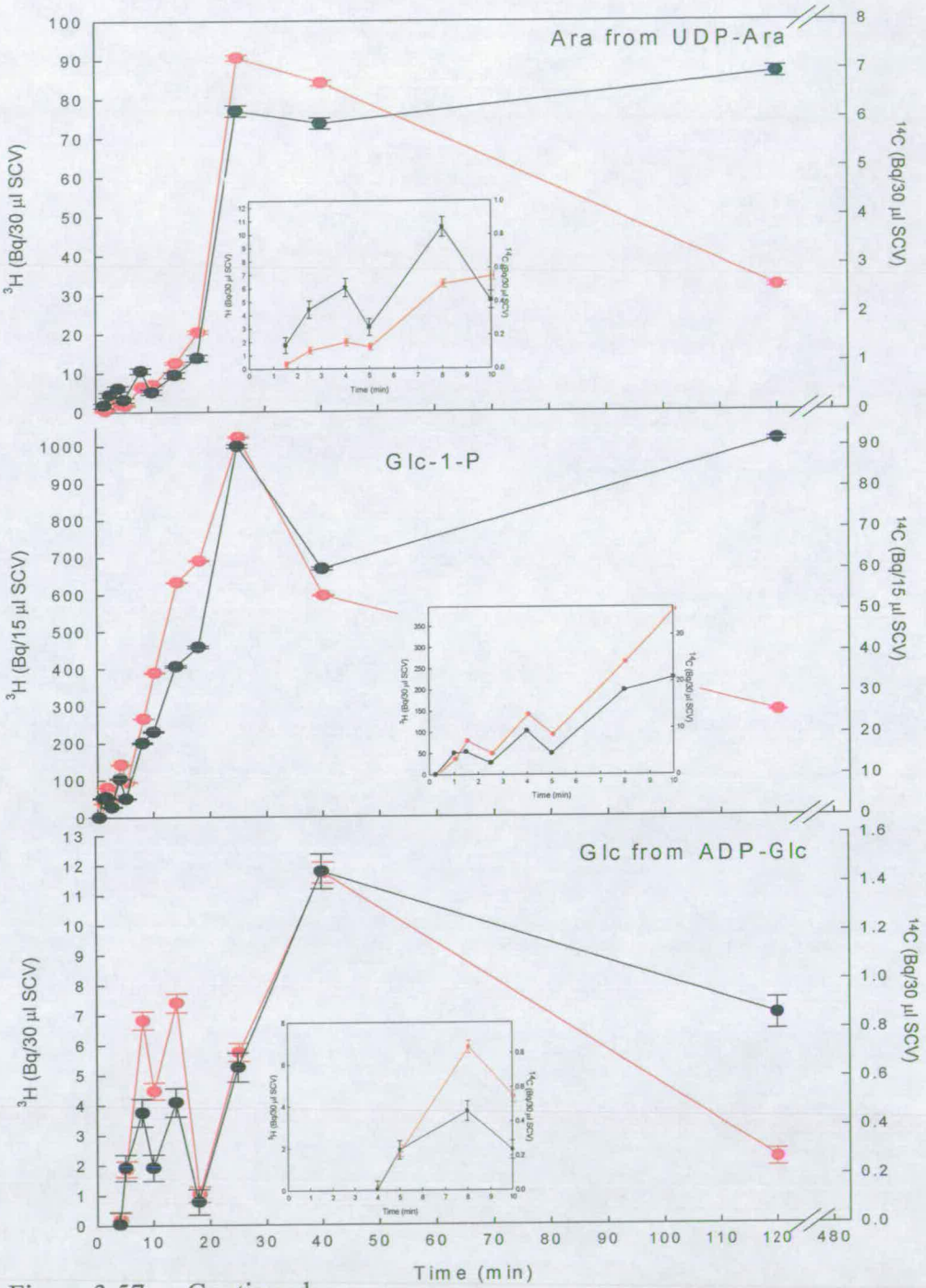

Figure 3.57 Continued.

Continued overleaf

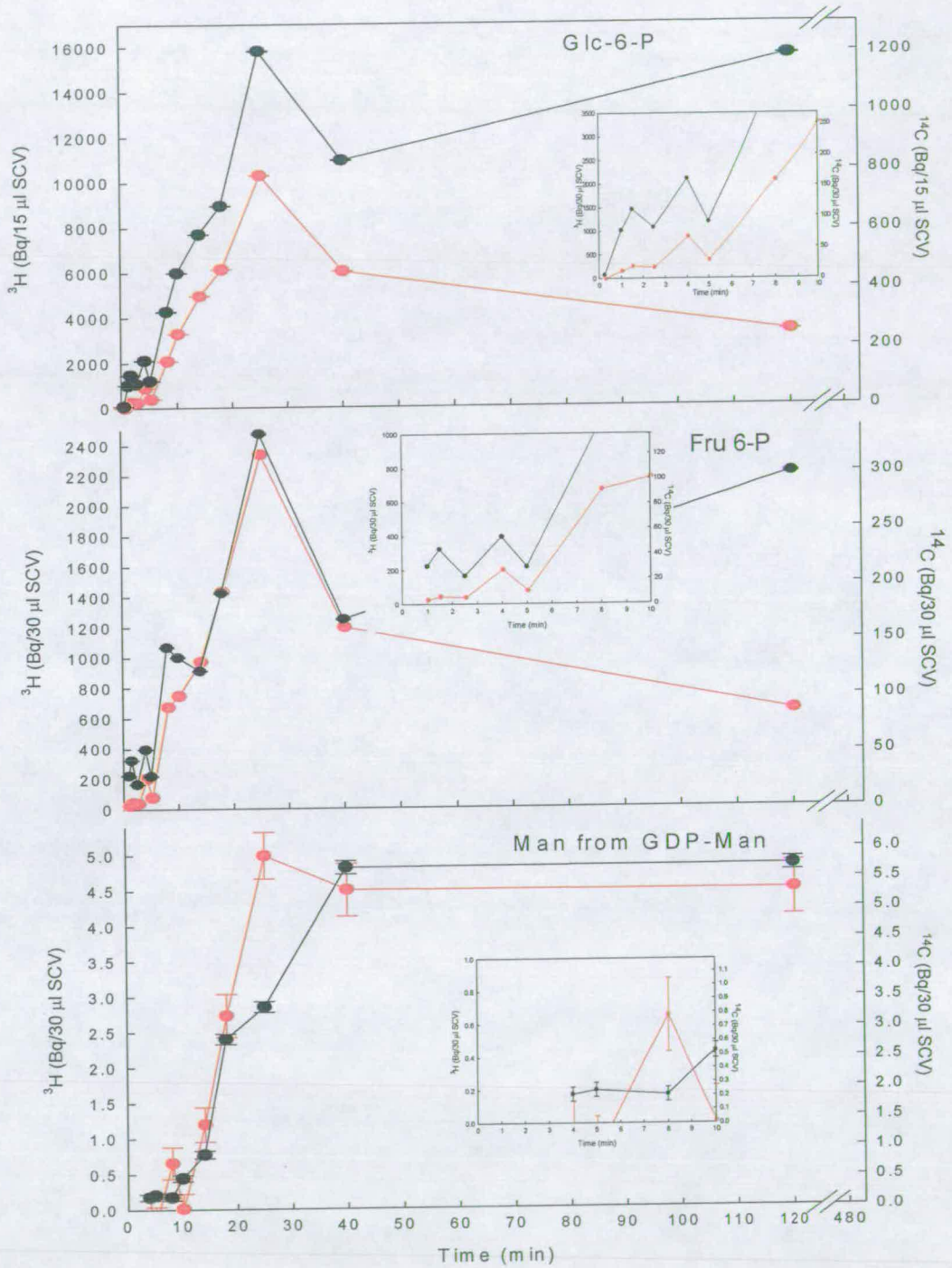

Figure 3.57 Continued.

Continued overleaf

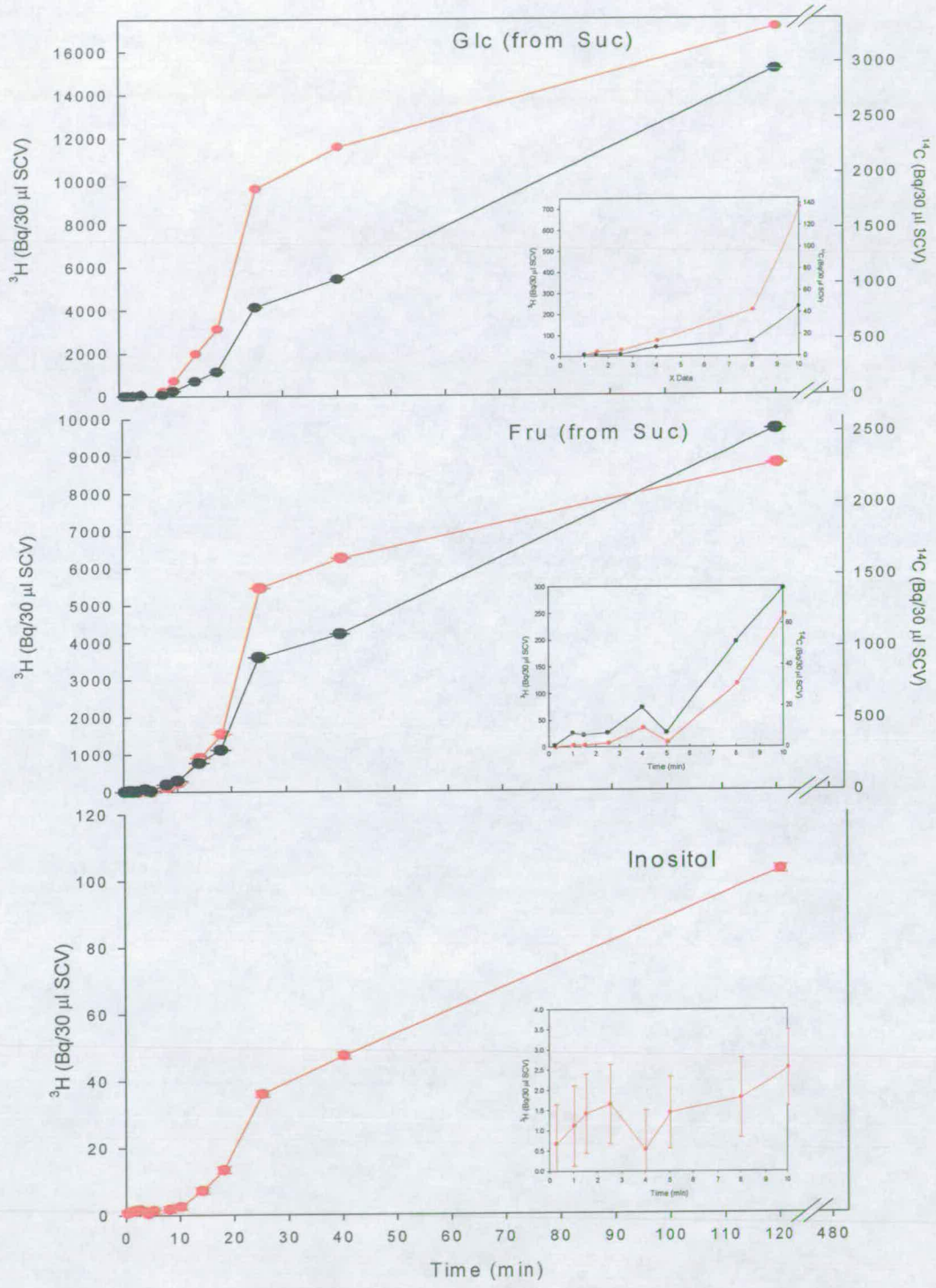

Figure 3.57 Continued.

Continued overleaf

approximately 20 min and remains at a constant plateau for at least 2 h. This suggests that the [U-^{14}C]Fru has a slower uptake rate from the medium than [^{3}H]Gal.

The 'core' metabolite closest to the source of ^{3}H is UDP-Gal. This metabolite pool is represented in the 'Gal from UDP-Gal' graph. The radiolabelling trends described for Gal 1-P also apply to 'Gal from UDP-Gal'. Previous experimentation has shown that [U-^{14}C]Fru is taken up by *Arabidopsis* cell-suspension within 2 h (Fig. 3.4).

The next 'core' metabolite distanced by an additional metabolic step from both the ^{3}H source and UDP-Gal is UDP-Glc. In the 'Glc from UDP-Glc' graph, the lag-period of ^{3}H and ^{14}C entry are similar to that of 'Gal from UDP-Gal' and Gal 1-P. However, the UDP-Glc metabolite pool has a slightly greater initial maximum rate of ^{14}C entry at ~2.5 min than the 'Gal from UDP-Gal' and Gal 1-P pool. This may be because fewer metabolic steps are required to convert [^{14}C]Fru to UDP-Glc than to UDP-Gal.

The 'core' metabolites that become radiolabelled with ^{3}H after UDP-Glc are Glc 1-P followed by Glc 6-P. The Glc 1-P and Glc 6-P graphs show that the maximum initial rate of ^{3}H entry into each of these metabolite pools occurs at approximately 5 min. This is longer than the time needed to reach the maximum initial rate of ^{3}H entry into Gal 1-P, 'Gal from UDP-Gal' and 'Glc from UDP-Glc'. The maximum initial rate of ^{14}C entry into Glc 1-P occurs at 5 min. This is approximately 4 min later than the time taken to reach the maximum initial rate of ^{14}C entry into Glc 6-P, which is metabolically closer to the ^{14}C-labelled source.

Fru 6-P is the 'core' metabolite that is furthest away from the source of ^{3}H and closest to the source of ^{14}C in the metabolic pathway. The radiolabelling kinetics of Fru 6-P closely match those of Glc 6-P.

The 'core' metabolites show an overall expected trend where the closer a metabolite is situated in the pathway to a radiolabelled source, the sooner the metabolite achieves a maximum initial rate of radiolabelling.

It is known that UDP-GlcA and UDP-GalA may arise from the parent 'core' metabolites UDP-Gal, UDP-Glc or Glc 6-P. In the 'GlcA from UDP-GlcA' and 'GalA from UDP-GalA' graphs the maximum initial rate of ^{3}H entry into these metabolite pools occurs at approximately 4 min. It expected that a metabolite that is more 'distanced' in a biochemical pathway from a radiolabelled source will not become radiolabelled until its precursor has been radiolabelled. As the maximum initial rate of ^{3}H entry into Glc 6-P occurs after that of 'GlcA from UDP-GlcA' and 'GalA from UDP-GalA', it is suggested that Glc 6-P may not be the parent 'core' metabolite of GlcA or GalA. The data obtained for 'Xyl from UDP-Xyl' also agree with this. UDP-Xyl, shown in the 'Xyl from UDP-Xyl' graph, is formed from UDP-GlcA and also obtains its maximum initial rate of ^{3}H entry before Glc 6-P. UDP-Xyl may also give rise to UDP-Ara. The graph of 'Ara from UDP-Ara' shows that the maximum initial rate of ^{3}H entry into UDP-Ara occurred at approximately 5 min. Although this is at approximately the same time that the maximum initial rate of ^{3}H entry in to Glc 6-P is achieved, it occurs after the maximum initial rate of its precursor UDP-Xyl.

The lag-times of ^{14}C entry into 'GlcA from UDP-GlcA', 'GalA from UDP-GalA', 'Xyl from UDP-Xyl' and 'Ara from UDP-Ara' are all longer than Glc 6-P.

These results are unable to give any information about the potential parent 'core' metabolite that each metabolite stemmed from because, as expected, they all become ^{14}C-labelled after Glc 6-P. Indeed, this would be expected if the parent core metabolites of UDP-GlcA, UDP-GalA, UDP-Xyl and UDP-Ara arose from any of the potential 'core' metabolites. The results of ^{14}C entry into the cytosolic inositol pool were unreliable as the originally [U-^{14}C]Fru that was fed to the cells was shown to be contaminated with [^{14}C]inositol (Fig. 3.54). The ^{3}H entry into the cytosolic pool was examined. It is clear from these results that the lag-time of ^{3}H entry into the inositol pool was greater than the lag-time for 'GlcA from UDP-GlcA', 'GalA from UDP-GalA', 'Xyl from UDP-Xyl' and 'Ara from UDP-Ara'. This suggests that these metabolites stem from a pathway that is 'closer' to the ^{3}H-labelled source than inositol. This indicates that the *myo*-inositol pathway is unlikely to be the predominating pathway in the formation of UDP-GlcA, UDP-GalA, UDP-Xyl and UDP-Ara.

GDP-Man may be formed from the parent 'core' metabolites Glc 1-P or Fru 6-P. As the 'Man from GDP-Man' graph shows both the ^{3}H and ^{14}C lag-times of entry into GDP-Man are slower than Glc 1-P and Fru 1-P no information can be concluded about the predominant parent 'core' metabolite of GDP-Man.

ADP-Glc is formed from Glc 1-P. The formation of ADP-Glc, however, is complicated by the fact that it may proceed through triose phosphates that are transported to the plastids. If this were the predominant method of ADP-Glc synthesis there would be many metabolic steps, distanced from the 'core' metabolites, that would be required to form ADP-Glc. This would result in longer lag-time of ^{3}H and ^{14}C entry into the ADP-Glc pool than if the predominant method

of ADP-Glc synethesis was in the cytosol. In the latter scenario the ADP-Glc would be transported, as ADP-Glc, into the plastids. The radiolabel kinetic results in the 'Glc from ADP-Glc' graph do not distinguish between these potential methods of starch synthesis. Indeed, the initial time points on the 'Glc from ADP-Glc' graph are scattered and do not allow the lag-period to be determined.

3.2.3.8 ^{3}H:^{14}C Ratios of the intermediary metabolites

The *Arabidopsis* cells were fed from the stock solution that contained both [1-^{3}H]Gal and [U-^{14}C]Fru. Minor discrepancies in the amount of ^{3}H and ^{14}C that cells received may have been caused by pipetting error and also error in the dispensation of cells. Analysis of the absolute amounts of ^{3}H and ^{14}C in each metabolite may over time be slightly distorted by this. This may also occur if the radiolabelled compound in question was not completely retrieved from the separation techniques employed in this study. A more reliable method of analysis of each of the intermediate metabolites is the ^{3}H:^{14}C (Bq/Bq) ratio. The information gained on the kinetics of the ^{3}H:^{14}C (Bq/Bq) ratios for each of the intermediary metabolites is advantageous because it does not rely on the absolute amount of ^{3}H and ^{14}C that was fed per cell. The original ^{3}H:^{14}C (Bq/Bq) ratio that the cells obtained will have been the same. In addition to this the analysis of the isotope ratios may overcome the problem that the cells may have taken time to 'adjust' to the 'shock' they may have suffered when they were dispensed into vials.

3.2.3.9 Isotope ratios of the 'core' metabolites, Gal 1-P, Glc (from Suc) and Fru (from Suc)

The ratios of the 'core' metabolites, Gal 1-P, Glc (from Suc) and Fru (from Suc) are shown in Fig. 3.58. The metabolite with the highest isotope ratio is expected to be

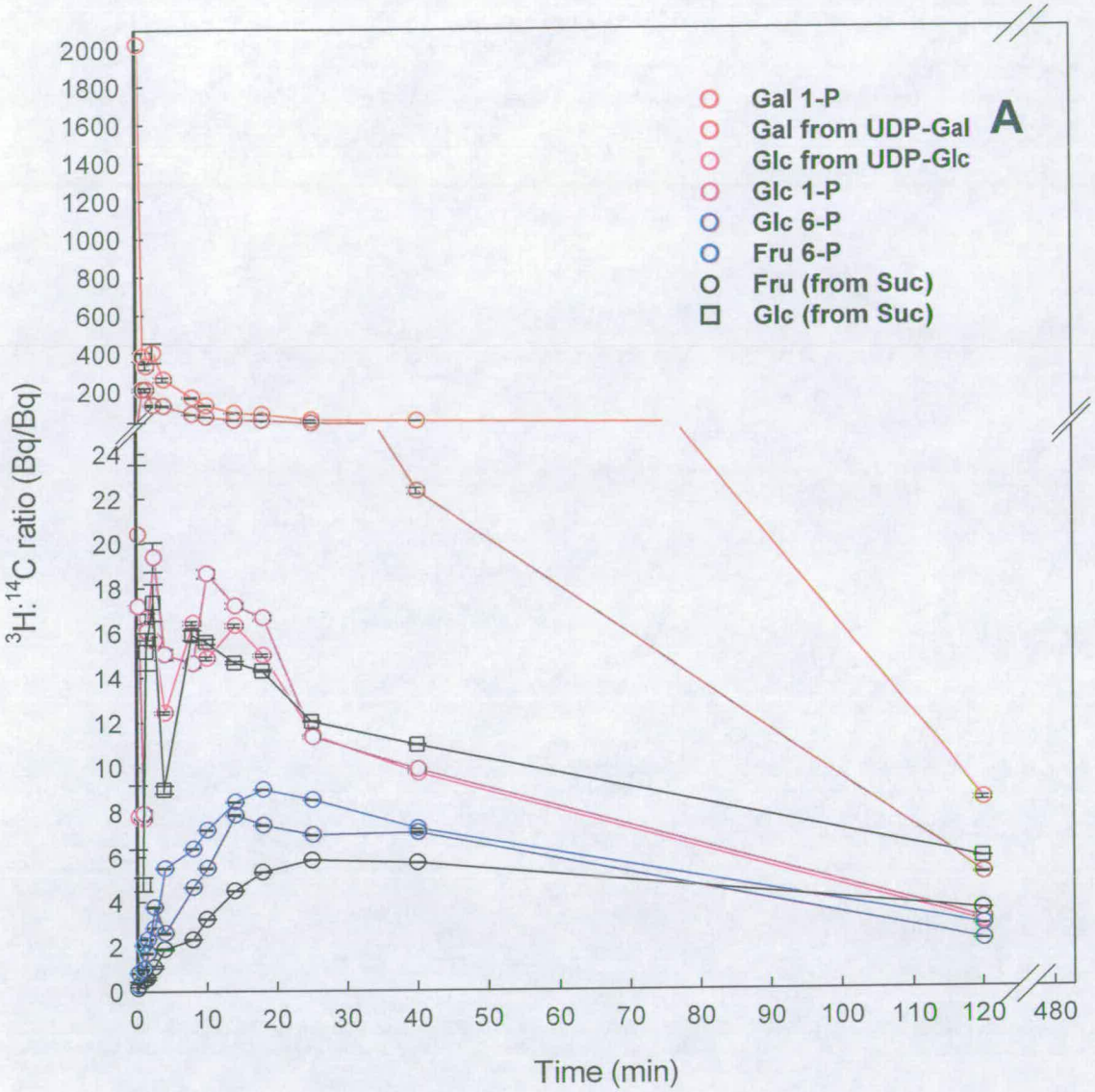

Figure 3.58 Kinetic study of the ^{3}H:^{14}C ratios of the metabolite intermediates purified from *Arabidopsis* cell-suspension culture

(**A**) ^{3}H:^{14}C (Bq/Bq) ratio kinetics of Gal 1-P, Fru (from Suc), Glc (from Suc) and the 'core' metabolite intermediates (Gal from UDP-Gal, Glc from UDP-Glc, Glc 1-P, Glc 6-P, Fru 6-P). ^{3}H:^{14}C (Bq/Bq) ratio kinetics of (**B**) GalA from UDP-GalA and the 'core' metabolites that UDP-GalA may stem from (Gal from UDP-Gal, Glc from UDP-Glc, Glc from Glc 6-P). ^{3}H:^{14}C (Bq/Bq) ratio kinetics of (**C**) GlcA from UDP-GlcA (**D**) Xyl from UDP-Xyl and (**E**) Ara from UDP-Ara and the 'core' metabolites that each of these compounds may stem from (Glc from UDP-Glc, Glc from Glc 6-P). (**F**) ^{3}H:^{14}C (Bq/Bq) ratio kinetics of Man from GDP-Man and the 'core' metabolites it may stem from (Glc 1-P, Fru 6-P). (**G**) ^{3}H:^{14}C (Bq/Bq) ratio kinetics of Glc from ADP-Glc, the 'core' metabolite it may potentially stem from (Glc 1-P) and Fru 6-P.
The error bars are unique to each time point and relate to the method used to detect the radiolabelled isotopes

Continued overleaf

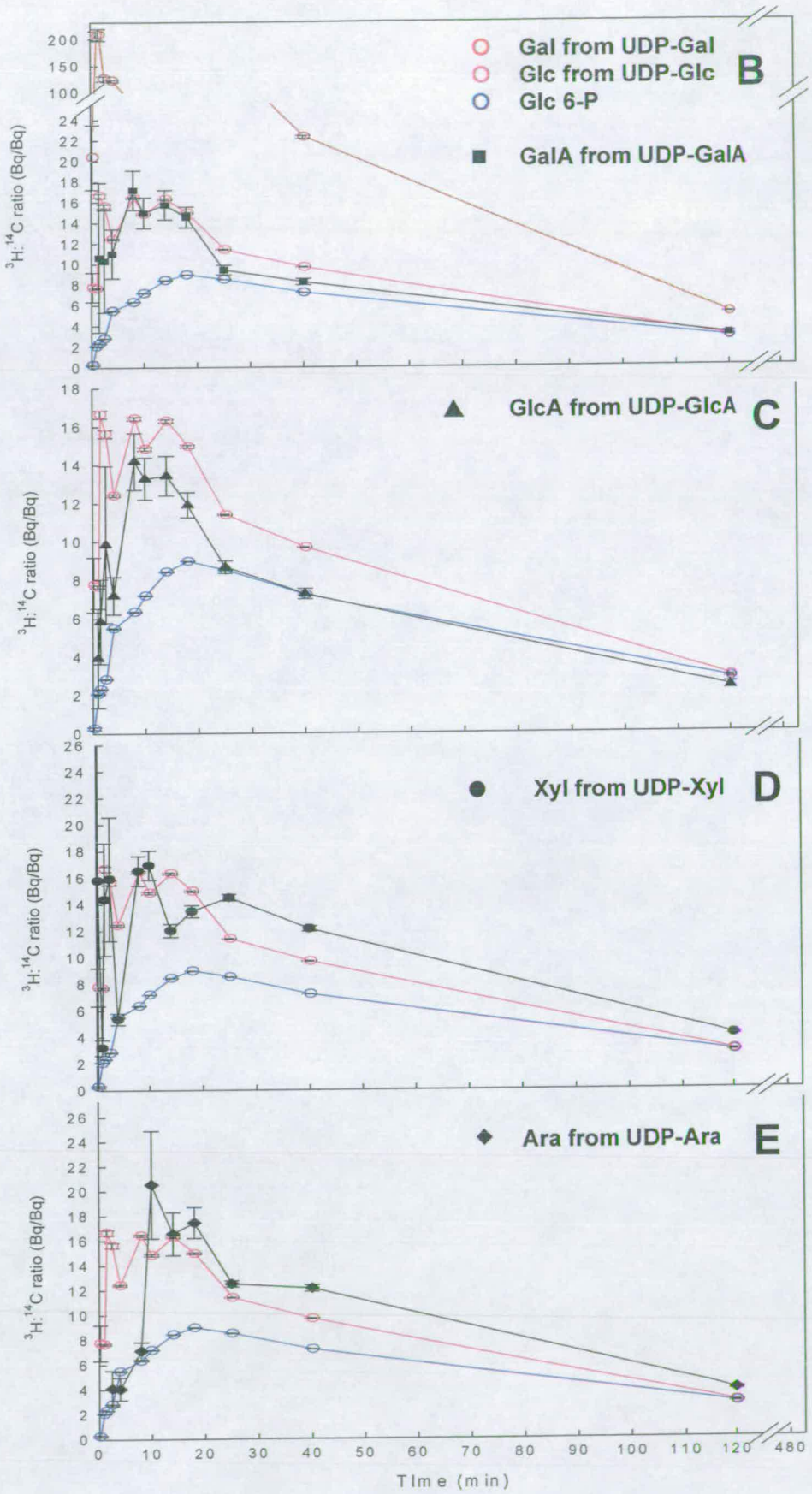

Figure 3.58 Continued

Continued overleaf

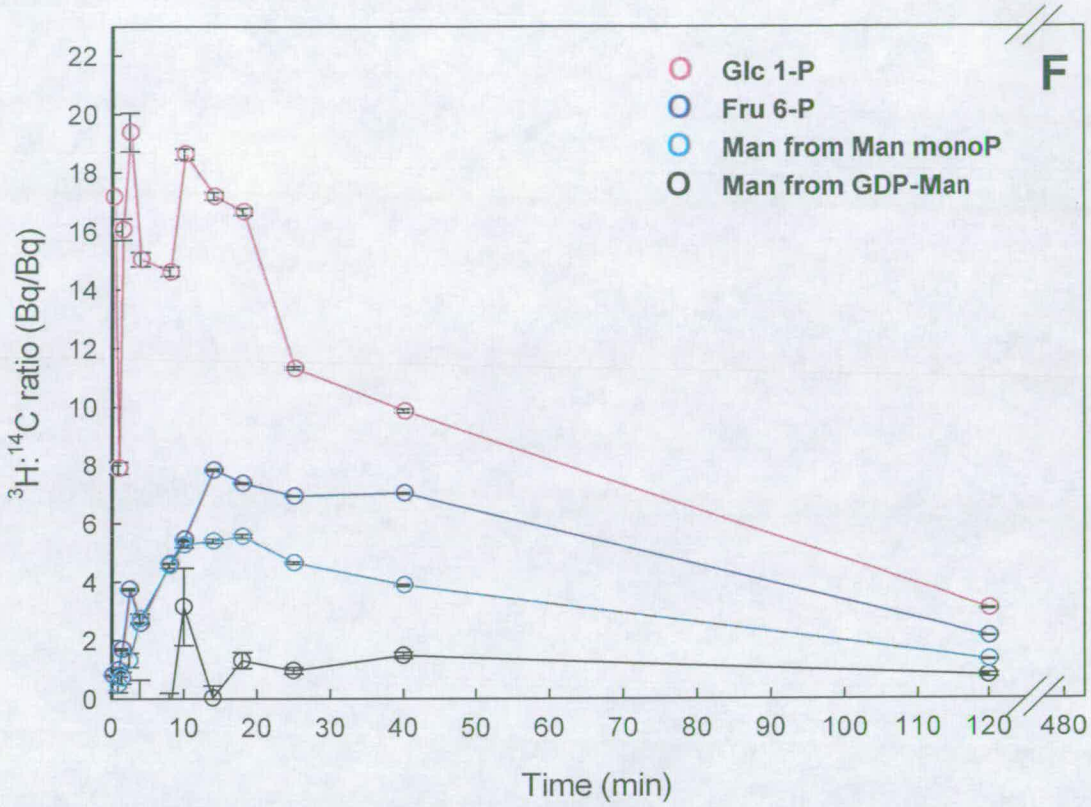

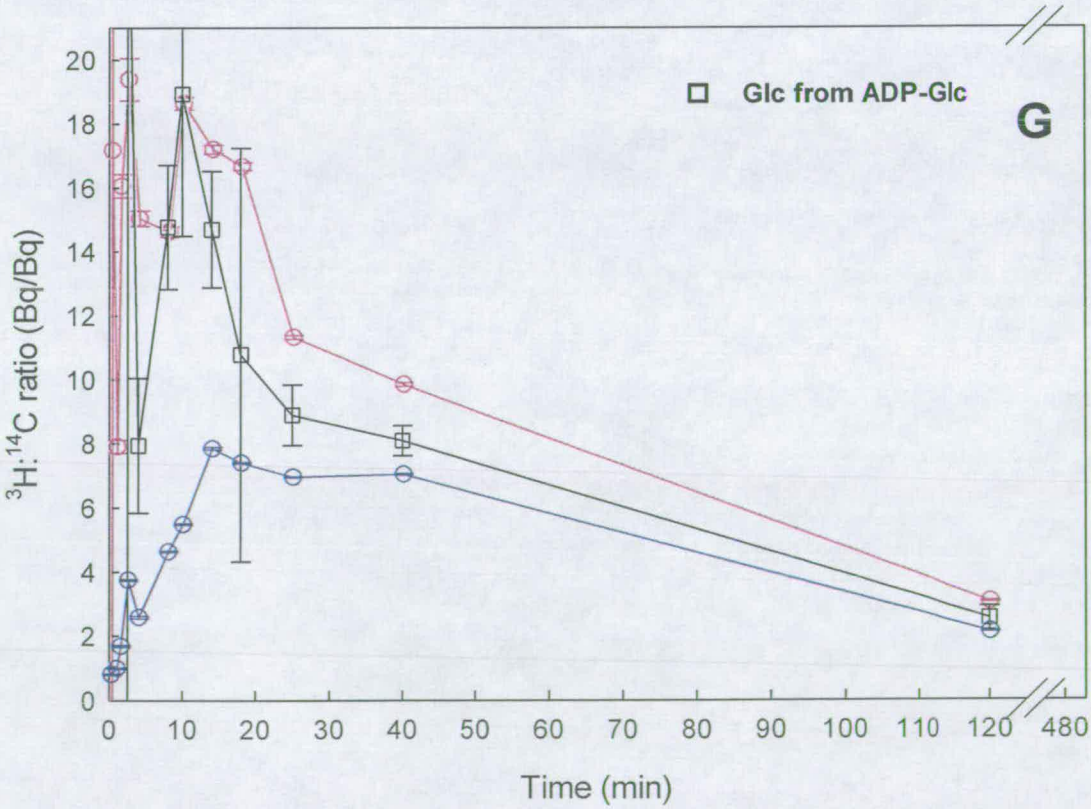

Figure 3.58 Continued

Continued overleaf

the metabolite closest to the originally supplied ^{3}H source, [1-^{3}H]Gal. This compound is Gal 1-P and, when analysed, the Gal 1-P has the most rapidly formed and highest ^{3}H:^{14}C (Bq/Bq) ratio of approximately 400 (Bq/Bq) in 15 s. There is also a rapid decline in the ratio once this peak has been reached. This suggests that, out of the metabolites analysed, Gal 1-P is closest to the ^{3}H source and becomes maximally radiolabelled with ^{3}H that is then lost when it is converted into another metabolite. The 'core' metabolite that is closest to the ^{3}H source in the biochemical pathway is UDP-Gal. UDP-Gal is distanced from the ^{3}H source by two metabolic reactions and may be directly formed from Gal 1-P. The 'Gal from UDP-Gal' pool reaches a maximum ^{3}H:^{14}C ratio peak of approximately 210 (Bq/Bq) after 1 min. The decline in ^{3}H occurs as per the Gal 1-P pool.

There are three metabolic reactions required to convert [^{3}H]Gal to UDP-Glc. UDP-Glc is formed directly from UDP-Gal. UDP-Glc obtains a maximum ^{3}H:^{14}C ratio of approximately 16.5 (Bq/Bq). The Glc 1-P plot in Fig. 3.58 (A) is very similar to that of 'Glc from UDP-Glc' and may suggest a rapid interconversion between these two metabolites that results in a similar ^{3}H:^{14}C ratio.

The 'core' metabolite Glc 6-P is formed from Glc 1-P. The ^{3}H:^{14}C ratio of Glc 6-P shows that the maximum ratio is obtained in 18 min and is approximately 9 (Bq/Bq). This value is much lower than the maximum obtained for Glc 1-P.

In comparison to the other 'core' metabolites Fru 6-P is metabolically furthest away from the source of ^{3}H and closest to the source of ^{14}C. Out of all of the 'core' metabolites Fru 6-P has the lowest maximum ^{3}H:^{14}C ratio of 7.8 (Bq/Bq) that is reached after the maximum obtained for Glc 6-P.

The formation of Suc proceeds via Suc 6-P that is formed from UDP-Glc and Fru 6-P. The difference between the isotope ratio kinetics of the 'core' metabolites UDP-Glc and Fru 6-P and the monosaccharides that form Suc is that the monosaccharides of Suc are end-products that may be turned over. 'Glc from UDP-Glc' and 'Fru from Fru 6-P' are intermediates. An end-product records the accumulated total radioactivity whereas an intermediate shows the radiolabel present in a metabolite pool at that moment. The isotope ratio kinetics of 'Glc from Suc' agrees with the 'core' metabolite that it is synthesised from ('Glc from UDP-Glc') (Fig. 3.58 A). The isotope ratio kinetics of 'Fru from Suc' show slightly lower values for 'Fru from Suc' than for Fru 6-P with the maximum $^{3}H:^{14}C$ ratio for 'Fru from Suc' (6 Bq/Bq) obtained by 25 min. The isotope ratios kinetics of the monosaccharides obtained from Suc clearly show that the isotope ratio of an end-product is, as predicted in the experimental outline (section 1.5), related to the 'core' metabolite that it was derived from.

As predicted in the experimental outline a $^{3}H:^{14}C$ ratio gradient is witnessed in the 'core' metabolites. Fig. 5.58 (A) clearly shows that, in general, the further the 'core' metabolite is from the source of ^{3}H the lower the $^{3}H:^{14}C$ ratio.

3.2.3.10 Predominant pathway of UDP-GalA and UDP-Glc formation based on the $^{3}H:^{14}C$ intermediate metabolite ratios

UDP-GalA could be derived from the 'core' metabolites UDP-Gal, UDP-Glc or Glc 6-P (Fig. 1.6). Examination of the $^{3}H:^{14}C$ (Bq/Bq) ratio kinetics indicates that 'GalA from UDP-GalA' obtains its maximum isotope ratio before Glc 6-P (Fig. 3.58 B). If Glc 6-P were the 'core' metabolite parent that gave rise to UDP-GalA via the *myo*-inositol pathway, it would be expected that UDP-Gal would obtain its maximum

isotope ratio after Glc 6-P. In addition to this, the maximum isotope ratio of Glc 6-P is lower than the maximum isotope ratio of 'GalA from UDP-GalA'. This suggests that the parent 'core' metabolite that UDP-GalA stemmed from is closer to the ^{3}H source than Glc 6-P.

The isotope ratio kinetics of 'Gal from UDP-Gal' are very different from those of 'GalA from UDP-GalA' (Fig. 3.58 B). If UDP-Gal gave rise to even a small proportion of the UDP-GalA the maximum isotope ratio of 'GalA from UDP-GalA' would be expected to be higher than it is.

The isotope ratio kinetics of 'GalA from UDP-GalA' closely match the isotope ratio kinetics of 'Glc from UDP-Glc'. If UDP-Glc were the predominant parent 'core' metabolite of UDP-GalA then UDP-GalA would be directly formed from UDP-GlcA. Fig. 3.58 C shows a comparison of 'GlcA from UDP-GlcA' against the potential 'core' metabolites that UDP-GlcA may be formed from. As 'GlcA from UDP-GlcA' obtains a higher maximum isotope ratio before Glc 6-P it is unlikely that Glc 6-P is the predominant parent 'core' metabolite. Indeed, the isotope ratio kinetics of 'GlcA from UDP-GlcA' matches that of 'Glc from UDP-Glc' more closely than Glc 6-P. This agrees with the isotope kinetics of the UDP-GlcA derivatives 'Xyl from UDP-Xyl' (Fig. 3.58 D) and 'Ara from UDP-Ara' (Fig. 3.58 E). When 'Xyl from UDP-Xyl' and 'Ara from UDP-Ara' are compared to the parent 'core' metabolites they may stem from their isotope ratio kinetics resemble the isotope ratio kinetics of 'Glc from UDP-Glc' and not Glc 6-P.

Overall, the ^{3}H:^{14}C ratio kinetics of 'GalA from UDP-GalA', 'GlcA from UDP-GlcA', 'Xyl from UDP-Xyl' and 'Ara from UDP-Ara' suggest that they predominantly arose from the parent 'core' metabolite UDP-Glc.

3.2.3.11 ^{3}H:^{14}C Ratio kinetics of GDP-Man and ADP-Glc

GDP-Man may be derived from the 'core' metabolites Glc 1-P or Fru 6-P. Fig. 3.58 F shows the ^{3}H:^{14}C ratio kinetics of 'Man from GDP-Man'. The large error in the initial timepoints, caused by the limited amount of radioactive GDP-Man, does not allow the early timepoints to be examined. The isotope ratio kinetics of 'Man from GDP-Man' (Fig. 3.58 F) are very different from Glc 1-P (Fig. 3.58 F). The isotope ratio of 'Man from GDP-Man' remains constant after 18 min at a ^{3}H:^{14}C ratio of about 1 (Bq/Bq). The Glc 1-P reaches its isotope ratio peak within 5 min with a ^{3}H:^{14}C ratio of approximately 18–20 (Bq/Bq) and does not start to decline until after 18 min when 'Man from GDP-Man' has already reached a plateau. The isotope ratio kinetics of 'Man from GDP-Man' are more likely to have stemmed from a 'core' metabolite that was more 'distanced' from the source of ^{3}H, such Fru 6-P, than Glc 1-P. However, the isotope ratio values of 'Man from GDP-Man' over time are much lower than the isotope ratio values obtained for Fru 6-P. This suggests that the formation of GDP-Man occurs by an unknown alternative route than suggested in section 1.2.3. Another explanation is that there may have been a loss of ^{3}H from GDP-Man potentially caused by the mild acid treatment.

As previously mentioned (section 3.2.2.6), triose phosphates that are transported into the plastids from the cytosol are proposed to be the precursors of Glc 1-P synthesis which, in turn, may form ADP-Glc. The formation of triose phosphates occurs by glycolysis. As glycolysis is 'distanced' from the 'core' metabolite pathway, the ^{3}H:^{14}C ratio values of ADP-Glc were expected to be lower than the results obtained for any of the 'core' metabolites. However, the isotope ratio kinetics of 'Glc from ADP-Glc' closely match the isotope ratio kinetics of Glc

1-P. As Glc 1-P is the direct precursor of ADP-Glc and both metabolites share similar ratio kinetics and values, ADP-Glc may be predominantly synthesised in the cytosol from Glc 1-P and transported into the plastids or Glc 1-P is transported into the plastids that is then converted to ADP-Glc.

3.2.3.12 Total quantity of radioactivity in the monosaccharide residues over time

Radiolabel tracer studies into end product predict a short lag period after the precursor becomes radiolabelled. As the precursor pool becomes maximally radiolabelled a maximum rate of incorporation into AIR should occur. When the radiolabel in the precursor pool is exhausted a plateau in the end product radiolabel occurs. Fig. 3.59 shows the kinetics of radiolabel entry into end products. The surprising element of these graphs is that there is a very long lag period prior to the maximum radiolabel entry into end product in comparison with the time taken for this to occur in the precursor pool (Fig. 3.59). A likely explanation for this is that the process of cell transfer from one container to another induces a state of cell stress. If the cells were not allowed to acclimatise to their new environment for long enough, the induced stress may alter their normal biosynthetic processes. Indeed, uptake of the radiolabel appears to be rapid, but radiolabel incorporation into plant cell wall polysaccharide residues is intuitively slow.

It is clear from the graphs presented in Fig. 3.59 that the further the precursor is from the source of ^{3}H the longer the lag period of ^{3}H entry into the end product. This may explain the graphs of both Gal and Xyl. For example, the rate of maximum ^{3}H entry into Gal starts after 3 min where this takes 10 min for Xyl.

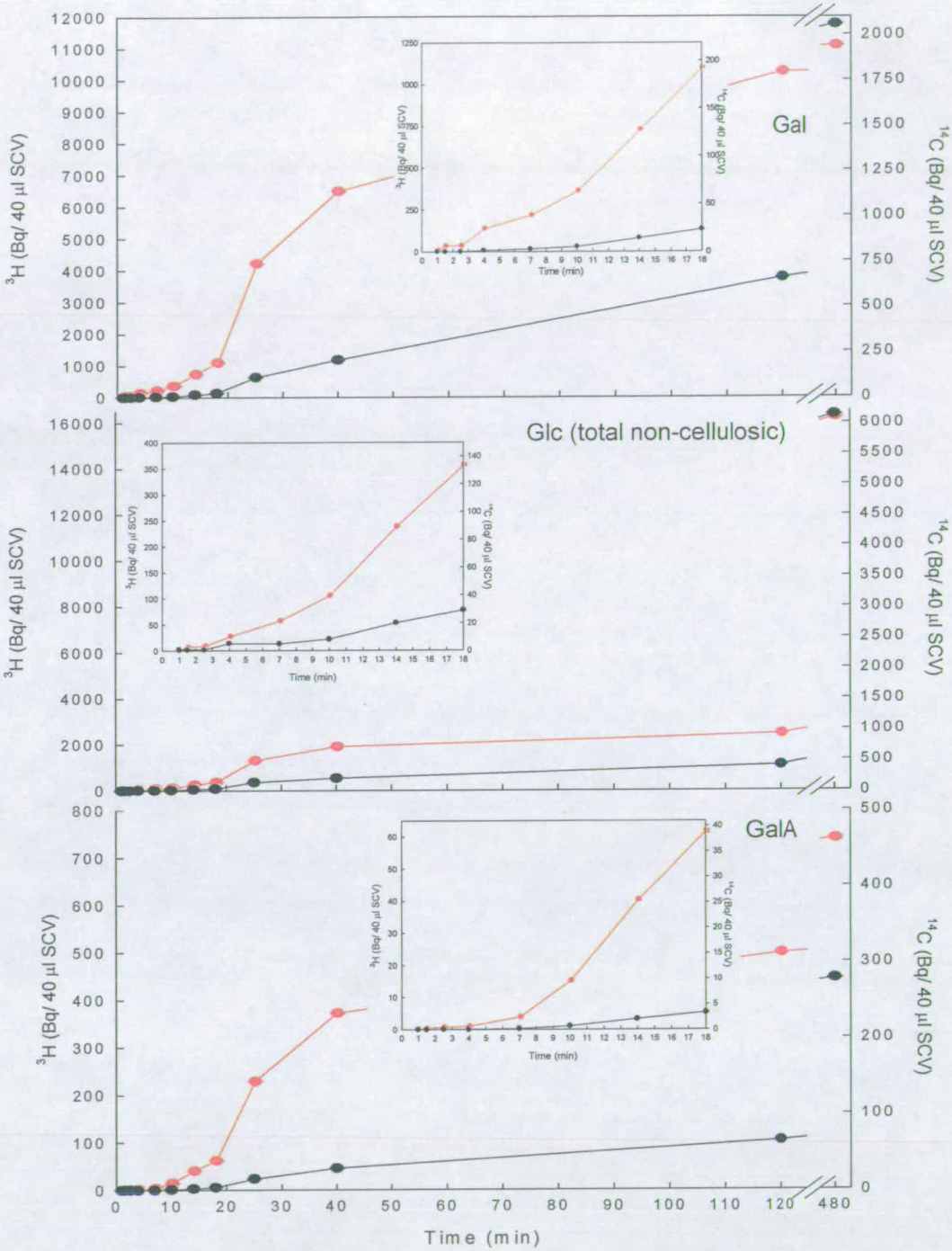

Figure 3.59 Kinetic study of the ^{3}H and ^{14}C levels in the monosaccharides of the AIR of *Arabidopsis* cell-suspension culture

The graphs shown inset magnify the initial values and the axes are proportional to the larger graph. The error bars are unique to each time point and relate to the method used to detect the radiolabelled isotopes. The (—) represents ^{3}H and the (—) represents ^{14}C.

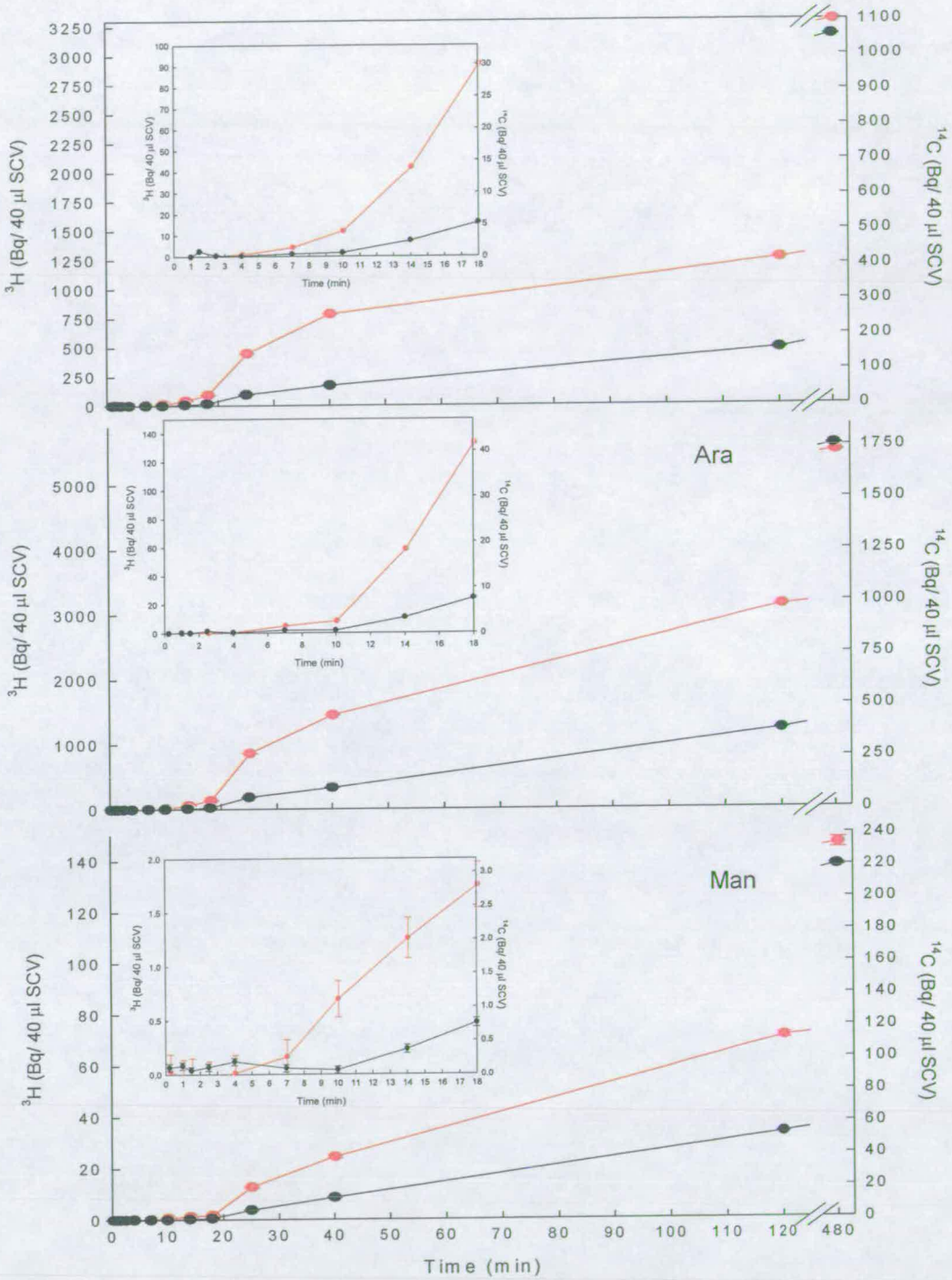

Figure 3.59 Continued.

Continued overleaf

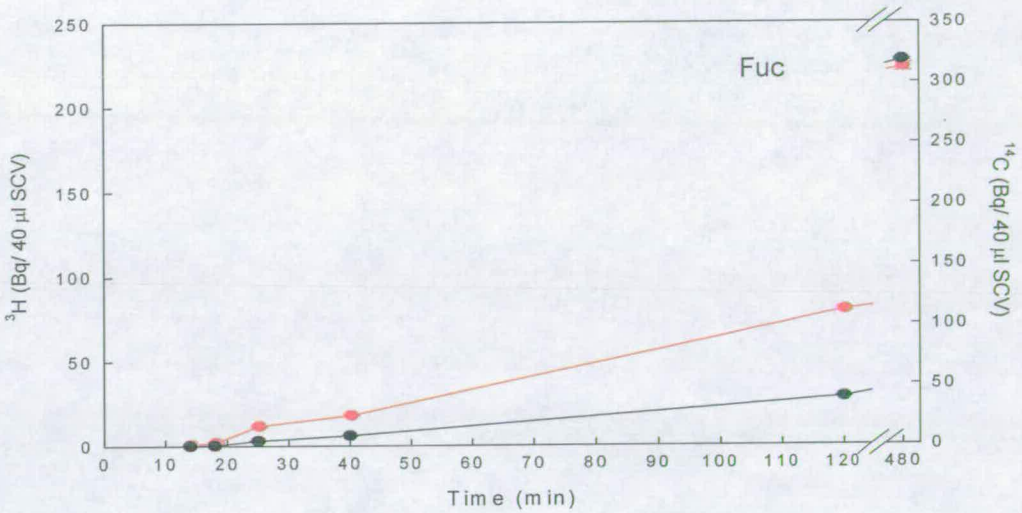

Figure 3.59 Continued.

3.2.3.13 ^{3}H:^{14}C Ratios of the monosaccharide residues of AIR over time

The ratios of the monosaccharide residues over 8 h are shown in Fig. 3.60. The ratios noted here are a cumulative total of the radiolabelled precursors that have been incorporated into an end product 'sink'. The Gal isotope ratio is the highest ratio throughout the timecourse. Although slightly delayed, the decline in the Gal isotope ratio is very similar to that of the Gal 1-P and 'Gal from UDP-Gal' (Fig. 3.60). This is thought to be a classic metabolite and end product relationship.

The ratios shown for GalA, Xyl and Ara are very similar. Their maximum ^{3}H:^{14}C ratios occur at approximately 10 min. The decline in the isotope ratio is a steady slow decline.

The ratios of Man and Fuc are exceptionally low. Owing to the initial large error bars in the early timepoints it is difficult to analyse what occurred during the first 18 min.

To make a comparison with the previous experiments (section 3.2.1, section 3.2.2) the 8 h timepoint results are shown in Fig. 3.61 and show much the same trend as in Fig. 3.22 and Fig. 3.38.

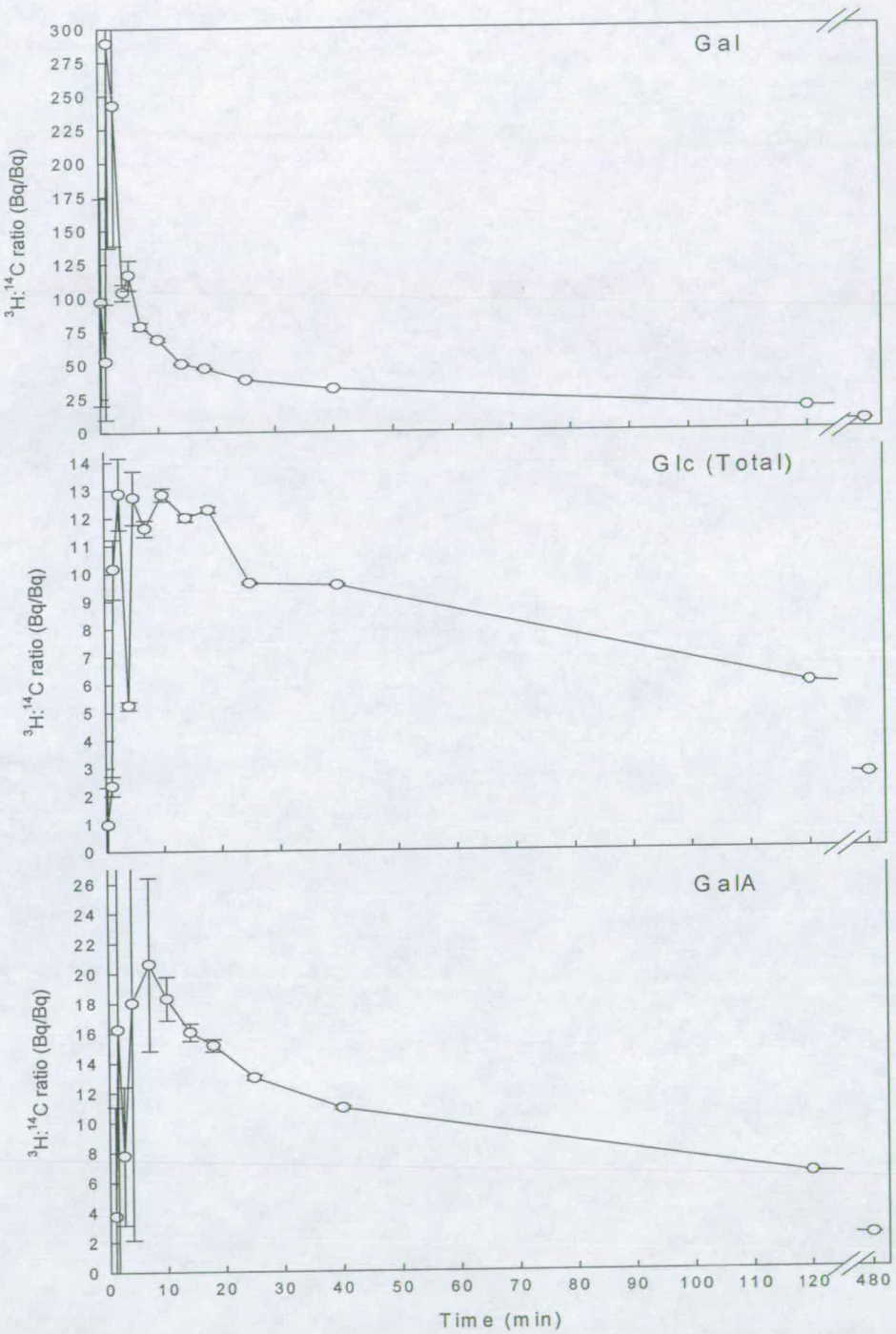

Figure 3.60 Kinetic study of the ^{3}H:^{14}C ratios of monosaccharides purified from the AIR of *Arabidopsis* cell-suspension culture

The error bars are unique to each time point and relate to the method used to detect the radiolabelled isotopes

Continued overleaf

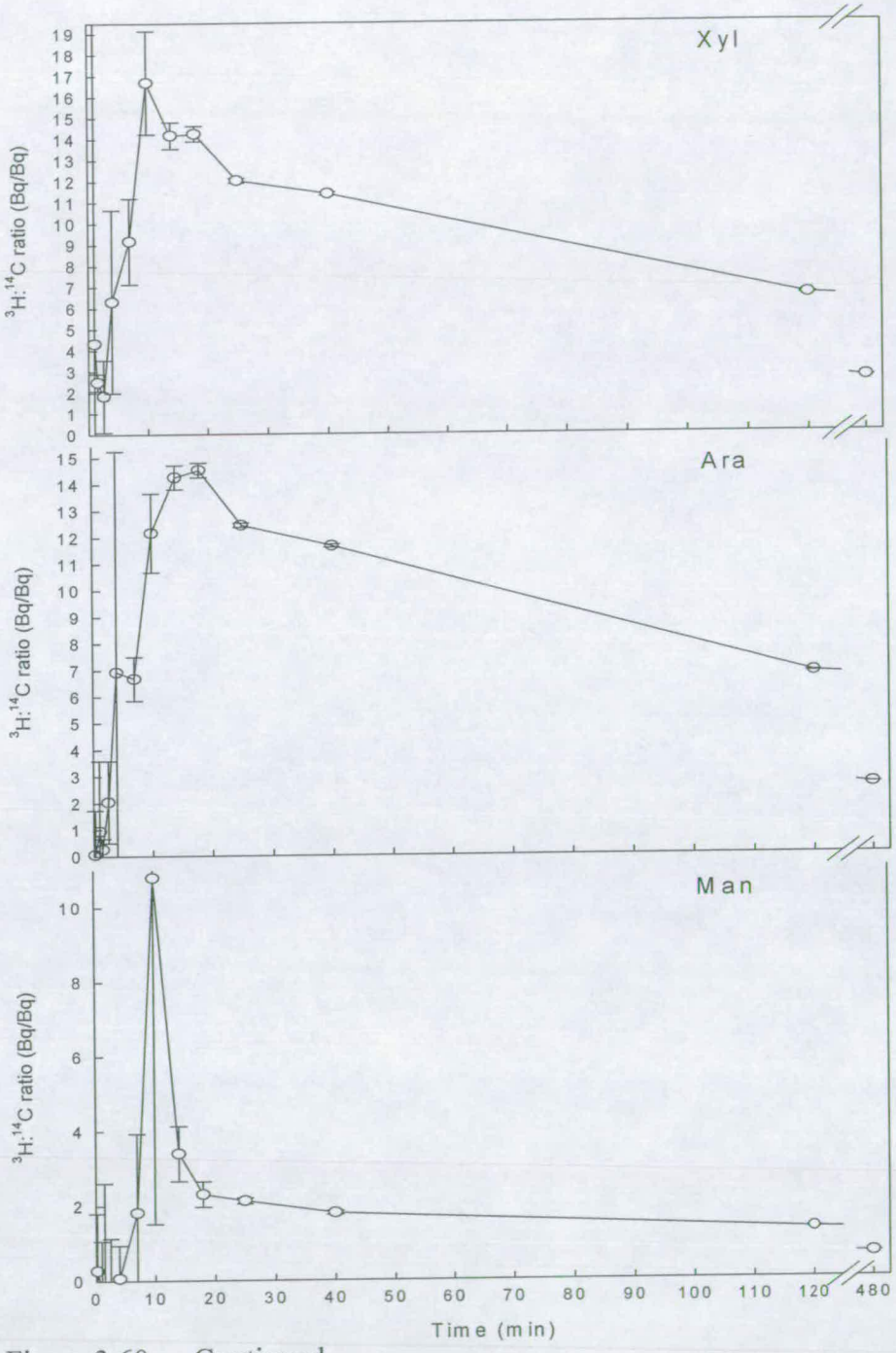

Figure 3.60 Continued.

Continued overleaf

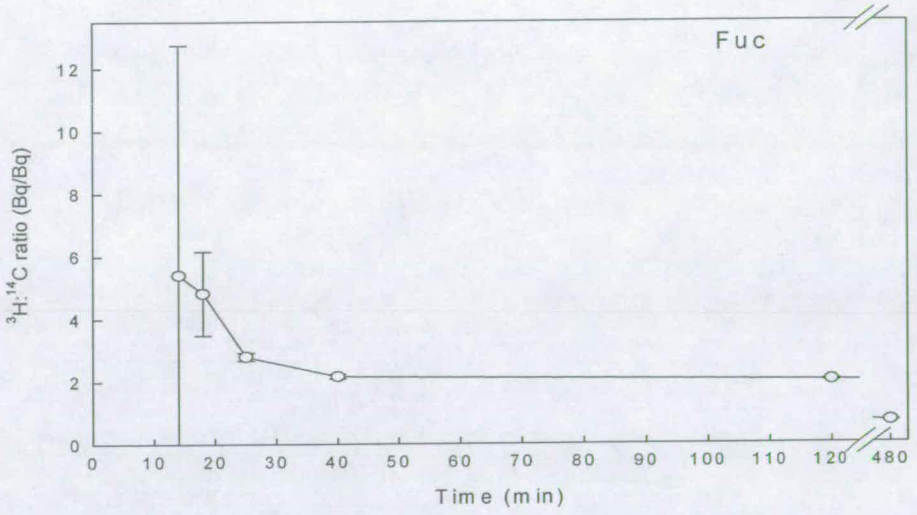

Figure 3.60 Continued.

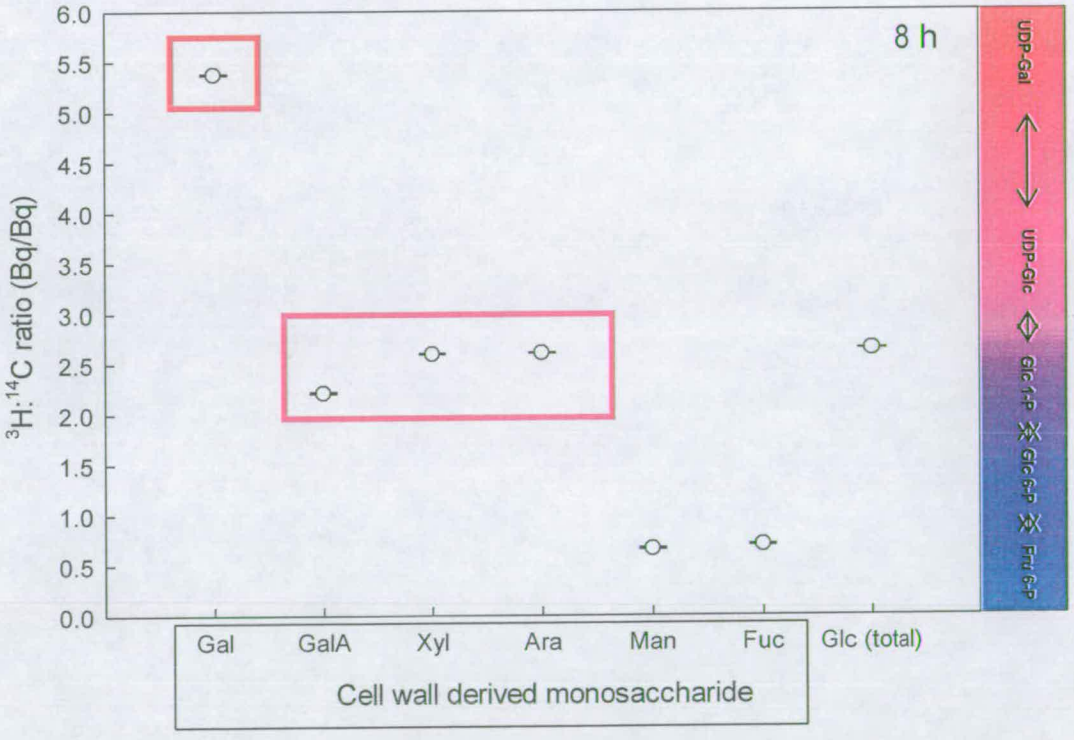

Figure 3.61 ^{3}H:^{14}C Ratios of monosaccharides purified from the AIR of *Arabidopsis* cell-suspension culture at 8 h

The colour gradient indicates the 'core' metabolites that each of the cell-wall monosaccharides may have stemmed from. The increased level of red in the colour gradient represents a high ^{3}H:^{14}C ratio as this is 'closer' to the ^{3}H source. An increased level of blue indicates a lower ^{3}H:^{14}C ratio as this is more 'distanced' from the ^{3}H source. The boxes that surround the compounds isolated from the AIR indicate the area of the colour gradient (and hence 'core' metabolite) that the isolated compounds are most likely to stem from. The error bars are unique to each time point and relate to the method used to detect the radiolabelled isotopes

4. Discussion

Attempts have been made to determine the predominant pathway of sugar nucleotide synthesis with an approach that involves the provision of a precursor in excess concentrations. Examples of this include the work carried out by Roberts *et al.* (1973) and Maiti *et al.* (1978) who, in order to study the contribution of the *myo*-inositol pathway to cell wall uronic acid residue synthesis, provided excess exogenous levels of *myo*-inositol to the plant material they worked with (section 1.2.1.2). The limited ability of the plants to convert [^{14}C]Glc into ^{14}C-labelled uronic acid residues was an indication to the researchers that the increase in the intracellular *myo*-inositol pool no longer required the conversion of [^{14}C]Glc to *myo*-inositol. The difficulty in the interpretation of such results, with respect to the predominating pathway of UDP-GlcA, is that the provision of a precursor in excess concentrations may only serve as a 'scavenger' pathway. The excess concentrations of *myo*-inositol may have stimulated the *myo*-inositol pathway that would otherwise not have been in operation. This argument also holds when the intracellular concentration of a precursor in a pathway is altered. Biffen *et al.* (1991) raised or lowered the intracellular concentration of *myo*-inositol in soybean cells by the provision of exogenous inositol or dGlc, respectively (section 1.2.1.2). Biffen *et al.* (1991) determined that despite the alteration in intracellular *myo*-inositol concentration the final amount of pectin uronic acid residues remained unchanged. In this case it could be argued that if the UDP-Glc dehydrogenase pathway predominated in pectin uronic acid residue formation the alteration of the cellular *myo*-inositol concentration would be irrelevant to plant cell wall synthesis. However, it could equally be argued

that the UDP-Glc dehydrogenase pathway became enhanced/repressed to compensate for the excess/limited concentration of *myo*-inositol.

More recently, with the advent of molecular genetics, researchers have tended to favour mutant studies to determine the importance of certain genes in each of the pathways. Both Wilcox *et al.* (2000) and Hitz *et al.* (2002) isolated viable soybean seeds with greatly reduced levels of phytate by mutating a gene involved in the *myo*-inositol pathway (section 1.2.1.2). The involvement of the *myo*-inositol pathway in seed development and ultimately cell wall synthesis may not be realised in these mutant studies. Indeed, it is not possible to distinguish whether the alternative UDP-Glc dehydrogenase pathway was the predominant pathway or whether the UDP-Glc dehydrogense pathway was stimulated due to the restriction in the *myo*-inositol pathway.

Kärkönen *et al.* (2005b, In press) studied maize plants that were homozygous for a mutation in one of the UDP-Glc dehydrogenase genes (*UDPGDH-A1*) (section 1.2.1.1.2). The *udpgdh-A1* homozygote had a 35 – 45% reduction of Ara:Gal and Xyl:Gal ratios in non-cellulosic polysaccharides in comparison to the wild-type controls. Although this showed that *UDPGDH-A1* contributed to a large portion of the cell wall pentose residues the UDP-Glc dehydrogenase is not necessarily the predominant pathway. Indeed, the majority of cell wall pentose residues are still formed either by another isoenzyme or by the alternative pathway.

The main approaches that have been used to study competing pathways are flawed. Indeed, as more than one pathway is known to exist in the formation of UDP-GalA, UDP-GlcA and GDP-Man, the alteration of 'normal' cellular conditions could stimulate a pathway that would otherwise not be in operation. In this project

the study of 'normal' biochemical pathways was of key importance. To study cell metabolism under 'normal' conditions the amount of [1-^{3}H]Gal and [U-^{14}C]Glc or [U-^{14}C]Fru fed to the cells was kept to trace concentrations. As exogenously supplied Gal has been reported to be toxic to plants in concentrations of 1–10 mM (Hughes *et al.*, 1974; Loughman *et al.*, 1989; Maretzki *et al.*, 1978), the [^{3}H]Gal concentration utilised in the main experiments was never higher than 51 μM. This meant that Gal was unlikely to be toxic to the *Arabidopsis* cell-suspension culture. It was also important to limit the exogenously supplied [^{3}H]Gal concentration so that all of the ^{3}H was taken up in a short period of time and incorporated into end products. For this reason the [^{3}H]Gal concentration fed to the cells was less than the apparent K_m for Gal of 240 μM.

As the experimental strategy relied heavily on the final ^{3}H:^{14}C ratio of cellular metabolites or AIR-derived monosaccharides, it was important that ^{3}H was not lost as a result of any of the treatments used in their biosynthesis, extraction or purification. (^{3}H,^{14}C)-Labelled monosaccharides exposed to 2 M TFA for up to 4 h were found to maintain their isotope ratio despite their degradation. It was also thought that ^{3}H could be lost from C1 when a transglycosylase acted upon a sugar nucleotide. This was tested by the administration of [1-^{3}H, 1-^{14}C]Ara with a known ^{3}H:^{14}C ratio to a *Arabidopsis* cells. It was predicted that if transglycosylation resulted in a loss of ^{3}H at C1, cell wall derived Ara and Xyl would have a lower ^{3}H:^{14}C ratio than the originally fed radiolabelled Ara stock solution. The results show that transglycosylation does not result in the loss of ^{3}H at C1 (Fig. 3.12).

For the main experimental approach of this project to work, it was necessary to form an isotope gradient amongst the 'core' metabolites. The bulk non-

radiolabelled carbon source that maintained the *Arabidopsis* cell-suspension culture was glycerol. This was proposed to maintain the main metabolic flux of the 'core' metabolites in the direction of Fru 6-P to UDP-Gal. The administration of trace amounts of [1-^{3}H]Gal and [U-^{14}C]Fru or [U-^{14}C]Glc, at opposite ends of the 'core' metabolite pathway, was predicted to form a gradient of ^{3}H:^{14}C ratios amongst the 'core' metabolites. The isotope ratio gradient amongst the 'core' metabolites is very clear (Fig. 3.58). Fig. 3.58 shows that the more metabolically 'distanced' a 'core' metabolite is from the ^{3}H source, the lower the maximum ^{3}H:^{14}C ratio that 'core' metabolite obtains.

The ^{3}H:^{14}C ratios of the isolated cell-wall monosaccharides also give evidence of an isotope gradient. Fig. 3.22, Fig. 3.38 and Fig. 3.61 show a similar trend in the distribution pattern of the cell-wall monosaccharide isotope ratios. Indeed, Gal thought to be derived from UDP-Gal, has the highest isotope ratio in comparison to the other cell-wall derived monosaccharides. This was found to be independent of whether the Gal isotope ratio was obtained from TFA-hydrolysed AIR or from xyloglucan oligosaccharides (Fig 3.38). UDP-Gal is expected to have the highest isotope ratio as it is the 'core' metabolite that is metabolically closest to the ^{3}H source. Cell wall-derived monosaccharides such as Man and Fuc are known to be formed from a 'core' metabolite that is more 'distanced' from the ^{3}H source than Gal and, as would be expected if an isotope gradient existed, have a much lower ^{3}H:^{14}C ratio than Gal (Fig. 3.22, Fig. 3.61). It is clear that a steep isotope gradient is formed with the experimental outline despite the few metabolic steps involved in the 'core' metabolites.

Both the ^{3}H:^{14}C ratio kinetics of the 'core' metabolites and the isotope ratios of cell wall-derived monosaccharides indicate that a ^{3}H:^{14}C gradient is established in the 'core' metabolites and validate the experimental approach that was utilised.

4.1 Predominant pathway involved in UDP-GalA and UDP-GlcA synthesis

The predominant pathway involved in UDP-GalA and UDP-GlcA synthesis is debated. In a textbook chapter written by Carpita *et al.* (2001) it is mentioned that UDP-GalA may be formed directly from UDP-Gal. If UDP-GalA was not predominantly formed from UDP-Gal it could be formed directly from UDP-GlcA. However, UDP-GlcA itself can be directly formed from UDP-Glc by UDP-Glc dehydrogenase or by the *myo*-inositol pathway from Glc 6-P (Fig. 1.2). In 1979 two separate papers were published on the formation of UDP-GlcA in carrot cell-suspension cultures (Verma *et al.* 1979; Asamizu *et al.* 1979) (section 1.2.1.2). Verma *et al.* (1979) concluded that carrot cell-suspension cultures predominantly formed UDP-GlcA from UDP-Glc. In contrast to these results Asamizu *et al.* (1979) concluded that the *myo*-inositol pathway predominantly formed UDP-GlcA.

4.1.1 AIR-derived ^{3}H:^{14}C ratios

In this project all of the potential pathways that could form UDP-GalA and UDP-GlcA were investigated in a single experimental approach. Initially cell-suspension cultures were fed [1-^{3}H]Gal or [U-^{14}C]Glc (section 3.2.1). The ^{3}H-labelled and ^{14}C-labelled AIRs were hydrolysed and the hydrolysates combined in a ^{3}H:^{14}C (cpm/cpm) ratio of 5:1. The isotope ratios of the monosaccharides in the hydrolysate were determined (Fig. 3.22). In the second experiment this was repeated but an additional set of samples were fed [1-^{3}H]Gal and [U-^{14}C]Fru (section 3.2.2). The

administration of [U-^{14}C]Fru was expected to extend the 'core' metabolite pathway by one additional metabolite. The second main experiment involved the combination of undigested ^{3}H-labelled AIR and undigested ^{14}C-labelled AIR, each with a known total quantity of radioactivity. Five different treatments were employed to release the AIR-derived monosaccharides from different polysaccharide sources. The isotope ratio of each of the monosaccharides was subsequently determined (Fig. 3.38). The third final main experiment (section 3.2.3) analysed the isotope ratios of monosaccharides from AIR TFA-hydrolysate over a time course of 8 h (Fig 3.60, Fig. 3.61).

The ^{3}H:^{14}C ratio of GalA is clearly lower than that of Gal (Fig. 3.22, Fig. 3.38, Fig. 3.61). This suggests that the parent 'core' metabolite of UDP-GalA is more metabolically 'distanced' from the source of ^{3}H than UDP-Gal, which is known to be the parent 'core' metabolite of Gal (Fig. 4.1 A). If UDP-GalA is not formed from UDP-Gal the direct precursor of UDP-GalA would be UDP-GlcA (Fig. 4.1 B). It is known that UDP-GlcA may give rise to UDP-GalA, UDP-Api, UDP-Xyl and, by epimerisation of UDP-Xyl, UDP-Ara (Fig. 1.2). The AIR-derived monosaccharides GalA, Ara, Xyl (Fig. 3.38, Fig. 3.61) and Api (Fig. 3.22) all share similar isotope ratios. This suggests that they all share a common parent 'core' metabolite (Fig. 4.1 C). The identity of this parent 'core' metabolite is suggested by the ^{3}H:^{14}C ratio values of Man, Fuc and Rha. GDP-Man and GDP-Fuc may only arise from the parent 'core' metabolites Glc 1-P or Glc 6-P. If UDP-GalA, GDP-Man and GDP-Fuc arose from either Glc 1-P or Glc 6-P, the isotope ratio of GalA would be less than or equal to the isotope ratios of Man and Fuc (Fig. 4.1, D1). As GalA has a higher isotope ratio than Man and Fuc and a lower ratio than Gal, this

suggests the predominant parent 'core' metabolite that gave rise to UDP-GalA was UDP-Glc (Fig. 4.1 D2). Rha residues of cell wall polysaccharides are thought to arise from UDP-Rha. The parent 'core' metabolite that UDP-Rha stems from is UDP-Glc. Rha was determined to have a similar isotope ratio value to GalA, Ara, Xyl (Fig. 3.38) and Api (Fig. 3.22). This suggests that UDP-Rha, UDP-GalA, UDP-Ara, UDP-Api and UDP-Xyl all share a common parent 'core' metabolite — UDP-Glc (Fig. 4.1 E).

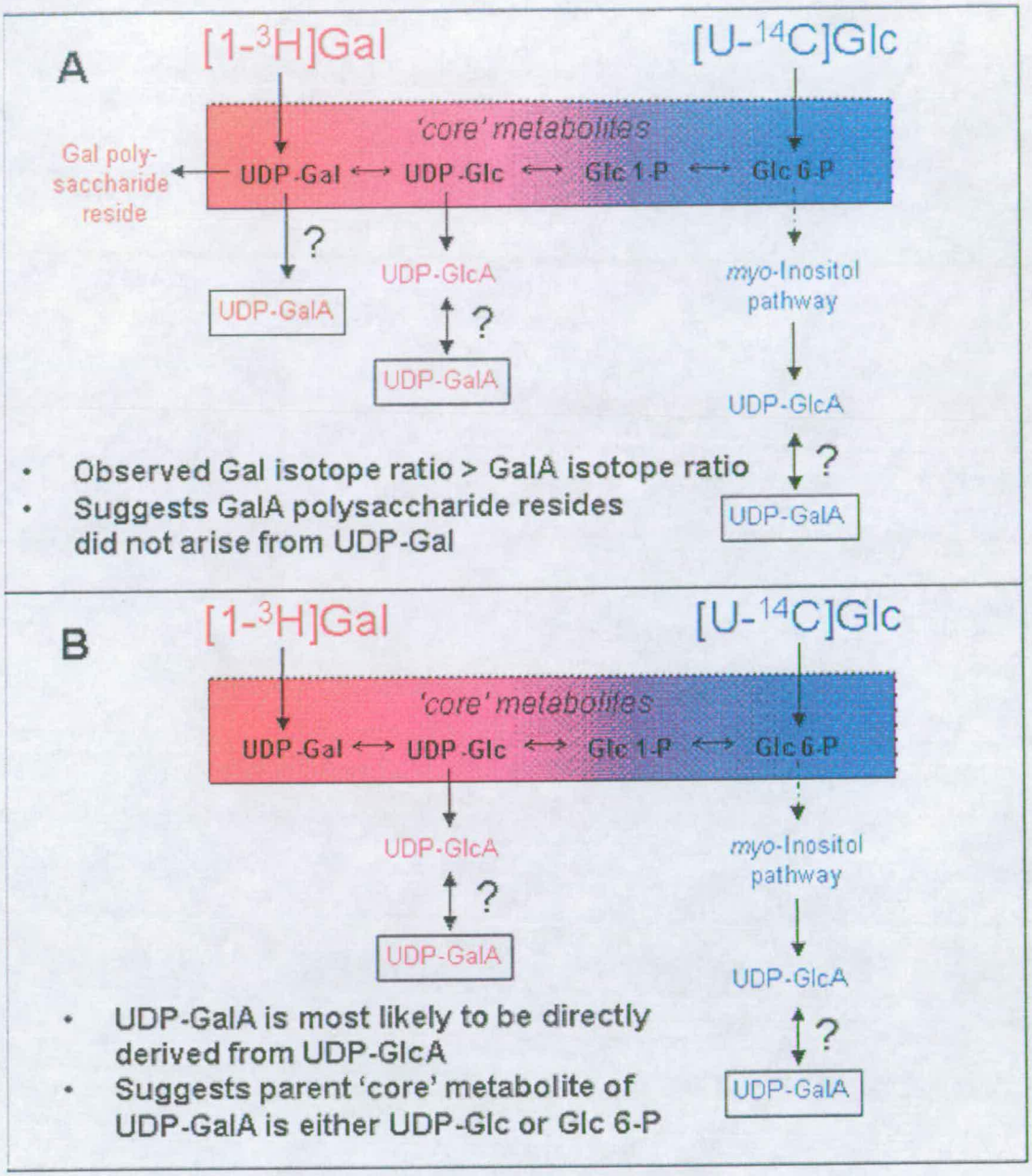

Figure 4.1 Determination of the parent 'core' metabolite of UDP-Gal in relation to the isotope ratio values obtained from AIR-derived monosaccharides

The results discussed in boxes A – E relate to the isotope ratio values shown in Fig. 3.22. A – D relate to to Fig. 3.61 and A – C relate to Fig 3.38. The colour gradient indicates the 'core' metabolites that each of the cell-wall monosaccharides may have stemmed from. The increased level of red in the colour gradient represents a high $^{3}H:^{14}C$ ratio as this is 'closer' to the ^{3}H source. An increased level of blue indicates a lower $^{3}H:^{14}C$ ratio as this is more 'distanced' from the ^{3}H source.

Continued overleaf

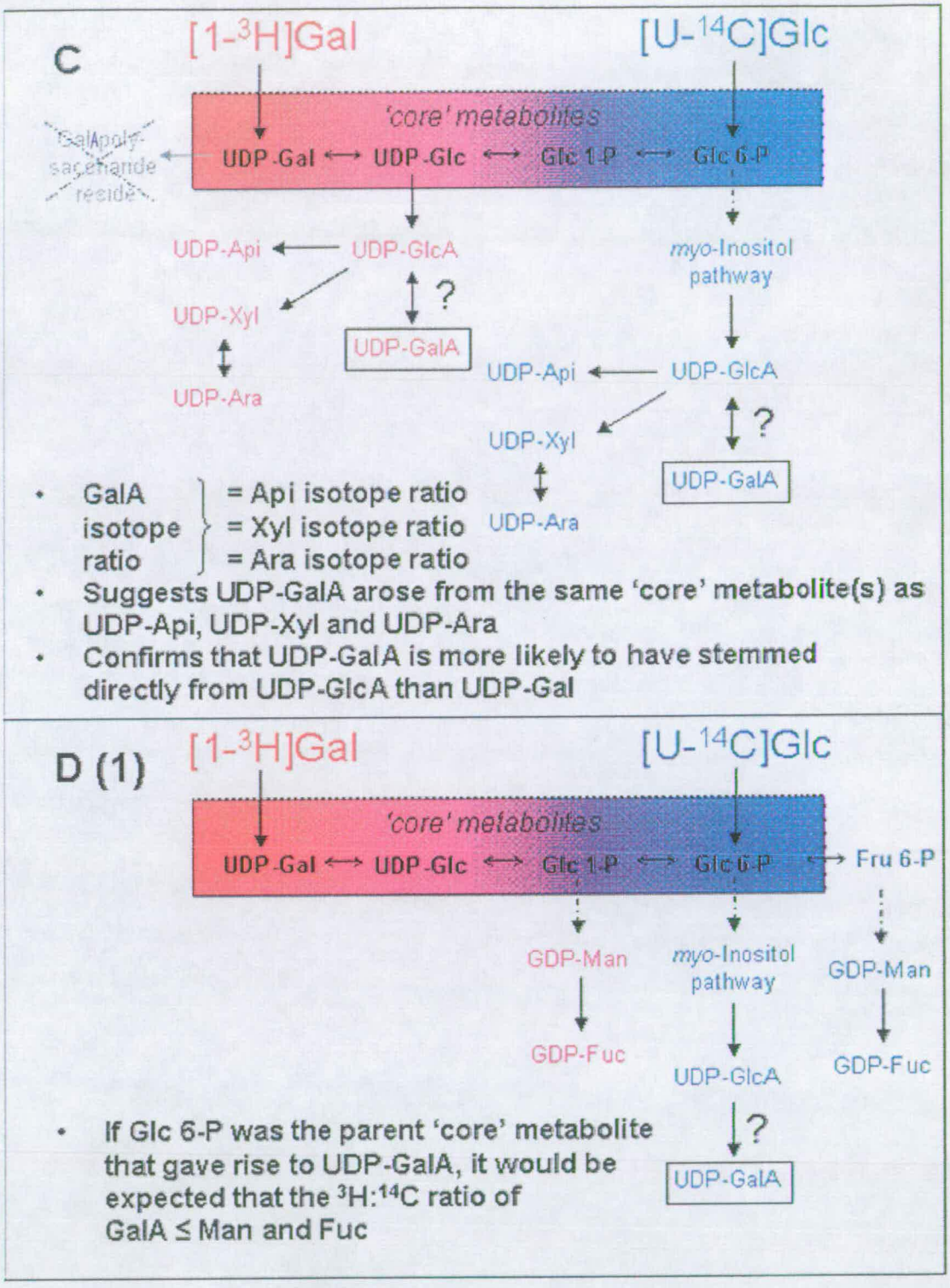

Figure 4.1 Continued

Continued overleaf

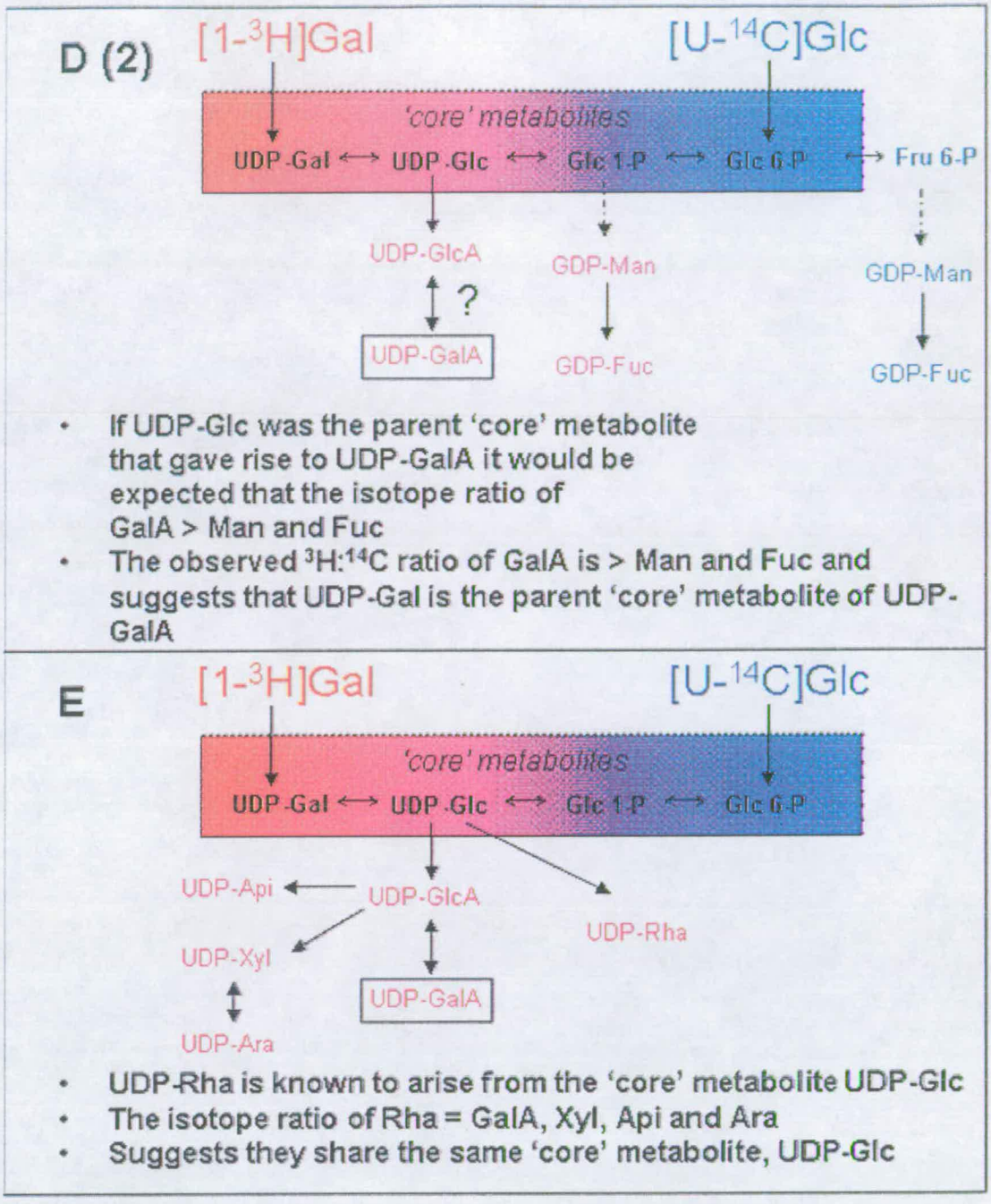

Figure 4.1 Continued

4.1.2 ^{3}H:^{14}C ratios of intermediary metabolites

The ^{3}H:^{14}C ratio kinetics of 'GalA from UDP-GalA' and the potential 'core' metabolites that UDP-GalA may stem from were compared (Fig. 3.58 B). The results showed that the 'GalA from UDP-GalA' isotope ratio values, over time, closely matched the parent 'core' metabolite isotope ratio values of UDP-Glc and not UDP-Gal or Glc 6-P. The isotope ratio kinetics of 'GlcA from UDP-GlcA', 'Xyl from UDP-Xyl' and 'Ara from UDP-Ara' were also examined against the potential 'core' metabolites that they may stem from. The results show that the isotope ratio kinetics of UDP-GlcA, UDP-Xyl and UDP-Ara are very distinct from the isotope ratio kinetics of Glc 6-P but that they are similar to the isotope ratio kinetics of UDP-Glc. The ^{3}H:^{14}C ratios of the intermediary metabolites strongly suggest that UDP-GalA, UDP-GlcA, UDP-Ara and UDP-Xyl predominantly stem from the 'core' metabolite UDP-Glc. The isolation of inositol from the ethanol-soluble fraction would have enabled a direct comparison of ^{3}H:^{14}C ratio kinetics of inositol and the UDP-GlcA that may stem from the *myo*-inositol pathway. Unfortunately the [U-^{14}C]Fru that was fed to the cells was contaminated with [^{14}C]inositol (Fig. 3.54). The ^{3}H-labelling kinetics of inositol indicates that there is a greater lag-time for inositol than 'GlcA from UDP-GlcA' (Fig. 3.57). As a precursor must become radiolabelled before its product this indicates that the ^{3}H that UDP-GlcA acquires is not predominantly from the *myo*-inositol pathway.

4.1.3 Summary of the predominant pathway involved in UDP-GalA and UDP-GlcA synthesis

It is clear from the AIR-derived ^{3}H:^{14}C ratios (Fig. 3.22, Fig. 3.38, Fig. 3.61) and the kinetics of the ^{3}H:^{14}C ratios of the intermediary metabolites (Fig. 3.57) that the

predominant pathway of UDP-GalA synthesis is not via dehydrogenase action on UDP-Gal. This pathway was mentioned by Carpita *et al.* (2001) and, as shown by the results of this project, is not a predominant pathway in UDP-GalA synthesis. In *Arabidopsis* cell-suspension culture the predominant pathway of UDP-GalA and UDP-GlcA synthesis occurs via the UDP-Glc dehydrogenase pathway and not the *myo*-inositol pathway. The results obtained in this project disagree with those presented by Asamizu *et al.* (1979) (section 1.2.1.2) where carrot cell suspension cultures, provided with 0.6 mM *myo*-inositol, were fed either [U-^{14}C]Glc or *myo*-[^{3}H]inositol. The specific activity of the ^{14}C-labelled and ^{3}H-labelled uronic acid residues was forty-two times lower than the originally supplied [U-^{14}C]Glc. The specific activity of the ^{3}H-labelled uronic acid residues was eighteen times lower than the originally supplied *myo*-[^{3}H]inositol. Although the authors claim that this was evidence that the *myo*-inositol pathway predominated in cell wall uronic acid residues, the provision of 0.6 mM *myo*-inositol may have stimulated the *myo*-inositol pathway that would otherwise not be in operation.

Verma *et al.* (1979) fed the carrot cell-suspension cultures *myo*-[^{3}H]inositol, which was expected to feed into the *myo*-inositol pathway alone, and [^{14}C]Glc that could enter either of the competing pathways (section 1.2.1.2). The cellular *myo*-inositol ^{3}H:^{14}C ratio was > 10-fold higher than that of cell-wall Ara, Xyl and GalA residues and led the researchers to conclude that carrot cell-suspension cultures predominantly formed UDP-GlcA from UDP-Glc. In contrast to the claims made by Asamizu *et al.* (1979), and in agreement with this project, Verma *et al.* (1979) concluded that the UDP-GlcA was predominantly formed by the UDP-Glc dehydrogenase pathway. The use of radiolabelled tracers by Verma *et al.* (1979)

enabled the researchers to study 'normal' cellular metabolism without the potential to enhance an alternative pathway. Although the results presented in this project agree with Verma *et al.* (1979) a direct comparison between *Arabidopsis* metabolism and carrot metabolism may not be made as each may utilise a different pathway for plant cell wall residue formation.

The results of this project strongly disagree with the conclusions formed by Kanter *et al.* (2005) who isolated *Arabidopsis* plants with T-DNA insertion lines in each of three *myo*-inositol oxygenase isoforms. The researchers claimed that their results showed 'strong evidence' that the gene that had been mutated in each case contributed to plant cell wall residues. However, each of the mutants had wild-type phenotypes. As discussed in section 1.2.1.2, the data presented by Kanter *et al.* (2005) suggest that the pentoses and uronic acids involved in plant cell wall residue synthesis in the mutant plants are either formed by other *myo*-inositol oxygenase isoforms and/or by the UDP-Glc dehydrogenase pathway. The results presented here suggest that the wild-type plant cell wall composition witnessed in the mutants formed by Kanter *et al.* (2005) was mainly attributable to the UDP-Glc dehydrogenase pathway that normally predominates in cell wall residue precursors. However, this assumes that the cell wall synthesis of *Arabidopsis* cell-suspension culture is similar to that of *Arabidopsis* plants.

4.2 Predominant pathway involved in GDP-Man synthesis

4.2.1 AIR-derived ^{3}H:^{14}C ratios

Radiolabelled Man and Fuc could not be detected in the second main experiment (section 3.2.2) owing to the limited amount of radioactivity fed to the cells. The isolation of AIR-derived Man was achieved in the first (section 3.2.1) and final (section 3.2.3) main experiments where [U-^{14}C]Glc and [U-^{14}C]Fru, respectively, were fed to the cells. Of all the obtained AIR-derived monosaccharides, Man and Fuc had the lowest ^{3}H:^{14}C ratio. GDP-Man may arise from the 'core' metabolites Glc 1-P or Glc 6-P (when cells were fed [U-^{14}C]Glc) or from Glc 1-P or Fru 6-P (when cells were fed [U-^{14}C]Fru) (Fig. 4.2 A). UDP-GalA, UDP-Xyl, UDP-Ara and UDP-Api may stem from the 'core' metabolites UDP-Glc or Glc 1-P and, in the case of UDP-GalA, UDP-Gal. Because the isotope ratios of GalA, Xyl, Ara, Api are higher than the ^{3}H:^{14}C ratios of Man and Fuc, the parent 'core' metabolite of Man and Fuc cannot be determined on the sole basis of the AIR ^{3}H:^{14}C ratios alone (Fig. 4.2 A). One potential method by which to determine the parent 'core' metabolite that Man and Fuc predominantly arose from, based on the AIR ^{3}H:^{14}C ratios only, would be to isolate a compound from an end product that was known to stem from Glc 6-P. A compound that is known to arise from the 'core' metabolite Glc 6-P is inositol. The isolation of inositol from the end product phosphatidylinositol could determine the parent 'core' metabolite that both Man and Fuc stemmed from (Fig. 4.2 B).

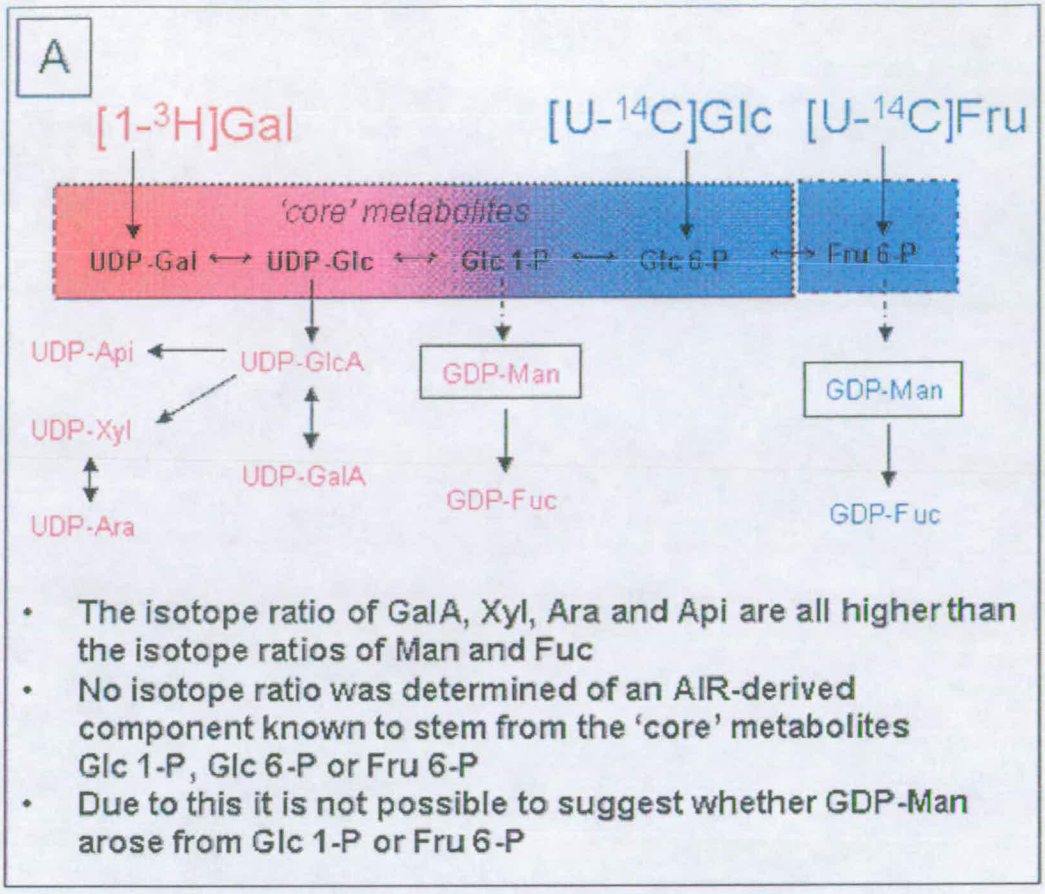

Figure 4.2 Inability to determine the parent 'core' metabolite that GDP-Man stemmed from with AIR-derived isotope ratios alone and potential method to solve this

The isotope ratios of AIR-derived Man and Fuc could not be linked to the parent 'core' metabolite that they predominantly stemmed from (**A**). A potential method of to determine this would be to isolate inositol from phosphatidylinositol (**B**). The ^{3}H:^{14}C ratio kinetics of the intermediary metabolites and the ^{3}H:^{14}C ratio of the AIR-derived monosaccharides indicated that the parent 'core' metabolite of GDP-Man is Fru 6-P (**C**). The colour gradient indicates the 'core' metabolites that each of the cell-wall monosaccharides may have stemmed from. The increased level of red in the colour gradient represents a high ^{3}H:^{14}C ratio as this is 'closer' to the ^{3}H source. An increased level of blue indicates a lower ^{3}H:^{14}C ratio as this is more 'distanced' from the ^{3}H source.
Continued overleaf

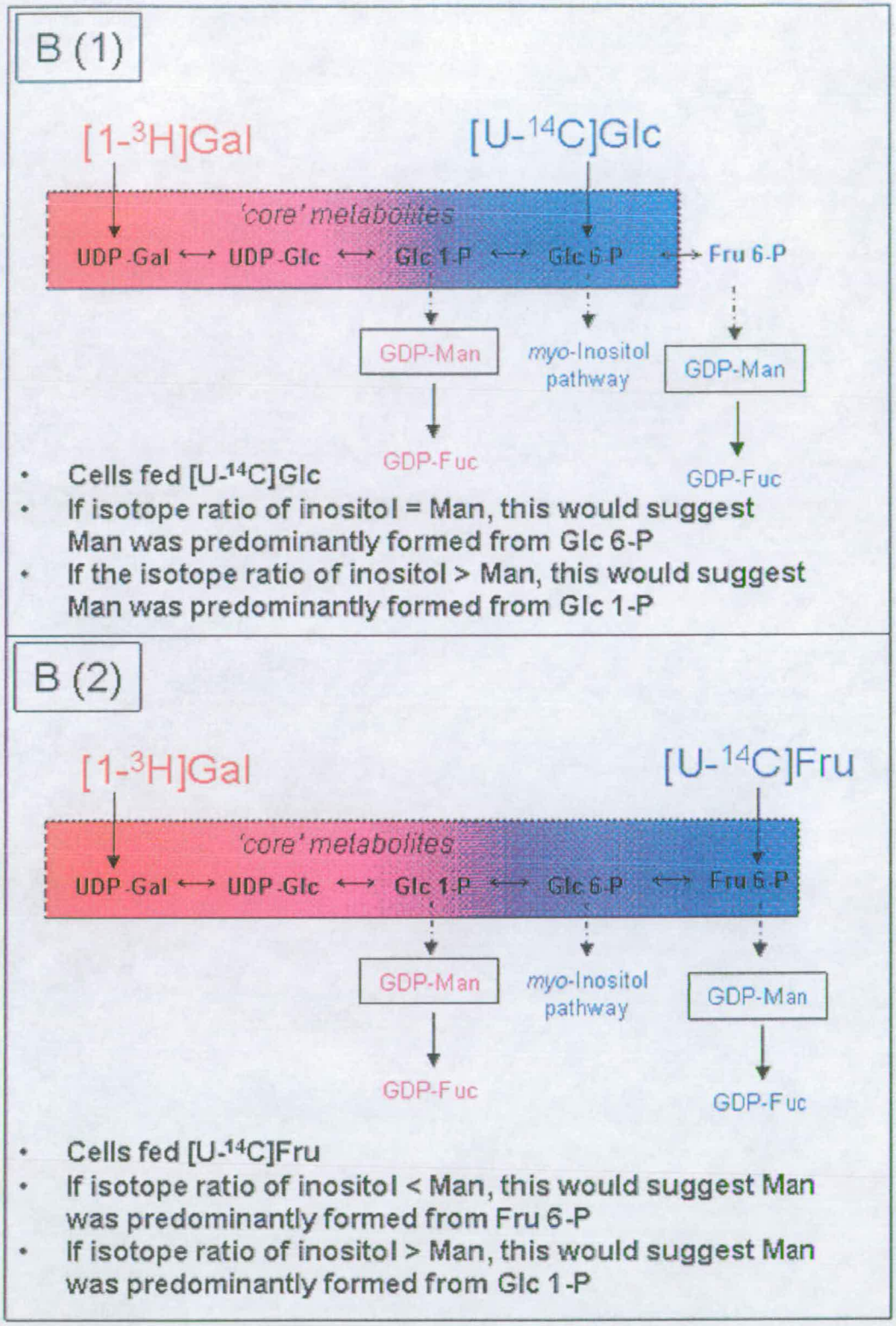

Figure 4.2 Continued

Continued overleaf

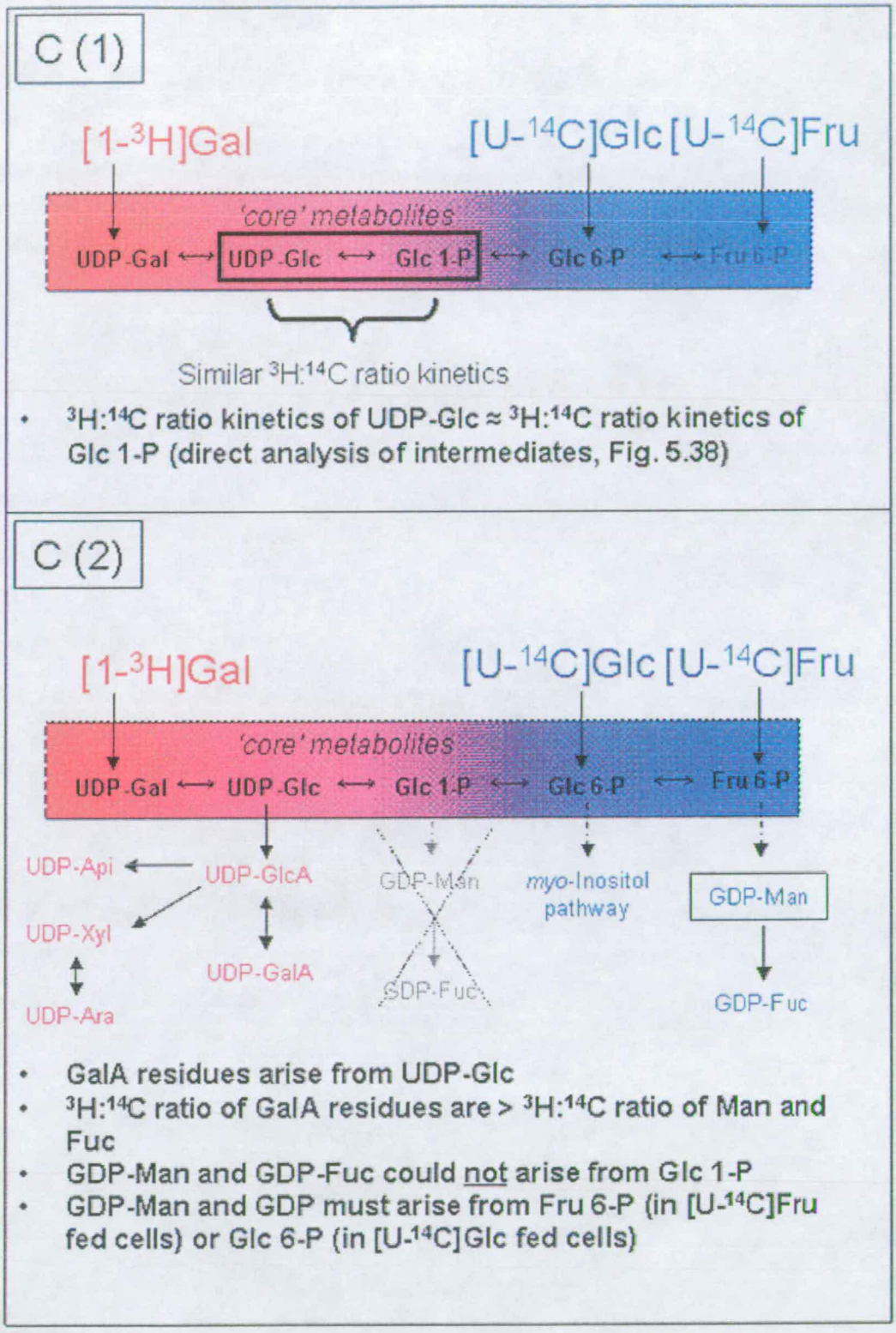

Figure 4.2 Continued

4.2.2 ^{3}H:^{14}C ratios of intermediary metabolites

The isotope ratios of Man and Fuc are difficult to interpret owing to the lack of reliable results in the first ~15 min of the time course. The isotope ratio value of GDP-Man, remains at 1 (Bq/Bq) from 15 min onwards. This value is far lower than the potential 'core' metabolites that may give rise to GDP-Man. This suggests that either a loss of ^{3}H has occurred or, that an unknown pathway from a more metabolically distanced 'core' metabolite is in operation.

4.2.3 Summary of the predominant pathway involved in GDP-Man synthesis

It is known that the ^{3}H:^{14}C ratio kinetics of UDP-Glc are very similar to Glc 1-P by direct analysis of the intermediates in the time-course experiment (Fig. 3.58, Fig. 4.2 C1). It is observed that the ^{3}H:^{14}C ratio for cell wall-derived GalA is greater than the ratios for Man and Fuc. As cell wall-derived GalA residues are known to predominantly arise from the parent 'core' metabolite UDP-Glc (section 4.1.3), Man and Fuc do not stem from the 'core' metabolite Glc 1-P. The parent 'core' metabolite of GDP-Man must be Fru 6-P (in [U-^{14}C]Fru fed cells) or Glc 6-P (in [U-^{14}C]Glc fed cells) (Fig. 4.2 C2).

Despite the variety of Man-containing plant polysaccharides there has been little investigation into the predominant pathway that forms GDP-Man. The results of this project suggest that GDP-Man is predominantly synthesised by the GDP-Man pyrophosphorylase pathway. Publications on the alternative pathway in plants that involves GDP-Man 2-epimerase are sparse. The addition of GDP-[^{14}C]Man to particulate fractions of mung bean seedlings (Elbein *et al.*, 1969) or *P. sylvestris* membrane preparations (Dalessandro *et al.*, 1986) resulted in the formation of ^{14}C-

labelled Glc polymer residues thought to have arisen from glucomannan. These results indicate that GDP-Man 2-epimerase may exist in mung bean seedlings and *P. sylvestris* but they do not indicate that this is the predominant method of GDP-Man synthesis.

Attempts made to assess the importance of GDP-Man pyrophosphorylase in tomato plants involved mutant studies (Keller *et al.*, 1999, section 1.2.3.2). Transformants, selected on the basis of reduced GDP-Man pyrophosphorylase activity, had 41–72% of the GDP-Man pyrophosphorylase activity of wild-type plants. In comparison to wild-type plants the transformants grown on soil started to deteriorate after 10 weeks and sections of the plant that corresponded to the strongest reduction in GDP-Man pyrophosphorylase were dead by 3 months. It was determined that the Man content of the transformant plant cell walls was significantly reduced to 30–50% of the levels found in the leaves of wild-type plants. This indicated that GDP-Man pyrophosphorylase contributed to the Man residues of tomato plants. However, it is clear that 50–70% of the Man residues were still able to be synthesised either by an alternative GDP-Man pyrophosphorylase isoform or by the epimerization of GDP-Man. This suggests that GDP-Man pyrophosphorylase may not necessarily predominate in GDP-Man synthesis.

The experiments conducted in this project were able to assess both competing pathways of GDP-Man synthesis. The predominant pathway of GDP-Man synthesis was found not to occur by the action of GDP-Man 2-epimerase but by the GDP-Man pyrophosphorylase pathway.

4.3 Cellulosic precursor — UDP-Glc or GDP-Glc

Although generally assumed there has, to date, been no conclusive evidence to demonstrate that cellulose is formed from UDP-Glc. The second main experiment (section 3.2.2) attempted to incorporate experimental procedures that would enable the discrimination between the use of UDP-Glc and GDP-Glc as the cellulosic precursor. AIR was digested with cellulase. When cells were fed [U-^{14}C]Glc the ^{3}H:^{14}C ratio value of the Glc monosaccharide obtained from the digest was similar to those of GalA, Xyl, Ara, Rha and Glc derived from other polysaccharide sources (total, *ex* starch, *ex* xyloglucan). This suggested that the Glc from cellulose and the other investigated polysaccharide sources had the same 'core' metabolite as GalA, Xyl, Ara and Rha, which was indicated to be UDP-Glc in this project. When cells were fed [U-^{14}C]Fru a slightly different trend emerged. The isotope ratios of Glc (*ex* xyloglucan) still match those of GalA, Xyl, Ara and Rha. However, the other Glc (total, *ex* starch, *ex* cellulose) isotope ratios no longer match the isotope ratios of GalA, Xyl, Ara and Rha. No explanation can be offered for this anomaly.

If this experiment were repeated another method that could be used to obtain cellulosic Glc residues would be to digest the AIR TFA-insoluble fraction with Driselase. The Glc residues obtained by the digest could be purified and assayed as cellulosic Glc. This would be an alternative method to obtain a ^{3}H:^{14}C ratio of Glc known to arise from cellulose that could be compared to the Glc that was obtained by a cellulase digest. If the enzyme preparation is able to digest Glc containing polymers, other than cellulose, the final ^{3}H:^{14}C ratio may be altered. The use of Driselase on the AIR TFA-insoluble fraction (cellulose) eliminates this potential problem.

The potential precursors of cellulose are GDP-Glc (formed from Glc 1-P) and UDP-Glc. The ^{3}H:^{14}C ratio kinetics of 'Glc from UDP-Glc' and Glc 1-P are very similar. Owing to this the experimental approach (section 1.5) may not be suitable to determine the precursor of cellulose because the ^{3}H:^{14}C ratios obtained by the cellulosic Glc residues may have a similar ratio whether they were derived from UDP-Glc or GDP-Glc.

4.4 Predominant pathway of Rib utilised for RNA synthesis

Rib was isolated from the AIR. Rib is not documented as a monosaccharide component of cell walls and is mainly thought to have arisen from RNA. A simple test to determine if the AIR-derived Rib arose from RNA would be to digest the AIR with an RNase and determine if alcohol-soluble Rib residues or alcohol-soluble compounds that contained Rib were contained in the sample. The undigested AIR could be hydrolysed with TFA and investigated to determine if any further Rib could be solubilised that was not from RNA.

Rib 5-P is thought to be a precursor of Rib from RNA. Fig. 3.23 illustrates the flow of ^{3}H from [1-^{3}H]Gal. It is generally assumed that Rib used to form RNA is derived from the pentose phosphate pathway (Horecker, 2002). If [1-^{3}H]Gal was metabolised to [1-^{3}H]Glc 6-P that then proceeded via 6-Phosphoglucono-δ-lactone from the ^{3}H from C1 would be lost (Fig. 3.23). However, as shown in Fig. 3.23, it is possible for Rib 5-P to become tritiated at C1 and C5 by alternative routes that stem from ^{3}H-labelled glyceraldehyde 3-P and Fru 6-P. As Rib 5-P is greatly 'distanced' from the 'core' metabolites and many metabolic steps are required to form [1,5-^{3}H]Rib 5-P from [1-^{3}H]Gal, it would be expected that Rib 5-P would have a lower or similar ^{3}H:^{14}C ratio as monosaccharides derived from Fru 6-P. It is therefore

surprising that the isotope ratio of Rib is repeatedly comparable to those of cell-wall derived GalA, Xyl, Ara and Api (Fig. 3.22, Fig. 3.38) and suggests they may share a common 'core' metabolite. One novel explanation for this might be that Xyl is acted on by an epimerase to form Rib (Fig. 4.3). An alternative explanation for the Rib

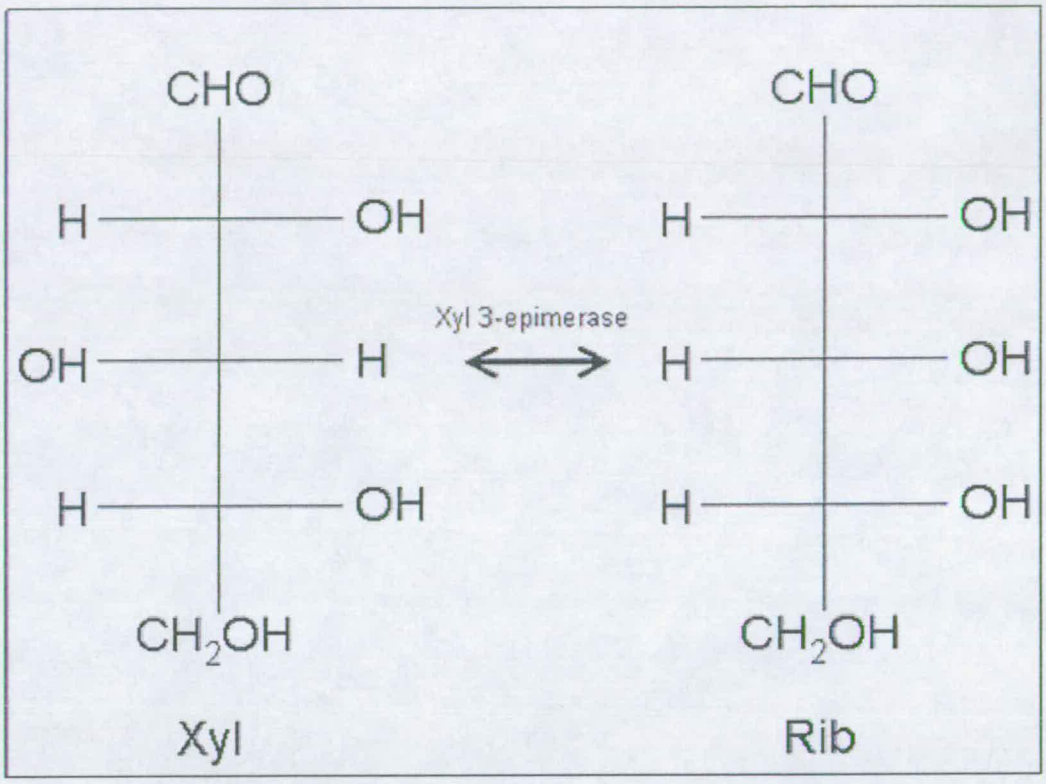

Figure 4.3 Potential formation of Rib from Xyl

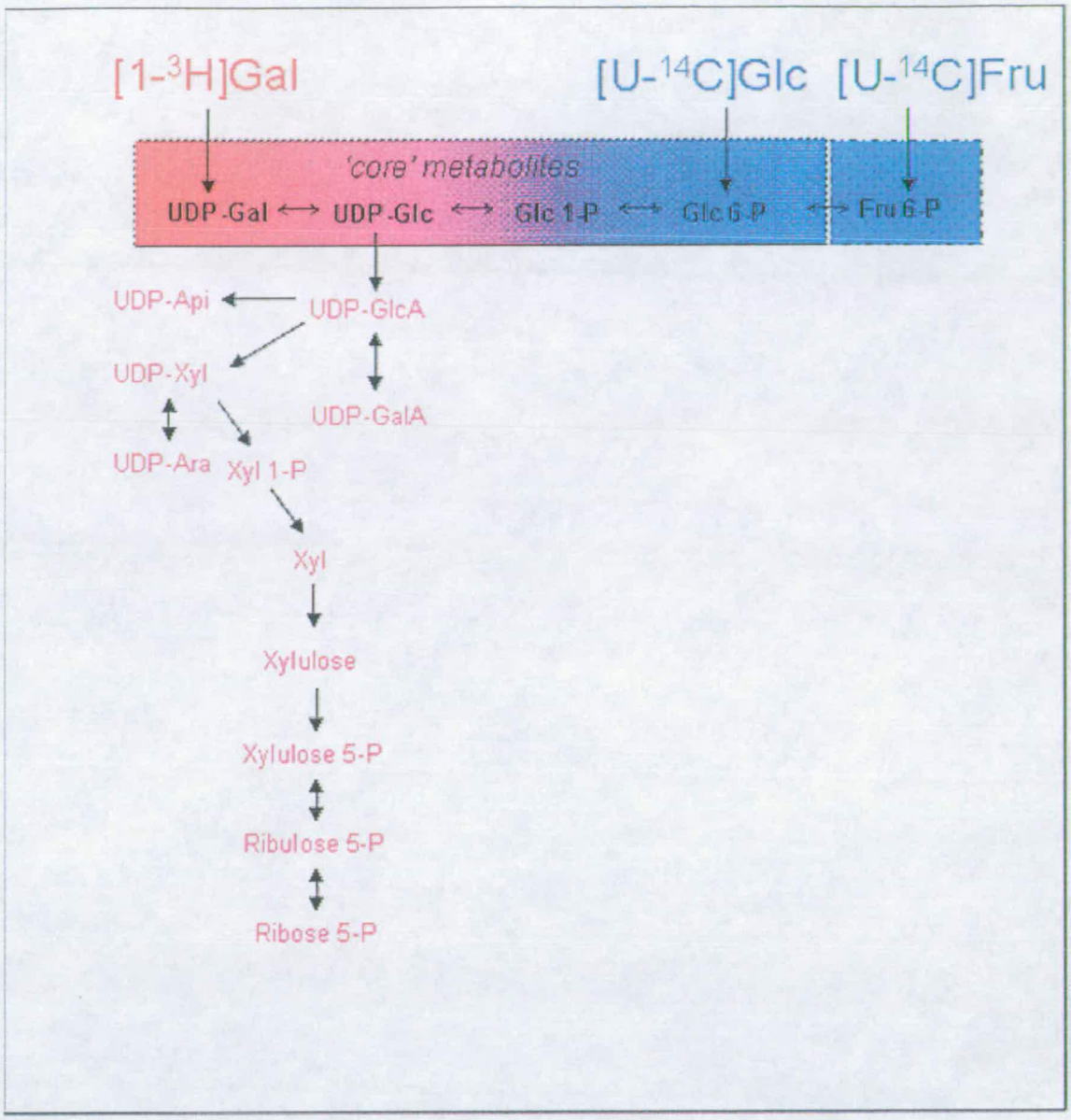

Figure 4.4 Suggested pathway to explain the similarity in the AIR-derived isotope ratios of Rib, Api, Xyl, Ara, GalA

If UDP-Xyl entered a pathway that formed the RNA precursor Rib 5-P the isotope ratios of AIR-derived Api, Xyl, Ara, GalA and Rib would be likely to be similar. As indicated in the figure, this would be independent of whether UDP-Xyl arose from the 'core' metabolite UDP-Glc or Glc 6-P and whether the ^{14}C-labelled source were [U-^{14}C]Fru or [U-^{14}C]Glc. The colour gradient indicates the 'core' metabolites that each of the cell-wall monosaccharides may have stemmed from. The increased level of red in the colour gradient represents a high ^{3}H:^{14}C ratio as this is 'closer' to the ^{3}H source. An increased level of blue indicates a lower ^{3}H:^{14}C ratio as this is more 'distanced' from the ^{3}H source.

isotope ratio involves the pathway shown in Fig. 4.4 where the formation of Rib 5-P may occur via UDP-Xyl. When the cell wall monosaccharides were isolated from *Arabidopsis* cell-suspension cultures fed [1-^{3}H, 1-^{14}C]Ara, the only cell wall monosaccharides expected were Ara and Xyl. This is because the Ara scavenger pathway is generally assumed to feed into a confined branch of the sugar nucleotide interconversion pathway (Fig. 3.10). It was therefore unexpected that radiolabelled Glc and Gal were obtained (Fig. 3.11). Their discovery suggested that UDP-Xyl might have been converted to Xyl that then entered the pentose phosphate pathway (Fig. 3.10). The similarity between the originally fed [1-^{3}H,1-^{14}C]Ara stock and the Xyl, Ara, Glc and Gal residues showed that ^{3}H was not lost in the formation of Glc and Gal (Fig. 3.12). As the Rib isotope ratios shown in Fig. 3.22 and Fig. 3.38 match the ratios of GalA, Xyl, Ara and Api, it seems likely that the predominating pathway of Rib 5-P formation stems from UDP-Xyl rather than via the pentose phosphate pathway in *Arabidopsis* cell-suspension cultures. This is because the Rib precursor shares the same 'core' metabolite as these monosaccharides and no ^{3}H is lost in the conversion of UDP-Xyl to Rib 5-P.

4.5 Starch synthesis

At present there are two proposals that relate to the pathway of starch synthesis (Fig. 4.5). The first 'classic' model suggests that ADP-Glc is formed in the plastid and utilised for starch synthesis (Neuhaus *et al.*, 2005). The second model proposes that ADP-Glc is formed in the cytosol, transported into the plastid, and utilised for starch synthesis (Baroja-Fernández *et al.*, 2005).

If starch synthesis occurred via the 'classic' model it would be expected that the ^{3}H:^{14}C ratio of 'Glc from ADP-Glc' would approximate that of Fru 6-P. This is

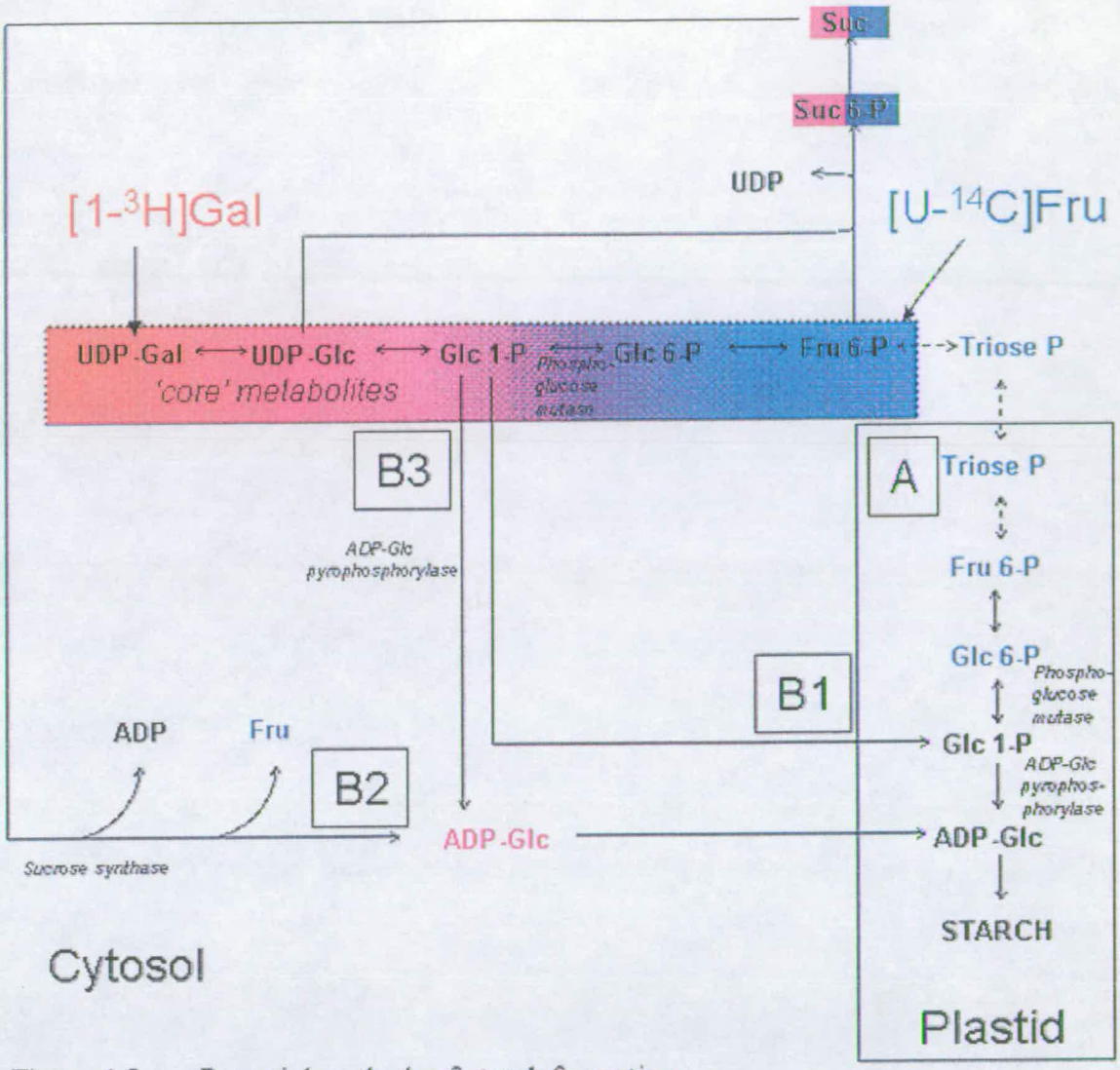

Figure 4.5 Potential methods of starch formation

(A) Starch could be formed by the 'classic' method from plastid-derived ADP-Glc. Alternative starch could be formed from **(B1)** Glc 1-P that is transported into the plastid or **(B2)** cytosolic ADP-Glc that is transported into the plastid from a sucrose precursor or **(B3)** a Glc 1-P precursor. The colour gradient indicates the 'core' metabolites that each of the cell-wall onosaccharides may have stemmed from. The increased level of red in the colour gradient represents a high ^{3}H:^{14}C ratio as this is 'closer' to the ^{3}H source. An increased level of blue indicates a lower ^{3}H:^{14}C ratio as this is more 'distanced' from the ^{3}H source.

because the 'core' metabolite Fru 6-P must first form triose phosphates that are transported into the plastid that act as the indirect precursor ADP-Glc (Fig. 4.5 A). However, the $^{3}H:^{14}C$ ratio values and kinetics of 'Glc from ADP-Glc' and its direct precursor Glc 1-P are similar and differ greatly from the $^{3}H:^{14}C$ ratio values and kinetics of Fru 6-P (Fig. 3.58 G). This suggests that either cytosolic Glc 1-P itself is predominantly transported into the plastid and converted into ADP-Glc (Fig. 4.5 B1) or that ADP-Glc is predominantly formed in the cytosol and transported into the plastid (Fig. 4.5 B2, B3). Starch biosynthesis in maize and barley in endosperm cells has been shown to occur by the import of ADP-Glc from the cytosol into the plastid (Denyer *et al.*, 1996). Baroja- Fernández *et al.* (2004) suggest that the biosynthesis of starch in potato leaves utilises ADP-Glc that is transported into the plastid from the cytosol. Indeed, the expression of bacterial ADP-Glc pyrophosphorylase in the cytosol of potato reduced the amount of starch in the leaves and tubers and reduced the concentration of ADP-Glc in the leaves. Baroja- Fernández *et al.* (2005) suggest that the formation of ADP-Glc may occur by a cytosolic ADP-Glc producing sucrose synthase (Fig. 4.5 B3). If this were the case the $^{3}H:^{14}C$ ratio kinetics of 'Glc from Suc' should match those of 'Glc from ADP-Glc'. Indeed, the results shown in Fig. 3.58 G show this to be the case. However, it is not possible to determine if the starch precursor is cytosolic Glc 1-P that is transported into the plastids (Fig. 4.5 B1) or whether cytosolic ADP-Glc (forrmed from Suc, Fig. 4.5 B or Glc 1-P, Fig. 4.5 B) is the starch precursor as the 'core' metabolites UDP-Glc (initially used to form the Glc residue of Suc) and Glc 1-P have similar $^{3}H:^{14}C$ ratio kinetics. Arguments against the work carried out by Baroja- Fernández *et al.* (2005) suggest that *Arabidopsis* mutants that lack plastidial phophoglucose mutase or plastidial ADP-Glc

pyrophosphorylase lack starch in the leaf tissue (Neuhaus *et al.*, 2005). If a mutant lacked plastidial ADP-Glc pyrophosphorylase, the transport of cytosolic Glc 1-P into the plastid would not result in the formation of ADP-Glc or starch (Fig. 4.5 B1). However, if a mutant lacks plastidial phophoglucose mutase the transport of cytosolic ADP-Glc or cytosolic Glc 1-P into the plastid should result in the formation of starch and cannot be explained (Fig. 4.5 B1, B2, B3).

4.6 Summary

In this project the use of a novel experimental approach (section 1.5) has been used to study the competing pathways of sugar nucleotide synthesis. The experimental approach enabled the competing pathways to be studied without alteration to 'normal' cellular conditions that the cells were maintained in. In addition to this all of the competing pathways could be studied in a single experiment.

A summary of the results obtained in this project on the competing pathways of sugar nucleotide synthesis are outlined in Fig. 4.6. The original experimental aim was to determine the predominant pathway involved in UDP-GlcA, UDP-GalA and GDP-Man synthesis. However, the experimental approach has potentially had wider implications on RNA (section 4.4) and starch synthesis (section 4.5). Analysis of the results has strongly suggested that UDP-GalA and UDP-GlcA predominantly arise from the 'core' metabolite UDP-Glc. The main pathway of UDP-GalA synthesis is by the UDP-GlcA 4-epimerase pathway and UDP-GlcA by the UDP-Glc dehydrogenase pathway. The ^{3}H:^{14}C kinetic ratios of the intermediary metabolites combined with the results from the AIR-derived ^{3}H:^{14}C ratios indicate that the parent 'core' metabolite of GDP-Man is Glc 6-P (in [U-^{14}C]Glc fed cells) or Fru 6-P (in [U-

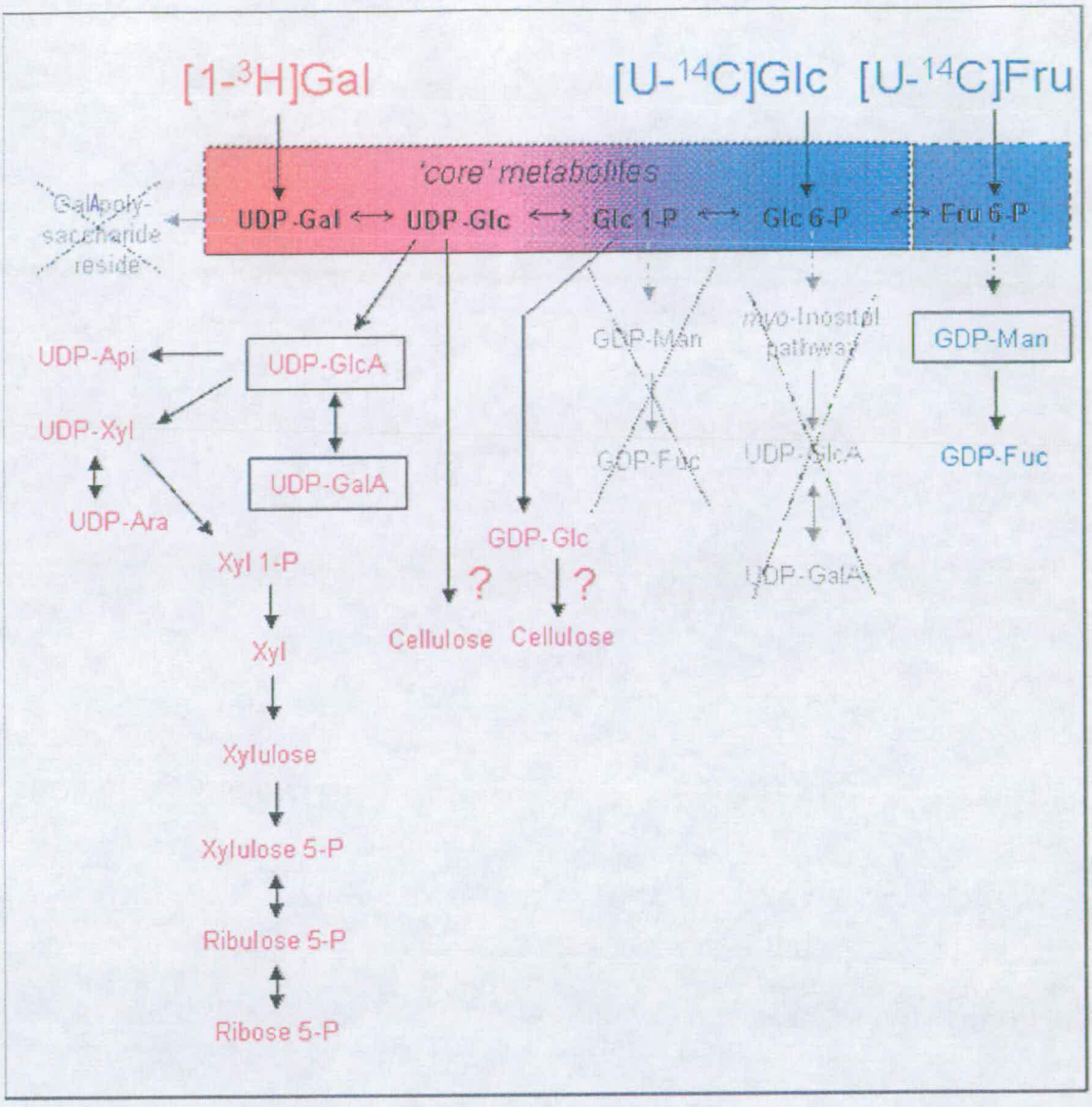

Figure 4.6 Sumary of the predominant pathways of sugar nucleotide synthesis in *Arabidopsis* cell-suspension cultures

The colour gradient indicates the 'core' metabolites that each of the cell-wall onosaccharides may have stemmed from. The increased level of red in the colour gradient represents a high $^{3}H:^{14}C$ ratio as this is 'closer' to the ^{3}H source. An increased level of blue indicates a lower $^{3}H:^{14}C$ ratio as this is more 'distanced' from the ^{3}H source.

^{14}C]Fru fed cells). The main pathway of GDP-Man synthesis is by the GDP-Man pyrophosphorylase pathway. Although these results are specific to *Arabidopsis* cell-suspension cultures, future work could adopt the experimental approach that has been used and apply this to whole plant cultures. Indeed, [1-^{3}H]Gal and either [U-^{14}C]Glc or [U-^{14}C]Fru could be fed to *Arabidopsis* seedling liquid cultures and the various tissues analysed for ^{3}H:^{14}C ratios of the AIR-derived monosaccharides.

References

Albersheim P. (1962) Hormonal control of *myo*-inositol incorporation into pectin. *The Journal of Biological Chemistry*. 238: 1608–1610

Amino S., Takeuchi Y., Komamine A. (1985) Changes in intracellular UDP-sugar levels during the cell cycle in a synchronous culture of *Catharanthus roseus*. *Physiologia Plantarum*. 64: 197–201

Asamizu T., Nishi A. (1979) Biosynthesis of cell-wall polysaccharides in cultured carrot cells. *Planta*. 146: 49–54

Baroja-Fernández E., Muñoz F. J., Zandueta-Criado A., Moran-Zorzano M. T., iale A. M., Alonso-Casajus N., Romero-Pozueta J. (2004) Most of the ADP-glucose linked to starch biosynthesis occurs outside the chloroplast in source leaves. *Proceedings of the National Academy of Sciences in the United States of America*. 101: 13080–13085

Baroja-Fernández E., Muñoz F. J., Romero-Pozueta J. (2005) Response to Neuhaus *et al.*: No need to shift the paradigm on the metabolic pathway to transitory starch in leaves. *Trends in Plant Science*. 10: 156–158

Baydoun E. A.-H., Fry S. C. (1988) [2-^{3}H]Mannose incorporation in cultured plant cells: investigation of L-galactose residues of the primary cell wall. *Journal of Plant Physiology*. 132: 484–490

Bewley J. D., Black M. (1994) Seeds: Physiology of Development and Germination (2^{nd} Ed.) Plenum Press, New York

Biffen M., Hanke D. E. (1990) Reduction in the level of intracellular *myo*-inositol in cultured soybean (*Glycine max*) cells inhibits cell division. *Biochemical Journal*. 265: 809–814

Biffen M., Hanke D. E. (1991) Metabolic fate of *myo*-inositol in soybean callus cells. *Plant Science*. 75: 203–213

Bindschedler L. V., Wheatley E., Gay E., Cole J., Cottage A., Bolwell G. P (2005) Characterisation and expression of the pathway from UDP-glucose to UDP-Xyl in differentiating tobacco tissue. *Plant Molecular Biology*. 57: 285–301

Brett C. T. (1981) Polysaccharide synthesis from GDP-glucose in pea epicotyl slices. *Journal of Experimental Biology*. 32: 1067–1077

Brett C. T., Waldron K. (1996) Physiology and Biochemistry of Plant Cell Walls (2nd Ed.) Chapman and Hall, London

Cabib E., Leloir L. F. (1954) Guanosine diphosphate mannose. *The Journal of Biological Chemistry*. 206: 779–790

Caputto R., Leloir L. F., Cardini C. E., Paladini A. C. (1950) Isolation of the coenzyme of the galactose phosphate-glucose phosphate transformation. ***The Journal of Biological Chemistry*** **184: 333–350**

Cardini C. E., Paladini A. C., Caputto R., Leloir L.F (1950) Uridine diphosphate glucose – the coenzyme of the galactose glucose phosphate isomerization. *Nature* 165: 191–192

Carpita N. C. (1996) Structure and biogenesis of the cell walls of grasses. *Annual Review of Plant Physiology and Plant Molecular Biology*. 47: 445–476

Carpita N. C., Delmer D. P. (1980) Concentration and metabolic turnover of UDP-glucose in developing cotton fibres. *The Journal of Biological Chemistry.* 256: 308–315

Carpita N. C., Kanabus J. (1987) Extraction of starch by dimethyl sulfoxide and quantitation by enzymatic assay. *Analytical Biochemistry.* 161: 132–139

Carpita N., McCann M. (2001) *In*: Biochemistry and Molecular Biology of Plants, Courier Companies Inc, USA

Chen M., Loewus F. A. (1977) *myo*-Inositol metabolism in *Lilium longiflorum* pollen. *Plant Physiology.* 59: 653–657

Chen M., Loewus M. W., Loewus F. A. (1977) Effect of a *myo*-inositiol antagonist, 2-*O*,C-methylene *myo*-inositol, on the metabolism of *myo*-inositol-2-^{3}H and D-glucose-1-^{14}C in *Lilium longiflorum* pollen. *Plant Physiology.* 59: 658–633

Conklin P. L., Norris S. R., Wheeler G. L., Williams E. H., Smirnoff N., Last R. L. (1999) Genetic evidence for the role of GDP-mannose in plant ascorbic acid (vitamin C) biosynthesis. *Proceedings of the National Aademy of Sciences of the United States of America.* USA. 96: 4198–4203

Cumming D. F. (1970) Separation and identification of soluble nucleotides in cambial and young xylem tissue of *Larix-decidua* mill. *Biochemical Journal.* 116: 189–198

Dalessandro G., Piro G., Northcote D. H. (1986) Glucomannan-synthase activity in differentiating cells of *Pinus sylvestris* L. *Planta.* 169: 564–574

Dankert M., Goncales I. R. J., Recondo E. (1964) Adenosine diphosphate glucose – orthophosphate adenylyltransferase in wheat germ. *Biochimica et Biophysica Acta.* 81: 78–85

Davies A. J., Perugini M. A., Smith B. J., Stewart J. D., Ilg T., Hodder A. N., Handman E. (2004) Properties of GDP-mannose pyrophosphorylase, a critical enzyme and drug target in *Leishmania mexicana*. *The Journal of Biological Chemistry*. 279: 12462–12468

Davies M. D., Dickinson D. B. (1972) Properties of uridine diphophoglucose dehydrogenase from pollen of *Lilium longiflorum*. *Archives of Biochemistry and Biophysics*. 152: 53–61

DeAsua L. J., Carminatti H., Passeron S. (1966) Guanosine diphosphate D-mannose pyrophosphorylase from *Gleditschia macracantha*. *Biochimica et Biophysica Acta*. 128: 582–585

Delmer P. D., Amor Y. (1995) Cellulose biosynthesis. *The Plant Cell*. 7: 987–1000

Denyer K., Dunlap F., Thorbjornsen T., Keeling P., Smith A. M. (1996) The major form of ADP-glucose pyrophosphorylase in maize endosperm starch is extraplastidial. *Plant Physiology*. 112: 779–785

Edison B. T., Chan J., Vandersall A. A., Elvebak II L. E., Smith J. J., Doong R. L., Mohnen D. (1996) Metabolism of UDP-galacturonic acid in tobacco cell free membrane preparations. *Plant Physiology*. 111: 101 *Supplement*.

Edstrom R. D., Heath E. C. (1967) The biosynthesis of cell wall lipopolysaccharide in *Escherichia coli*. VI. Enzymatic transfer of galactose, *N*-acetylglucosamine, and colitose into the polymer. *The Journal of Biological Chemistry*. 242: 3581

Elbein A. D., Hassid W. Z. (1966) The enzymatic synthesis of a glucomannan. *Biochemical and Biophysical Research Communications*. 23: 311–318

Elbein A. D. (1969) Biosynthesis of a cell wall glucomannan in mung bean seedlings. *Journal of Biological Chemistry*. 244: 1608–1616

Eshdat Y., Mirelman D. (1972) An improved method for the recovery of compounds from paper chromatograms. *Journal of Chromatography*. 65: 458–459

Evans E. A., Sheppard H. C., Turner J. C., Warrell D. C. (1974) A new approach to specific labelling of organic compounds with tritium: catalysed exchange in solution with tritium gas. *Journal of Labelled Compounds*. 10: 569 – 587

Feingold D. S., Avigad G. (1980) Sugar nucleotide transformations in plants. *In* The Biochemistry of Plants: A Comprehensive Treatise. Stumpf P. K. and Conn E. E., Academic Press, London, pp 101–170

Feingold D. S., Barber G. A. (1990) Nucleotide sugars. In Methods in Plant Biochemistry (Dey P. M., ed.). pp 39–78

Feingold D. S., Neufeld E. F., Hassid W. Z. (1958) Synthesis of a β-1,3-linked glucan by extracts of *Phaseolus aureus* seedlings. *The Journal of Biological Chemistry*. 233: 783–788

Feingold D. S., Neufeld E. F., Hassid W. Z. (1960) The 4-epimerisation and decarboxylation of uridine diphosphate D-glucuronic acid by extracts from *Phaseolus aureus* seedlings. *Journal of Biological Chemistry*. 235: 910–913

Flowers H. M., Batra K. K., Kemp J., Hassid W. Z. (1968) Biosynthesis of insoluble glucans from uridine diphosphate-D-glucose with enzyme preparations from *Phaseolus aureus* and *Lupinus albus*. *Plant Physiology*. 43: 1703–1709

Flowers H. M., Batra K. K., Kemp J., Hassid W. Z. (1969) Biosynthesis of cellulose *in vitro* from guanosine diphosphate D-glucose with enzymic preparations

from *Phaseolus aureus* and *Lupinus albus*. *Journal of Biological Chemistry* 244: 4969–4974

Fry S. C. (2000) The growing plant cell wall. Chemical and metabolic analysis. 2nd Edition. Blackburn Press, Caldwell, New Jersey

Fry S. C., D. H. Northcote (1983) Sugar nucleotide precursors of arabinopyranosyl, arabinofuranosyl, and xylopyransosyl residues in spinach polysaccharides. *Plant Physiology*. 73: 1055–1061

Gaunt M. A., Maitra U. S., Ankel H. (1974) Uridine diphosphate galacturonate 4-epimerase from the blue-green alga *Anabaena flos-aquae*. *The Journal of Biological Chemistry*. 249: 2366–2372

Gibeaut D. M., Cramer G. R., Seemann J. R. (2001) Growth, cell walls and UDP-glucose dehydrogenase activity of *Arabidopsis thaliana* grown in elevated carbon dioxide. *Journal of Plant Physiology*. 158: 569–576

Ginsberg V., Stumpf P. K., Hassid W. Z. (1956) The isolation of uridine diphosphate derivatives of D-glucose, D-galactose, D-xylose, and L-arabinose from mung bean seedlings. *The Journal of Biological Chemistry*. 223: 977–983

Gonzalez H. S., Pontis H. G., (1963) *Plant Physiology*. 54: 186–191

Gu X., Bar-Peled M. (2004) The biosynthesis of UDP-galacturonic acid in plants. Functional cloning and characterization of *Arabidopsis* UDP-D-glucuronic acid 4-epimerase. *Plant Physiology*. 136: 4256–4264

Hayashi T., Koyama T., Matsuda K. (1988) Formation of UDP-xylose and xyloglucan in soybean Golgi membranes. *Plant Physiology*. 87: 341–345

Hinterberg B., Klos C., Tenhaken R. (2002) Recombinant UDP-glucose dehydrogenase from soybean. *Plant Physiology*. 40: 1011–1017

Hitz W. D., Carlson T. J., Kerr P. S., Sebastian S. A. (2002) Biochemical and molecular characterization of a mutation that confers a decreased raffinosaccharide and phytic acid phenotype on soybean seeds. *Plant Physiology*. 128: 650–660

Horecker B. L. (2002) The pentose phosphate pathway. *The Journal of Biological Chemistry*. 277: 47965–47971

Hughes R., Street H. E. (1974) Galactose as an inhibitor of the expansion of root cells. *Annals of Botany*. 38: 555–564

Ishitani M., Majumder A. L., Bornhouser A., Michalowski C. B., Jensen R. C., Bohnert H. J. (1996) Co-ordinate transcriptional induction of *myo*-inositol metabolism during environmental stress. *Plant Journal*. 9: 537–548

Irvine R. F., Letcher A. J., Lander D. J., Drøbak B. K., Dawson A. P., Musgrave A. (1989) Phosphatidylinositol (4,5)bisphosphate and phosphatidylinositol (4)phosphate in plant tissues. *Plant Physiology*. 89: 888–892

Jung P., Tanner W., Wolter K. (1972) The fate of *myo*-inositol in *Fraxinus* tissue cultures. *Phytochemistry*. 11: 1655–1659

Kanter U., Usadel B., Guerineau F., Yong L., Pauly M., Tenhaken (2005) The inositol oxygenase gene family of *Arabidopsis* is involved in the biosynthesis of nucleotide sugar precursors for cell-wall matrix polysaccharides. *Planta*. 221: 243–254

Kärkönen A. (2005) Biosynthesis of UDP-GlcA: via UDPGDH or the *myo*-inositol oxidation pathway? *Plant Biosystems*. 139: 46–49

Kärkönen A., Fry S. C. (2005a) Novel characteristics of UDP-glucose dehydrogenase activities in maize: non-involvement of alcohol dehydrogenases in cell wall polysaccharide biosynthesis. *Planta*. In Press.

Kärkönen A., Murigneux A., Martinant J-P., Pepey E., Tatout C., Dudley B. J., Fry S. C. (2005b) UDP-Glucose dehydrogenases of maize — a role in cell wall pentose biosynthesis. *Biochemical Journal*. In Press.

Katan R., Avigad G. (1965) Soluble nucleotide pool of sugar beet root. *Israel Journal of Chemistry*. 3: 110

Kauss H. (1965) Uridine diphosphate rhamnose from golden brown alga ochromonas. *Biochemical and Biophysical Research Communications*. 18: 170–173

Kauss H., Kandler O. (1962) Adenosindiphosphatglucose aus *Chlorella*. *Zeitschrift für Naturforschung Part B-Chemie Biochemie Biophysik Biologie und verwanten gebiete*. 17b: 858–860

Keller R., Springer F., Renz A., Kossmann J. (1999) Antisense inhibition of the GDP-mannose pyrophosphorylase reduces the ascorbate content in transgenic plants leading to developmental changes during senescence. *The Plant Journal*. 19: 131–141

Kessler G., Neufeld E. F., Feingold D. S., Hassid W. Z. (1961) Metabolism of D-glucuronic acid and D-galacturonic acid by *Phaseolus aureus* seedlings. *The Journal of Biological Chemistry*. 236: 308–312

Kimura S., Kondo T. (2002) Recent progress in cellulose biosynthesis. Journal of Plant Research. 115: 297–302

Lehle L., Tanner W., Kandler O. (1970) *myo*-Inositol, a co-factor in the biosynthesis of raffinose. *Hoppe-Seylers Zeitschrift für Physiologische Chemie*. 351: 1494–1498

Li Y., He N., Guan H., Du G., Chen J. (2003) A novel polygalacturonic acid bioflocculant REA-11 produced by *Corynebacterium glutamicum*: a proposed

biosynthetic pathway and experimental confirmation. *Applied Microbiology and Biotechnology*. 63: 200 – 206

Liljebjelke K., Adolphson R., Baker K., Doong R. L., Mohnen D. (1995) Enzymatic synthesis and purification of uridine diphospate[^{14}C]galacturonic acid: a substrate for pectin biosynthesis. *Analytical Biochemistry*. 225: 296–304

Lin T. Y., Hassid W. Z. (1966) Isolation of guanosine diphosphate uronic acids from a marine brown alga, *Fucus gardneri* Silva. *The Journal of Biological Chemistry*. 241: 3283–3293

Loewus M. A. (1977) Hydrogen isotope effects in the cyclization of D-glucose 6-phosphate by myo-inositol-1-phosphate synthase. *Journal of Biological Chemistry*. 252: 7221–7223

Loewus M. W., Loewus F. A. (1980) The C-5 hydrogen isotope-effect in myo-inositol 1-phosphate synthase as evidence for the *myo*-inositol oxidation-pathway. *Carbohydrate Research*. 82: 333–342

Loewus F. A., Murthy P. P. N. (2000) *myo*-Inositol metabolism in plants. *Plant Science*. 150: 1–19

Loewus F. A., Kelly S., Neufeld E. F. (1962) Metabolism of *myo*-inositol in plants: conversion to pectin, hemicellulose, D-xylose and sugar acids. *Proceedings of the National Acadamey of Sciences*. 48: 421–425

Loughman B. C., Ratcliffe R. G., Schwabe J. W. R. (1989) Galactose metabolism in *Zea mays* root tissues observed by ^{31}P-NMR spectroscopy. *Plant Science*. 59: 11–23

Maiti I. B., Loewus F. A. (1978) Evidence for a functional *myo*-inositol oxidation pathway in *Lilium longiflorum* pollen. *Plant Physiology*. 62: 280–283

Maretzki A., Thom M. (1978) Characteristics of a galactose-adapted sugarcane cell line grown in suspension culture. *Plant Physiology*. 61: 544–548

McNeil M., Darvill A. G., Fry S. C., Albersheim P. (1984) Structure and function of the primary cell wall of plants. *Annual Review Biochemistry*. 53: 625–663

Mølhøj M., Verma R., Reiter W-D. (2004) The biosynthesis of D-galacturonate in plants. Functional cloning and characterization of a membrane-anchored UDP-D-glucuronate 4-epimerase from *Arabidopsis*. *Plant Physiology*. 135: 1221–1230

Muñoz R., López R., Frutos M., García E. (1999) First molecular characterization of a uridine diphosphate galacturonate 4-epimerase: an enzyme required for capsular biosynthesis in *Streptococcus pneumoniae* type 1. *Molecular Microbiology*. 31: 703–713

Murashige T, Skoog F (1962) A revised medium for rapid growth and bioassay with tobacco tissue culture. *Physiol. Plant*. 15: 473–497

Nelson D. E., Koukoumanos M., Bohnert H. J. (1999) *myo*-Inositol-dependent sodium uptake in ice plant. *Plant Physiology*. 119: 165–172

Neufeld E. F., Feingold D. S. (1961) Isolation of uridine diphosphate-galacturonic acid from seedlings of *Phaseolus aureus*. *Biochimica et Biophysica Acta*. 53: 589–590

Neuhaus E. H., Häusler R. E., Sonnewald U. (2005) No need to shift the paradigm on the metabolic pathway to transitory starch in leaves. *Trends in Plant Science*. 10: 154–156

Ning B., Elbein A. D. (2000) Cloning, expression and characterization of the pig liver GDP-mannose pyrophosphorylase. Evidence that GDP-mannose and GDP-Glc

pyrophosphorylases are different proteins. *European Journal of Biochemistry.* 267:6866–6874

Passeron S., Recondo E., Dankert M. (1964) Biosynthesis of adenosine diphosphate D-hexoses. *Biochimica et Biophysica Acta.* 89: 372–374

Perrin R. M. (2001) How many cellulose synthases make a plant? *Current Biology.* 11: R213–R216

Peng L. C., Kawagoe Y., Hogan P., Delmer D. (2002) Sitosterol-beta-glucoside as primer for cellulose synthesis in plants. *Science.* 295: 147–150

Preiss J. (1991) Biology and molecular biology of starch synthesis and its regulation. *Oxford Surveys of Plant Molecular and Cell Biology.* 7: 59–114

Raboy V., Gerbasi P. F., Young K. A., Stoneberg S. D., Pickett S. G., Bauman A. T., Murthy P. P. N., Sheridan W. F., Ertl D. S. (2000) Origin and seed phenotype of maize *low phytic acid 1-1* and *low phytic acid 2-1*. *Plant Physiology.* 124: 355–368

Reiter W-D., Vanzin G. F. (2001) Molecular genetics of nucleotide sugar interconversion pathways in plants. *Plant Molecular Biology.* 47: 95–113

Roberts R. M., Loewus F. (1966) Inositol metabolism in plants. III. Conversion of *myo*-inositol-2-^{3}H to cell wall polysaccharides in sycamore (*Acer pseudoplatanus* L.) cell culture. *Plant Physiology.* 41: 1489–1498

Roberts R. M., Cetorelli J. J. (1973) UDP-Glucuronic acid pyrophosphorylase and the formation of UDP-glucuronic acid in plants. In Biogenesis of Plant Cell Wall Polysaccharides (Loewus F., ed.). pp. 49–68

Roberts R. M., Loewus F. (1973) The conversion of [6-^{14}C]glucose to cell wall polysaccharide material in *Zea mays* in the presence of high endogenous levels of *myo*-inositol. *Plant Physiology*. 52: 646–650

Roberts R. M., Deshusses J., Loewus F. (1968) Inositol metabolism in plants. V. Conversion of *myo*-inositol to uronic acid and pentose units of acidic polysaccharides in root–tips of *Zea mays*. *Plant Physiology*. 43: 979–989

Robertson D., Beech I., Bolwell G. P. (1995) Regulation of the enzymes of UDP-sugar metabolism during differentiation of French bean. *Phytochemistry*. 39: 21–28

Robertson D., Smith C., Bowell G. P. (1996) Inducible UDP-glucose dehydrogenase from French bean (*Phaseolus vulgaris* L.) locates to vascular tissue and has alcohol dehydrogenase activity. *Biochemical Journal*. 313: 311–317

Sacchetti S., Bartolucci S., Rossi M., Cannio R. (2004) Identification of a GDP-mannose pyrophosphorylase gene from *Sulfolobus solfataricus*. *Gene*. 332: 149–157

Samac D. A., Litterer L., Temple G., Jung H-J. G., Somers D. A. (2004) Expression of UDP-Glucose dehydrogenase reduces cell-wall polysaccharide concentration and increases xylose content in alfalfa stems. *Applied Biochemistry and Biotechnology*. 113: 1167–1182

Sanderman H., Grisebach H. (1968a) Apiose biosynthesis. 3. Occurrence of UDP-apiose and other UDP-sugars in parsley (*Apium petroselinum* L.). *European Journal of Biochemistry*. 6: 404–410

Sanderman H., Grisebach H. (1968b) Occurrence of UDP-apiose in parsley (*Apium petroselinum* L.). *Biochimica et Biophysica Acta*. 156: 435–436

Sasaki K., Taylor I. E. P. (1984) Specific labelling of cell wall polysaccharides with *myo*-[2-^{3}H]inositol during germination and growth of *Phaseolus vulgaris* L. *Plant and Cell Physiology*. 25: 989–997

Seitz B., Klos C., Wurm M., Tenhaken R. (2000) Matrix polysaccharide precursors in *Arabidopsis* cell walls are synthesized by alternate pathways with organ-specific expression patterns. *The Plant Journal*. 21: 537–546

Selvendran R. R., Isherwood F. A. (1967) Identification of guanosine diphosphate derivatives of D-xylose, D-mannose, D-glucose and D-galactose in mature strawberry leaves. *Biochemical Journal*. 105: 723–738

Smart C. C., Flores S. (1997) Overexpression of D-*myo*-inositol-3-phosphate synthase leads to elevated levels of inositol in *Arabidopsis*. *Plant Molecular Biology*. 33: 811–820

Solms J., Hassid W. Z. (1957) Isolation of uridine diphosphate *N*-acetylglucosamine and uridine diphosphate glucuronic acid from mung bean seedlings. *The Journal of Biological Chemistry*. 228: 357–364

Stewart D. C., Copeland L. (1998) Uridine 5'-diphosphate-glucose dehydrogenase from soybean nodules. *Plant Physiology*. 116: 349-355

Strominger J. L., Mapson L. W. (1957) Uridine diphosphoglucose dehydrogenase of pea seedlings. *Biochemical Journal*. 66: 567–562

Strominger J. L., Kalckar H. M., Axelrod J., Maxwell E. S. (1954) Enzymatic oxidation of uridine diphosphate glucose to uridine diphosphate glucuronic acid. *Journal of American Chemistry Society*. 76: 6411

Stroud D. B. E., Hassid W. Z. (1964) Synthesis of 4-keto-sugar phosphates. *Biochemical and Biophysical Research Communications*. 15: 65–69

Su J. C., Hassid W. Z (1962a) Carbohydrates and nucleotides in red alga *Porphyra perforata*. 1. Isolation and identification of carbohydrates. *Biochemistry*. 1: 468–474

Su J. C., Hassid W. Z (1962b) Carbohydrates and nucleotides in red alga *Porphyra perforata*. 2. Separation and identification of nucleotides. *Biochemistry*. 1: 474–480

Szumilo T., Drake R. R., York J. L., Elbein A. D. (1993) GDP-mannose pyrophosphorylase. *The Journal of Biological Chemistry*. 268: 17943–17950

Tenhaken R., Thulke O. (1996) Cloning of an enzyme that synthesises a key nucleotide-sugar precursor of hemicellulose biosynthesis from soybean: UDP-glucose dehydrogenase. *Plant Physiology*. 112: 1127–1134

Turner W., Botha F. C. (2002) Purification and kinetic properties of UDP-glucose dehydrogenase from sugarcane. *Archives of Biochemistry and Biophysics*. 407: 209–216

Usadel B., Schlüter U., Mølhøj M., Gipmans M., Verma R., Kossmann J., Reiter W-D., Pauly M. (2004) Identification and characterization of a UDP-D-glucuronate 4-epimerase in *Arabidopsis*. *FEBS Letters*. 569: 327–331

Verma D. C., Dougall D. K. (1979) Biosynthesis of *myo*-inositol and its role as a precursor of cell-wall polysaccharides in suspension cultures of wild-carrot cells. *Planta*. 146: 55–62

Wakabayashi K., Sakurai N., Kuraishi S. (1989) Effects of ABA on synthesis of cell-wall polysaccharides in segments of etiolated squash hypocotyls. I. Changes in incorporation of glucose and *myo*-inositol into cell-wall components. Plant Cell Physiology. 30: 99–105

Walbot V. (2000) A green chapter in the book of life. *Nature*. 408: 794–795

Warit S., Zhang N., Short A., Walmsley R. M., Oliver S. G., Stateva L. I. (2000) Glycosylation deficiency phenotypes resulting from depletion of GDP-mannose pyrophosphorylase in two yeast species. *Molecular Microbiology*. 36: 1156–1166

Wilcox J. R., Premachandra G. S., Young K. A., Raboy V. (2000) Isolation of high seed inorganic P, low-phytate soybean mutants. *Crop Science*. 40: 1601–1605

Witt H.-J. (1992) UDP-glucose metabolism during differentiation and dedifferentiation of *Riella helicophylla*. *Journal of Plant Physiology*. 140: 276–281

Wheeler G. L., Jones M. A., Smirnoff N. (1998) The biosynthetic pathway of vitamin C in higher plants. *Nature*. 393: 365–369

Woulucka B A., Persiau G., Doorsselaere J. Van., Davey M. W., Demol H., Vanderkerckhove J., Montagu M. Van., Zabeau M., Boerjan W. (2001) Partial purification and identification of GDP-mannose 3",5"-epimerase of *Arabidopsis thaliana*, a key enzyme of the plant vitamin C pathway. *Proceedings of the National Academy of Sciences*. 98: 14843–14848

Zhang L., Radziejewska-Lebrecht J., Krajewska-Pietrasik D., Toivanen P., Skurnik M. (1997) Molecular and chemical characterization of the lippopolysaccharide O-antigen and its role in the virulence of *Yersinia enterocolitica* serotype O:8. *Molecular Microbiology*. 23: 63–76

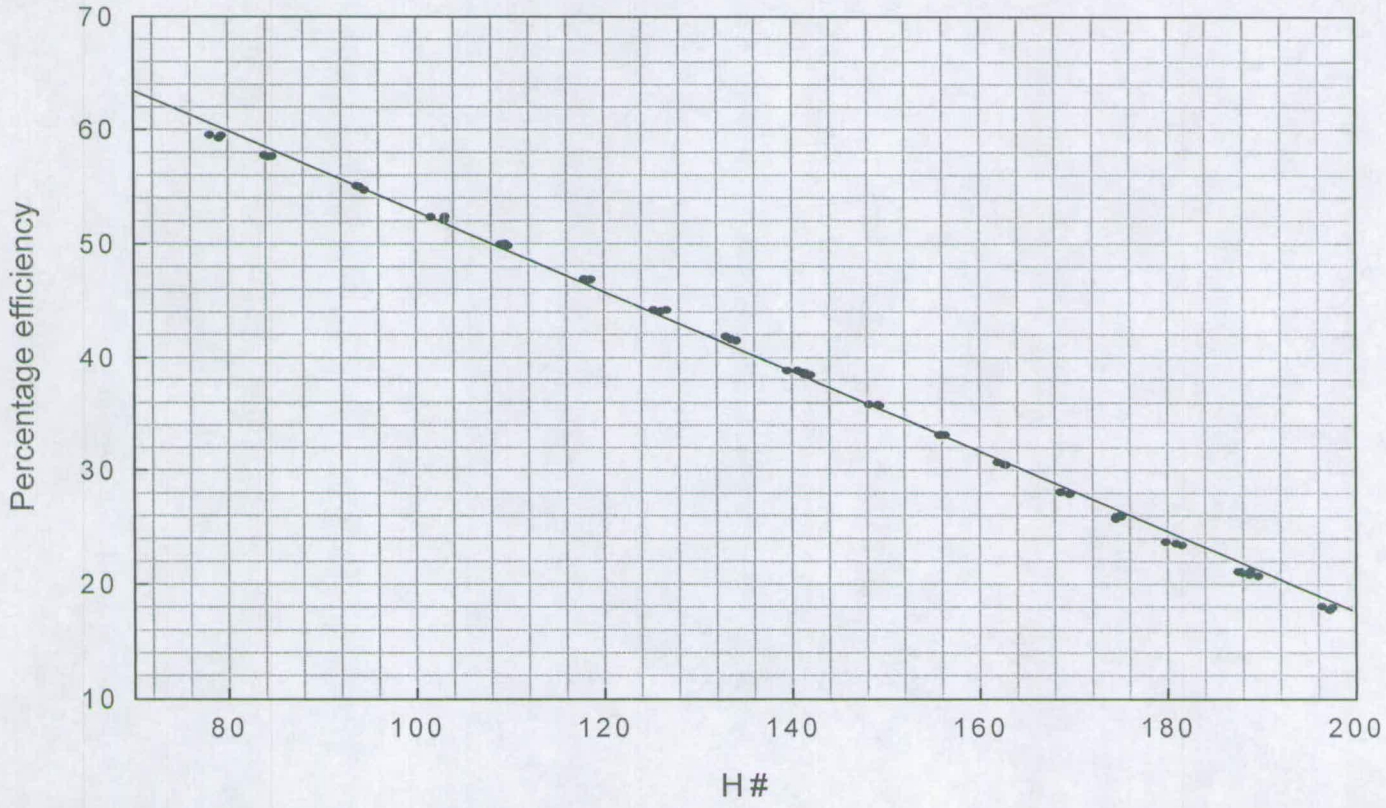

Appendix 1 Quench curve of ^{14}C assayed on a dual ^{14}C and ^{3}H channel on a Beckman LS 6500 multi-purpose scintillation counter

The scintillant was 10 ml of OptiPhase, and the sample was 1 ml of aqueous solution.

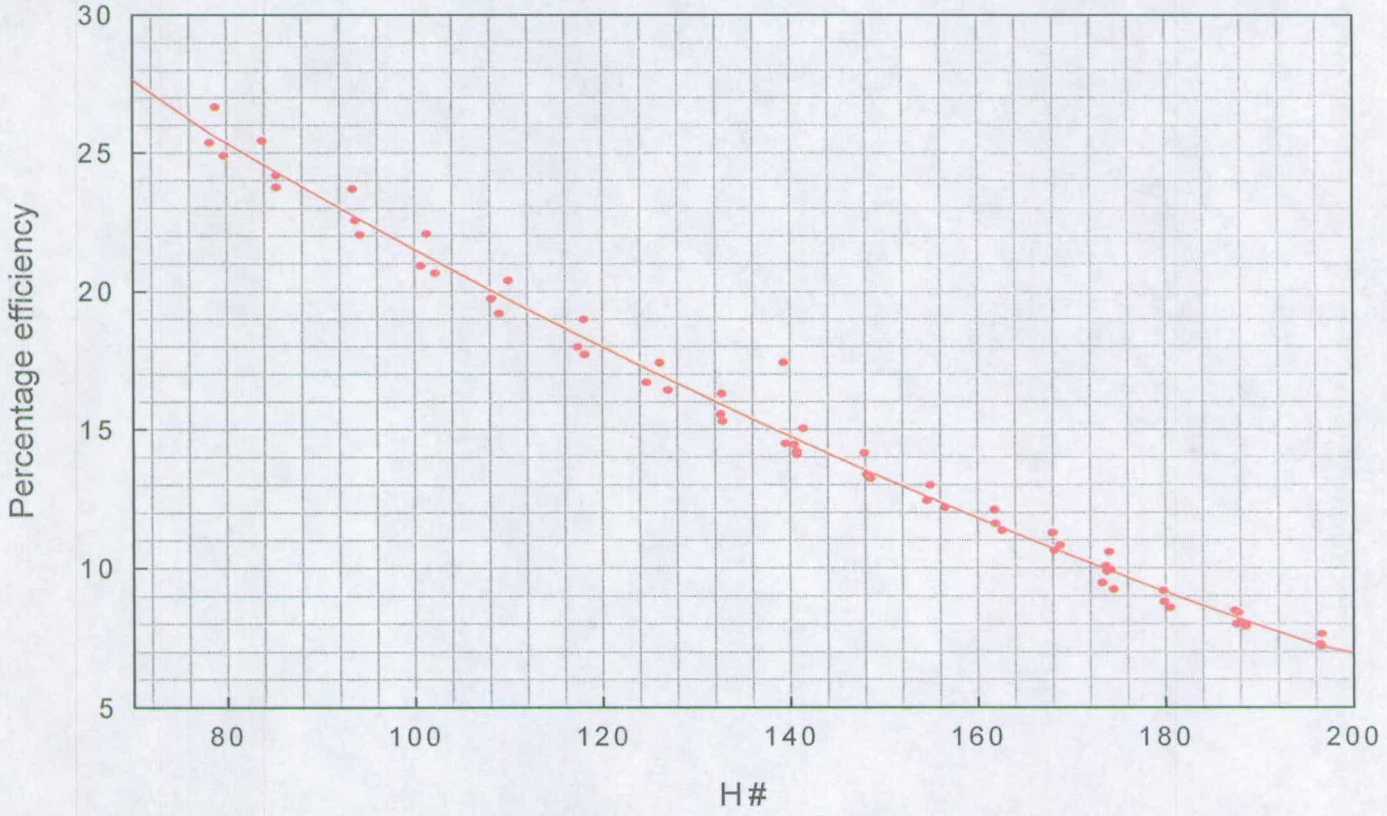

Appendix 2 Quench curve of ^{3}H assayed on a dual ^{14}C and ^{3}H channel on a Beckman LS 6500 multi-purpose scintillation counter

Other details as in Appendix 1.

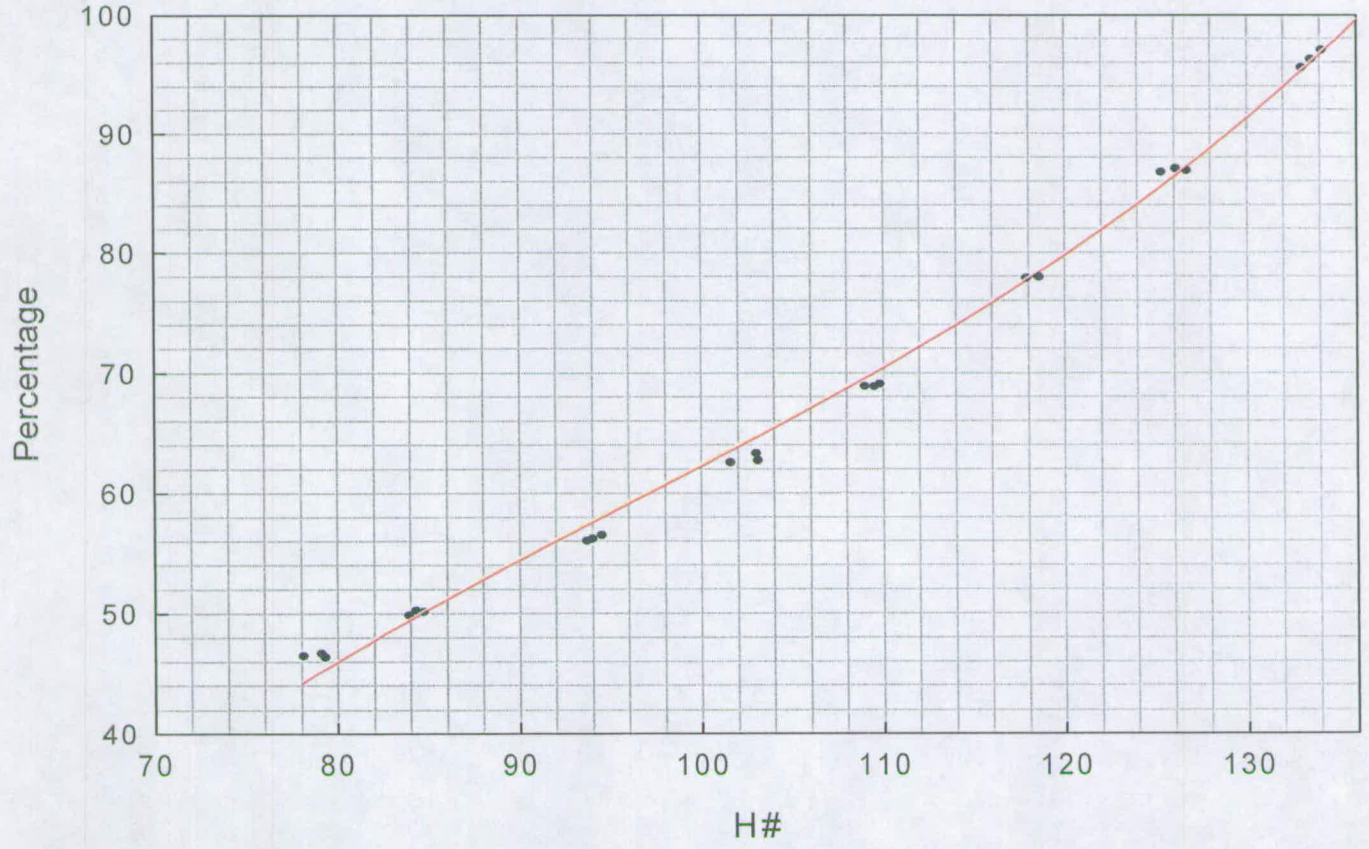

Appendix 3 Percentage of ^{14}C falsely detected as ^{3}H when assayed on a dual ^{14}C and ^{3}H channel

Other details as in Appendix 1.

		Apparent 3H			Apparent 14C					True								
	Time (h)	Total counts registered in 10 min	Minus back-ground count	Sample error (2σ) combined with error of lowest no. of counts (2σ)	Total counts registered in 10 min	Minus back-ground count	Sample error (2σ) combined with error of background (2σ)	Average H#	% false 3H	3H (counts in 10 min)	Counting efficiency * 3H	Counting efficiency * 14C	3H (Bq)	3H error (± Bq)	14C (Bq)	14C error (± Bq)	3H:14C ratio (Bq/Bq)	Error of ratio
Gal/A (A)	Control	11084	10971	212	1778	1665	87	83	50	10139	25	59	68.27	1.54	4.74	0.25	14.39	0.82
	0	12751	12638	227	1945	1832	91	85	50	11722	24	58	80.56	1.66	5.31	0.26	15.17	0.82
	2	6106	5993	158	394	881	67	87	50	5553	24	57	38.56	1.19	2.60	0.20	14.84	1.22
	4	2649	2736	103	548	435	52	86	50	2519	24	57	17.31	0.83	1.27	0.15	13.61	1.75
	8	339	226	43	235	122	38	85	50	165	24	58	1.13	0.39	0.35	0.11	3.21	1.50
Gal/A (B)	Control	14845	14732	245	1798	1685	88	83	50	13830	25	59	94.49	1.77	4.84	0.25	19.51	1.08
	0	14797	14684	244	1941	1828	91	85	48	13807	24	58	91.13	1.72	5.16	0.26	17.65	0.94
	2	8267	8154	183	1050	937	69	87	50	7686	24	57	52.28	1.33	2.69	0.20	19.42	1.51
	4	4347	4234	134	678	565	57	86	50	3952	24	57	26.88	0.99	1.62	0.16	16.56	1.77
	8	606	493	54	304	191	42	85	50	398	24	58	2.68	0.46	0.54	0.12	4.92	1.36
Ara (A)	Control	41307	41194	407	5083	4970	144	83	43	38759	25	59	258.39	2.68	14.16	0.41	18.25	0.57
	0	38383	38870	335	4364	4851	143	85	50	36445	24	58	250.48	2.89	14.06	0.41	17.81	0.56
	2	37673	37560	383	4684	4571	133	87	50	35275	24	57	242.44	2.84	13.25	0.40	18.30	0.60
	4	34952	34839	375	4303	4190	133	86	50	32744	24	57	220.50	2.68	11.94	0.38	18.47	0.63
	8	14631	14518	243	1807	1694	88	85	50	13671	24	58	93.96	1.78	4.95	0.26	18.97	1.05
Ara (B)	Control	42803	42690	414	4606	4493	138	83	50	40444	25	59	275.13	2.97	12.91	0.40	21.31	0.69
	0	39785	39672	339	4172	4059	131	85	50	37643	24	58	258.71	2.83	11.77	0.38	21.99	0.75
	2	33363	33250	366	3539	3426	121	87	50	31537	24	57	216.75	2.65	9.93	0.35	21.83	0.82
	4	31223	31110	354	3253	3140	116	86	50	29540	24	57	203.02	2.56	9.18	0.34	22.11	0.87
	8	11312	11799	219	1254	1141	74	85	50	11229	24	58	77.38	1.61	3.37	0.22	23.17	1.58
Xyl (A)	Control	33628	33515	367	4572	4459	137	83	50	31286	25	59	212.83	2.67	12.81	0.39	16.61	0.55
	0	28760	28647	340	3926	3813	127	85	50	26741	24	58	181.91	2.47	10.96	0.37	16.60	0.60
	2	23751	23638	309	3097	2984	114	87	50	22146	24	57	150.65	2.24	8.57	0.33	17.57	0.72
	4	19669	19556	281	2568	2455	104	86	43	18353	24	57	122.35	2.00	6.99	0.30	17.49	0.79
	8	5935	5822	156	839	726	62	85	50	5459	24	58	37.14	1.14	2.09	0.18	17.80	1.62
Xyl (B)	Control	31680	31567	357	3636	3523	123	83	50	29806	25	59	202.76	2.57	10.12	0.35	20.03	0.74
	0	27964	27851	335	3211	3098	116	85	50	26302	24	58	180.77	2.44	8.98	0.34	20.13	0.80
	2	24358	24245	313	2813	2700	108	87	50	22895	24	57	154.18	2.23	7.69	0.31	20.04	0.86
	4	20080	19967	284	2201	2088	97	86	50	18923	24	57	127.43	2.02	5.95	0.28	21.42	1.05
	8	5363	5856	156	753	640	59	85	50	5536	24	58	37.26	1.12	1.82	0.17	20.45	2.00
Gal (A)	Control	96144	96031	621	9533	9420	137	83	50	91321	25	59	614.96	4.38	26.84	0.56	22.91	0.51
	0	78771	78658	562	8005	7892	180	85	50	74712	24	58	513.48	4.05	23.08	0.53	22.25	0.54
	2	83312	83199	578	8703	8590	186	87	50	78904	24	57	531.34	4.09	24.47	0.54	21.71	0.50
	4	103822	103709	645	9063	8950	132	86	43	93324	24	57	662.16	4.48	25.50	0.55	25.97	0.58
	8	38716	38603	394	3989	3876	128	85	43	36704	24	58	244.69	2.76	11.04	0.37	22.16	0.78
Gal (B)	Control	124540	124427	706	10853	10740	210	83	50	119057	25	59	818.26	5.06	31.40	0.61	26.06	0.53
	0	115805	115692	681	9830	9717	200	85	50	110804	24	58	746.15	4.78	27.65	0.57	26.79	0.57
	2	109966	109853	664	9690	9577	198	87	50	105065	24	57	705.75	4.65	28.25	0.58	26.04	0.57
	4	80257	80144	567	8275	8162	183	86	50	76063	24	57	512.21	4.01	23.25	0.52	22.03	0.52
	8	48640	48527	442	4036	3985	130	85	43	46574	24	58	310.50	3.07	11.35	0.37	27.35	0.93
Man (A)	Control	503	390	50	253	140	39	85	50	320	24	58	2.20	0.43	0.41	0.11	5.42	1.66
	0	433	320	47	263	150	40	84	50	245	25	58	1.67	0.42	0.43	0.11	3.87	1.41
	2	420	307	46	259	146	39	84	50	234	25	58	1.59	0.41	0.42	0.11	3.79	1.42
	4	375	262	44	255	142	39	85	50	191	24	58	1.31	0.41	0.41	0.11	3.19	1.32
	8	241	128	38	207	94	37	84	50	81	25	58	0.55	0.36	0.27	0.11	2.04	1.55
Man (B)	Control	649	536	55	316	203	42	85	50	435	24	58	2.99	0.48	0.59	0.12	5.06	1.33
	0	607	494	54	288	175	41	84	50	407	25	58	2.85	0.47	0.52	0.12	5.51	1.58
	2	765	652	59	330	217	43	84	50	544	25	58	3.77	0.51	0.64	0.13	5.90	1.41
	4	686	573	57	331	218	43	85	50	464	24	58	3.25	0.50	0.64	0.13	5.05	1.26
	8	358	245	43	215	102	37	84	50	194	25	58	1.36	0.40	0.30	0.11	4.52	2.11

Appendix 4 Data set for Fig. 3.8. Effect of TFA on [^{3}H, ^{14}C]monosaccharides

(*) The counting efficiency was obtained from Appendices 1 − 2. The percentage of ^{14}C falsely detected as ^{3}H was determined from Appendix 3. The ^{3}H background was 113 ± 21.3 counts/10 min and for ^{14}C 130 ± 22.8 counts/10 min.

Continued overleaf

		Apparent 3H			Apparent 14C						Counting efficiency *							
	Time (h)	Total counts registered in 10 min	Minus back-ground count	Sample error (2σ) combined with error of lowest no. of counts (2σ)	Total counts registered in 10 min	Minus back-ground count	Sample error (2σ) combined with error of background (2σ)	Average H#	% false 3H	True 3H (counts in 10 min)	3H	14C	3H (Bq)	3H error (± Bq)	14C (Bq)	14C error (± Bq)	3H:14C ratio (Bq/Bq)	Error of ratio
Fuc (A)	Control	490	377	49	402	289	46	85	55	218	24	58	1.62	0.50	0.88	0.14	1.83	0.64
	0	348	235	43	320	207	42	84	50	132	25	58	0.92	0.42	0.61	0.13	1.51	0.76
	2	592	479	53	489	376	50	84	50	291	25	58	2.02	0.51	1.11	0.15	1.82	0.52
	4	305	192	41	267	154	40	85	50	115	24	58	0.79	0.39	0.45	0.12	1.76	0.99
	8	285	172	40	266	153	40	84	50	96	25	58	0.66	0.38	0.45	0.12	1.47	0.95
Fuc (B)	Control	685	572	57	536	423	52	85	50	361	24	58	2.48	0.53	1.24	0.15	2.00	0.49
	0	479	366	49	381	268	45	84	50	232	25	58	1.59	0.46	0.78	0.13	2.03	0.68
	2	676	563	56	550	437	52	84	50	345	25	58	2.39	0.53	1.29	0.15	1.86	0.47
	4	685	572	57	541	428	52	85	50	358	24	58	2.49	0.53	1.26	0.15	1.97	0.49
	8	394	281	45	324	211	43	84	50	176	25	58	1.20	0.42	0.60	0.12	1.98	0.80
Rha (A)	Control	13127	13014	230	1873	1760	30	85	49	12152	24	58	81.01	1.65	5.01	0.26	16.16	0.88
	0	12471	12358	224	1802	1689	88	84	50	11514	25	58	79.13	1.66	4.90	0.25	16.16	0.91
	2	12263	12150	222	1643	1530	84	84	48	11416	25	58	75.35	1.57	4.32	0.24	17.43	1.03
	4	10487	10374	206	1479	1366	80	85	50	9631	24	58	65.93	1.50	3.93	0.23	16.79	1.06
	8	4554	4441	137	707	594	58	84	50	4144	25	58	27.31	1.00	1.69	0.16	16.49	1.71
Rha (B)	Control	14105	13992	238	1715	1602	86	85	45	13271	24	58	86.74	1.66	4.49	0.24	19.33	1.10
	0	13023	12910	229	1578	1465	83	84	45	12251	25	58	80.07	1.59	4.10	0.23	19.51	1.17
	2	11895	11782	219	1501	1388	81	84	50	11088	25	58	74.67	1.57	3.95	0.23	18.88	1.17
	4	11278	11165	213	1392	1279	78	85	49	10538	24	58	70.26	1.52	3.64	0.22	19.28	1.25
	8	5658	5545	152	752	639	59	84	45	5257	25	58	34.03	1.06	1.78	0.16	19.17	1.88
Glc (A)	Control	73310	73197	542	5661	5548	152	85	45	70700	24	58	466.67	3.72	15.67	0.43	29.78	0.85
	0	62673	62560	501	4793	4680	140	84	50	60220	25	58	413.86	3.58	13.57	0.41	30.51	0.95
	2	65188	65075	511	5119	5006	145	84	50	62572	25	58	425.66	3.61	14.39	0.42	29.59	0.89
	4	67980	67867	522	5194	5081	146	85	50	65327	24	58	439.31	3.65	14.48	0.42	30.39	0.91
	8	31649	31536	356	2413	2300	101	84	49	30409	25	58	202.73	2.47	6.55	0.29	30.94	1.41
Glc (B)	Control	75138	75025	549	5683	5570	152	82	49	72236	25	59	481.37	3.80	15.87	0.43	30.37	0.87
	0	74272	74159	545	5637	5524	152	85	50	71397	24	58	490.70	3.89	16.01	0.44	30.65	0.88
	2	67574	67461	520	5103	4990	145	83	50	64366	25	59	437.48	3.64	14.22	0.41	30.77	0.93
	4	61075	60962	495	4683	4570	139	80	45	58306	26	60	385.00	3.36	12.80	0.39	30.08	0.95
	8	30490	30377	350	2309	2196	99	84	50	29279	25	58	193.18	2.47	6.31	0.28	31.56	1.47
Glc (C)	Control	4330	4217	133	503	390	50	82	48	4030	25	59	26.60	0.94	1.10	0.14	24.14	3.23
	0	4743	4630	139	544	431	52	85	50	4415	24	58	30.34	1.02	1.26	0.15	24.06	3.01
	2	4699	4586	139	561	448	53	83	49	4366	25	59	29.11	0.99	1.28	0.15	22.81	2.79
	4	4293	4180	133	530	417	51	80	50	3972	26	60	27.30	0.98	1.21	0.15	22.58	2.90
	8	2068	1955	93	344	231	44	84	50	1840	25	58	12.33	0.69	0.66	0.12	18.82	3.70
Glc (D)	Control	3526	3413	121	473	360	49	82	50	3233	25	59	22.22	0.90	1.04	0.14	21.29	3.03
	0	3004	2891	112	365	252	44	85	50	2765	24	58	19.20	0.83	0.74	0.13	25.83	4.70
	2	3446	3333	119	454	341	48	83	50	3163	25	59	21.96	0.89	1.01	0.14	21.83	3.22
	4	3146	3033	114	448	335	48	80	50	2866	26	60	19.49	0.84	0.96	0.14	20.25	3.04
	8	1674	1561	85	308	195	42	84	50	1464	25	58	10.06	0.65	0.57	0.12	17.64	3.95
Rib (A)	Control	7359	7246	173	1239	1126	74	82	50	6683	25	59	45.33	1.29	3.26	0.21	14.07	1.01
	0	7027	6914	169	1243	1130	74	85	50	6349	24	58	44.09	1.28	3.33	0.22	13.23	0.95
	2	5160	5047	145	901	788	64	83	50	4653	25	59	31.98	1.09	2.30	0.19	13.88	1.23
	4	3605	3492	122	654	541	56	80	50	3222	26	60	22.56	0.94	1.60	0.17	14.14	1.56
	8	805	692	61	199	86	36	84	50	649	25	58	4.41	0.48	0.25	0.10	17.87	7.78
Rib (B)	Control	6944	6831	168	947	834	66	82	50	6414	25	59	44.06	1.24	2.44	0.19	18.06	1.51
	0	6588	6475	164	986	873	67	85	50	6039	24	58	41.50	1.22	2.53	0.19	16.40	1.34
	2	4933	4820	142	709	596	58	83	50	4522	25	59	31.08	1.05	1.73	0.17	17.99	1.85
	4	3612	3499	122	546	433	52	80	50	3283	26	60	22.33	0.90	1.24	0.15	17.95	2.27
	8	751	638	59	188	75	36	84	50	601	25	58	4.04	0.46	0.21	0.10	18.32	9.26

Appendix 4 Continued

		Apparent 3H		Apparent 14C				True							
		Total counts registered in 20 min	Deduct back-ground counts	Total counts registered in 20 min	Deduct back-ground counts	Average #H number	% false 3H	3H (counts in 20 min)	Counting efficiency * 3H	Counting efficiency * 14C	3H (Bq)	14C (Bq)	Average 3H:14C ratio (Bq/Bq)	Standard error of ratio
Gal	A	1214940	1214737	102639	102444	102	61	1152246	22	53	4466	162.61		
	B	1117817	1117614	80439	80184	101	60	1063504	22	53	4098	126.08		
	C	2521703	2521500	132612	132357	103	62	2402239	21	52	9421	308.26	30.18	1.20
Glc	A	69502	69299	5900	5645	104	63	65771	21	52	261	9.05		
	B	44900	44697	3845	3590	104	63	42453	21	52	168	5.75		
	C	89810	89607	9247	8992	104	63	83987	21	52	333	14.41	27.09	1.62
Rha	A	182021	181818	20333	20078	102	61	169570	22	53	657	31.87		
	B	172765	172562	15796	15541	103	62	162327	22	53	639	24.31		
	C	267623	267420	27820	27565	103	62	250330	21	52	982	44.17	22.83	1.21
Api	A	7332	7129	972	717	105	63	6677	22	53	27	1.16		
	B	7668	7465	932	677	105	63	7038	22	53	28	1.10		
	C	12353	12150	1394	1139	106	65	11410	21	52	46	1.86	20.51	0.54
Xyl	A	444945	444742	48118	47863	102	61	415546	22	53	1611	75.37		
	B	420277	420074	38734	38479	103	62	396217	22	53	1554	61.67		
	C	622217	622014	63432	63177	102	61	583476	21	52	2262	100.28	19.15	0.80
Ara	A	510961	510758	53064	52809	103	62	478016	22	53	1875	84.63		
	B	537416	537213	47237	46982	103	62	508084	22	53	1992	75.29		
	C	846410	846207	80035	79780	103	62	796743	21	52	3124	127.85	20.29	0.85
GalA	A	217390	217187	25925	25670	103	62	201272	22	53	789	41.14		
	B	253995	253792	24602	24347	104	63	238575	22	53	947	33.02		
	C	352431	352228	42654	42399	104	63	325729	21	52	1293	67.95	20.82	1.40
GlcA ?	A	6204	6001	1261	1006	103	62	5377	22	53	21	1.61		
	B	7427	7224	1133	878	103	62	6680	22	53	26	1.41		
	C	8630	8427	1571	1316	103	62	7611	21	52	30	2.11	15.28	1.38
Man	A	7885	7682	2484	2229	103	62	6300	22	53	25	3.57		
	B	11562	11359	3056	2801	102	61	9650	22	53	37	4.45		
	C	16569	16366	4966	4711	103	62	13445	21	52	53	7.55	7.44	0.40
Fuc	A	10003	9800	4419	4164	103	62	7218	21	52	28	6.67		
	B	9249	9046	3709	3454	102	61	6939	22	53	27	5.48		
	C	18211	18008	6642	6387	103	62	14048	21	52	55	10.24	4.84	0.27
Rib	A	93701	93498	12316	12061	103	62	86020	21	52	337	19.33		
	B	104368	104165	11171	10916	102	61	97506	22	53	378	17.33		
	C	143841	143638	16253	15998	102	61	133873	21	52	542	25.39	16.84	0.94
Asp ?	A	7873	7670	7308	7053	103	62	3297	21	52	13	11.30		
	B	7307	7704	6825	6570	103	62	3631	22	53	14	10.53		
	C	16416	16213	13567	13312	104	63	7893	21	52	31	21.33	0.88	0.05

Appendix 5 Data set for Fig. 3.22. [^{3}H, ^{14}C]Monosaccharides obtained by TFA hydrolysis of *Arabidopsis* AIR

(*) The counting efficiency was obtained from Appendices 1 – 2. The percentage of ^{14}C falsely detected as ^{3}H was determined from Appendix 3. The ^{3}H background was 203 ± 28.5 counts/20 min and that for ^{14}C was 255 ± 31.9 counts/20 min. In cases where a five-carbon compound was examined it was necessary to adjust the final ^{3}H:^{14}C ratio and its error by a factor of 5/6. In the four-carbon compound Asp, the final ratio and its error was multiplied by 4/6.

	..1..	..2..	..3..	..4..	..5..
	Digested AIR from cells fed [3H]Gal (dpm/100 μl)	Intended [3H]Gal (dpm in 300 μl)	Digested AIR from cells fed [14C]Glc (A -- D) or [14C]Fru (E -- H) (dpm/100 μl)	Intended [14C]Glc at 1/5 level of intended [3H]Gal (dpm)	Intended [14C]Glc at 1/3 level of intended [3H]Gal (dpm)
A	31739	95217	114810	19043	N/A
B	33520	100560	95064	20112	N/A
C	36687	110061	110353	22012	N/A
D	32453	97359	99449	19472	32453
E	26355	79065	24690	15813	26355
F	23184	69552	24186	13910	23184
G	29473	88419	19716	17684	29473
H	23935	71805	21807	14361	N/A

Appendix 6 Data set for section 2.11

A worked example of how the tabulated numbers were derived is shown in section 2.9.1 part 1. (**1**) The amount of ^{3}H (dpm/100 μl) that was present in the digested AIR sample was based on a 47% counting efficiency. (**2**) The intended [^{3}H]Gal (dpm/300 μl) that was to be used to combine ^{3}H-labelled AIR with ^{14}C-labelled AIR was three times the level in column 1. (**3**) The amount of ^{14}C was based on a 93% counting efficiency. (**4**) To combine ^{3}H-labelled AIR with ^{14}C-labelled AIR in a 5:1 ^{3}H:^{14}C (dpm/dpm) ratio, the required amount of ^{14}C (dpm) was one fifth of the amount of ^{3}H in the ^{3}H-labelled AIR. (**5**) In sample D, E, F and G a 3:1 ^{3}H:^{14}C (dpm/dpm) ratio was used throughout the experiment and, in order to compare all of the final isotope ratios (Appendix 8), the intended level of ^{14}C has been included in the above calculations. With the knowledge of the amount of ^{3}H and ^{14}C that had been intended in each sample, any deviation in these values due to the dispensation of a suspension, could be accounted for.

		A		B		C		D	
	Sample	14C[Glc]	3H[Gal]	14C[Glc]	3H[Gal]	14C[Glc]	3H[Gal]	14C[Glc]	3H[Gal]
cpm	1	12303	23440	17638	22749	16065	21773	37777	25465
	2	16095	21122	20701	20863	16472	22344	31716	20459
	3	14599	19697	18190	19755	16290	21050	23529	21954
	4	15994	20402	20621	19454	15184	23470	23388	20812
	5	14364	20704	16255	19671	20125	21651	26018	20454
	6	14476	18476	14567	19425	17043	21953	27551	19352
	Average cpm	14639	20640	17995	20320	16863	22040	28330	21416
	Intended dpm for 3H:14C ratio of 5:1	19043	95217	20112	100560	22012	110061	19472	97359
	Intended dpm for 3H:14C ratio of 3:1	N/A	N/A	N/A	N/A	N/A	N/A	32453	N/A
	Counting efficiency solid AIR	76.9	21.7	89.5	20.2	76.6	20.0	87.3	22.0
	Intended cpm (based on 5:1 3H:14C ratio)	17138.7	21423.8	18100.8	22626.0	19810.8	24763.7	17524.8	21905.8
	Correction factor 1	1.39	0.91	1.03	0.99	1.23	1.14	0.46	0.86
	2	1.06	1.01	0.87	1.08	1.20	1.11	0.55	1.07
	3	1.17	1.09	1.00	1.15	1.22	1.18	0.74	1.00
	4	1.07	1.05	0.88	1.16	1.30	1.06	0.75	1.05
	5	1.19	1.03	1.11	1.15	0.98	1.14	0.67	1.07
	6	1.18	1.16	1.24	1.16	1.16	1.13	0.64	1.13
	3H/14C correction factor 1	0.66		0.97		0.92		1.85	
	2	0.95		1.24		0.92		1.94	
	3	0.93		1.15		0.97		1.34	
	4	0.98		1.32		0.81		1.40	
	5	0.87		1.03		1.16		1.59	
	6	0.98		0.94		0.97		1.78	

		E		F		G		H	
	Sample	14C[Fru]	3H[Gal]	14C[Fru]	3H[Gal]	14C[Fru]	3H[Gal]	14C[Fru]	3H[Gal]
cpm	1	25538	17403	19970	17667	33110	16236	13134	19067
	2	22776	18666	18903	20048	30595	18258	17156	20376
	3	22545	19972	21094	18108	32822	18479	14167	19489
	4	24301	18678	19503	19211	32536	18279	14755	18788
	5	22002	17736	20061	17682	33117	18680	12965	17890
	6	24016	17678	23415	16936	30235	18687	16932	16142
	Average cpm	23530	18356	20491	18275	32069	18103	14852	18625
	Intended dpm for 3H:14C ratio of 5:1	15813	79065	13910	69552	17683	88419	14361	71805
	Intended dpm for 3H:14C ratio of 3:1	26355	N/A	23184	N/A	29473	N/A	N/A	N/A
	Counting efficiency solid AIR	89.3	23.2	88.4	26.3	108.8	20.5	103.4	25.9
	Intended cpm	14231.7	17789.6	12519.0	15649.2	15914.7	19894.3	12924.9	16156.1
	Correction factor 1	0.56	1.02	0.63	0.89	0.48	1.23	0.98	0.85
	2	0.62	0.95	0.66	0.78	0.52	1.09	0.75	0.79
	3	0.63	0.89	0.59	0.86	0.48	1.08	0.91	0.83
	4	0.59	0.95	0.64	0.81	0.49	1.09	0.88	0.86
	5	0.65	1.00	0.62	0.89	0.48	1.07	1.00	0.90
	6	0.59	1.01	0.53	0.92	0.53	1.06	0.76	1.00
	3H/14C correction factor 1	1.83		1.41		2.55		0.86	
	2	1.53		1.18		2.09		1.05	
	3	1.41		1.46		2.22		0.91	
	4	1.63		1.27		2.23		0.98	
	5	1.55		1.42		2.22		0.91	
	6	1.70		1.73		2.02		1.31	

Appendix 7 Correction factor calculated to compensate for error in the dispensation of a suspension. Data set for section 2.11

A worked example of how the tabulated numbers were derived is shown in section 2.9.1 part 2. The AIR formed for each of the [^{3}H]Gal, [U-^{14}C]Glc and [^{14}C]Fru fed cell-suspensions (A – E) was sub-divided into six portions (Sample 1 – 6) that were to be treated with either (Sample 1) cellulase, (Sample 2) EPGase, (Sample 3), Termamyl® 120L, (Sample 4) Driselase and (Sample 5) TFA. The cpm values detected in each of the AIR-suspension samples (1 – 6) were averaged. With the knowledge of the intended dpm (Appendix 6) for each sample, the counting efficiency of solid AIR was calculated. The overall average counting efficiencies of solid AIR for ^{3}H (22.5%) and ^{14}C (90.0%) were used to determine the intended cpm of each sample. The deviation between the intended cpm of each sample and the actual cpm value detected was calculated (correction factor 1 – 6). The overall deviation factor from the originally intended 5:1 ^{3}H:^{14}C ratio for each of the partnered ^{3}H-labelled AIR and ^{14}C-labelled AIR samples was determined (^{3}H:^{14}C correction factor 1 – 6).

		Apparent 3H		Apparent 14C												
		Machine-reported counts (cpm)	Back-ground deducted (cpm)	Machine-reported counts (cpm)	Back-ground deducted (cpm)	Average H# number	% false 3H	True 3H (cpm)	Counting efficiency * 3H	Counting efficiency * 14C	3H (Bq)	14C (Bq)	Error factor due to formation of a sus-pension	3H:14C ratio (Bq/Bq)	Average 3H:14C ratio (Bq/Bq)	Standard Error
Gal (ex. XG oligo)	A	355	340	40	19	81	50	330	25	59	330	31	0.7	28.2		
	B	427	412	56	35	76	45	397	27	60	397	59	1.0	24.3		
	C	356	341	54	33	78	46	326	27	60	326	56	0.9	20.4		
	D	399	384	95	74	80	49	348	26	59	348	125	1.9	33.1	26.5	2.4
	E	374	359	93	72	80	50	323	26	59	323	121	1.8	31.3		
	F	248	233	52	31	79	49	218	26	59	218	52	1.4	37.9		
	G	288	273	90	69	81	50	239	25	59	239	117	2.5	35.5		
	H	263	248	43	22	85	50	238	25	58	238	38	0.9	21.4	31.5	3.2
Gal (TFA)	A	2890	2879	293	273	85	50	2743	26	58	179	8	0.9	19.8		
	B	2914	2903	320	300	84	50	2754	26	58	180	9	1.0	21.6		
	C	2970	2959	411	391	84	50	2763	26	58	181	11	1.2	18.7		
	D	3790	3779	467	447	83	50	3555	26	58	232	13	1.6	47.9	27.0	6.1
	E	2203	2192	371	351	84	50	2016	26	58	132	10	1.6	33.8		
	F	2593	2582	389	369	84	50	2397	26	58	157	11	1.4	35.0		
	G	2740	2729	646	626	84	50	2416	26	58	158	18	2.2	32.4		
	H	2437	2426	269	249	84	50	2302	26	58	150	7	0.9	19.1	30.1	3.2
Glc (cellulase)	A	321	310	95	75	84	50	273	26	58	18	2	0.7	5.5		
	B	313	302	109	89	83	50	258	26	58	17	3	1.0	6.4		
	C	608	597	69	49	84	50	573	26	58	37	1	0.9	24.8		
	D	296	285	125	105	83	50	232	26	58	15	3	1.9	15.6	13.0	3.9
	E	356	345	209	189	83	50	251	26	58	16	5	1.8	9.3		
	F	455	444	245	225	83	50	331	26	58	22	6	1.4	7.9		
	G	220	209	203	183	83	50	118	26	58	8	5	2.5	6.2		
	H	291	280	132	112	84	50	224	26	58	15	3	0.9	3.9	6.8	1.0
Glc (TFA)	A	2070	2059	529	509	85	50	1805	26	58	118	15	0.9	7.0		
	B	1697	1686	381	361	83	50	1506	26	58	98	10	1.0	9.8		
	C	5993	5982	567	547	84	50	5709	26	58	373	16	1.2	27.6		
	D	1905	1894	639	619	84	50	1584	26	58	104	18	1.6	15.4	14.9	3.9
	E	1593	1582	703	683	84	50	1240	26	58	81	20	1.6	10.7		
	F	1464	1453	662	642	83	50	1132	26	58	74	18	1.4	9.5		
	G	1650	1639	1105	1085	83	50	1097	26	58	72	31	2.2	8.5		
	H	1254	1243	513	493	84	50	996	26	58	65	14	0.9	4.2	8.2	1.2
Glc (IsoP, Driselase)	A	300	289	103	81	84	50	248	26	58	16	2	1.0	6.9		
	B	336	325	102	80	85	50	285	26	58	19	2	1.3	10.7		
	C	418	407	89	67	85	50	374	25	58	25	2	0.8	10.4		
	D	358	347	94	72	86	50	311	25	58	21	2	1.4	23.4	12.8	3.1
	E	368	357	133	111	86	50	302	25	58	20	3	1.6	17.2		
	F	320	309	99	77	86	50	271	25	57	18	2	1.3	16.9		
	G	369	358	160	138	84	50	289	26	58	19	4	2.2	17.7		
	H	333	322	83	61	85	50	292	25	58	19	2	1.0	10.8	15.7	1.4

Appendix 8 ^{3}H:^{14}C Ratios of monosaccharides obtained by different methods from the AIR. Data set for Fig. 3.38

(*) The counting efficiency was obtained from Appendices 1 − 2. The percentage of ^{14}C falsely detected as ^{3}H was determined from Appendix 3. In cases where a five-carbon compound was examined it was necessary to adjust the final ^{3}H:^{14}C ratio and its error by a factor of 5/6. Samples A − D were cells that had originally fed [U-^{14}C]Glc. Samples E − F had originally been fed [U-^{14}C]Fru. The error factor due to the formation of a suspension was obtained from Appendix 7.

Continued overleaf

		Apparent 3H		Apparent 14C												
		Machine-reported counts (cpm)	Back-ground deducted (cpm)	Machine-reported counts (cpm)	Back-ground deducted (cpm)	Average H# number	% false 3H	True 3H (cpm)	Counting efficiency * 3H	Counting efficiency * 14C	3H (Bq)	14C (Bq)	Error factor due to formation of a sus-pension	3H:14C ratio (Bq/Bq)	Average 3H:14C ratio (Bq/Bq)	Standard Error
Glc (IsoP, Cellulase)	A	616	574	101	79	95	55	531	23	59	38	2	0.7	11.2		
	B	704	662	142	120	95	55	597	23	59	43	3	1.0	12.2		
	C	671	629	137	114	94	55	567	23	59	41	3	0.9	11.6		
	D	896	854	327	305	96	55	688	23	59	50	9	1.9	17.9	13.2	1.4
	E	602	561	215	193	95	55	455	23	59	33	5	1.8	18.2		
	F	535	493	152	130	95	55	422	23	59	30	4	1.4	19.4		
	G	587	545	258	236	95	55	417	23	59	30	7	2.5	19.0		
	H	556	514	107	85	95	55	468	23	59	33	2	0.9	11.9	17.1	1.5
Xyl (IsoP, Driselase)	A	284	273	86	63	77	48	243	27	60	15	2	1.0	7.1		
	B	288	277	81	59	78	48	249	27	60	16	2	1.3	10.5		
	C	311	300	69	47	79	48	278	26	59	18	1	0.8	9.0		
	D	301	290	75	53	79	48	264	26	59	17	2	1.4	21.8	12.1	2.9
	E	354	343	106	84	78	48	302	26	60	19	2	1.6	18.5		
	F	284	273	81	59	78	48	245	26	60	16	2	1.3	16.5		
	G	304	293	123	101	78	48	245	27	60	15	3	2.2	16.9		
	H	289	278	68	45	78	48	256	26	60	16	1	1.0	10.5	15.6	1.5
Xyl (IsoP, Cellulase)	A	580	538	80	58	96	55	507	23	59	36	2	0.7	12.0		
	B	616	574	111	89	95	55	526	23	59	38	3	1.0	12.1		
	C	600	558	107	85	95	55	512	23	59	37	2	0.9	11.7		
	D	756	714	252	230	95	55	589	23	59	42	6	1.9	16.7	13.1	1.0
	E	619	577	171	149	95	55	495	23	59	35	4	1.8	21.4		
	F	501	459	115	93	95	55	409	23	59	29	3	1.4	21.8		
	G	579	537	199	177	95	55	440	23	59	32	5	2.5	22.3		
	H	591	550	86	64	95	55	515	23	59	37	2	0.9	14.6	20.0	1.6
Xyl (TFA)	E	418	376	130	108	96	55	317	23	59	23	3	1.6	15.9		
	F	444	402	129	107	95	55	344	23	59	25	3	1.4	16.0		
	G	520	478	191	169	95	55	386	23	59	28	5	2.2	17.8		
	H	502	460	131	109	96	55	400	23	59	29	3	0.9	7.0	14.2	2.1
Rha (EPGase)	A	90	79	30	10	94	55	73	24	55	5	0	1.0	15.6		
	B	130	119	45	25	93	55	106	24	55	8	1	1.2	12.5		
	C	121	110	37	17	94	55	100	24	55	7	1	0.9	12.4		
	D	199	188	76	56	94	55	157	24	55	11	2	1.9	21.2	15.4	1.8
	E	120	109	48	28	93	55	94	24	55	7	1	1.5	20.0		
	F	134	123	44	24	94	55	110	24	55	8	1	1.2	21.0		
	G	120	109	55	35	94	55	89	24	55	6	1	1.2	11.8		
	H	263	252	64	44	94	55	228	24	55	16	1	1.1	12.8	16.4	2.1
Rha (TFA)	A	328	317	54	34	83	50	300	26	58	20	1	0.9	17.6		
	B	541	530	56	36	84	50	512	26	58	33	1	1.0	33.9		
	C	358	347	72	52	84	50	321	26	58	21	1	1.2	16.4		
	D	418	407	80	60	85	50	377	26	58	25	2	1.6	37.7	26.4	4.7
	E	121	110	44	24	84	50	98	26	58	6	1	1.6	23.9		
	F	140	129	47	27	85	50	115	26	58	8	1	1.4	22.7		
	G	161	150	69	49	84	50	126	26	58	8	1	2.2	21.6		
	H	447	436	39	19	84	50	427	26	58	28	1	0.9	46.72 ?	22.7	0.5

Appendix 8 Continued

Continued overleaf

		Apparent 3H		Apparent 14C												
		Machine-reported counts (cpm)	Back-ground deducted (cpm)	Machine-reported counts (cpm)	Back-ground deducted (cpm)	Average H# number	% false 3H	True 3H (cpm)	Counting efficiency * 3H	Counting efficiency * 14C	3H (Bq)	14C (Bq)	Error factor due to formation of a sus-pension	3H:14C ratio (Bq/Bq)	Average 3H:14C ratio (Bq/Bq)	Standard Error
Ara (Driselase)	A	904	893	153	136	93	55	818	24	55	58	4	1.0	11.5		
	B	816	805	164	147	91	54	726	24	56	50	4	1.3	12.6		
	C	907	896	135	118	93	55	832	24	55	59	4	0.8	11.2		
	D	931	920	206	189	94	56	814	24	55	58	6	1.4	19.6	13.7	1.7
	E	754	743	175	158	93	55	656	24	55	47	5	1.6	22.0		
	F	789	778	156	139	92	55	701	24	55	49	4	1.3	20.6		
	G	891	880	281	264	91	54	737	24	56	51	8	2.2	20.0		
	H	760	749	126	109	92	55	689	24	55	48	3	1.0	11.9	18.6	2.0
Ara (TFA)	A	1433	1422	194	174	85	50	1336	25	58	88	5	0.9	12.7		
	B	1253	1242	192	172	85	50	1156	25	58	76	5	1.0	13.2		
	C	1510	1499	290	270	85	50	1364	25	58	90	8	1.2	11.2		
	D	2107	2096	385	365	85	50	1913	25	58	126	11	1.6	26.4	15.8	3.1
	E	1436	1425	308	288	85	50	1280	25	58	85	8	1.6	21.8		
	F	1299	1288	268	248	85	50	1163	25	58	77	7	1.4	21.0		
	G	1254	1243	413	393	85	50	1046	25	58	69	11	2.2	18.6		
	H	1129	1118	187	167	85	50	1034	25	58	68	5	0.9	10.7	18.0	2.2
GalA (TFA)	A	372	361	44	24	84	50	349	26	58	23	1	0.9	28.5		
	B	308	297	52	32	85	50	281	26	58	18	1	1.0	20.5		
	C	332	321	69	49	85	50	297	26	58	19	1	1.2	16.0		
	D	382	371	79	59	85	50	342	26	58	22	2	1.6	35.0	25.0	3.7
	E	143	132	40	20	84	50	123	26	58	8	1	1.6	36.9		
	F	155	144	40	20	85	50	133	26	58	9	1	1.4	35.7		
	G	104	93	58	38	84	50	74	26	58	5	1	2.2	16.7		
	H	195	184	37	17	84	50	175	26	58	11	0	0.9	21.3	27.6	4.4
GalA (Driselase)	A	1361	1350	281	261	91	54	1209	24	56	84	8	1.0	10.5		
	B	1474	1463	362	342	93	55	1274	24	55	90	10	1.3	11.5		
	C	1583	1572	305	285	93	56	1412	24	55	100	9	0.8	9.4		
	D	1723	1712	456	436	93	55	1472	24	55	104	13	1.4	18.5	12.5	1.8
	E	1631	1620	518	498	91	54	1351	24	56	94	15	1.6	17.0		
	F	1688	1677	418	398	92	55	1458	24	55	103	12	1.3	18.1		
	G	1799	1788	708	688	92	55	1410	24	55	100	21	2.2	17.8		
	H	1580	1569	335	315	92	55	1396	24	55	99	10	1.0	10.2	15.8	1.6
GalA(EPGase, oligo)	A	268	257	56	36	84	50	239	26	58	16	1	1.0	14.5		
	B	404	393	72	52	84	50	367	26	58	24	2	1.2	19.7		
	C	250	239	54	34	85	50	222	26	58	15	1	0.9	13.7		
	D	337	326	101	81	84	50	286	26	58	19	2	1.9	26.0	18.5	2.5
	E	791	780	70	50	84	50	755	26	58	49	1	1.5	87.59 ?		
	F	354	343	67	47	84	50	319	26	58	21	1	1.2	30.3		
	G	404	393	85	65	84	50	361	26	58	24	2	1.2	24.9		
	H	353	342	71	51	84	50	317	26	58	21	1	1.1	15.0	23.4	3.7

Appendix 8 Continued

Continued overleaf

		Apparent 3H		Apparent 14C												
		Machine-reported counts (cpm)	Back-ground deducted (cpm)	Machine-reported counts (cpm)	Back-ground deducted (cpm)	Average H# number	% false 3H	True 3H (cpm)	Counting efficiency * 3H	Counting efficiency * 14C	3H (Bq)	14C (Bq)	Error factor due to formation of a sus-pension	3H:14C ratio (Bq/Bq)	Average 3H:14C ratio (Bq/Bq)	Standard Error
Rib (TFA)	A	283	272	65	45	85	50	249	25	57	16	1	0.9	9.0		
	B	291	280	69	49	84	50	255	26	58	17	1	1.0	10.1		
	C	368	357	87	67	84	50	324	26	57	21	2	1.2	10.5		
	D	360	349	93	73	85	50	312	25	57	21	2	1.6	21.2	12.7	2.5
	E	311	300	104	84	85	50	259	25	57	17	2	1.6	15.0		
	F	304	293	97	77	85	50	255	25	57	17	2	1.4	14.8		
	G	318	307	137	117	85	50	249	26	57	16	3	2.2	14.7		
	H	285	274	69	49	84	50	250	26	58	16	1	0.9	8.7	13.3	1.3
Glc (ex. Starch)	A	196	186	69	49	74	45	163	27	62	10	1	0.9	7.0		
	B	143	133	50	30	75	45	119	27	61	7	1	1.2	10.3		
	C	472	462	51	31	74	45	448	27	62	28	1	1.2	37.3 ?		
	D	100	89	55	35	75	45	73	27	61	5	1	1.3	10.6	9.3	1.0
	E	180	170	94	75	75	45	136	27	61	8	2	1.4	9.8		
	F	155	145	94	75	75	45	111	27	61	7	2	1.5	8.2		
	G	141	131	141	122	76	45	76	27	61	5	3	2.2	5.3		
	H	124	113	79	59	76	45	87	27	61	5	2	0.9	3.1	6.6	1.3

Appendix 8 Continued

		Apparent 3H			Apparent 14C						Counting efficiency *							
	Time (min)	Total counts registered in 1 h	Minus back-ground count	Sample error (2σ) combined with error of back-ground error (2σ)	Total counts registered in 1 h	Minus back-ground count	Sample error (2σ) combined with error of back-ground error (2σ)	Average H# number	% false 3H	True 3H (counts)	3H	14C	3H (Bq)	3H error (± Bq)	14C (Bq)	14C error (± Bq)	3H:14C ratio (Bq/Bq)	Error of ratio
Gal from Gal monophosphate(s) (Z- 2)	0	4263	0		1175	0	0											
	0.25	18184	13921	300	1335	160	160	73	45	13848.9	27	62	14.25	0.33	0.07	0.05	198.76	124.93
	1	224393	220130	956	2881	1706	1706	73	45	219362	27	62	225.68	0.99	0.76	0.06	295.28	22.13
	1.5	263576	259313	1035	3567	2392	2392	73	45	258237	27	62	265.68	1.07	1.07	0.06	247.90	14.33
	2.5	209438	205175	925	3271	2096	2096	74	45	204232	27	62	210.11	0.96	0.95	0.06	220.15	14.07
	4	465315	461052	1371	6643	5468	5468	74	45	458591	27	62	471.80	1.42	2.45	0.08	192.59	6.26
	8	630277	626014	1593	12119	10944	10944	75	45	621089	27	61	638.98	1.66	4.98	0.11	128.22	2.72
	10	556993	552730	1498	15095	13920	13920	73	45	546466	27	62	562.21	1.56	6.24	0.11	90.15	1.67
	14	543034	538771	1480	22072	20897	20897	73	45	529367	27	62	544.62	1.55	9.36	0.14	58.17	0.87
	18	502263	498000	1423	21000	19825	19825	75	45	489079	27	61	503.17	1.50	9.03	0.14	55.74	0.85
	25	991838	987575	1996	60916	59741	59741	72	45	960692	27	62	988.37	2.12	26.77	0.22	36.93	0.32
	40	373948	369685	1230	32453	31278	31278	74	45	355610	27	62	365.85	1.32	14.01	0.16	26.11	0.32
	120	412370	408107	1291	59876	58701	58701	74	45	381691	27	62	392.69	1.42	26.30	0.22	14.93	0.14
Gal from UDP-Gal (Z- 1)	0	4227	0		2043	0												
	0.25	13059	8832	263	2990	947	142	73	45	8406	27	62	8.65	0.31	0.42	0.06	20.39	3.13
	1	501294	497067	1422	7506	5463	195	72	45	494609	27	62	508.86	1.48	2.45	0.09	207.90	7.46
	1.5	300002	295775	1103	5284	3241	171	73	45	294317	27	62	302.79	1.15	1.45	0.08	208.53	11.03
	2.5	293110	288883	1091	7270	5227	193	72	45	286531	27	62	294.79	1.14	2.34	0.09	125.88	4.67
	4	993971	989744	1998	20547	18504	300	73	45	981417	27	62	1009.69	2.08	8.29	0.13	121.79	1.99
	8	1020540	1016313	2025	31954	29911	369	72	45	1002853	27	62	1031.74	2.12	13.40	0.17	76.99	0.96
	10	703613	699386	1683	27108	25065	341	72	45	688107	27	62	707.93	1.77	11.23	0.15	63.04	0.87
	14	456812	452585	1358	24071	22028	323	73	45	442672	27	62	455.42	1.44	9.87	0.14	46.15	0.69
	18	465214	460987	1370	26225	24182	336	72	45	450105	27	62	463.07	1.45	10.83	0.15	42.74	0.61
	25	1139195	1134968	2139	86407	84364	595	72	45	1097004	27	62	1128.61	2.28	37.80	0.27	29.86	0.22
	40	1100572	1096345	2102	109989	107946	669	72	45	1047769	27	62	1077.95	2.27	48.36	0.30	22.29	0.15
	120	417064	412837	1298	157227	155184	798	72	45	343004	27	62	352.88	1.57	69.53	0.36	5.08	0.03
Glc from UDP-Glc (Z- 1)	0	1742	0		1628	0												
	0.25	4571	2829	159	2099	738	122	72	45	2497	27	62	2.57	0.21	0.33	0.05	7.77	1.43
	1	260854	259112	1025	69714	68353	534	72	45	228353	27	62	234.93	1.19	30.62	0.24	7.67	0.07
	1.5	249437	247695	1002	33517	32156	375	71	45	233225	27	62	239.94	1.10	14.41	0.17	16.65	0.21
	2.5	218755	217013	939	31257	29896	363	72	45	203560	27	62	209.42	1.04	13.39	0.16	15.64	0.20
	4	955740	953998	1957	165246	163885	817	74	45	880250	27	62	912.36	2.20	73.43	0.37	12.43	0.07
	8	1544176	1542434	2487	204150	202789	907	72	45	1451179	27	62	1492.98	2.72	90.86	0.41	16.43	0.08
	10	1138984	1137242	2136	165799	164438	818	72	45	1063245	27	62	1093.87	2.35	73.67	0.37	14.85	0.08
	14	1316438	1314696	2296	176654	175293	844	73	45	1235814	27	62	1280.90	2.54	78.54	0.38	16.31	0.08
	18	1586128	1584386	2520	230255	228894	963	73	45	1481384	27	62	1535.43	2.80	102.55	0.43	14.97	0.07
	25	3242592	3240850	3602	604154	602793	1557	73	45	2969593	27	62	3077.94	4.07	270.07	0.70	11.40	0.03
	40	2967299	2965557	3446	641124	639763	1603	73	45	2677663	27	62	2775.36	3.94	286.63	0.72	9.68	0.03
	120	1526907	1525165	2473	899392	898031	1898	73	45	1121051	27	62	1161.95	3.23	402.34	0.85	2.89	0.01

Appendix 9 Kinetics of radiolabel incorporation into intermediary metabolites. Data set for section 3.2.3, Fig. 3.57 and Fig. 3.58.

(*) The counting efficiency was obtained from Appendices 1 − 2. The percentage of ^{14}C falsely detected as ^{3}H was determined from Appendix 3. In cases where a five-carbon compound was examined it was necessary to adjust the final ^{3}H:^{14}C ratio and its error by a factor of 5/6. The zone number (Z) relates to the area of electrophoretogram (Fig. 3.40) that each compound was originally taken from. The background counts is taken to be the sample that contains the lowest level of ^{3}H and ^{14}C in the time course.

Continued overleaf

	Time (min)	Apparent 3H: Total counts registered in 1 h	Apparent 3H: Minus background count	Apparent 3H: Sample error (2σ) combined with error of background error (2σ)	Apparent 14C: Total counts registered in 1 h	Apparent 14C: Minus background count	Apparent 14C: Sample error (2σ) combined with error of background error (2σ)	Average H# number	% false 3H	True 3H (counts)	Counting efficiency * 3H	Counting efficiency * 14C	3H (Bq)	3H error (± Bq)	14C (Bq)	14C error (± Bq)	3H:14C ratio (Bq/Bq)	Error of ratio
GlcA from UDP-GlcA (Z, 1)	0	1292			1196													
	0.25	1713	0		1144	0												
	1	2161	448	125	1351	207	100	73	45	355	27	62	0.37	0.16	0.09	0.04	3.28	2.17
	1.5	2694	981	133	1467	323	103	74	45	836	27	61	0.86	0.17	0.15	0.05	4.87	1.84
	2.5	2966	1253	137	1408	264	102	73	45	1134	27	62	1.17	0.18	0.12	0.05	8.22	3.41
	4	5208	3495	166	2119	975	115	74	45	3056	27	62	3.14	0.21	0.44	0.05	6.00	0.81
	8	9694	7981	214	2347	1203	119	73	45	7439	27	62	7.65	0.25	0.54	0.05	11.83	1.23
	10	11859	10146	233	2770	1626	126	74	45	9414	27	62	9.69	0.27	0.73	0.06	11.08	0.91
	14	12970	11257	242	2930	1786	128	74	45	10453	27	62	10.75	0.28	0.80	0.06	11.20	0.86
	18	17709	15996	279	3938	2794	143	75	45	14739	27	61	15.16	0.32	1.27	0.07	9.93	0.55
	25	23668	21955	319	6334	5190	173	74	45	19619	27	62	20.18	0.37	2.33	0.08	7.23	0.28
	40	21726	20013	306	6603	5459	177	74	45	17556	27	61	18.06	0.36	2.49	0.08	6.05	0.23
	120	7313	5600	190	4883	3739	156	75	45	3918	27	61	4.03	0.25	1.70	0.07	1.97	0.15
GalA from UDP-GalA (Z, 1)	0	1090			1112													
	0.25	1359			1122													
	1	1259	0		1109	0												
	1.5	2027	768	115	1260	151	98	71	45	700	27	62	0.72	0.15	0.07	0.04	8.87	6.04
	2.5	2337	1078	120	1330	218	99	73	45	980	27	62	1.01	0.16	0.10	0.04	8.59	4.13
	4	3964	2705	145	1627	515	105	72	45	2473	27	62	2.54	0.18	0.23	0.05	9.19	1.98
	8	9737	8478	210	2180	1068	115	72	45	7997	27	62	8.23	0.25	0.48	0.05	14.33	1.60
	10	10009	8750	212	2349	1237	118	74	45	8193	27	61	8.43	0.25	0.56	0.05	12.47	1.24
	14	11306	10047	224	2487	1375	120	73	45	9428	27	62	9.70	0.26	0.62	0.05	13.12	1.20
	18	14836	13577	254	3112	2000	130	74	45	12677	27	62	13.04	0.29	0.90	0.06	12.13	0.84
	25	16700	15441	268	4500	3388	150	73	45	13917	27	62	14.32	0.32	1.52	0.07	7.86	0.39
	40	23209	21950	313	6541	5429	175	73	45	19507	27	62	20.07	0.37	2.43	0.08	6.88	0.26
	120	10389	9130	216	6180	5068	171	74	45	6849	27	61	7.05	0.28	2.31	0.08	2.54	0.13
Xyl from UDP-Xyl (Z, 1)	0	1648	0		2112	0												
	0.25	1911	263	119	2148	36	131	75	45	247	27	61	0.26	0.19	0.02	0.06	13.15	48.63
	1	3729	2081	147	3243	1131	146	74	45	1572	27	61	1.65	0.22	0.52	0.07	2.67	0.49
	1.5	4855	3207	161	2591	479	137	75	45	2992	27	61	3.14	0.22	0.22	0.06	11.98	3.53
	2.5	5125	3477	165	2593	481	137	77	45	3261	26	61	3.48	0.23	0.22	0.06	13.26	3.88
	4	8545	6897	202	4595	2483	164	75	45	5780	27	61	6.06	0.27	1.13	0.07	4.46	0.36
	8	20659	19011	299	4650	2538	165	76	45	17869	26	61	19.09	0.36	1.16	0.07	13.77	0.93
	10	22108	20460	308	4780	2668	166	76	45	19259	26	61	20.58	0.37	1.21	0.08	14.11	0.92
	14	30166	28518	357	7217	5105	193	74	45	26221	27	62	27.49	0.43	2.29	0.09	10.01	0.41
	18	44414	42766	429	8902	6790	210	75	45	39710	27	61	41.63	0.50	3.09	0.10	11.22	0.37
	25	133331	131683	735	21636	19524	308	74	45	122897	27	61	128.82	0.84	8.89	0.14	12.07	0.21
	40	125745	124097	714	23801	21689	322	75	45	114337	27	61	119.85	0.82	9.88	0.15	10.11	0.17
	120	58512	56864	491	28068	25956	347	74	45	45184	27	62	47.36	0.63	11.63	0.16	3.39	0.06

Appendix 9

Continued overleaf

	Time (min)	Apparent 3H: Total counts registered in 1 h	Apparent 3H: Minus background count	Apparent 3H: Sample error (2σ) combined with error of background error (2σ)	Apparent 14C: Total counts registered in 1 h	Apparent 14C: Minus background count	Apparent 14C: Sample error (2σ) combined with error of background error (2σ)	Average H# number	% false 3H	True 3H (counts)	Counting efficiency * 3H	Counting efficiency * 14C	3H (Bq)	3H error (± Bq)	14C (Bq)	14C error (± Bq)	3H:14C ratio (Bq/Bq)	Error of ratio
Ara from UDP-Ara (Z_1)	0	4221	4221			1256												
	0.25	4521	4521			1300												
	1	3891	3891			1571												
	1.5	4335	4335	0		1568	0											
	2.5	5531	5531	1196	199	2031	463	75	45	988	27	61	1.04	0.24	0.21	0.05	4.09	1.43
	4	6265	6265	1930	206	2321	753	75	45	1591	27	61	1.67	0.25	0.34	0.06	4.06	0.91
	8	10889	10889	6554	247	3140	1572	74	45	5846	27	62	6.01	0.29	0.70	0.06	7.12	0.71
	10	10872	10872	6537	247	2154	586	76	45	6273	27	61	6.58	0.29	0.27	0.06	20.54	4.37
	14	16334	16334	11999	288	2893	1325	77	45	11403	26	60	12.18	0.34	0.61	0.06	16.55	1.73
	18	24044	24044	19709	337	3637	2069	77	45	18778	26	60	20.06	0.39	0.96	0.07	17.45	1.26
	25	97971	97971	93636	640	14777	13209	74	45	87692	27	61	90.22	0.71	6.02	0.12	12.50	0.26
	40	89886	89886	85551	614	14201	12633	75	45	79866	27	61	83.72	0.70	5.75	0.11	12.13	0.26
	120	41858	41858	37523	430	16721	15153	74	45	30704	27	62	31.59	0.52	6.79	0.12	3.88	0.09
Glc from Glc 1-P (Z_2)	0	1032	0		1373	0												
	0.25	1856	824	107	1477	104	107	75	45	777	27	61	0.81	0.16	0.05	0.05	17.17	17.90
	1	41686	40654	413	11817	10444	230	73	45	35954	27	62	36.99	0.49	4.68	0.10	7.91	0.20
	1.5	83098	82066	580	12402	11029	235	74	45	77103	27	62	79.32	0.64	4.94	0.11	16.05	0.37
	2.5	50879	49847	456	6994	5621	183	75	45	47318	27	61	49.60	0.51	2.56	0.08	19.38	0.66
	4	147889	146857	772	22047	20674	306	74	45	137554	27	61	141.52	0.85	9.41	0.14	15.03	0.24
	8	271655	270623	1044	41181	39808	413	75	45	252710	27	61	264.89	1.18	18.13	0.19	14.61	0.16
	10	399364	398332	1266	47896	46523	444	74	45	377397	27	62	388.27	1.38	20.84	0.20	18.63	0.19
	14	639883	638851	1601	82057	80684	578	75	45	602543	27	61	631.60	1.78	36.74	0.26	17.19	0.13
	18	713283	712251	1690	93850	92477	617	74	45	670636	27	62	689.96	1.85	41.43	0.28	16.65	0.12
	25	1085782	1084750	2085	203100	201727	904	74	45	993973	27	62	1022.61	2.34	90.38	0.41	11.31	0.06
	40	628646	627614	1587	134099	132726	736	75	45	567887	27	61	595.27	1.83	60.44	0.34	9.85	0.06
	120	359370	358338	1201	202826	201453	904	75	45	267684	27	61	280.59	1.58	91.74	0.41	3.06	0.02
Glc from ADP-Glc (Z_3)	0	4771			1365													
	0.25	3686			1384													
	1	4440			1532													
	1.5	5715	0		1517	0												
	2.5	5891	176	215	1531	14	110	74	45	170	27	62	0.17	0.25	0.01	0.05	28.06	226.59
	4	7782	2067	224	2046	529	119	73	45	1829	27	62	1.88	0.26	0.24	0.05	7.94	2.10
	8	12811	7096	265	2548	1031	128	74	45	6632	27	62	6.82	0.30	0.46	0.06	14.77	1.94
	10	10298	4583	245	2044	527	119	74	45	4346	27	62	4.47	0.28	0.24	0.05	18.93	4.45
	14	13272	7557	269	2623	1106	129	75	45	7059	27	61	7.40	0.31	0.50	0.06	14.69	1.82
	18	6787	1072	215	1726	209	114	75	45	978	27	61	1.03	0.26	0.10	0.05	10.78	6.46
	25	11952	6237	259	2960	1443	134	74	45	5588	27	62	5.75	0.30	0.65	0.06	8.89	0.95
	40	18551	12836	305	4700	3183	158	74	45	11404	27	61	11.73	0.35	1.45	0.07	8.09	0.47
	120	8689	2974	232	3405	1888	140	74	45	2124	27	61	2.19	0.28	0.86	0.06	2.54	0.38
Glc from Glc 6-P (Z_2)	0	3850	0		8	0												
	0.25	11049	7199	244	12739	12731	226	75	45	1470	27	62	1.50	0.41	5.70	0.12	0.26	0.07
	1	237842	233992	983	173350	173342	833	73	45	155988	27	62	160.48	1.49	77.66	0.40	2.07	0.02
	1.5	369934	366084	1223	250458	250450	1001	74	45	253381	27	62	260.68	1.86	112.21	0.47	2.32	0.02
	2.5	314160	310310	1128	181786	181778	853	74	45	228510	27	61	234.17	1.62	82.78	0.41	2.83	0.02
	4	1027734	1023884	2031	361175	361167	1202	74	45	861359	27	62	886.17	2.71	161.66	0.57	5.48	0.03
	8	2348472	2344622	3067	718628	718620	1695	75	45	2021243	27	61	2074.56	3.97	327.24	0.82	6.34	0.02
	10	3657045	3653195	3827	1005483	1005475	2005	74	45	3200731	27	62	3292.93	4.85	458.21	0.96	7.19	0.02
	14	5428376	5424526	4661	1314525	1314517	2293	74	45	4832993	27	62	4960.52	5.90	588.35	1.09	8.43	0.02
	18	6649347	6645497	5159	1501195	1501187	2450	74	45	5969963	27	62	6141.94	6.43	684.28	1.18	8.98	0.02
	25	11199575	11195725	6694	2652484	2652476	3257	74	45	10002111	27	62	10290.24	8.34	1209.35	1.59	8.51	0.01
	40	6701275	6697425	5179	1838186	1838178	2712	75	45	5870245	27	61	6028.32	6.54	837.06	1.32	7.20	0.01
	120	4407371	4403521	4201	2612928	2612920	3233	75	45	3227707	27	61	3315.49	5.88	1189.85	1.58	2.79	0.01

Appendix 9

Continued overleaf

		Apparent 3H			Apparent 14C													
	Time (min)	Total counts registered in 1 h	Minus back-ground count	Sample error (2σ) combined with error of back-ground error (2σ)	Total counts registered in 1 h	Minus back-ground count	Sample error (2σ) combined with error of back-ground error (2σ)	Average H# number	% false 3H	True 3H (counts)	Counting efficiency * 3H	Counting efficiency * 14C	3H (Bq)	3H error (± Bq)	14C (Bq)	14C error (± Bq)	3H:14C ratio (Bq/Bq)	Error of ratio
Glc from Suc (Z. 4)	0	855			1281			95	55									
	0.25	992	0		1444	0		96	58									
	1	8904	7912	199	4576	3132	155	94	55	6189	23	55	7.56	0.31	1.58	0.08	4.78	0.31
	1.5	21191	20199	298	4403	2959	153	96	58	18498	22	54	23.09	0.42	1.52	0.08	15.17	0.83
	2.5	28441	27449	343	4999	3555	161	95	55	25494	23	55	31.47	0.47	1.81	0.08	17.37	0.83
	4	72201	71209	541	18137	16693	280	95	55	62028	23	55	76.58	0.75	8.51	0.14	9.00	0.17
	8	196693	195701	889	28814	27370	348	94	58	179963	23	55	219.74	1.17	13.82	0.18	15.90	0.22
	10	617492	616500	1573	89831	88387	604	96	55	567887	22	54	708.97	2.10	45.47	0.31	15.59	0.12
	14	1731941	1730949	2633	263716	262272	1030	95	55	1586699	23	55	1958.89	3.49	133.68	0.52	14.65	0.06
	18	2789427	2788435	3341	432930	431486	1318	94	55	2551118	23	55	3114.92	4.39	217.92	0.67	14.29	0.05
	25	8659950	8658958	5886	1571887	1570443	2509	95	55	7795214	23	55	9623.72	7.90	800.43	1.28	12.02	0.02
	40	10433880	10432888	6461	2049102	2047658	2864	96	58	9255485	22	54	11554.91	8.82	1053.32	1.47	10.97	0.02
	120	16998090	16997098	8246	5770727	5769283	4805	95	55	13823992	23	55	17066.66	11.78	2940.51	2.45	5.80	0.01
Fru from Suc (Z. 4)	0	1861	0		2130	0												
	0.25	2648	787	134	3665	1535	152	75	45	96	27	61	0.10	0.21	0.70	0.07	0.14	0.30
	1	11899	10038	235	17233	15103	278	73	45	3242	27	62	3.33	0.37	6.77	0.12	0.49	0.06
	1.5	11216	9355	229	15348	13218	264	73	45	3407	27	62	3.51	0.36	5.92	0.12	0.59	0.06
	2.5	15933	14072	267	17441	15311	280	75	45	7182	27	61	7.53	0.41	6.97	0.13	1.08	0.06
	4	55400	53539	479	44476	42346	432	75	45	34483	27	61	36.15	0.68	19.28	0.20	1.87	0.04
	8	164975	163114	817	114465	112335	683	76	45	112563	27	61	117.99	1.12	51.15	0.31	2.31	0.03
	10	320531	318670	1136	174582	172452	841	74	45	241066	27	62	248.01	1.45	77.26	0.38	3.21	0.02
	14	1054554	1052693	2056	441783	439653	1333	76	45	854849	27	61	896.07	2.57	200.21	0.61	4.48	0.02
	18	1757777	1755916	2853	640245	638115	1603	75	45	1468764	27	61	1539.59	3.25	290.58	0.73	5.30	0.02
	25	6239085	6237224	4996	2088852	2086722	2892	72	45	5298199	27	62	5450.82	5.94	934.91	1.30	5.83	0.01
	40	7048212	7046351	5310	2412385	2410255	3108	76	45	5961736	27	61	6249.20	6.45	1097.57	1.42	5.69	0.01
	120	10856730	10854869	6590	5536840	5534710	4707	75	45	8364250	27	61	8767.56	8.49	2520.36	2.14	3.48	0.00
Man from GDP-Man (Z. 3)	0	4562			1346													
	0.25	4487			1491													
	1	4355			1385													
	1.5	4227			1312													
	2.5	3672	0		1368	0												
	4	3801	129	173	1826	458	113	75	45	-77	27	61	-0.08	0.21	0.21	0.05	-0.38	-1.02
	8	4243	571	178	1491	123	107	73	45	-166	27	62	-0.17	0.21	0.24	0.05	-0.71	-0.89
	10	4505	833	181	1826	458	113	75	45	627	27	61	0.66	0.22	0.21	0.05	3.15	1.32
	14	4219	547	178	2556	1188	125	70	45	13	28	63	0.01	0.22	0.52	0.06	0.02	0.41
	18	5744	2072	194	3382	2014	138	74	45	1166	27	61	1.20	0.24	0.92	0.06	1.31	0.28
	25	9140	5468	226	7620	6252	190	74	45	2655	27	61	2.73	0.30	2.85	0.09	0.96	0.11
	40	11865	8193	249	8798	7430	202	74	45	4850	27	61	4.99	0.33	3.38	0.09	1.47	0.11
	120	13781	10109	264	14118	12750	249	73	45	4372	27	62	4.50	0.37	5.71	0.11	0.79	0.07
Inositol (Z-4)	0	32512	0		73957	0		71	45		27	62						
	0.25	35953	3441	524	80146	6189	785	72	45	656	27	62	1	1.0				
	1	39702	7190	538	87508	13551	804	73	45	1092	27	62	1	1.0				
	1.5	37514	5002	530	81993	8036	790	73	45	1386	27	62	1	1.0				
	2.5	37863	5351	531	82258	8301	791	73	45	1615	27	62	2	1.0				
	4	35591	3079	522	79625	5668	784	72	45	528	27	62	1	1.0				
		25269	-7243	481	54710	-19247	717	73	45	1418	27	62	1	0.9				
	8	38772	6260	534	83941	9984	795	73	45	1767	27	62	2	1.0				
	10	32878	366	512	69251	-4706	757	73	45	2484	27	62	3	0.9				
	14	38728	6216	534	72109	-1848	764	73	45	7048	27	62	7	1.0				
	18	46126	13614	561	75766	1809	774	74	45	12800	27	62	13	1.0				
	25	70734	38222	643	80935	6978	787	72	45	35082	27	62	36	1.0				
	40	79271	46759	669	75323	1366	773	74	45	46144	27	62	47	1.1				
	120	146367	113855	846	104704	30747	845	73	45	100019	27	62	103	1.2				

Appendix 9

Continued overleaf

		Apparent 3H			Apparent 14C													
	Time (min)	Total counts registered in 1 h	Minus back-ground count	Sample error (2σ) combined with error of back-ground error (2σ)	Total counts registered in 1 h	Minus back-ground count	Sample error (2σ) combined with error of back-ground error (2σ)	Average H# number	% false 3H	True 3H (counts)	Counting efficiency * 3H	Counting efficiency * 14C	3H (Bq)	3H error (± Bq)	14C (Bq)	14C error (± Bq)	3H:14C ratio (Bq/Bq)	Error of ratio
Gal	0	97318			1715													
	0.25	91416	0		1574	0												
	1	100657	9241	877	1861	287	117	80	45	9112	26	60	9.93	0.96	0.13	0.05	74.11	31.06
	1.5	125248	33832	931	1939	365	118	81	45	33668	25	59	36.86	1.03	0.17	0.06	214.53	69.81
	2.5	126231	34815	933	1992	418	119	80	45	34627	26	60	37.72	1.02	0.20	0.06	193.29	55.37
	4	220997	129581	1118	4455	2881	155	81	45	128284	25	59	140.43	1.24	1.36	0.07	103.53	5.65
	8	295247	203831	1244	7496	5922	190	81	45	201166	25	59	220.21	1.38	2.79	0.09	78.98	2.59
	10	427004	335588	1440	12761	11187	239	82	45	330554	25	59	363.65	1.61	5.27	0.11	69.04	1.51
	14	769104	677688	1855	32066	30492	367	82	45	663967	25	59	730.44	2.08	14.36	0.17	50.88	0.63
	18	1110358	1018942	2193	50915	49341	458	82	45	996739	25	59	1096.52	2.46	23.23	0.22	47.20	0.45
	25	4042472	3951056	4066	234515	232941	972	81	45	3846233	25	59	4210.44	4.58	109.67	0.46	38.39	0.17
	40	6217380	6125964	5023	439236	437662	1328	81	45	5929016	25	59	6490.44	5.69	206.06	0.63	31.50	0.10
	120	10028295	9936879	6362	1398563	1396989	2367	82	45	9308234	25	59	10240.08	7.47	657.72	1.11	15.57	0.03
	480	12168627	12077211	7003	4372732	4371158	4183	81	45	10110190	25	59	11067.53	8.93	2057.98	1.97	5.38	0.01
Glc (Total)	0	1528			1814													
	0.25	1299	0		1549	0												
	1	3852	2553	143	3418	1869	141	83	45	1712	25	59	1.90	0.22	0.88	0.07	2.16	0.30
	1.5	8256	6957	195	3217	1668	138	82	45	6206	25	59	6.83	0.26	0.79	0.07	8.69	0.79
	2.5	10222	8923	215	3267	1718	139	81	45	8150	25	59	8.92	0.28	0.81	0.07	11.03	0.96
	4	31523	30224	362	12913	11364	241	81	45	25110	25	59	27.49	0.48	5.35	0.11	5.14	0.14
	8	57709	56410	486	12270	10721	235	83	45	51585	25	59	57.32	0.60	5.05	0.11	11.36	0.28
	10	105465	104166	653	19310	17761	289	82	45	96174	25	59	105.80	0.79	8.36	0.14	12.65	0.23
	14	237066	235767	976	44011	42462	427	82	45	216659	25	59	238.35	1.17	19.99	0.20	11.92	0.13
	18	350272	348973	1186	63511	61962	510	83	45	321090	25	59	356.77	1.43	29.17	0.24	12.23	0.11
	25	1276390	1275091	2261	280961	279412	1063	84	45	1149356	25	58	1287.36	2.80	133.82	0.51	9.62	0.04
	40	1898211	1896912	2756	423755	422206	1304	83	45	1706919	25	59	1896.58	3.39	198.78	0.61	9.54	0.03
	120	2609221	2607922	3231	871719	870170	1869	82	45	2216345	25	59	2438.22	4.11	409.68	0.88	5.95	0.02
	480	20072091	20070792	8961	12818505	12816956	7161	85	45	14303162	25	58	16216.74	13.01	6138.39	3.43	2.64	0.00
GlcA	0	736			1240													
	0.25	692			1162													
	1	735	0		1156	0												
	1.5	1026	291	84	1223	67	98	81	45	261	25	59	0.29	0.14	0.03	0.05	7.53	11.56
	2.5	1032	297	84	1227	71	98	81	45	265	25	59	0.29	0.14	0.03	0.05	7.23	10.55
	4	964	229	82	1284	128	99	81	45	172	25	59	0.19	0.14	0.06	0.05	2.60	2.79
	8	2011	1276	105	1354	198	100	83	45	1187	25	59	1.32	0.16	0.09	0.05	11.80	6.14
	10	5425	4690	157	1787	631	109	83	45	4406	25	59	4.90	0.21	0.30	0.05	13.73	2.43
	14	8139	7404	188	2431	1275	120	81	45	6830	25	59	7.48	0.24	0.60	0.06	10.38	1.03
	18	9451	8716	202	2713	1557	124	81	45	8015	25	59	8.77	0.26	0.73	0.06	9.98	0.85
	25	23506	22771	311	5686	4530	165	82	45	20732	25	59	22.81	0.39	2.13	0.08	8.91	0.36
	40	27975	27240	339	7927	6771	191	81	45	24193	25	59	26.48	0.43	3.19	0.09	6.92	0.22
	120	21015	20280	295	10668	9512	217	82	45	16000	25	25	17.60	0.40	10.46	0.24	1.40	0.05
	480	81063	80328	572	68657	67501	528	83	45	49953	25	59	55.50	0.87	31.78	0.25	1.46	0.03

Appendix 10 Kinetics of radiolabel incorporation into the monosaccharide components of the AIR. Data set for section 3.2.3, Fig. 3.39, Fig. 3.60 and Fig. 3.61

Additional details as per Appendix 10.

Continued overleaf

		Apparent 3H			Apparent 14C													
	Time (min)	Total counts registered in 1 h	Minus back-ground count	Sample error (2σ) combined with error of back-ground error (2σ)	Total counts registered in 1 h	Minus back-ground count	Sample error (2σ) combined with error of back-ground error (2σ)	Average H# number	% false 3H	True 3H (counts)	Counting efficiency * 3H	Counting efficiency * 14C	3H (Bq)	3H error (± Bq)	14C (Bq)	14C error (± Bq)	3H:14C ratio (Bq/Bq)	Error of ratio
GalA	0	910			1121													
	0.25	703	0		1137	0												
	1	845	142	79	1196	59	96	70	45	115	28	64	0.11	0.12	0.03	0.04	3.74	7.33
	1.5	1018	315	83	1172	35	96	70	45	299	28	64	0.30	0.13	0.02	0.04	16.23	44.83
	2.5	1497	794	94	1312	175	99	71	45	715	28	63	0.72	0.14	0.08	0.04	7.79	4.63
	4	1812	1109	100	1249	112	97	69	45	1059	28	64	1.05	0.14	0.05	0.04	18.02	15.86
	8	4861	4158	149	1506	369	103	69	45	3992	28	64	3.96	0.18	0.16	0.04	20.61	5.80
	10	16841	16138	265	2741	1604	124	70	45	15416	28	64	15.29	0.29	0.70	0.05	18.31	1.46
	14	43686	42983	421	5983	4846	169	70	45	40802	28	64	40.48	0.45	2.10	0.07	16.04	0.59
	18	66369	65666	518	8947	7810	201	69	45	62152	28	64	61.66	0.55	3.39	0.09	15.16	0.41
	25	241826	241123	985	34398	33261	377	71	45	226155	28	63	228.44	1.07	14.67	0.17	12.98	0.16
	40	404787	404084	1274	66486	65349	520	69	45	374677	28	64	371.70	1.36	28.36	0.23	10.92	0.10
	120	580516	579813	1525	153164	152027	786	67	45	511401	29	65	498.44	1.67	64.97	0.34	6.39	0.04
	480	1015675	1014972	2016	631796	630659	1591	71	45	731176	28	63	738.56	2.59	278.07	0.70	2.21	0.01
Xyl	0	3804			3489													
	0.25	3890	0		3485	0												
	1	3967	77	177	3514	29	167	82	45	64	25	59	0.07	0.27	0.01	0.08	4.33	29.95
	1.5	6934	3044	208	5246	1761	187	82	45	2251	25	59	2.48	0.31	0.83	0.09	2.49	0.41
	2.5	4356	466	182	3821	336	171	82	45	315	25	59	0.35	0.27	0.16	0.08	1.82	1.72
	4	4889	999	188	3758	273	170	83	45	876	25	59	0.97	0.28	0.13	0.08	6.31	4.33
	8	8158	4354	220	4333	844	177	82	45	3974	25	59	4.37	0.31	0.40	0.08	9.17	2.03
	10	15189	11385	276	4752	1263	181	84	45	10817	25	58	12.12	0.37	0.60	0.09	16.69	2.45
	14	44188	40384	439	8764	5275	221	83	45	38010	25	59	42.23	0.55	2.48	0.10	14.17	0.62
	18	90825	87021	616	14793	11304	270	83	45	81934	25	59	91.04	0.75	5.32	0.13	14.25	0.36
	25	438579	434775	1330	69074	65585	539	82	45	405262	25	59	445.83	1.58	30.88	0.25	12.03	0.11
	40	765448	761644	1754	125553	122064	718	83	45	706715	25	59	785.24	2.11	57.47	0.34	11.39	0.07
	120	1273407	1269603	2260	337209	333720	1167	84	45	1119429	25	58	1253.84	2.85	159.83	0.56	6.54	0.03
	480	3934699	3930895	3969	2208473	2204984	2975	84	45	2938652	25	58	3291.50	5.56	1056.03	1.42	2.60	0.01
Ara	0	2509			3562													
	0.25	1141	0		1630	0												
	1	1249	108	98	1816	186	118	95	55	6	23	55	0.01	0.19	0.09	0.06	0.06	1.66
	1.5	1266	125	98	1753	123	117	95	55	57	23	55	0.07	0.19	0.06	0.06	0.94	2.65
	2.5	1731	590	107	2468	838	128	96	58	108	22	54	0.14	0.21	0.43	0.07	0.26	0.41
	4	1547	406	104	1890	260	119	95	55	263	23	55	0.32	0.19	0.13	0.06	2.04	1.54
	8	5773	4632	166	2825	1195	134	96	58	3945	22	54	4.92	0.27	0.61	0.07	6.68	0.83
	10	8591	7450	197	2762	1132	133	95	55	6828	23	55	8.43	0.29	0.58	0.07	12.18	1.49
	14	52207	51066	462	8336	6706	200	95	55	47378	23	55	58.49	0.62	3.42	0.10	14.26	0.45
	18	117287	116146	688	16618	14988	270	95	55	107902	23	55	133.21	0.91	7.64	0.14	14.53	0.28
	25	764886	763745	1750	115058	113428	683	94	55	701360	23	55	856.36	2.29	57.29	0.35	12.46	0.08
	40	1283320	1282179	2267	204399	202769	908	95	55	1170656	23	55	1445.25	3.01	103.35	0.46	11.65	0.06
	120	2931585	2930444	3425	744317	742687	1727	96	58	2503399	22	54	3125.34	4.79	382.04	0.89	6.82	0.02
	480	6367881	6366740	5047	3417464	3415834	3698	96	58	4402636	22	54	5496.42	7.81	1757.12	1.90	2.61	0.00

Appendix 10 Continued

Continued overleaf

		Apparent 3H			Apparent 14C													
	Time (min)	Total counts registered in 1 h	Minus back-ground count	Sample error (2σ) combined with error of back-ground error (2σ)	Total counts registered in 1 h	Minus back-ground count	Sample error (2σ) combined with error of back-ground error (2σ)	Average H# number	% false 3H	True 3H (counts)	Counting efficiency * 3H	Counting efficiency * 14C	3H (Bq)	3H error (± Bq)	14C (Bq)	14C error (± Bq)	3H:14C ratio (Bq/Bq)	Error of ratio
Man	0	993	0		1539	0												
	0.25	1120	127	92	1762	223	115	79	45	27	26	60	0.03	0.16	0.10	0.05	0.28	1.53
	1	1091	98	91	1810	271	115	80	45	-24	26	60	-0.03	0.16	0.13	0.05	-0.21	-1.27
	1.5	1040	47	90	1661	122	113	80	45	-8	26	60	-0.01	0.16	0.06	0.05	-0.15	-2.76
	2.5	1058	65	91	1765	226	115	80	45	-37	26	60	-0.04	0.16	0.11	0.05	-0.38	-1.52
	4	1183	190	93	1936	397	118	82	45	11	25	59	0.01	0.17	0.19	0.06	0.07	0.88
	8	1226	233	94	1729	190	114	80	45	148	26	60	0.16	0.16	0.09	0.05	1.81	2.12
	10	1688	695	104	1676	137	113	82	45	633	25	59	0.70	0.17	0.06	0.05	10.80	9.28
	14	2498	1505	118	2326	787	124	81	45	1151	25	59	1.26	0.19	0.37	0.06	3.40	0.74
	18	3269	2276	131	3123	1584	136	84	45	1563	25	58	1.75	0.21	0.76	0.07	2.31	0.34
	25	18336	17343	278	14261	12722	251	80	45	11618	26	60	12.66	0.41	5.94	0.12	2.13	0.08
	40	36185	35192	386	30257	28718	357	81	45	22269	25	59	24.38	0.57	13.52	0.17	1.80	0.05
	120	117345	116352	688	115621	114082	685	80	45	65015	26	60	70.82	1.06	53.26	0.32	1.33	0.02
	480	344614	343621	1176	468991	467452	1372	81	45	133268	25	59	145.89	1.98	220.08	0.65	0.66	0.01
Fuc	0	4408			3878													
	0.25	4777			4037													
	1	4919			4167													
	1.5	5644			4967													
	2.5	4667			4046													
	4	4847			4095													
	8	4229			3519													
	10	4263	0		3425	0												
	14	4672	409	189	3573	148	169	82	45	342	25	59	0.38	0.28	0.07	0.08	5.40	7.35
	18	6238	1975	205	4217	792	176	83	45	1619	25	59	1.80	0.30	0.37	0.08	4.82	1.34
	25	18691	14428	303	12247	8822	251	83	45	10458	25	59	11.62	0.44	4.15	0.12	2.80	0.13
	40	28408	24145	362	21107	17682	314	83	45	16188	25	59	17.99	0.53	8.32	0.15	2.16	0.07
	120	114096	109833	688	87836	84411	605	83	45	71848	25	59	79.83	1.02	39.74	0.28	2.01	0.03
	480	509299	505036	1433	679846	676421	1653	83	45	200646	25	59	222.94	2.43	318.47	0.78	0.70	0.01

Appendix 10 Continued

Continued overleaf

Wee t ☺ the professional skier
Thank you for all the times you kept me entertained both in and out of the lab!
You will always be the loveliest of the loveliest!
x